# Assessment of *Pseudomonas* Quinolone Signal Response Protein PqsE and Preliminary Functional Annotation of Hypothetical Protein PA0803 from *Pseudomonas aeruginosa*

# Dissertation

zur Erlangung des akademischen Grades
eines Doktors der Naturwissenschaften der Fakultät Chemie
der Technischen Universität Dortmund

Vorgelegt von

**Shen Yu**

Technische Universität Dortmund
und
Max-Planck-Institut für molekulare Physiologie

Dortmund 2009

# ACKNOWLEDGEMENTS

The following work was carried out under the guidance of Dr. Wulf Blankenfeldt and Prof. Dr. Roger Goody at the department of Biophysical Chemistry, Max-Planck-Institute of Molecular Physiology, during the period from March 2005 to December 2008.

Here, I would like to give my sincere gratefulness to:

**Prof. Dr. Roger Goody** for the possibility to work at the MPI and for his consistent help, discussions and encouragements,
**Dr. Wulf Blankenfeldt**, as my mentor, for introducing me to this project and for patient guidance in my academic and personal development,
**Prof. Dr. Roland Winter** for being very kind to spend time to be my second thesis advisor,
**IMPRS-CB** for educational and financial support as the study program of my PhD training,
**Prof. Dr. Susanne Häussler and her group**, as our collaborator, for their help in the transcriptiome assay of PqsE and their kind gift of various ligands,
**Dr. Ingrid Vetter and the Crystallography community in the MPI** for data collection at the synchrotrons as well as many helps in handling experimental difficulties,
**Dr. Petra Janning** for coaching mass spectrometry techniques,
**Ms. Janine Seeliger and Ingrid Hoffmann** for purification of some PqsE constructs and for carrying out some kinetic measurements of PqsE,
**Ms. Petra Geue, Ms. Nathalie Bleimling, and Ms. Christiane Pfaff** for numerous helps in the lab,
**All colleagues at the MPI-DO, especially members of the AG Blankenfeldt** for enjoyable working atomosphere,

and last but not least

**Mom and Dad**, who are in Beijing, for all you've done for me.

Eidesstattliche Erklärung

Hiermit erkläre ich an Eides Statt, dass ich diese Arbeit selbständig und nur mit den angegebenen Hilfsmitteln angefertigt habe.

Dortmund, December. 2009

# INDEX

**INDEX**

## INDEX

**INDEX**

## INDEX

# 1 INTRODUCTION

## 1.1 INFECTION, VIRULENCE AND VIRULENCE FACTORS

An infection refers to the detrimental colonization of a host organism by a foreign species. Many human diseases are caused by microbial infection and are therefore termed "infectious diseases". The microscopic pathogens can be parasites, protozoa, fungi, bacteria, viruses or prions.

Statistics reported by the World Health Organization showed that in year 2002 alone, 14.7 million people were killed by infectious diseases. Surprisingly, despite HIV/AIDS causing 2.8 million deaths and being the top single disease killer, more mortalities (3.9 millions) resulted from lower respiratory infections caused by bacteria. Humanity has been fighting bacterial infections for centuries, but the constant treatment with antibiotics has been driving the pathogenic bacteria to evolve to resistant strains which are clinically more challenging to eradicate. The need for developing novel antibiotics remains high at the present time.

Virulence describes the ability of a pathogen to invade its hosts. For bacterial pathogens, important features include the number of infecting bacteria, the route to entry into the host, effects of host defence mechanisms (e.g. fever) and intrinsic characterics of the bacteria called virulence factors.

Virulence factors are proteins or small molecules synthesized and released by a pathogen in order to facilitate the invasion process. Bacterial virulence factors may function in various pathogenic steps, such as adhesion, host body entry, survival in host environment and inhibition of host immune response. Some virulence factors may also poison host cells or damage host tissues for different purposes, like obtaining nutrition from the host.

It is important to study virulence factors since in many cases they are the direct cause of diseases. Previously, studies focused on how these toxins or inhibitors are synthesized in the bacteria. In recent years, in search of novel antibiotic targets, the research on virulence factors has been extended to a much broader realm, covering for example the control of virulence factor production and self-protection of the pathogen from the malicious effects of its own virulence factors.

## 1.2 CONTROL OF VIRULENCE: QUORUM SENSING

### 1.2.1 The concept of quorum sensing

Although plants and animals are in continuous contact with potential pathogens, a successful infection is rare. This is because these potential hosts possess innate immune systems that defend them from infections.

Generally speaking, host immunity relies both on constitutive barriers and inducible responses. For example, both plants and animals have receptors that can recognize the presence of microbial threats by detecting microbe-associated molecular patterns such as bacterial flagellin or peptidoglycans. Recognition triggers the activation of mitogen-activated protein kinases (MAPKs) and various hormone signalling pathways. The signalling induces strong defensive actions like production and accumulation of antimicrobial compounds or programmed cell death.

On the other side of the infection war, pathogens have to develop strategies to overcome host defences. One of them is called quorum sensing (QS). These bacteria keep virulence factor production at a very low level as long as the cell density is low. They can thereby proliferate in the host environment without triggering defensive alarms until the bacteria reach a concentration that is appropriate for a massive production of virulence factors, thus swamping out the host immunity response.

### 1.2.2 The discovery of quorum sensing

The molecular mechanism of QS was first discovered in a Gram-negative marine bacterium, *Vibrio fischeri*, which lives in symbiosis with marine animals such as the bobtail squid *Euprymna scolopes*. The animal provides the bacteria with an exclusive sugar and amino acid rich ecological niche. The bacterium in turn emits photons (bioluminescence), a function that hides the outline of the animal when viewed from below. Reasonably, the bacterium only produces bioluminescence at high cell density. However, adding sterile culture supernatant of a high-density culture to fresh, low cell density cultures of this bacterium induces the low-density culture to emit light. This led to the discovery of the responsible signalling molecule N-(3-oxo) hexanoyl-L-homoserine lactone (3O-C6HSL) (Kaplan and Greenberg, 1985).

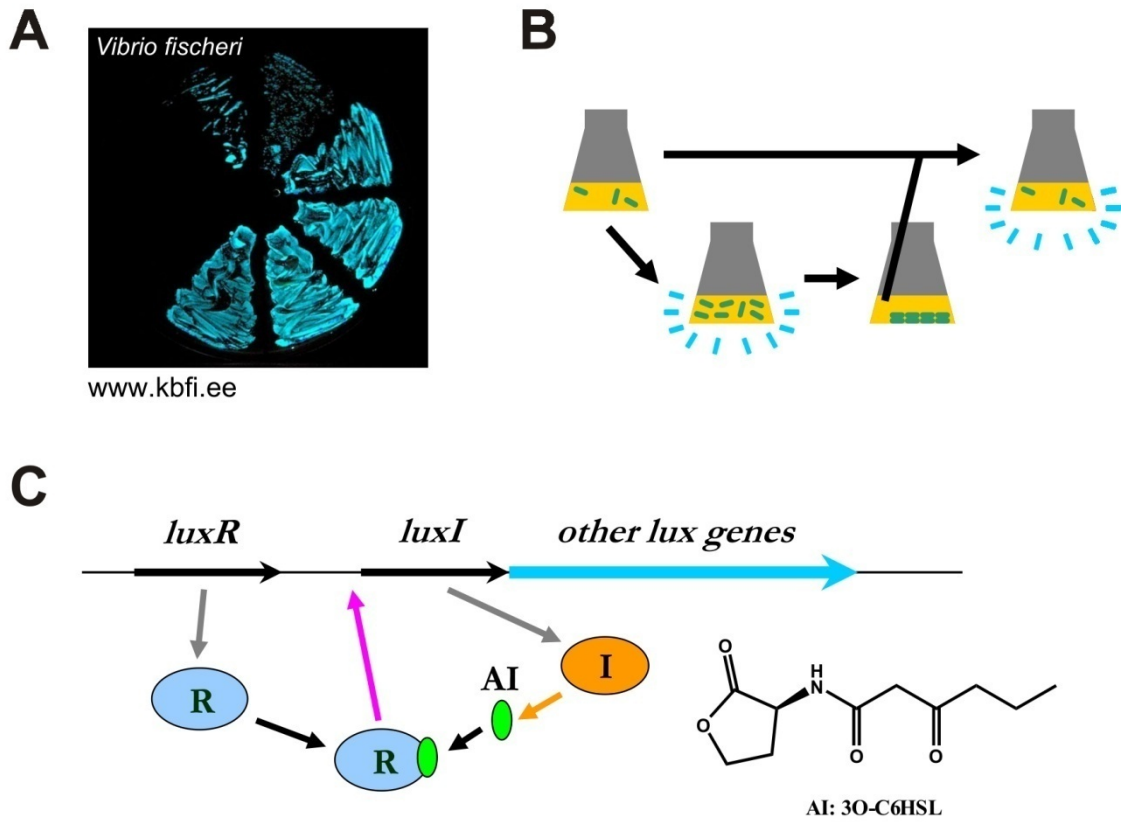


**Figure 1.1: Concepts of QS. A) A photograph of *V. fischeri* exhibiting bioluminescence. B) Scheme of the discovery of QS. C) A typical R/I two-component QS module (LuxR/I from *V. fischeri*, using 3O-C6HSL as AI). Pink arrow: activation.**

In *V. fischeri*, 3O-C6HSL is synthesized from S-adenosyl methionine (SAM) and an acyl-carrier protein by a synthase encoded by the *luxI* gene. As it is produced at a basal level by each cell, the concentration of the signal builds up in the environment as bacteria proliferate, and this indicates the cell density. Once a threshold signal concentration (i.e., a cell density threshold) is reached, it is sensed and bound by the LuxR sensor protein, which is encoded by *luxR* and also acts as a transcriptional regulator by activating the expression of the *lux* operon. Interestingly, *luxI* is also a member of the *lux* operon, together with other *lux* genes that are responsible for bioluminescence. Therefore, the R/I protein forms a positive feedback loop in terms of signal transduction and the acyl-HSL (AHL) is termed an auto-inducer (AI) (Kaplan *et al.*, 1985;Kaplan and Greenberg, 1987;Fuqua et al., 1994). Upon activation of the LuxR/I, a burst of 3O-C6HSL concentration occurs, driving simultaneously the expression of other Lux proteins that "switch-on" the bioluminescence (Figure 1.1). It is necessary to point out that although the positive feedback circuit is a

characteristic feature of a LuxR/I type two component QS system, the transcription regulator R protein can activate genes including, but not limited to, the I protein. Each LuxR-like transcription factor recognizes a particular nucleic acid sequence at the promoter region that may occur multiple times in the genome and thereby controls the expression of a particular set of genes, which is termed a "regulon".

### 1.2.3 LuxR-like transcription regulator in atomic detail

Because this research work is dedicated to understanding proteins at the molecular level, structural data will be extensively discussed. Therefore shown here is a crystal structure of a transcription regulator R protein, as it will be referred to in various discussions through the following chapters. Due to experimental difficulties, only a few LuxR-like transcription regulators have been studied structurally. Most notably, the crystal structure of the TraR protein from *Agrobacterium tumefaciens* has been determined in 2002 (Vannini et al., 2002), bound with the TraBox DNA (5'-ATG-TGC-AGA-TCT-GCA-CAT-3') and the N-(3-oxo) octanoyl-L-homoserine lactone (3O-C8HSL) auto-inducer. This structure revealed some common features of the LuxR-like transcription factors.

Like LuxR, the TraR protein folds into two domains: an N-terminal ligand-binding domain (LBD) and the C-terminal DNA-binding domain. The DNA-binding domain has a helix-turn-helix (HTH) motif, but without an apo structure available it is not possible yet to describe the LBD without the auto-inducer. However, upon AI binding, the ligand-binding domain forms a very tight dimer, with one AI bound to each monomer, and this dimerization brings the two HTH domains together to bind the TraBox (Figure 1.2A). It therefore explains how the LuxR-like proteins recognize DNA sequences that have perfect dyad symmetry.

While the HTH domain follows the same mechanism of DNA binding as other HTH domain containing proteins, i.e., by inserting one of the helices into the major groove of double stranded DNA, the LuxR-like transcription regulators have the characteristic of recognizing a specific AHL signal molecule. It is therefore important to examine in detail how the LBD sequesters the corresponding AHL. From the TraR structure, the LBD (residue 1-162) exhibits structure similarities with the ubiquitous GAF/PAS domains. It consists of a five-stranded antiparallel β-sheet, packed against three α-helices on each side.

The 3O-C8HSL molecule is deeply inserted between the β-sheet and three helices (Figure 1.2B).

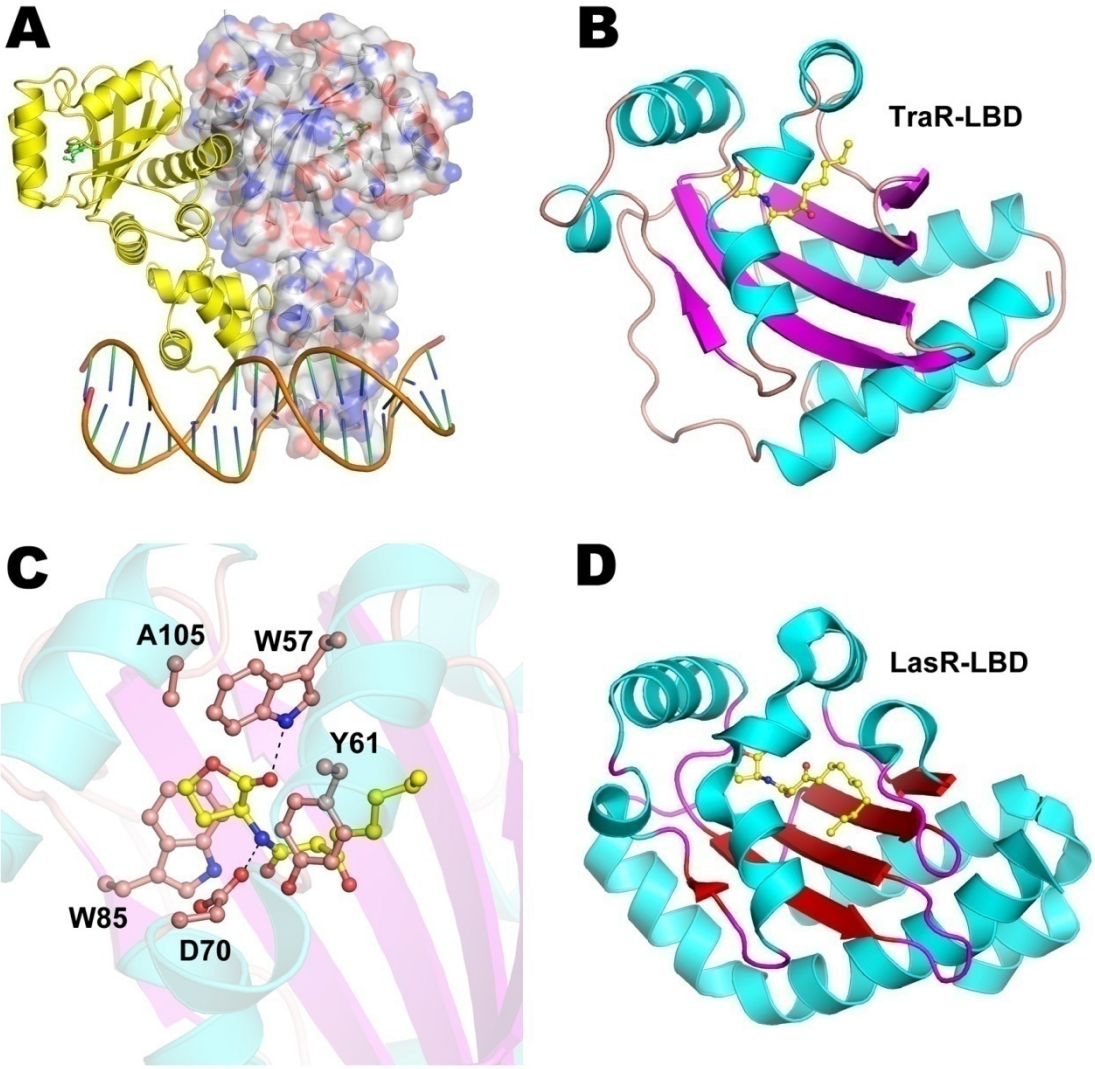


**Figure 1.2: Structure of a LuxR-like transcription factor TraR. A) Cartoon representation of the TraR dimer bound to AI and DNA. Surface presentation of one chain is also shown. PDB ID: 1H0M. B) Ligand binding domain of TraR. C) Binding pocket of AI. D) Ligand binding domain of LasR. PDB ID: 2UV0.**

The AI molecule does not appear to be involved in dimerization directly. On the contrary, it is completely embedded in a closed cavity with no access to external solvents (Figure 1.2C). The molecule is encompassed mostly by hydrophobic residues including conserved Trp57, Tyr61, Trp85 and Ala105, reflecting the rather hydrophobic nature of the AI molecule. Two hydrogen bonds appear to be critical in AHL binding: one between the

carbonyl oxygen atom of the HSL moiety and the ε nitrogen (NE1) of Trp57, the other between the nitrogen atom of the AI molecule and one ε oxygen (OD2) of Asp70.

In 2007, the crystal structure of the LBD of LasR (Section 2.5.1) in complex with its AI molecule 3O-C12HSL had been published (Bottomley et al., 2007). The fold completely resembles a GAF/PAS domain as well (Figure 1.2D) and the LasR molecule utilizes exactly the same set of conserved residues to bind its AI as shown in Figure 1.2C. The 12-carbon long acyl chain, however, adopts a different spatial configuration.

## 1.3 *PSEUDOMONAS AERUGINOSA*

*Pseudomonas aeruginosa* is a ubiquitous Gram-negative bacterium. It can be found in soil, water, or many other natural and artificial environments throughout the world. It thrives in both aerobic and anaerobic conditions, and can feed on a wide range of organic materials and is therefore very versatile. *P. aeruginosa* is an important opportunistic pathogen to both plants and animals, including humans. Extensive studies carried out in, e.g., *Arabidopsis thaliana* (Walker et al., 2004), *Caenorhabditis elegans* (Mahajan-Miklos et al., 1999b), and *Drosophila* (D'Argenio et al., 2001) show that the bacterium uses common virulence factors against different hosts (Rahme et al., 1995;Rahme et al., 2000). In humans, *P. aeruginosa* typically infects the pulmonary tract, urinary tract, burns, wounds, and may also cause blood infections. If *P. aeruginosa* colonizations occur in critical body organs such as the lungs, the urinary tract, and kidneys, the results can be fatal. In fact, the bacterium is a leading cause of many infections. For example, about 10% of hospital-acquired infections are from *Pseudomonas*; it is common for cystic fibrosis patients to have *P. aeruginosa* infection in the lungs; *P. aeruginosa* also serves as the most common cause of burn wound infections.

*P. aeruginosa* uses the virulence factor exotoxin A to ADP-ribosylate eukaryotic elongation factor 2 in the host cell. Without elongation factor 2, eukaryotic cells cannot synthesize proteins and undergo necrosis. The release of intracellular contents induces an immunologic response. The bacterium is therefore termed an “opportunistic” pathogen that is unable to infect immunocompetent individuals. Nevertheless, however opportunistic the pathogen is, *P. aeruginosa* remains a severe threat to the survival and well-being of immunocompromised patients.

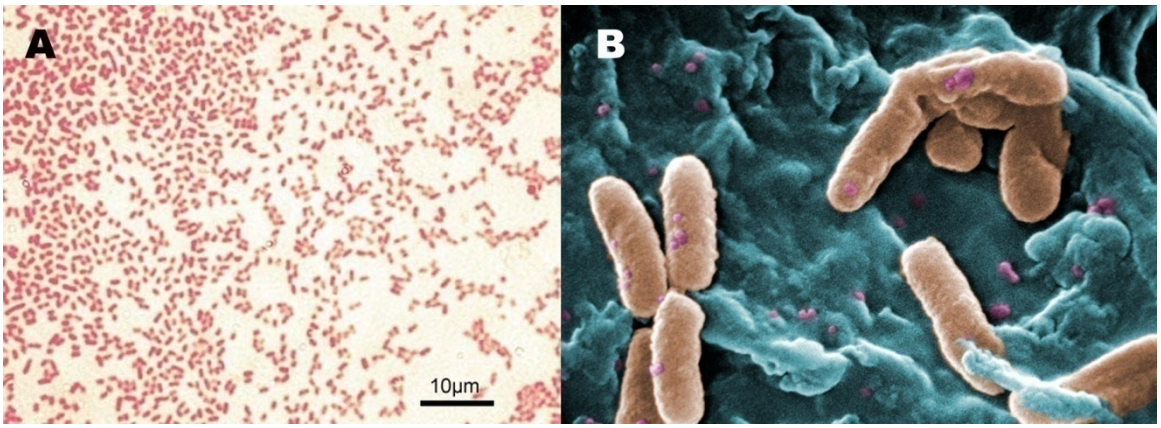


**Figure 1.3: *Pseudomonas aeruginosa*. A) A microscopic image showing Gram staining of *P. aeruginosa* (Source: ATCC 27853, 1:1000). The pink color of the bacteria indicates that they are Gram-negative, as opposed to purple in the Gram-positive cases. B) A colorized picture depicting a scanning electron micrograph of *P. aeruginosa*. (Source: Centers for Disease Control and Prevention's Public Health Image Library, ID 10043).**

One of the most notorious characteristics of *P. aeruginosa* infection is the resistance to many antibiotics. This low susceptibility is attributable to a concerted action of multidrug efflux pumps with chromosomally-encoded antibiotic resistance genes and the low permeability of the bacterial cellular envelopes. Besides, the bacterium switches at one stage from planktonic growth to a biofilm phenotype. The biofilm is build from extracellular polymeric substances and gives the bacterial community extra protection from antibiotics. Hence, once the *P. aeruginosa* infection establishes in the host, it is very difficult to eradicate it by traditional antibiotic treatment. Medical research in recent years therefore shifted to search for targets in the regulation mechanisms of biofilm formation and virulence factor production. Thus it is no wonder why a universal switch mechanism that controls both characteristics (Section 1.4) has become a new hot-spot in *P. aeruginosa* research.

## 1.4 QUORUM SENSING IN *PSEUDOMONAS AERUGINOSA*

### 1.4.1 AHL based QS systems in *P. aeruginosa*

The same principle also applies to how *P. aeruginosa* regulates the expression of many virulence genes. One class of virulence factors made by P. aeruginosa is the phenazines (Section 1.5). Due to their unclear but indispensible role in pathogenesis,

phenazines are presumably molecules that alert the host surveillance. In fact, at least one phenazine compound, pyocyanin, has been shown to elicit the induced system resistance in plants (Audenaert et al., 2002). In order to maintain its presence unnoticed by host defence before a critical mass is reached, multiple layers of quorum sensing control exist in this phenazine-producing bacterium.

Apart from phenazine production, the QS systems in *P. aeruginosa* also directly or indirectly control the timing and production of a large arsenal of other virulence factors like elastase, alkaline protease, exotoxin A, rhamnolipids, lectins, superoxide dismutases, as well as biofilm formation (Smith and Iglewski, 2003), estimated to be 6% - 10% of the genome (Schuster et al., 2003).

In *Pseudomonas aeruginosa*, two AHL based QS modules, termed LasR/I and RhlR/I, were discovered (Gambello and Iglewski, 1991;Brint and Ohman, 1995). LasR and RhlR are LuxR-like transcription regulators, whereas LasI makes N-(3-oxo) dodecanoyl homoserine lactone (3O-C12HSL) as the AI for LasR, while RhlI makes N-butanoyl homoserine lactone (C4HSL) for RhlR. The relationship between these two systems was believed to be hierarchical, because activated LasR drives the expression of *lasI* as well as *rhlR* and *rhlI* (Latifi et al., 1996). However, the relationship between LasR/I and RhlR/I is not simply a linear, hierachical one. It has been recently discovered that there are QS systems based on non-AHL autoinducers, such as acyl-quinolone (AQ) based signals (Pesci et al., 1999). In addition, the expression of QS regulated genes is reported to depend significantly on growth environments (Duan and Surette, 2007).

There are prominent differences between the target promoters of LasR and RhlR. Transcriptome studies using *lasI* and *rhlI* single and double mutants in the presence or absence of one or both autoinducers revealed that some genes are *las* specific, some respond to both AHLs but not 3O-C12HSL alone, while others are *rhl* specific (Schuster and Greenberg, 2006). The differential recognition of QS target promoters by LasR and RhlR depends on the recognition of conserved *las-rhl* boxes that serve as binding sites for either or both regulators (Schuster and Greenberg, 2007). However, analysis showed that although *rhl*-responsive promoters significantly retain the dyad symmetry, such symmetry of the *las-rhl* boxes was not required for LasR binding (Schuster et al., 2004b). These findings suggest that the LasR/I and RhlR/I each control different regulons.

In addition to LasR and RhlR, there are two other LuxR-like transcription regulators in the *P. aeruginosa* genome, named QscR (Chugani et al., 2001) and VqsR (Juhas et al.,

2004). Unlike the typical R/I two component systems, however, QscR and VqsR are orphaned transcription factors without the association of a cognate AHL synthase. The exact roles of these LuxR-like proteins are yet unclear, but they do participate in co-regulation of expression of QS-dependent genes (Juhas et al., 2005;Lequette et al., 2006), possibly by forming heterodimers with the LasR or RhlR protein (Ledgham et al., 2003).

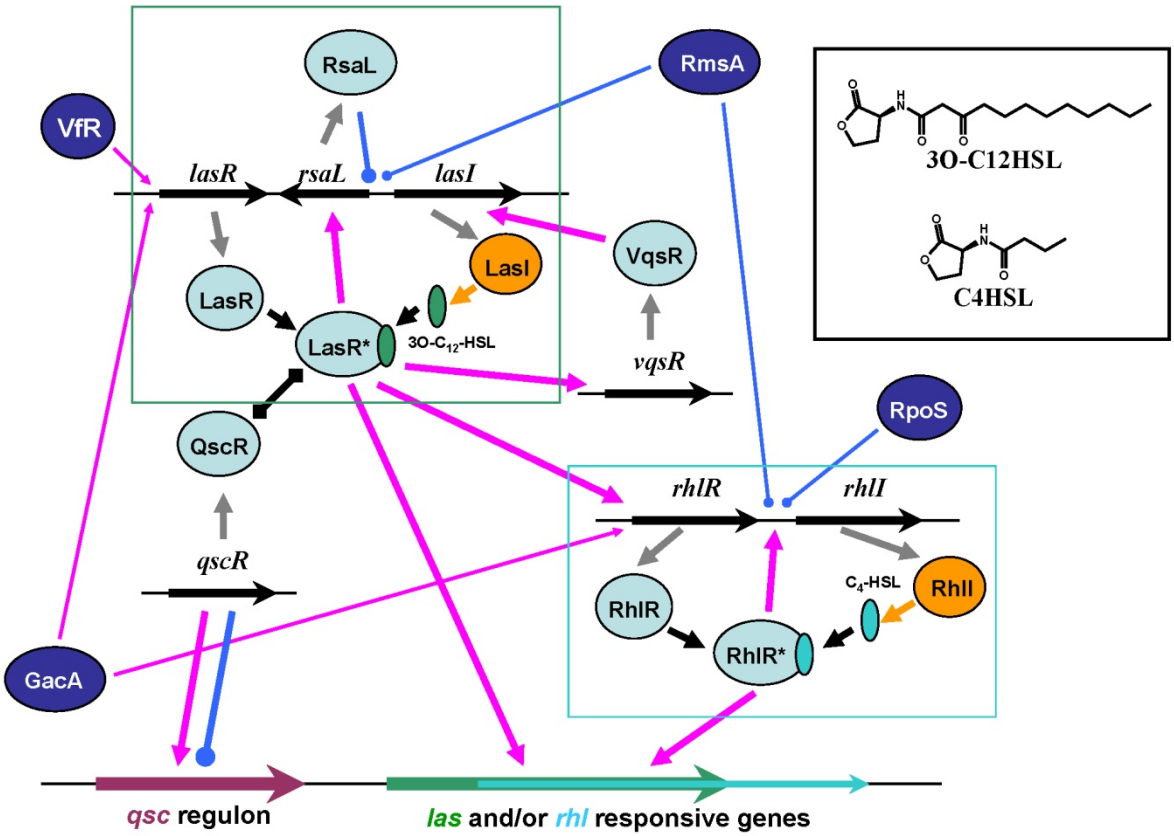


**Figure 1.4: AHL-based QS system in *P. aeruginosa*. LuxR-like proteins are depicted in light-blue ovals, AHL synthases in orange, while global regulators are in deep blue. In order to simplify the view, some global regulators are not shown here but are summarized in Table 1.1. The *las* and *rhl* modules are boxed respectively. Magenta arrow: positive regulation; blue dot-end lines: negative regulation. Molecules in the black box: chemical structures of the two AIs.**

*P. aeruginosa* is a highly environmentally adaptable bacterium with a large, dynamic genome of over 6 million base pairs that encode 4000-5000 genes. It has been estimated that approximately 10% of the genome is devoted to regulatory elements. It is therefore not surprising that many global factors also participate as fine-tuners of the multi-signal QS system (Table 1.1).

| Regulator | Description | Link with QS | Phenotypes affected |
|---|---|---|---|
| VfR | Cyclic AMP receptor protein | ↑ lasR | Exotoxin A, proteases |
| RsaL | Repressor of QS | ↓ lasI | Elastase, pyocyanin, HCN |
| RpoS | Stationary phase sigma factor | ↓ rhlI | LecA, elastase, pyocyanin, swarming |
| RpoN | Alternative sigma factor | ↓ lasRI, rhlI, can ↑ rhlI | Elastase, rhamnolipid, HCN |
| MvaT | HNS-like transcription regulator | Involved in the growth phase dependency of QS | LecA, elastase, pyocyanin, swarming, biofilms, MexEF-OprN efflux pump |
| VqsM | Transcription regulator | ↑ lasI and rhlI | Protease, elastase, swimming and swarming motility |
| RsmA | Post-transcriptional regulator | ↓ lasI and rhlI | Protease, pyocyanin, LecA, HCN, swarming |
| DksA | Transcription regulator | ↓ rhlI | Elastase, rhamnolipid |
| GacA | Global activator | ↑ lasR and rhlR | Pyocyanin, lipase, HCN |
| PhoB | Response regulator | ↑ rhlR under phosphate limited conditions | Pyocyanin |
| PQS | Pseudomonas quinolone signal | ↑ rhl QS | Elastase, LecA, pyocyanin, biofilm formation |
| PmpR | YebC protein family | ↓ pqsR, pqsA, pqsH and rhlR | Phenazines, pyocyanin |
| PtxR | Transcription regulator | ↓ pqsA-E and rhlI, ↑ lasI. | Pyocyanin, exotoxin A, rhamnolipids |
| PPK1 | Polyphosphate kinase | ↑ AHL production | Elastase, rhamnolipids, biofilm formation |
| AlgR | Transcription regulator | ↓ rhlI in biofilms | Biofilm maturation, rhamnolipids |

**Table 1.1: A summary of the main regulators known to modulate AHL and AQ-dependent QS in *P. aeruginosa*.**

RsaL, for example, is a global negative regulator of AHL-based QS. Its encoding gene locates directly between the *lasR* and *lasI* gene. RsaL transcription is initiated by activated LasR, which binds to the bi-directional rsaL-lasI promoter. However, RsaL also binds, as a repressor, to a site immediately adjacent to this promoter. When both RsaL and LasR bind to DNA, the repressor activity is dominant. It therefore creates a negative feedback loop that counteracts the LasR/I positive feedback loop. In addition, RsaL can

also directly repress some QS controlled genes, such as those responsible for pyocyanin production (Rampioni et al., 2007). Given the very upstream position of LasR/I, RsaL serves as a master off-switch of QS that functions both directly and indirectly.

*P. aeruginosa* encodes two AHL acylases, PvdQ and QuiP, that have quorum quenching function (Huang et al., 2006;Sio et al., 2006). These enzymes cleave off the fatty acid chain from the AHL resulting in HSL, thereby facilitating homoeostasis of the 3O-C12HSL level within the cell community. Interesting to note, some bacteria that may live in the same environment as *Pseudomonas*, such as *Bacillus*, *Burkholderia* or *Streptomyces*, encode AHL lactonase that cleaves open the HSL moiety and silences the cross-species QS as if they could decide willingly whether or not they act in concert with *Pseudomonas* (Dong et al., 2002;Ulrich, 2004;Park et al., 2005).

### 1.4.2 Discovery of Acyl-Quinolone (AQ) Signaling

If LasR/I and RhlR/I are the only QS modules in *Pseudomonas aeruginosa*, because they are hierarchically connected (see Figure 1.4), disruption of the upstream *lasR* gene should abolish the AHL synthesis with little or no expression of *lasI* and *rhlR/I*, and thereby no expression of AHL QS-controlled genes should occur. However, Pesci *et al.* (Pesci *et al.*, 1999) observed that the culture supernatant of a *ΔlasR* mutant of *P. aeruginosa* PAO1 can still induce significant expression of *lasB*, a gene for elastase previously known to be controlled by LasR/I QS. This suggested that a non-AHL QS signal is present in *P. aeruginosa*. It was shown that this signal requires a functional RhlR/I module because lasB cannot be activated in a *ΔrhlR/rhlI* double mutant. The signal molecule that is responsible for this phenomenon was purified from the culture fluid and identified to be 2-heptyl-3-hydroxy-4-quinolone (Figure 1.6), termed the *Pseudomonas* Quinolone Signal (PQS).

Since then, more than 55 quinolone metabolites were identified in *P. aeruginosa*, among which 2-heptyl-4-quinolone (HHQ, Figure 1.6), 2-nonyl-4-quinolone (NHQ) and 2-heptyl-4-quinolone Noxide (HHQNO) possess an acyl chain at the 2- position and are therefore classified together with PQS into the acyl-quinolone (AQ) compounds (Lepine et al., 2004). Interestingly, HHQ, an immediate precursor of PQS, was recently shown to be a QS signal as well (Xiao et al., 2006a).

### 1.4.3 Components of the PQS quorum sensing module

The gene cluster which directs the biosynthesis of PQS and other AQs in *P. aeruginosa* was identified by a random transposon mutagenesis screen for regulators of pyocyanin production and termed the *pqs* operon. It consists of five genes and they are therefore named *pqsABCDE* (Gallagher et al., 2002).

PqsA was identified as an anthranilate coenzyme A ligase that activates the precursor (Coleman et al., 2008). PqsD was responsible for the biosynthesis of 2,4-dihydroxyquinoline and therefore possibly assembling HHQ (Zhang et al., 2008;Bera et al., 2009). PqsB and PqsC have not yet been studied *in vitro* but their sequences show similarities with β-keto-acyl-acyl carrier protein synthetases. Anthranilate is converted by the *pqsABCD* gene products into HHQ (Deziel et al., 2004), which can pass between cells and be converted intracellularly into PQS by the gene product of *pqsH*, a probable FAD-dependent monoxygenase, which locates elsewhere in the genome (Gallagher *et al.*, 2002;Deziel *et al.*, 2004). The role of PqsE, a putative metallo-β-lactamase, has remained a mystery since its discovery (Figure 1.5).

Another gene *pqsL*, the product of which also resembles a probable FAD-dependent monoxygenase, was suggested to play a role in PQS biosynthesis due to the fact that a mutation in *pqsL* resulted in overproduction of PQS (D'Argenio et al., 2002). Profiling of the AQ production revealed that no AQ N-oxides were detected in a *pqsL* mutant, indicating that this gene may function by oxidizing the N-atom of the quinolones and is involved in the biosynthesis of these particular AQ compounds (Lepine *et al.*, 2004).

The expression of the *pqs* operon is regulated by a LysR-family regulator PqsR (also named MvfR), the gene of which locates close to *pqsE* but transcribes in the opposite direction (Deziel et al., 2005). It has been recently shown that both HHQ and PQS are autoinducers for PqsR, with the later being more potent in terms of enhancing the PqsR binding to the *pqsABCDE* promoter (Xiao *et al.*, 2006a). Besides, in a *pqsH* mutant that produces only HHQ, normal PqsR-dependent gene expression and virulence remains, except pyocyanin production. This on one hand reiterated the importance of PQS in regulation of phenazine biosynthesis, but on the other hand demonstrated that the presence of *pqsABCDE* and *pqsR* were sufficient to form a QS-module that resembles the LasR/I and RhlR/I modules, only differing from the later ones by replacing the sole synthase of AHL with four HHQ synthases (PqsA, B, C and D).

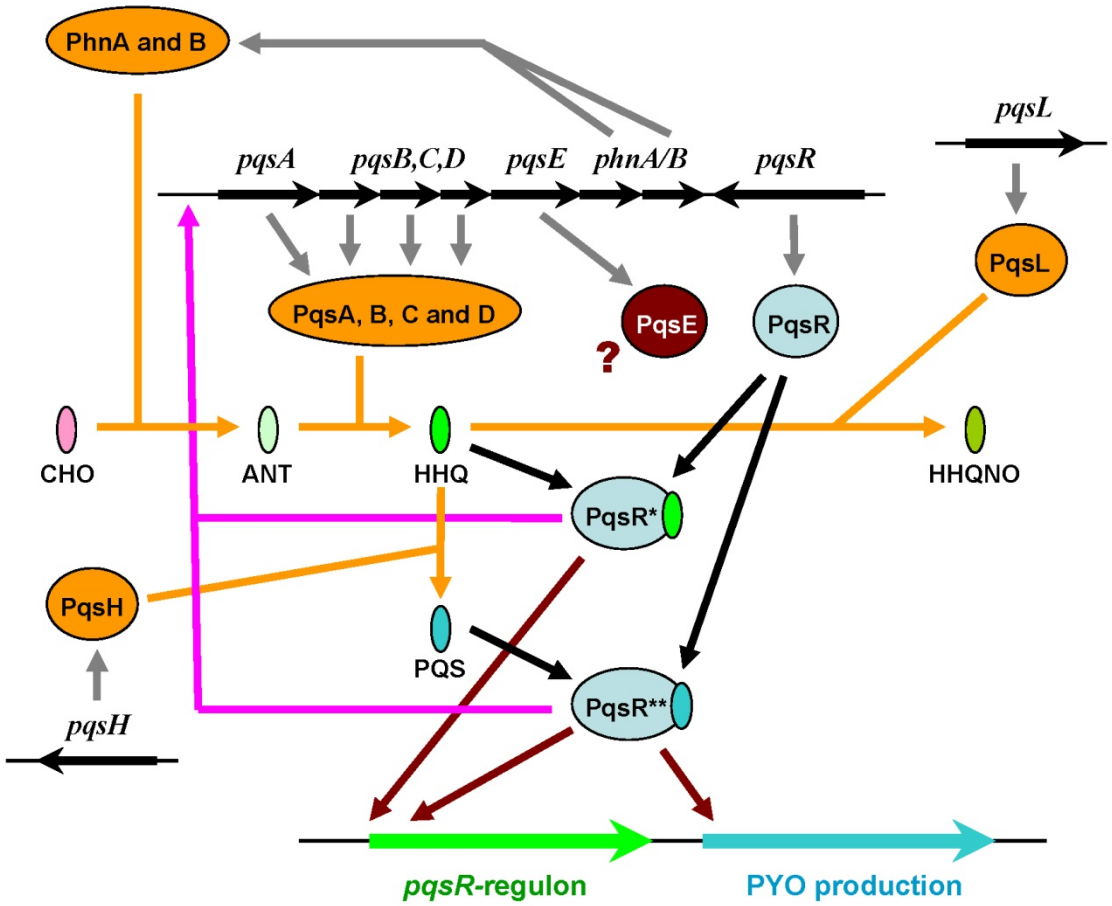


**Figure 1.5: Components of AQ-based QS in P. aeruginosa. CHO: chorismate; ANT: anthranilate. PqsE and PqsE-dependent positive regulations are colored dark red; other positive regulations are colored in magenta. Synthases and related chemical conversions are colored orange. Question mark indicates unknown function.**

Located between *pqsE* and *pqsR* are genes that encode the last two major components of the PQS module: *phnA* and *phnB*. Sequence analysis shows that the products of these genes are homologues to the anthranilate synthases TrpE/G. Their biochemical function is to convert chorismate to anthranilate. The rational of maintaining an additional set of anthranilate synthases can be that when PqsR gets activated, the presence of PhnA/B ensures the supply of precursor for PQS biosynthesis. They do not overlap TrpE/G activity before PqsR activation because *phnA* and *phnB* are co-regulated with the *pqs* operon.

### 1.4.4 Physiological roles of PQS

The role of PQS and HHQ in AQ-based cell-cell communication will be explained in detail in the following section. PQS, however, has been shown to have multiple functions (Figure 1.6).

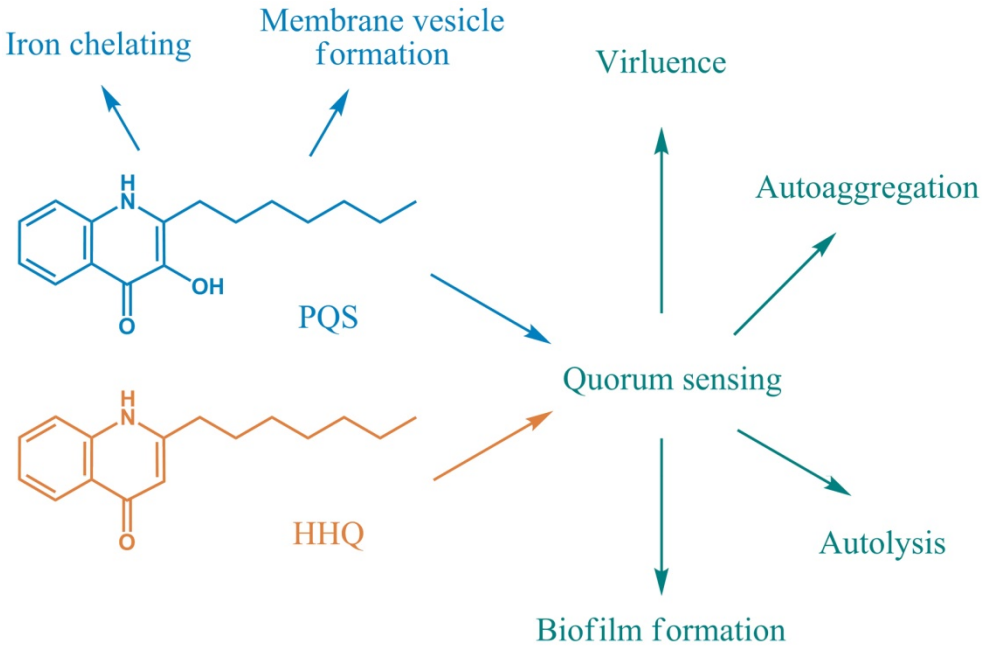


**Figure 1.6: Chemical Structure and functions of PQS and HHQ.**

It is apparent that PQS is poorly soluble in water, due to its relatively long acyl chain and the rather hydrophobic nature of the quinolone moiety. Therefore, over 50% of PQS is associated with the cell envelope. Binding of PQS to the cell envelope results in the release of membrane vesicles (MVs) that contain toxins, DNA, antibiotics and PQS (Mashburn and Whiteley, 2005). This mechanism provides a way for the insoluble PQS to travel within a *P. aeruginosa* population.

PQS solubility in *P. aeruginosa* cultures is also greatly facilitated by the biosurfactant properties of the rhamnolipids (Calfee et al., 2005), the production of which is dependent on both AHL and AQ-signalling (Diggle et al., 2003). Notably, MV formation is abolished in *P. aeruginosa ΔpqsH* mutants that are unable to convert HHQ to PQS (Mashburn *et al.*, 2005) but can be restored by provision of exogeneous PQS (Mashburn-Warren et al., 2008).

Recent studies of cell-to-cell signaling mediated by QS systems show growing evidence that QS can also be strongly affected by environmental factors other than cell density. Transcriptome profiling of *P. aeruginosa* PAO1 cultures supplemented with PQS

revealed an induction of the iron acquisition systems as well as the oxidative stress response upon PQS supplementation (Bredenbruch et al., 2006). When PQS was added to a culture, a rapid loss of free iron was observed. ESI/MS analysis showed that PQS chelates iron in a 3:1 complex. This demonstrated that PQS influences *P. aeruginosa* iron homeostasis (Bredenbruch *et al.*, 2006). A biophysical analysis by Diggle *et al.* (2007) uncovered that PQS forms a complex with Fe(III) at physiological pH (7.4). However, taken into consideration the recent finding that PQS can directly bind via its 3-hydroxyl group to the 4‘-phosphate group of bacterial lipopolysaccharide (Mashburn-Warren *et al.*, 2008), PQS is not likely to act as a siderophore but rather as an iron trap. In fact, when PQS was supplied to a *P. aeruginosa* mutant unable to produce pyoverdine or pyochelin, PQS associated with the cell envelope and inhibited bacterial growth, suggesting that PQS could play a role in iron entrapment to facilitate siderophore-mediated iron delivery (Diggle et al., 2007). In natural environments, where competition for iron is important, PQS may aid *P. aeruginosa* growth by trapping iron, storing it in the cell membrane for future use, and starve competing species of bacteria of free iron as well. PQS in iron-rich media induces many genes associated with oxidative stress (Bredenbruch *et al.*, 2006). It is thus possible that the PQS-Fe(III) complex plays an important role in this context, since ferric ligand complexes including some siderophores are capable of generating lethal oxidants such as the hydroxyl radical (DeWitte et al., 2001). This however requires further examination, because the PQS-regulated pyocyanin, for example, has also substantial oxidative capability.

In iron-rich environments, the *Pseudomonas aeruginosa* Fur (ferric uptake regulator) protein represses expression of two small regulatory RNAs encoded by *prrF1* and *prrF2*. More recently, effects of iron and *prrF* regulation on *P. aeruginosa* physiology were examined by Oglesby and co-workers. PrrF was shown to repress genes encoding anthranilate degradation enzymes, i.e. *antABC* (Oglesby et al., 2008). This means that when iron concentration shifts towards repletion, anthranilate, a PQS precursor, gets degraded more quickly. Therefore in iron-depletion conditions, anthranilate is expected to accumulate and the bacterium should produce PQS actively. Indeed, under iron-limiting conditions, PQS production was greatly decreased in a *ΔprrF12* mutant as compared with the wild type. The addition of anthranilate to the growth medium restored PQS production to the *ΔprrF12* mutant, demonstrating that the defect in PQS production is a consequence of anthranilate

degradation (Oglesby *et al.*, 2008). This experiment reveals a direct regulatory link between iron and PQS via PrrF RNAs.

Another interesting observation is that since Fe activates *antA*, the bacterium should produce little PQS in high-iron conditions. This is however not true for the wild type PAO1 (Oglesby *et al.*, 2008), suggesting that Fe can activate either the anthranilate biosynthesis pathway via chorismate, or more likely, the tryptophan degradation pathway via kynurenine to keep homoeostasis of anthranilate.

PQS has also been shown to be involved in biofilm formation (Diggle *et al.*, 2003). Biofilms formed by a *pqsA* mutant contained less extracellular DNA than biofilms formed by the wild type. In addition, the mutant biofilms were less susceptible to treatment with sodium dodecyl sulfate than a wild type biofilm (Allesen-Holm et al., 2006). Extracellular DNA is one of the major matrix components in *P. aeruginosa* biofilms. QS-controlled DNA release from *P. aeruginosa* strains involves lysis of a sub-population of cells. A *P. aeruginosa ΔpqsL* mutant that overproduces PQS showed a high level of autolysis phenotype (D'Argenio *et al.*, 2002). PQS may therefore play an important community function in balancing viability and cell death under stressful conditions by promoting regulated autolysis within the population, thus enabling surviving bacteria to uptake nutrients from lysed cells and to make use of the extracellular DNA as a component of the biofilm matrix. This hypothesis was supported by a recent study showing that PQS can act as both a pro-oxidant and an inducer of an antioxidative stress response, thereby shaping the population structure of *P. aeruginosa* cultures according to cellular stress tolerances (Haussler et al., 2007).

Interestingly, it has been shown that *pqs* gene expression, DNA release and biofilm formation were favoured in media with low iron concentrations. When levels of iron were high, it was found that *pqsA* expression was significantly lower, DNA release was repressed and biofilms were structurally altered resulting in biofilms with higher susceptibility to antimicrobial compounds. The *pqs* operon was induced in particular sub-populations of biofilm cells under low iron conditions and repressed in biofilm cells under higher iron level (Yang et al., 2007). This observation, however, contradicts the more recent report showing that *P. aeruginosa* produces more PQS in high iron condition (Oglesby *et al.*, 2008). Although this discrepancy might be explained by different behavior of the bacterium in biofilms and in fluid culture, it nevertheless implies that the link

between iron levels, PQS and biofilm formation can be very intricate and requires further investigation.

### 1.4.5 Integration of the PQS module into the QS system

Recent findings on QS in *Pseudomonas aeruginosa* strongly suggest that the AHL modules and the PQS module, together with some global regulatory factors, form an intricate network that allows the bacterium to respond effectively to its growth environment. Figure 1.7 summarizes how the PQS module is inter-connected with the AHL modules.

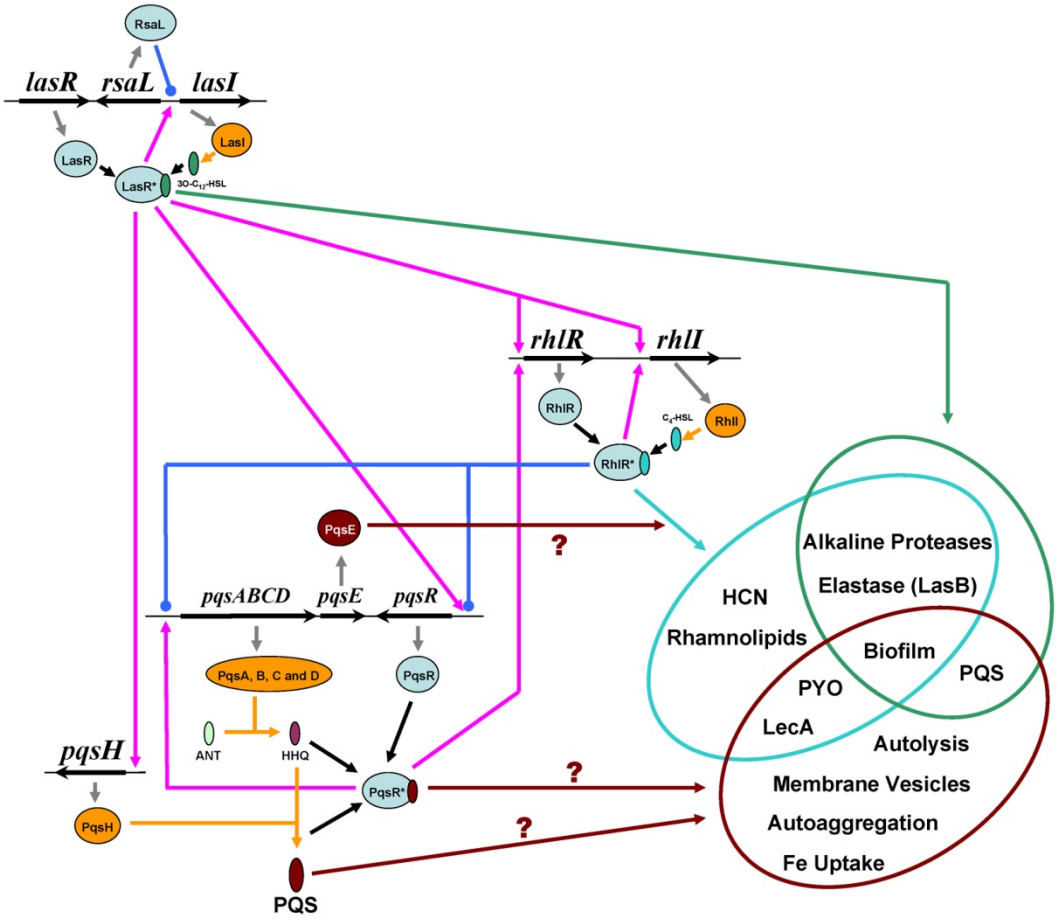


**Figure 1.7: Formation of the QS system in *P. aeruginosa*, emphasizing on interactions between the Las, Rhl, PQS modules and their regulated phenotypes. Global regulators, *qscR*, *vqsR* and *pqsL* are omitted for clarity. PqsE and PqsE-dependent positive regulations are colored dark red; other positive regulations are colored in magenta; negative regulations are depicted as blue dot-end lines. Synthases and related chemical conversions are colored orange. Question marks indicate unknown mechanisms.**

The transcription activator of the *pqs* operon, *pqsR*, as well as the *pqsH* gene are positively regulated by LasR (Gallagher *et al.*, 2002;Deziel *et al.*, 2005;Xiao *et al.*, 2006a). Conversely, RhlR negatively regulates both *pqsR* and *pqsA* (Xiao et al., 2006b). Taking into account that the PQS module positively regulates the RhlR/I module (McKnight et al., 2000), both AHL-dependent and AQ-dependent QS modules are closely linked and mutation of either system results in the attenuation of *P. aeruginosa* virulence.

Nevertheless, phenotypes that fall under QS control can still be segmented. As reviewed in a recent report (Dubern and Diggle, 2008), production of HCN and rhamnolipid seems to be directly controlled by the RhlR/I module, whereas autolysis, autoaggregation and membrane vesicle formation, together with Fe homoeostasis are mostly affected by perturbation of the PQS module. Complicated phenotypes, like biofilm formation, require a collective effort of many genes and are therefore difficult to assign to any of the three sections.

Pyocyanin production is known to be abolished in all *rhl* and *pqs* mutants. Since the relationship between these two modules is very complex, it is difficult to draw a conclusion on how pyocyanin production is modulated in *P. aeruginosa*.

### 1.4.6 PqsE

The most intriguing gene in the *pqsABCDE* operon is the fifth gene, *pqsE*. *P. aeruginosa ΔpqsE* mutants produce similar AQ profiles but do not produce PQS-dependent virulence factors such as pyocyanin and lectin A (Figure 1.5). *In vivo*, *ΔpqsE* exhibits attenuated virulence in both *C. elegans* and mouse infection models (Gallagher *et al.*, 2002;Diggle *et al.*, 2003;Deziel *et al.*, 2005). None of these phenotypes can be restored by addition of exogenous PQS or HHQ. These data suggest that PqsE is a responder or an effector of AQ action. Since sequence analysis indicates that PqsE belongs to the family of metallohydrolases that includes the metallo-β-lactamases and AHL-degrading lactonases, it was originally hypothesized that PqsE may act on PQS to convert it to another signal molecule that drives expression of PQS-dependent genes (Gallagher *et al.*, 2002).

Farrow *et al.* reported recently that PqsE can activate PQS-regulated genes in the absence of PQS and PqsR (Farrow, III et al., 2008). The action of PqsE was *rhl*-dependent and PqsE could also enhance the ability of *E. coli* harboring a *rhlR*-containing plasmid to respond to C4-HSL (Figure 1.7). This makes it indispensible to elucidate the biochemical

function of PqsE in order to understand the associated downstream signal transduction mechanisms. Because PqsE functions in the *rhlR*-containing *E. coli* as well, it may possibly interact directly with either the RhlR protein or the C4HSL sigal. Alternatively, since PqsE is predicted to be an enyzme, it presumably converts a substrate that is common in both *E. coli* and *P. aeruginosa* into a co-activator of RhlR.

The AQ-independent action of PqsE suggests that the primary function of PqsR in regulating virulence is to drive the expression of *pqsE*. However, this fails to explain the observation that PQS, but not HHQ, restores pyocyanin and lectin A production in a *P. aeruginosa* PAO1 *ΔpqsA* mutant, since both PQS and HHQ can activate PqsR and thereby the expression of the *pqsABCDE* operon (Diggle *et al.*, 2007). Hence, even if the action of PqsE is not dependent on PQS, the presence of PQS appears to be part of the link between QS and virulence production in a yet undiscovered way.

## 1.5 PHENAZINES AND PYOCYANIN

Lives depend on macromolecules like proteins and nucleic acids, as they are indispensible for one of the most critical functions that define life: storing and passing genetic information. However, macromolecules are not the only players. It is well known that small molecules, generally referred as metabolites, work in concert with proteins and nucleic acids to play important roles in cellular function. Many are in fact essential, as they involve in critical process like bioenergetics. There are also many others, which are not required for the survival of the cells and therefore termed “secondary metabolites”.

It is nevertheless interesting to study these non-essential compounds, because many of them are found to have interesting chemical or biological properties, such as antibiotic, anti-tumor, anti-inflammation or antioxidant activities. Secondary metabolites therefore have become a new source of bioactive natural products actively pursued in pharmaceutical and agricultural industry. Recently, as our knowledge of biological systems expands, many old molecules that were previously identified to be secondary metabolites have been shown to play previously unidentified roles that are important for survival, therefore blurring the border between primary and secondary metabolites.

One class of these compounds are phenazines (Section 1.5), which are nitrogen-containing aromatic compounds (Figure 1.8) that are produced by diverse bacterial

genera, including *Streptomyces, Pseudomonas, Pelagiobacter* and *Vibrio*, under the control of quorum sensing (Section 1.2). They are generally water soluble and distinctly colored (Kerr, 2000). Phenazines have long been recognized as secondary metabolites (BU'LOCK, 1961), as they are natural products of restricted taxonomic distribution, formed mainly by cells that have stopped dividing and therefore have no obvious effect on cell growth. Early studies on phenazines were motivated by the fact that phenazines possess broadband antibiotic activity towards other bacteria, fungi, or plant/animal tissues (Laursen and Nielsen, 2004).

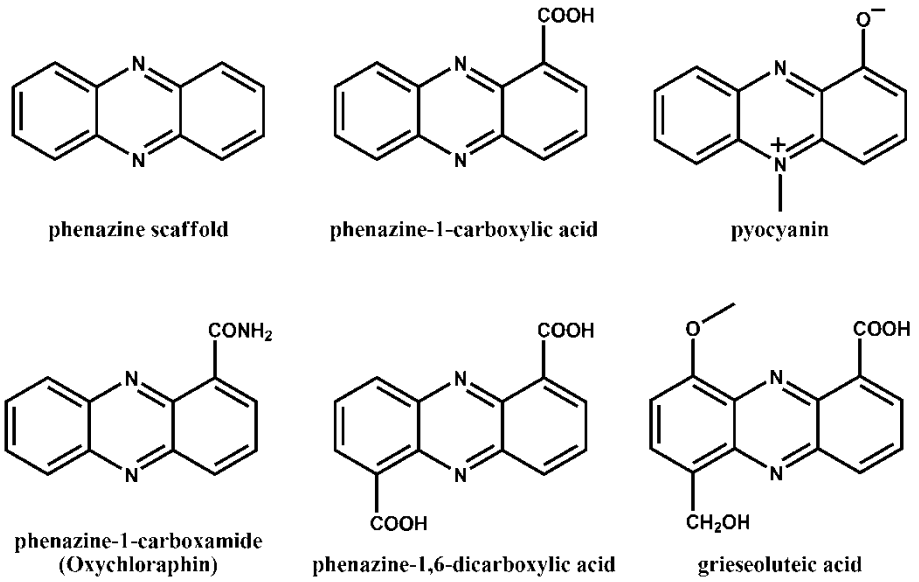


**Figure 1.8: Some phenazines derivatives.**

The lack of obvious metabolic functions of phenazines has led to several hypotheses on their role in nature. As phenazine-producing organisms survive longer than non-phenazine-producing species, it is likely that the phenazine production, due to the apparent antibiotic activity, helps the producing organism to protect its habitat against other microbial competitors. It is also possible that phenazines act as bacterial virulence factors to their hosts, i.e., they facilitate the development and continuation of the infections. *Pseudomonas aeruginosa* produces, e.g., pyocyanin and 1-hydroxyphenazine. These two phenazine derivatives are known to down-regulate the ciliary beat frequency of respiratory epithelial cells by reducing cAMP and ATP, altering the calcium concentration by inhibition of plasma membrane $Ca^{2+}$-ATPase, and inducing death in human neutrophils (leukocytes). These and other functions of the virulence factors lead to prolonged inflammation and

escalation of the disease. The importance of pyocyanin to the pathogenesis of *P. aeruginosa* infection was re-emphasized using *in vivo* and genomic approaches (Tan et al., 1999;Mahajan-Miklos et al., 1999a;Cao et al., 2001;Ran et al., 2003;Lau et al., 2003;Lau et al., 2004b).

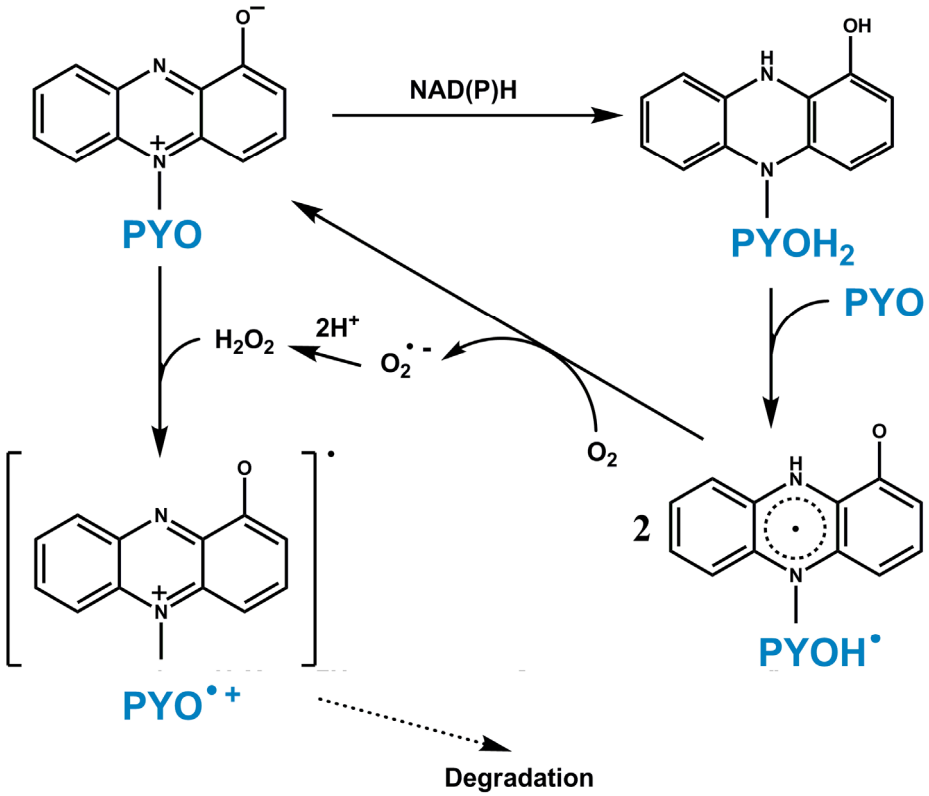


**Figure 1.9: Ability of pyocyanin to trigger reactive oxygen species.**

The mode of action of the phenazines appears to be complex. Despite the fact that phenazines have the ability to trigger the generation of reactive oxygen species and that many of them participate in redox reactions, there is no generally accepted evidence that any phenazine functions physiologically in a respiratory chain (Turner and Messenger, 1986). One example is pyocyanin, which can accept a single electron and form a stabilized anion radical. In earlier hypotheses, it was believed that this anion radical underwent redox cycling, leading to increased production of the toxic superoxide ($O_2^{\bullet-}$) and $H_2O_2$ ((Reszka et al., 2004), Figure 1.9). Thereby the production of radicals exceeds the degenerating capacity of cellular superoxide dismutase, and radicals accumulate in the cell, leading to cell injury or even death. Baron et al. (Baron and Rowe, 1981) questioned this hypothesis when it was observed that there is no correlation between the level of dismutase activity and resistance

toward pyocyanin. Instead, it was suggested that the pyocyanin radical was further stabilized by complexation with divalent metal cations in the physiological media, like $Mg^{2+}$. The zwitterionic properties of this complex would allow passage over cell membranes. When inside the cell, the phenazine radical can accept an electron and thereby interrupt electron transport and respiratory flow in the cell, which is essential for membrane-bound metabolic processes that require energy, such as the active transport. Therefore, the function of pyocyanin is not entirely dependent on the presense of molecular oxygen. In addition to their redox activity, phenazines are shown to possess polynucleotide intercalation, topoisomerase inhibition, and charge transfer abilities as well (Laursen *et al.*, 2004). Recently, pyocyanin has been shown to have other functions. It is a terminal signaling molecule for the expression of some quorum sensing controlled genes such as the *mexGHI-ompD* efflux pump and a putative mono-oxygenase PA2274 (Dietrich et al., 2006). It can alter redox homeostasis and carbon flux through central metabolic pathways (Price-Whelan et al., 2007) and activates superoxide stress response transcription regulater SoxR (Dietrich et al., 2008).

Despite the yet incomplete understanding of their physiological functions, pathogen mutants that are deficient in making phenazines exhibit attenuated virulence (Lau et al., 2004a). Besides, this class of chemically interesting compounds has also drawn attention to aspects of application. For example, the electron carrier property of pyocyanin could be utilized to make microbial fuel cells (http://parts.mit.edu/igem07/index.php/Glasgow/Plan).

### 1.5.1 Genetics of phenazine biosynthesis

Phenazine biosynthesis was first studied in the fluorescent *Pseudomonas* species. Mutants of *Pseudomonas aeruginosa*, selected by observed visual differences in coloration from the wild-type strain, were examined for altered patterns of phenazine synthesis. Three classes of mutants that were incapable of pyocyanin production were identified. Pigmentation patterns that were found to characterize the various mutant classes implicated precursor-product relationships, and a draft of a biochemical scheme covering the terminal reactions of pyocyanin biosynthesis was proposed (Byng et al., 1979).

According to this scheme, a cluster of seven genes (phzA–phzG) cloned from *P. fluorescens* 2-79 by Mavrodi et al. (Mavrodi et al., 1998) was found to be sufficient for PCA (Phenazine-1-carboxylic acid) production. As PCA serves as the common precursor for many different species-specific phenazines (Mavrodi et al., 2001;Chin et al., 2001;Delaney

et al., 2001), further investigations were carried out in various research groups. Timms-Wilson et al. (Timms-Wilson et al., 2000) used this gene cluster to transform *P. fluorescens* SBW25 into a PCA producer, enhancing the ability of this bacterium to reduce damping-off disease in pea seedlings caused by *Pythium ultimum* . This study proved that the use of the *phz* gene cluster is a tool to modify biological control strains. The *phz* gene cluster was subsequently detected in other fluorescent pseudomonads like *Pseudomonas aeruginosa*, *P. aureofaciens*, *P. chlororaphis* and *P. fluorescens* but initially not in phenazine producing isolates of *Burkholderia cepacia*, *Burkholderia phenazinium* or *Brevibacterium iodinum* (Mavrodi *et al.*, 2001). However, new data from recently sequenced microbial genomes have provided insight into the phenazine biosynthesis operons of *B. cepacia*, *Erwinia carotovora* subsp. *atroseptica*, *P. agglomerans*, and notably, the first Gram-positive bacterium, *Brevibacterium lingens*. Collectively, the data suggest that phenazine biosynthesis requires five genes encoding the proteins PhzA, PhzD, PhzE, PhzF, and PhzG (*P. fluorescens* nomenclature), with the *phzA* gene duplicated as *phzB* in *Pseudomonads*. Most gene clusters also encode a 3-deoxy-D-arabino-heptulosonate-7-phosphate (DAHP) synthase, PhzC, which catalyzes the first step of the shikimate pathway and acts to redirect intermediates from primary metabolism into phenazine biosynthesis (Figure 1.10) (Mavrodi et al., 2006).

An alternative mechanism was considered for the synthesis of PDC (Phenazine dicarboxylic acid) by *Streptomyces spp*. (Vantland et al., 1993;McDonald et al., 1999). PDC appears to be another common precursor that is modified further to create more complex phenazines in bacteria like *Streptomyces spp*. and *P. agglomerans* (Messenger and Turner, 1978;Vantland *et al.*, 1993;McDonald *et al.*, 1999).

The phenazine-producing *Pseudomonas* typically produces two or more phenazines, with the exception of *P. fluorescens* that produces only the yellow PCA compound. *P. aeruginosa* produces the characteristic bluish green phenazine pigment pyocyanin (5-N-methyl-1-hydroxyphenazine, PYO), together with PCA, 1-hydroxyphenazine, phenazine-1-carboxyamide, and two heavily modified phenazine derivatives aeruginosin A and B (Herbert and Holliman, 1969;Holliman, 1969;Flood et al., 1972;Byng *et al.*, 1979;Hassan and Fridovich, 1980).

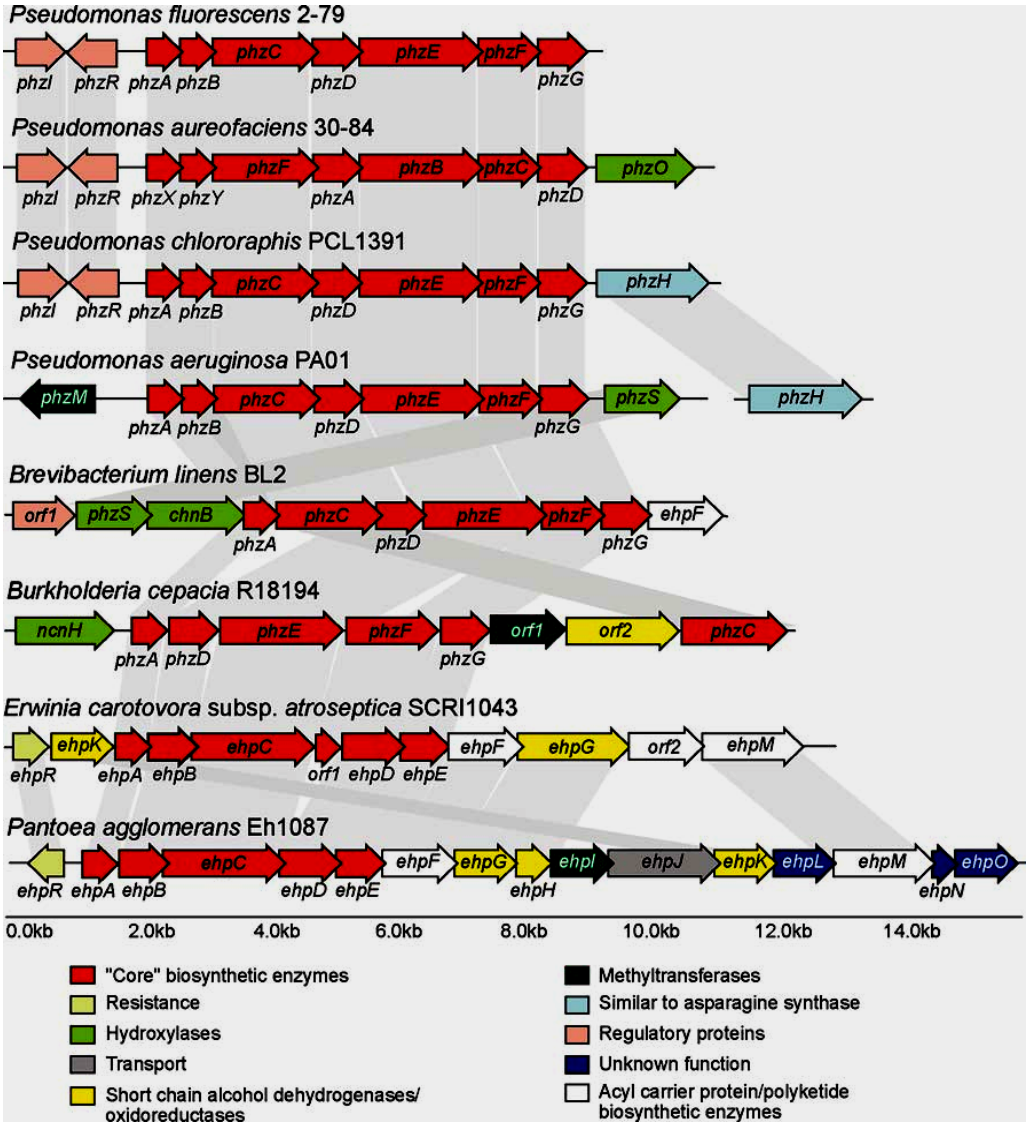


**Figure 1.10: Comparison of new phenazine biosynthetic loci from Br. linens BL2, *B. cepacia* R18194, and *E. carotovora* subsp. *atroseptica* SCRI1043 with those from *P. fluorescens* 2-79, *P. aureofaciens* 30-84, *P. aeruginosa* PAO1, and *P. agglomerans* Eh1087. Genes of similar function are connected with gray lines.**

The exact molecular pathways of synthesizing these phenazine derivatives are not yet clear. *P. aeruginosa* has in fact two *phz* operons, each encoding a set of PhzA-G enzymes and each sufficient to produce PCA. The biological rationale for this duplicity is not well understood. However, they are not totally identical. One *phz* operon has two neighboring genes, *phzM* and *phzS*. They are required to modify PCA to PYO. Given the importance of phenazines in the life span of this bacterium, it is possible that *P. aeruginosa* encodes two sets of PCA synthetic enzymes to achieve a high level of regulation.

### 1.5.2 Chemistry of phenazine biosynthesis

Studies in the early 1970s using radioactively labeled compounds added to bacterial cultures revealed that phenazine biosynthesis branched from the shikimic acid pathway as reviewed in (Turner *et al.*, 1986). Chorismic acid was identified as the branchpoint to phenazine synthesis (Longley et al., 1972), with the phenazine nucleus formed by the symmetrical condensation of two chorismate molecules (Hollstein and McCamey, 1973) and the amide nitrogen of glutamine serving as the immediate source of nitrogen in the heterocyclic nucleus (Galbraith et al., 2004).

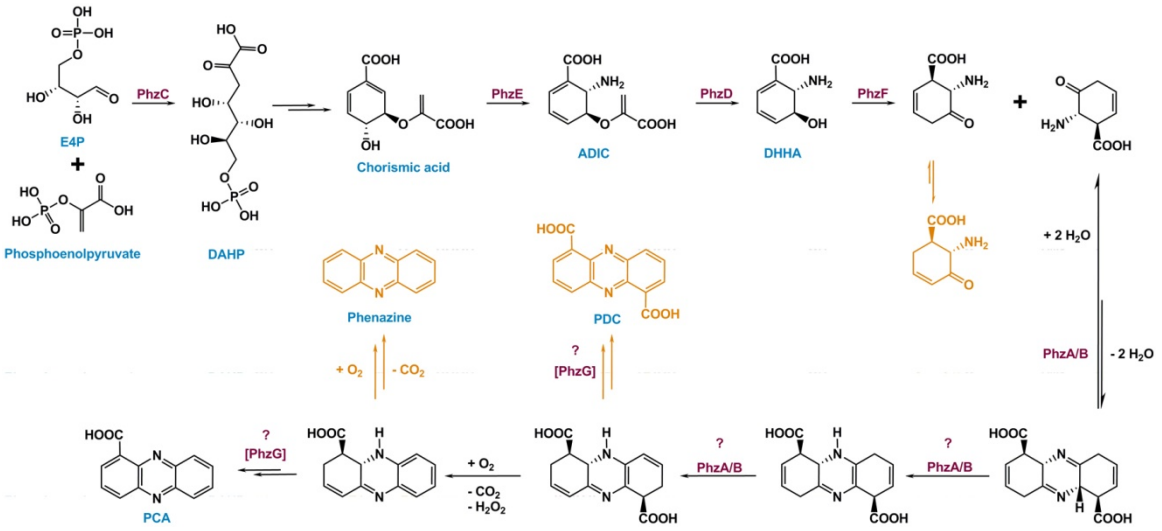


**Figure 1.11: Biosynthesis of phenazine-1-carboxylic acid (PCA). Phz enzymes are shown in purple. By-products are colored in orange. Question marks indicate unclear mechanisms.**

The model proposed by Mavrodi et al. (Mavrodi *et al.*, 1998) for the synthesis of the phenazine nucleus by the PhzA-G proteins was recently improved by biochemical and crystallographic studies of Ahuja et al. (Ahuja et al., 2008), Blankenfeldt et al. (Blankenfeldt et al., 2004) and Parsons et al. (Parsons et al., 2004). The current understanding of phenazine biosynthesis is summarized in Figure 1.11.

## 1.6 PHENAZINE RESISTANCE, EHPR AND PA0803

Many bacteria possess hydrolytic enzymes to neutralize lethal compounds into less harmful forms. β-lactamases are good examples of one class of these enzymes. They catalyze the hydrolysis of the lactam bond of β-lactam antibiotics and thus provide a major resistance mechanism to compounds like penicillin and cephalosporins. However, it is energetically counter-productive for antibiotic-producing bacteria to adopt such a strategy, especially given the fact that antibiotic production is usually under tight regulation. Therefore, in many antibiotic-producing bacteria, a "binding protein" is encoded as a key component of the self-protection system, which is believed to isolate the antibiotic before it leaves the cell and thus keeps the organism safe. Examples of such "binding proteins" include the BLMA/BLMT protein from *Streptomyces verticillu*s, which produces bleomycin (Kawano et al., 2000;Maruyama et al., 2001;Sugiyama et al., 2002) and the MRD protein from *Streptomyces lavendulae*, which produces Mitomycin C (Sheldon et al., 1997;Sheldon et al., 1999;Martin et al., 2002).

In a project carried out prior to this study, a phenazine resistance gene *ehpR* from *Pantoea agglomerans* (previously named *Erwinia herbicola*), which produces the phenazine antibiotic D-alanyl-grieseoluteic acid (AGA), was studied. *ehpR* was demonstrated to be responsible for phenazine resistance, since a plasmid carrying this gene conferred AGA resistance to other species and disruption of *ehpR* by transposon insertion in the plasmid abolished this function (Giddens et al., 2002). The Eh1087 strain is unlikely to possess another self-protection strategy from AGA because the removal of *ehpR* during the creation of EhΔAGA mutant resulted in a strain with AGA sensitivity similar to *E.coli*. EhΔAGA and *E.coli* can be transformed to be AGA-resistant by a plasmid encoding *ehpR*. Additionally, cells of EhΔAGA harbouring a plasmid with genes that can convert exogenously supplied non-toxic precursor grieseoluteic acid (GA, Figure 1.8) into toxic AGA is not viable, indicating sensitivity to AGA (Giddens *et al.*, 2002). It has been reported that both Eh1087 and EhΔAGA have similar, albeit low, sensitivity to PCA, suggesting that EhpR-mediated resistance does not protect *P. agglomerans* against all phenazine antibiotics.

Structural and functional evidence that the gene product indeed is a phenazine binding-protein were obtained. Despite low affinity between the protein and the ligand precursor, the structure of EhpR in complex with GA was determined at 1.0 Å resolution, providing insights to its mechanism (Figure 1.12). This demonstrated that phenazine

producing microorganism may utilize the binding-protein strategy to protect themselves against the toxic action of self-synthesized phenazines.

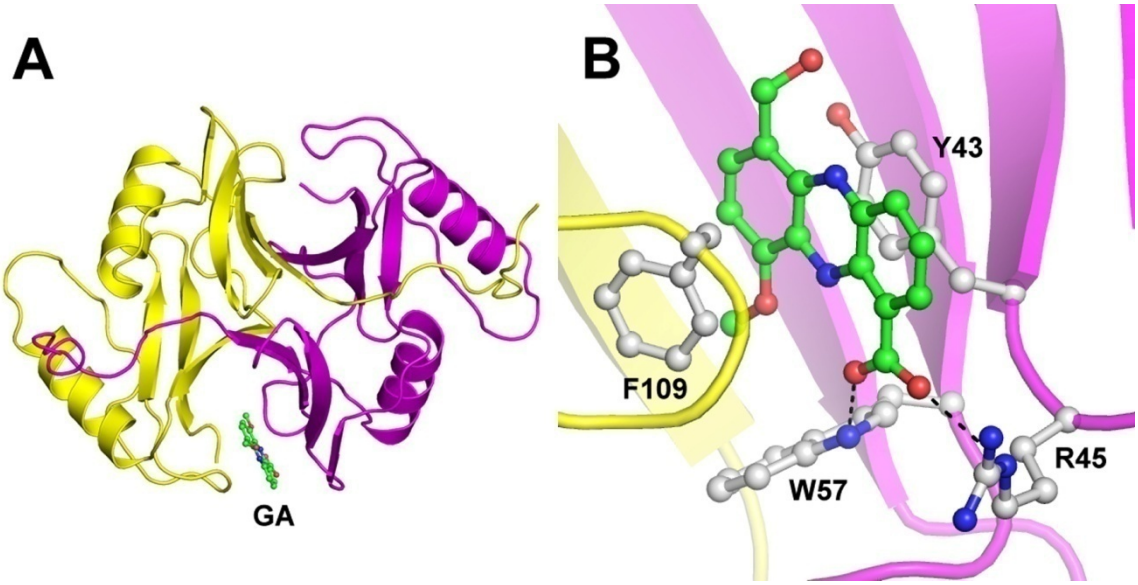


**Figure 1.12: Phenazine resistance mediated by EhpR. A) Cartoon presentation showing the topology of the EhpR-GA complex. Protein colored by chain. The GA molecule, shown as ball-and-stick, colored by atom with C atoms in green, is sequestered in a binding site formed at the dimer interface. B) Detailed view of the binding site. Side chains of key protein residues shown as ball-and-stick, colored by atom with C atoms in white. The GA molecule is sandwiched between Y43 and F109 via π–stacking interaction. Black dashes show the two key hydrogen bond: one between NE1 atom of Trp57 and O16 atom of the carboxyl group of GA; the other between NE atom of R42 and O17 atom of the carboxyl group of GA.**

Surprisingly, only few data are available on the topic of pyocyanin resistance in *Pseudomonas aeruginosa*, although this is one critical issue for this bacterium. It has been reported that in *P. aeruginosa*, superoxide dismutases (SOD) play a key role in the resistance mechanism by neutralizing the reactive oxygen species raised by pyocyanin. Intracellular superoxide and/or hydrogen peroxide production was observed to be 50-fold less in *P. aeruginosa* treated by exogeneous supplement of pyocyanin than in *E. coli*, and activity of SODs increased when pyocyanin was produced (Hassett et al., 1992). Mutants defective in an iron-cofactored SOD, *ΔsodB*, were found to produce no pyocyanin (Hassett et al., 1995).

However, at the time when these experiments were carried out, quorum sensing had not been well studied. The same author found out a few years later that the expression of SODs and catalases are under QS control (Hassett et al., 1999). Hence it might be meaningful to revisit these reports and interpret the results in the context of more recent findings. For example, the 1995 report demonstrate clearly that Fe-SOD is required for

optimum pyocyanin production. But since *P. aeruginosa* is a bacterial species very sensitive to environmental conditions, a mutant strain that is weak in handling oxidative stress might result in a dramatic change in its transcription profile, which was never monitored. The reduction in pyocyanin production might also be an indirect result of this gene deletion. In addition, it is not surprising that SOD activity will surge upon exogenous supply of pyocyanin, since these enzymes are known to function as a response to oxidative stress. In fact, in a similar experiment, *P. aeruginosa* showed less sensitivity than *E. coli* upon exposure to other redox-active compounds (paraquat, streptonigrin, and plumbagin) as well (Hassett *et al.*, 1992). It is therefore sensible to assume that the SODs, especially Fe-SOD, serve as a general, non-specific safety-net for phenazine resistance. There might be a counterpart of *ehpR* in the *P. aeruginosa* genome acting in concert with the SODs, which provides self-protection to the bacterium that is specific for pyocyanin.

A BLAST search with the EhpR sequence against the genome of *Pseudonomas aeruginosa* PAO1 shows that a 146-amino-acid protein encoded by gene PA0803 possesses highest homology to EhpR. Despite the fact that alignment of EhpR and the PA0803 gene product did not show very high sequence similarity and the binding residues of EhpR are not conserved in PA0803, the PA0803 protein is predicted to have the same fold as EhpR. Considering that the active phenazine compound is different, a potential pyocyanin binding protein may utilize a different set of residues at the active site. Therefore, structure and function of PA0803 should be determined to testify the hypothesis.

# 2 AIMS OF THIS STUDY

*Pseudomonas aeruginosa* is an opportunistic human pathogen that still respresents one of the leading causes of death in immunocompromised patients. It synthesizes an arsenal of virulence factors, notably the phenazine derivative pyocyanin. The physiological roles that pyocyanin plays seem to be complex: apart from being a major virulence factor in pathogenesis, it is also a signal molecule and an antibiotic.

Previous genetic studies on quinolone signaling in *P. aeruginosa* have identified the *pqsE* gene prerequisite for the biosynthesis of many virulence factors including pyocyanin. However, the molecular functions of PqsE remain unknown. The main aim of the first topic reported in this thesis is to identify the *in vitro* function of PqsE, in order to understand how PqsE links the presence of the PQS signal to the expression of downstream genes.

Pyocyanin has antibiotic activity. Nevertheless, *P. aeruginosa* is not affected by self-produced pyocyanin. The molecular mechanism for this protection is not well understood to date. In the *P. aeruginosa* genome, a lot of genes are not yet studied and are annotated as “hypothetical proteins”. One of them is predicted to have the fold of a known phenazine binding protein, EhpR. The second topic of this work represents a pioneering study searching for a phenazine-binding protein in the cytosol of *P. aeruginosa*. It aims at verifying whether this hypothetical protein PA0803 indeed can bind pyocyanin.

In order to shed light onto the molecular functions of PqsE and PA0803, these two proteins were cloned, expressed, purified and characterized *in vitro* via a broad spectrum of biochemical/biophysical techniques. High resolution structures of both proteins with and without a ligand/substrate were obtained by X-ray crystallography. In the course of this work, novel assays were developed or adapted to overcome the challenge of probing unknown protein functions.

# 3 PRINCIPLES OF X-RAY CRYSTALLOGRAPHY

## 3.1 CONCEPTS

Observation is one of the most important methods for scientists to study biological system. Virtually no significant discovery could be made without observation. Many phenomenons, like change of color, can be inspected directly by eye. Nevertheless, for smaller objects like the shape of a cell, the human eye is insufficient. Therefore, optical systems, like microscopes, are widely used to observe small objects.

The principle of the microscope lies on the usage of optical lens, which can refract rays of light that travel perpendicular to the lens to pass a particular point (focus, F and F', Figure 3.1), and can turn rays that travel via the focus to a parallel beam. Therefore, rays that are emitted from, e.g., point A will meet again at point A'. When captured by eyes, they would lead the observer to see an "image" of A at the position of A'. With proper usage of lens and positioning, an object can be magnified, enabling the observer to see it.

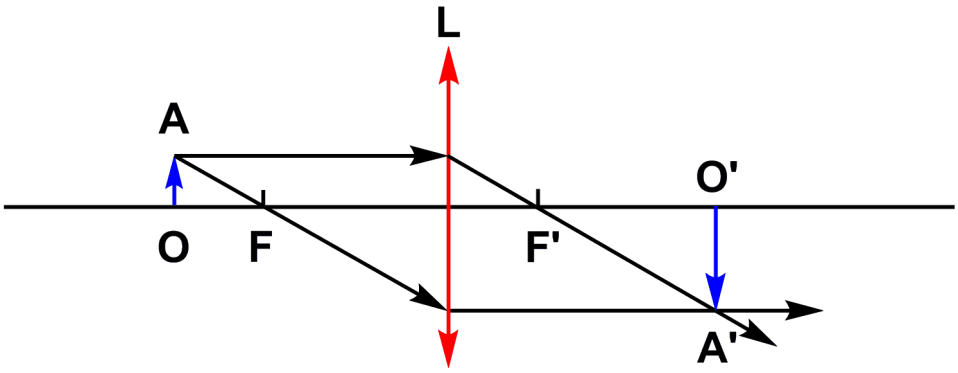


**Figure 3.1: Principle of image formation. L: lens; OA: object; O'A': image; black arrows: light rays; F and F': focus of the lens.**

Simply seeing the object is sometimes not enough, because discoveries often rely on observing the details of the objects. However, there are physical limits of the optical systems so that the examination of details can only reach certain extend, due to the intrinsic properties of the two indispensible requirements for observation: light and the lens. This is termed "resolution", which can be roughly defined to be the smallest spacing distance in the specimen that a microscope is able to distinguish. Contrary to common mis-perception, resolution is independent from magnification, because further magnification does not bring

additional details to the image created by the objective lens. As Ernst Abbe first described in 1873, because of the wave nature of the lights, the resolution of a microscope is determined by the wavelength of the light (λ), refractive index of the lens medium (n), and the aperture half angle (α), as show by Equation 1 below, where NA stands for the numerical aperture of the lens.

$$R = \frac{\lambda}{2n\sin\alpha} = \frac{\lambda}{2NA} \tag{1}$$

Typically, the light that human eyes can perceive falls in the range of λ=400-700 nm, and the finest grade lens have NA around 1.4. Therefore, the resolution limit of human eyes, which is in essence similar optical systems that focus the lights on retina, is about 0.2 μm. This is the same for all optical microscopes using visible light.

Modern biology requires understanding of biological systems on the molecular level. It is therefore desired by scientists to visualize, e.g., chemical bonds that fall in the range of a few angstroms. However, despite recent development in fluorescent microscopy using the stimulated emission depletion (STED) method fundamentally increased the resolution of microscopic systems further to below 100 nm (Klar et al., 2000), it is still a few orders of magnitude beyond the size of atoms and chemical bonds. Therefore an electronmagnetic wave with significantly shorter wavelength is needed to illuminate molecules. The required wavelength range falls to that of X-rays (λ=0.1 – 100 Å). The most typical source of X-rays used in protein crystallography today is the 1.54 Å Kα-Cu X-ray, emitted by an L-shell electron of copper atom replacing a displaced K-shell electron. Modern synchrotrons offer possibilities to utilize X-rays of fine-tunable X-rays, typically around 1 Å. With electronmagnetic waves of this wavelength, it is theoretically possible to resolve sub-angstrom resolution details.

However, there are two inherent problems using X-rays as the illumination source. First is the lack of X-ray refracting lenses. Fortunately, X-ray beams can be recorded directly with films or modern electronic detectors. If the origin of the refracted X-rays is known, directions of the rays can be calculated and their intensity measured. Therefore, the lens problem can be overcome by placing the specimen between a source and a detector, measuring diffracted X-rays, and subsequently calculating an image as if the rays are focused by a lens. The second problem is that single molecules diffract X-rays very weakly. It is therefore necessary to arrange the molecules to regular arrays, crystals to be pricise, and

utilize the interference phenomenon to enhance the intensity to a detectable scale. Generally speaking, protein crystallography is a method that uses an X-ray beam to illuminate a protein crystal, thereby construct an atomic-resolution 3D image of proteins.

It is therefore necessary for a crystallographer to (1) generate high-quality protein crystals from purified protein, (2) collect X-ray data and (3) compute the image of the protein molecule. Principles of these processes are explained in the following sections.

## 3.2 INTERFERENCE OF WAVES

As decribed in the previous section, a high-resolution image of a molecule is not directly obtainable with current technology, therefore an image has to be calculated from an intereference pattern. Undertanding of interference is therefore critical for crystallography and will be briefly reviewed in this section.

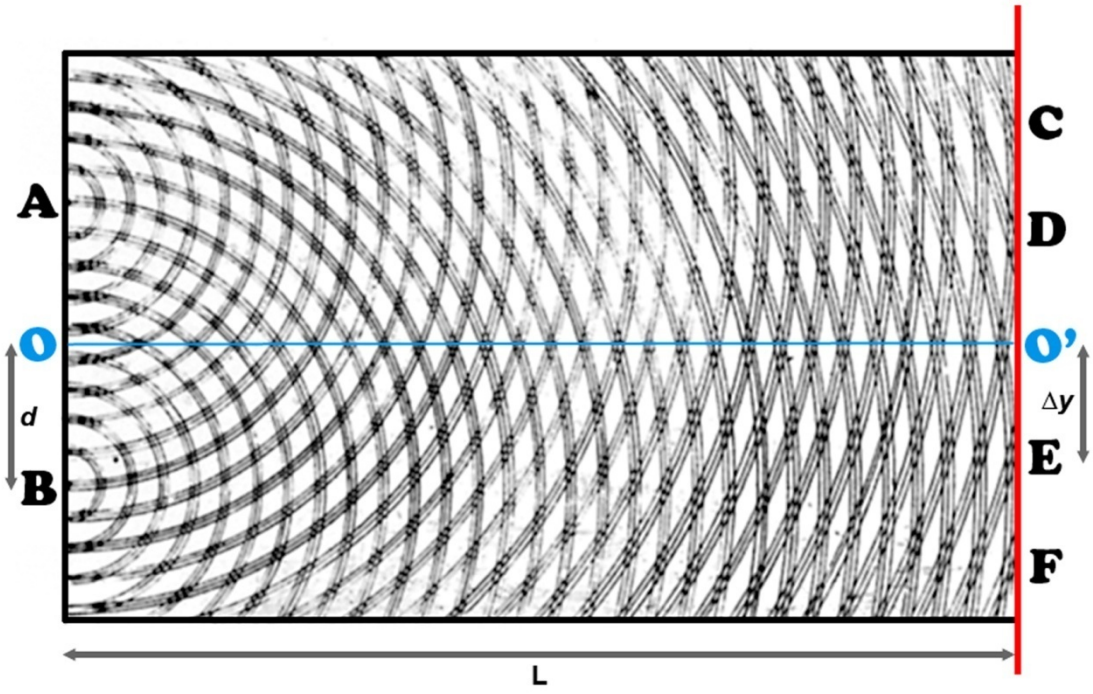


**Figure 3.2: The double-slit experiment by Thomas Young. Red bar: screen; A and B: two slits (AB is parallel to the screen); O: center of AB; line O-O' is perpendicular to AB. Constructive interference result in light bands at position C, D, E and F; while at O', because O'A = O'B, the interference is also constructive and therefore gives a bright band. Figure based on modification of Young's sketch.**

In physics, interference is the addition of two or more waves that result in a new wave pattern. In most cases, it refers to the interaction between correlated waves that come from the same source or share the same frequency. In crystallography, the nature of the wave is in most cases single wavelength X-rays, although modern techniques can sometimes decipher patterns from a non-monochromatic source. When two correlated waves exist in space, they add up constructively (in phase interference) at some points while cancel each other (out of phase interference) at some other points, thereby forming a stable interference pattern. In contrast to visible light, where the interference may be inspected by eye, X-rays have to be recorded by special detectors.

Interference is first observed experimentally in the laboratory of Thomas Young, using a double-slit set up (Figure 3.2), where a coherent light source illuminates a thin plate with two parallel slits A and B, and the light passing through the slits strikes a screen behind them, creating an interference pattern of bright and dark bands on the screen. It was proven that the position where the bright bands occur can be approximated by the equation

$$\frac{n\lambda}{d} = \frac{y}{L} \tag{2}$$

In Equation 2, λ is the wavelength of the light; d is the distance between slits A and B; L is the distance between slit AB and the screen; n is an integer; y is the position of the center of the light band on the screen. Rearrange of Equation 2 leads to

$$y = \frac{n\lambda L}{d} \tag{3}$$

Equation 3 reveals that when λ and L are known, the mathematical relationship between y and d are reciprocal. Defining $\Delta y = y_{n+1} - y_n$, Equation 3 can be rearranged to

$$d = \frac{\lambda L}{\Delta y} \tag{4}$$

Because the physical meaning of Δy are the distance between adjacent bright bands, it can be inferred from formula 4 that when λ, L (e.g., |OO'| in Figure 3.2) are known and Δy (|O'D| in Figure 3.2) can be measured, d, the distance between A and B can be solved. This is in fact a one dimensional example of using interference pattern to resolve a smaller distance d (|AB| in Figure 3.2).

## 3.3 CRYSTALIZATION OF PROTEINS

The crystal is one type of the solid states of matter, in which molecules are packed in a regular three-dimensional array. Therefore, a crystal can be used as a set of 3D slits that result in interference of X-ray beam.

Unfortunately, however, the mechanism of crystal formation is not yet fully understood. Therefore although there are principles to follow, crystallization of proteins remains an empirical process. It is only known that to obtain diffraction quality crystals, kinetic parameters have to be manipulated, so that the solution of a purified protein is slowly concentrated to super-saturation to allow nucleation of crystals (Figure 3.3A, purple zone). Then, because of nucleation, the concentration drops slightly to a zone in which nucleation does not continue but the existing crystallines are able to grow (Figure 3.3A, green zone).

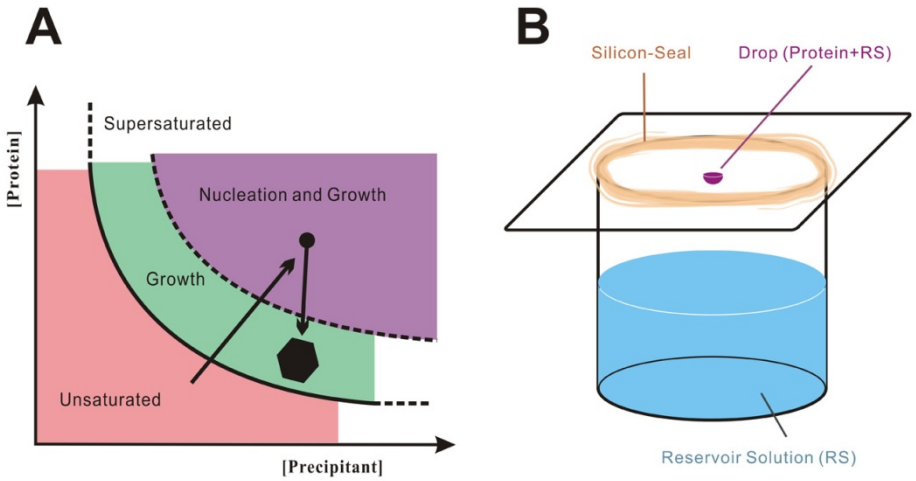


**Figure 3.3: A) Phase diagram of a typical protein solution. B) Scheme of the hanging-drop vapour diffusion crystallization method.**

Experimentally, crystallization is usually carried out with the vapour diffusion method. In brief, a solution containing hydrophilic precipitants is prepared and put in a reservoir such as a well in a cell-culture plate. Then the protein solution is mixed with this reservoir solution into a drop that is sealed, either hanging or sitting on a solid support, to the same well as the reservoir solution (Figure 3.3B). Because the reservoir solution has higher percentage of precipitant, solvent water is slowly drawn away from the drop via vapour diffusion in this enclosed system. In this way the protein is slowly concentrated and is hoped to fall out of solution in the form of crystals instead of amorphous precipitation.

Given the empirical nature of this set up and the fact that proteins are different in their properties, it is usually necessary to try many different conditions simultaneously to obtain a proper crystallization protocol, which is usually carried out at the beginning as high-throughput screening.

## 3.4 REFLECTIONS AND THE CRYSTAL CELL

### 3.4.1 Bragg's Law in real space

When X-rays hit atoms, the wave is scattered by the electron cloud of the atom. The resulting radiation has the same frequency (wavelength) but a shifted phase. Therefore, when a beam of X-ray waves hits an array of atoms, interference of scattered rays will occur and the pattern contains information on the atomic array. Reducing the shapes of the molecules to a point in space, the crystal structure can be reduced to a lattice and the scattered rays can be reduced to rays as if reflected by lattice planes. The mathematical relationship between constructive interference and lattice planes is termed Bragg's law (Figure 3.4 and Equation 5).

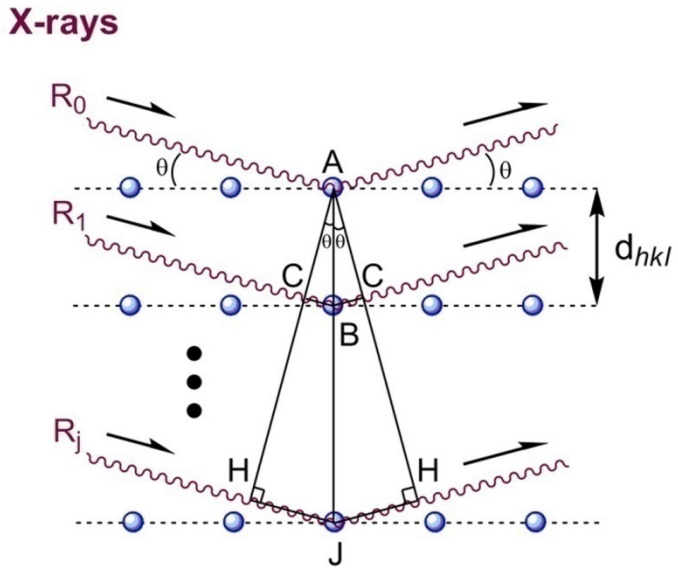


**Figure 3.4: Elastic scattering of X-rays by real space lattice.**

As shown in Figure 3.4, suppose a beam of x-rays hits planes of atoms and was reflected elastically, the difference between ray $R_1$ and $R_0$ would be 2 × BC, and since BC = AB × sinθ = $d_{hkl}$ × sinθ. The interference is only constructive when the difference of light paths is multiples of the wavelength λ (or, the phase shift is a multiple of 2π, Equation 5).

$$2d \sin\theta = n\lambda \tag{5}$$

If this equation is not satisfied, for example

$$2d \sin\theta = (n + k)\lambda \tag{6}$$

where n remains an integer, k is a fraction and 0< k < 1, there is always a plane J in the lattice, that j × k = m + ½ (m is an integer). Thereby the difference between ray $R_j$ and $R_0$, 2 × JH, satisfy equation

$$2jd \sin\theta = (jn + m + \frac{1}{2})\lambda \tag{8}$$

which means that the phase difference between $R_j$ and $R_0$ is π; and the two rays will cancel each other.

### 3.4.2 Construction of reciprocal space

Once high quality crystals of a protein can be obtained, structure determination can be carried out by shining X-rays onto the crystal. At a particular distance, some diffracted rays will add-up constructively while others will cancel each other, and thus a measurable interference pattern can be recorded using X-ray film or modern electronic detectors. The pattern contains information about 1) the lattice, or in other words the manner how molecules are packed in the crystal and 2) the shape of the diffracting matter, which is the electron envelope of the protein in this case, within a crystal cell. The second is exactly the information required to visualize the protein molecule. The packing of molecules is also critical because correct interpretation of the interference pattern relies on understanding the lattice.

Therefore, the first step is to obtain parameters describing the lattice or “unit cells” of the crystal. However, as shown in equation 4, the relationship between the lattice distance d and pattern spacing Δy is reciprocal. Besides, three dimensional cases (such as crystals), the pattern is no more bars but spots. Calculations hence can be greatly simplified

by introducing a system called "reciprocal space", which is in essence the space that the interference spots are in.

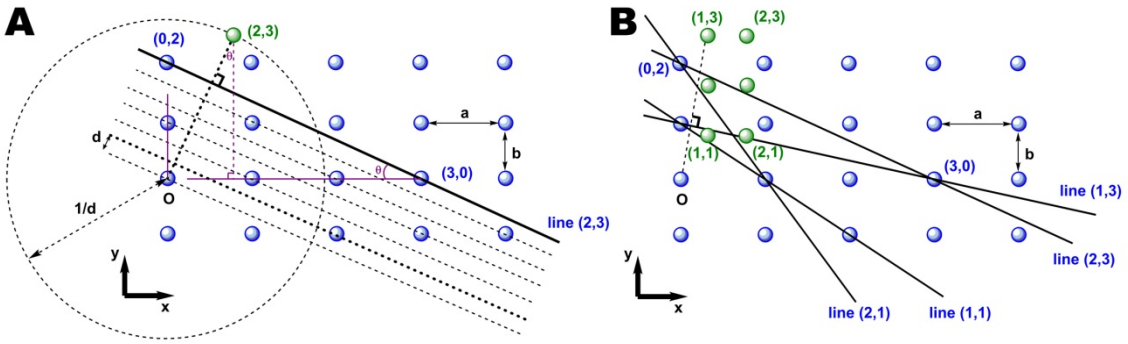


**Figure 3.5: Construction of the reciprocal lattice.**

Figure 3.5 is a simplified, two-dimensional illustration how reciprocal lattice is constructed from real lattice (can be also considered to be a plane in a 3D lattice with z = 0). The origin point O is arbitrarily selected in the real-space lattice and the lattice points can be given an index such as (0, 1), (1, 0) or (1, 1) etc to describe their relative position referring to the origin. Supposing the distances between lattice points in the x-direction is **a**, and in the y-direction **b**, then each indexed lattice point (i, j) will have a coordinate (i**a**, j**b**). Defining line series (h, k) as parallel lines that divide **a** into h equal parts and divide **b** into k equal parts, apparently one of these lines will pass (0, h) and (k, 0), which is shown in Figure 3.5 to represent the series of lines. By definition, another line in this series is the one that pass (1/h, 0) and (0, 1/k). It is also obvious that in each different series, there is always one line that passes the origin point O. Therefore the distance from origin O to line (1/h, 0) and (0, 1/k) is exactly the distance **d** between this series of parallel lines. The value of **d** equals **b**cosθ/k or **a**sinθ/h, where θ is the angle between line (h, k) and the x-axis. Now if a line normal to line (h, k) is drawn from the origin, then points on this new line will have the coordinates (**D**sinθ, **D**cosθ), where **D** is the distance of this point to origin O. Apparently when **D** = 1/**d**, the point will have coordinate (h/**a,** k/**b**). Because **a** and **b** are constants, points (h/**a**, k/**b**) composite a new array depending on combination of h and k.

In this way, a new lattice is created shown in Figure 3.5 as green points. Because the distances between these new lattice points are 1/a in the x-direction and 1/b in the y direction, this new lattice is termed the reciprocal lattice. This construction can be also

applied to three dimensional spaces, where planes instead of lines are given indices (h, k, l). As a consequence, the reciprocal lattice obtained after this construction is also a 3D object in a space termed the reciprocal space.

### 3.4.3 Bragg's Law in reciprocal space

As described in section 3.4.1, for constructive interference to occur, the relationship of the experimental system much satisfy Equation 5, the Bragg's law. Figure 3.6 shows how calculation of the lattice parameters can be simplified by utilizing reciprocal space concepts, usually referred to as "Ewald construction". Suppose X-ray $R_0$ passes an arbitrarily selected lattice point O in the crystal. A circle intersecting $R_0$ at point O, with its center C located on line $R_0$ and its radius equals $1/\lambda$ can be drawn (Figure 3.6A). Defining the other intersection as point B, if a reciprocal lattice point P with index (h, k) falls on this circle, then OP and BP are normal. By definition of the reciprocal lattice, $OP = 1/d_{hk}$, and OP is normal to line (h, k) in the real space lattice. Therefore, BP is parallel to line series (h, k) in real space. Defining the angle between BP and BO as θ, then

$$\sin\theta = \frac{BP}{BO} = \frac{1/d_{hk}}{2/\lambda} = \frac{\lambda}{2d_{hk}} \tag{9}$$

which can be rearranged to

$$2d\sin\theta = \lambda \tag{10}$$

Bragg's law is satisfied, so constructive interference will occur, giving reflected ray $R_p$, whose direction is exactly the same as CP. Extending the same principle to the three-dimensional situation, it can be proven that when reciprocal lattice point P(h, k, l) falls on the surface of the sphere C (called "Ewald sphere"), a constructive interference wave $R_p$, also called reflection (h,k,l), is produced as ray $R_0$ reflected by atomic plane (h, k, l) in real space.

By rotating the crystal, thereby both the real space and reciprocal space lattices, virtually all reciprocal lattice points can fall on sphere C, producing a series of reflected rays. When a detector is placed in the system as in Figure 3.6B, each reflected ray $R_p$ results in a spot (D) on the detector. Since the direction of $R_0$ (AO), the wavelength (λ, and $\lambda=1/OC=1/BC$), as well as the crystal-detector distance (AC) is known, direction and length of OP (therefore $d_{hk}$) can be derived by measuring the direction and length of AD.

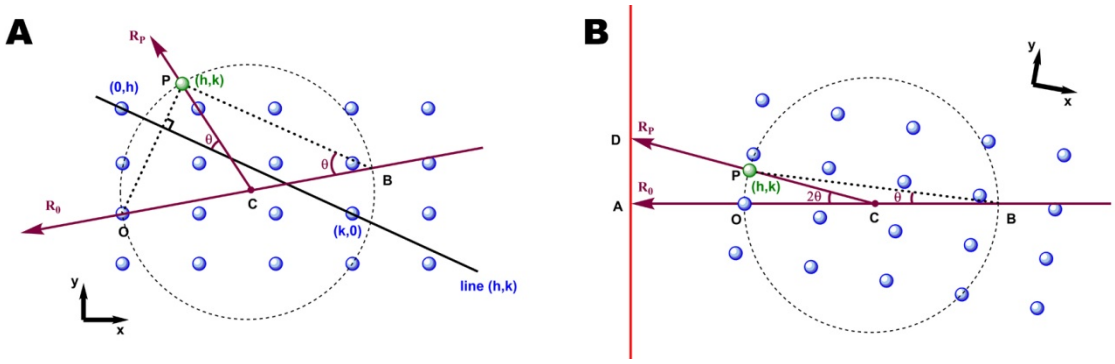


**Figure 3.6: A)Bragg's law in reciprocal space. B) Relationship beween X-ray measurement and the crystal lattice.**

In three dimensional cases the mathematical relationship is more complicated, but the same principles apply. In fact it can be proven that for orthogonal unit cells,

$$d_{100} = \frac{D\lambda}{L_{100}} \tag{11}$$

where λ is the x-ray wavelength, D is the crystal detector distance and L100 is the distance between detector origin and the (1,0,0) reflection. With the knowledge of the reciprocal lattice the parameters of real space lattice can be calculated.

## 3.5 ELECTRON DENSITY AND REFLECTIONS

What crystallography tries to determine is an image, to be more precise a description, of electron distribution in the crytal. Because the crystal is a three dimensional repetition of small unit cells, the overall electron distribution is a repetition of the electron envelope within one unit cell. This means, the electron distribution can be described by a three-dimensional periodic function ρ(x, y, z).

It has been proven that any complicated periodic function can be approximated by a sum of a series of simple trigonometric functions, in the form of

$$f(x) = \sum_{h=0}^{n} F_h \cos 2\pi(hx + \alpha_h) \tag{12}$$

where the basic wave function is cos2π(hx+α). One particularly useful basic function is [cos2π(hx)+ isin2π(hx)]. Calculations that relate real space and reciprocal space

could be greatly simplified by using this function as the basic periodic function. Equation 12 then becomes

$$f(x) = \sum_h F_h \left[\cos 2\pi(hx) + i \sin 2\pi(hx)\right] \tag{13}$$

Euler has proven that

$$\cos\theta + i\sin\theta = e^{i\theta} \tag{14}$$

then Equation 13 can be arranged to

$$f(x) = \sum_h F_h e^{2\pi i(hx)} \tag{15}$$

The same principle applies also to three-dimensional cases, so any 3-D periodic function

$$f(x,y,z) = \sum_h \sum_k \sum_l F_{hkl} e^{2\pi i(hx+ky+lz)} \tag{16}$$

Fourier has proven that for any function f(x,y,z), there exists a function F(h,k,l) that

$$F(h,k,l) = \int_x \int_y \int_z f(x,y,z) e^{2\pi i(hx+ky+lz)} dxdydz \tag{17}$$

and

$$f(x,y,z) = \int_h \int_k \int_l F(h,k,l) e^{-2\pi i(hx+ky+lz)} dhdkdl \tag{18}$$

where h,k,l have units reciprocal to those of x,y and z. So this operation, termed Fourier transformation, is a natural choice for relating real space and reciprocal space. When applied to this case, the variables bear physical meanings. Let x, y and z describe real-space coordinates within the crystal, then h, k, l are frequencies in x, y, z direction, respectively. In section 3.4 (Figure 3.5), it has been shown that the plane series that divides **a** (in x direction) into **n** parts (or, cutting the x-axis **n** times, exactly a frequency) will have reciprocal lattice index (**n**, k, l). Therefore, h, k, l are exactly variables represented by the reciprocal lattice indices. Since the data obtained in crystallography (a set of "reflections") can be expressed as a set of values defined by indices h, k and l, Fourier transformation makes the link between crystallographic data and the electron density function. However, since h, k, l are integers that represent the indices of discrete reflections, so the relationship is in fact a sum instead of an integral

$$\rho(x,y,z) = \frac{1}{V} \sum_h \sum_k \sum_l F_{hkl} e^{-2\pi i(hx+ky+lz)} \tag{19}$$

where V is the volume of unit cell, and $F_{hkl}$, termed a structure factor, is the function that describes reflection (h, k, l).

## 3.6 PHASING

Equation 19 shows how to obtain the electron density function from crystallographic data. However, there is one last practical problem remaining. $F_{hkl}$ is the function that describes reflection (h, k, l), which by nature is still a wave (sum of waves). But the X-ray film/detector could only counts x-ray doses, which provide us an intensity number but it does not tell which stage it is in the repetition (the phase). Since both amplitude and phase is required to give a full description of the reflection but only intensity could be measured, sophisticated techniques have to be developed to obtain the phases of each reflection.

There are different ways to obtain phases. One of them, when applicable, is termed molecular replacement. In this process, software tries to take advantage of the reversibility of Fourier transformation (Equation 17), by putting a homologous model into the target unit cell. A calculated electron density is transformed to theoretical structor factors and theoretical intensities, as if these reflections were recorded the same way as in the experiment. Then this theoretical set is compared with the experimental set. Because at this stage there is no way to tell how the molecule lies within the unit cell, different orientations as well as positions have to be sampled. In successful cases one particular orientation and position combination will shown significantly better correlation to the experimental intensities than others. Then electron density can be calculated using experimental intensities and theoretical phases, with the assumption that a similar molecule lies in the same manner in the unit cell as the model used for the search.

It is also possible to obtain phases experimentally. The method involves perturbing the X-ray diffraction properties of the protein by introducing heavy atoms without altering its structure. Because of the prevalence of seleno-methionine substitution and related anomalous scattering methods in recent years, isomorphous replacement methods will not be introduced.

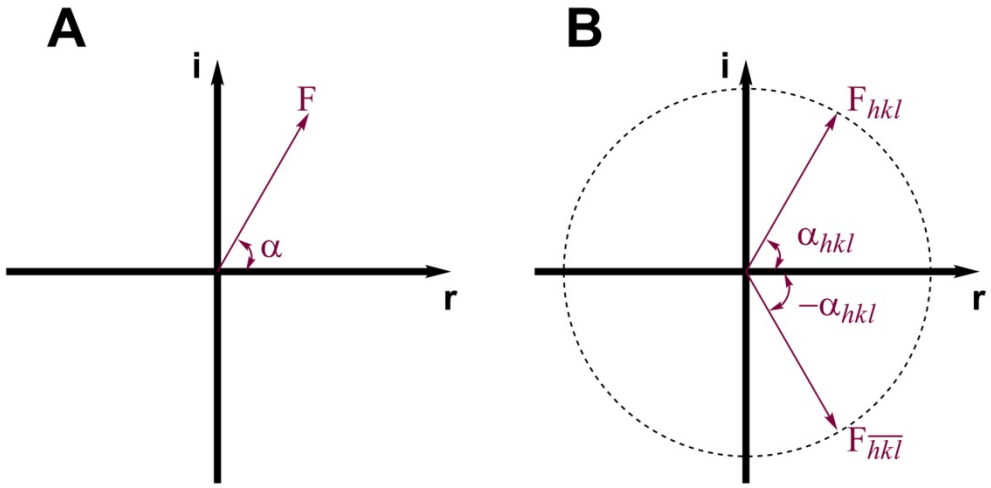


**Figure 3.7: A) Vector representation of a structure factor function on the complex number plane. B) Vector representation of Friedel's law.**

Anomalous scattering methods take advantage of centrosymmetrically related reflections which are called Friedel pairs. Because the origin of indexing was chosen arbitrarily, the h, k, l indices can be positive or minus. By definition, a reflection $F_{hkl}$ has the indices $F_{-h-k-l}$ if the origin is chosen from the other side of the reference plane. Hence, Friedel pairs are reflections of the same plane series from mirrored directions and therefore would have the same intensity (Equation 20, Fiedel's law). The concepts of structure factors, friedel pairs and related phasing techniques are best illustrated in the vector form.

$$|F_{hkl}| = |F_{\overline{hkl}}| \tag{20}$$

As described in the previous section (Equation 17), $F_{hkl}$ is a periodic function which can be regard as a sum of functions with basic form A(cosθ+isinθ). From knowledge of wave functions, periodic functions like $F_{hkl}$ can be interpreted as a vector

$$\vec{F} = |F|(\cos\alpha + i\sin\alpha) = |F| \cdot e^{i\alpha} \tag{21}$$

As shown in Figure 3.7A, vector F can be geometrically represented by an arrow on the complex number plane, with length |F|, and angle with the real axis α. Applying this to Friedel pairs, according to Friedel's law, $F_{hkl}$ and $F_{\overline{hkl}}$ are two vectors of the same length, but reversed angle regarding the real axis (Figure 3.7B).

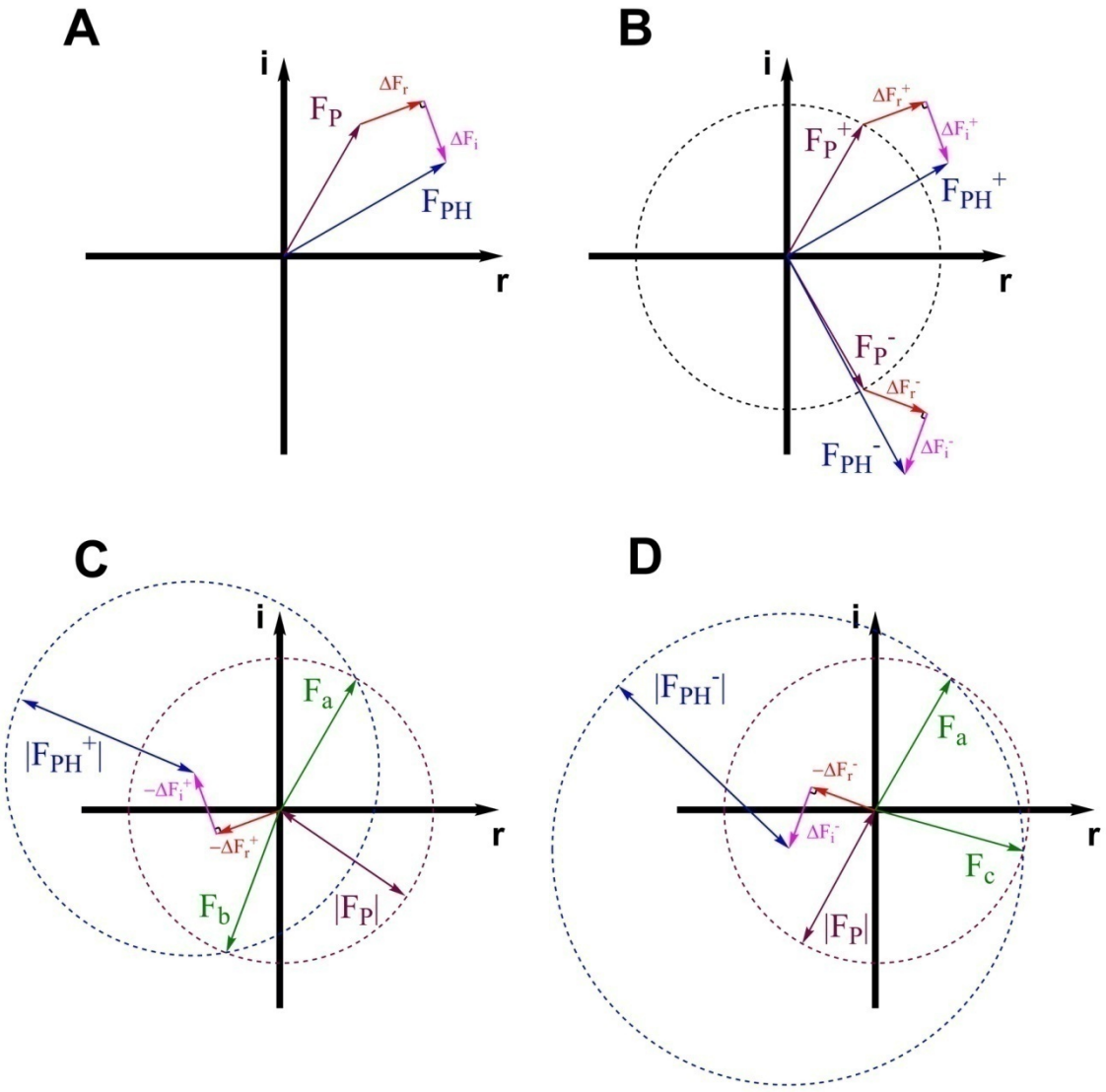


**Figure 3.8: A) Shift of structure factor vectors in presence of heavy atoms. B) The structure factors of heavy atom derivative FPH no longer follow Friedel's law but can be broken down as a sum of protein and heavy atom contributions. The protein contribution FP obeys Friedel's law and the heavy atom contribution FH can be further broken down to two perpendicular vectors ΔFr and ΔFi. C, D) Vector solution gives (in ideal cases) unique solution of the phase of FP+ (Fa).**

However, when heavy atoms, such as Se atoms in a Se-Met derivated protein, are introduced into the crystal, the structure factors are shifted both in phase and intensity due to the absorption of X-rays by the heavy atoms (Figure 3.8A). This shift can be expressed as the sum of two perpendicular vectors, $\Delta F_r$ and $\Delta F_i$. It can be proven that, in an anomalous scattering experiment, $\Delta F_r^+$ and $\Delta F_r^-$ are image of each other in the real axis,

while $\Delta F_i^+$ and $-\Delta F_i^-$ are image of each other in the imaginary axis. Because of this difference, Friedel's law no longer hold true (Figure 3.8B).

It is known that the amplitude of $\Delta F_r$ and $\Delta F_i$ are constant, while their phases depend on the position of the heavy atoms in the cell. Once the positions of the heavy atoms are known, $\Delta F_r$ and $\Delta F_i$ can be fully determined and structures factor vectors of protein atoms Fp can be determined by vector solutions (Figure 3.8C, D). Therefore, by incorporating heavy atoms into the protein the calculation of phases of tens of thousands of reflections can be reduced to determining the position of a small number of heavy atoms.

The most powerful method to determine heavy atom positions is the Patterson method, which makes use of a phase-independent function called the Patterson function:

$$P(u,v,w) = \frac{1}{V}\sum_h\sum_k\sum_l \left|F_{hkl}\right|^2 e^{-2\pi i(hu+kv+lw)} \tag{22}$$

Patterson function, like ρ(x, y, z) is a fourier sum. However, it is propotional to the square of $\boldsymbol{F}_{hkl}$, i.e. $I_{hkl}$. Therefore, the Patterson function can be calculated directly with any collected crystallography dataset (no phase information required).

The physical meaning of the Patterson function was shown to be vectors between atoms. Obviously there are more vectors between atoms than atoms themselves. So the Patterson map, which is the contour map defined by P(u,v,w), is even more complicated than the electron density map defined by ρ(x, y, z). But when it is applied to determine the heavy atom structure it is very efficient, because the difference Patterson map

$$\Delta P(u,v,w) = \frac{1}{V}\sum_h\sum_k\sum_l \left|\Delta F\right|^2 e^{-2\pi i(hu+kv+lw)} = \frac{1}{V}\sum_h\sum_k\sum_l \left(\left|F_{PH}\right| - \left|F_P\right|\right)^2 e^{-2\pi i(hu+kv+lw)} \tag{23}$$

can be directly calculated by the indexed intensities obtained by subtracting the derivative (PH) dataset by the native (Fp) dataset. In recent years, seleno-methionine phasing is the prevalent method used in crystallography. In this method, all methioines in a protein are replaced by seleno-methionine during protein expression. Since from the diffraction pattern unit cell parameters and symmetry (space group) can be determined, the number of selenium atoms in the unit cell is known. So when both native and seleno-methionine datasets are available, the difference Patterson map can be calculated. Then computer software can find peaks on this map, which are vectors between heavy atoms (e.g. Se atoms). From these vectors the positions of the heavy atoms can be calculated.

## 3.7 MODEL BUILDING AND REFINEMENT

Once the electron density function ρ(x, y, z) is derived with structure factor amplitudes and the corresponding phase values, it can be visualized by computer software showing the distribution of electron density within the real space unit cell (asymmetric unit). Applying existing knowledge about proteins and their building blocks – amino acids, such as the bulky side chains of aromatic amino acids and secondary structures, a model can be built to interpret the electron density. The model is in essence a list of atoms, each of which is specified with the position coordinates and temperature factor. The temperature factor describes the degree of movement for an atom to oscillate around the specified position. Flexible regions in the protein usually exhibit higher temperature factor.

However, the initial estimation of phases usually contains many errors, which in turn lead to errors in the initial electron density map. Correction of these errors, termed structure refinement, is usually carried out in two parts, in real space and reciprocal space, respectively.

In real space, crystallographers adjust the atom positions manually in a process similar to model building, so that the model 1) fits in the electron density 2) conforms as much as possible to our knowledge about proteins. For example, all natural amino acid must be L-amino acids; all pepetide bonds shall be planar; the carbonyl-moiety of the residues in an α-helix shall point to one direction; etc.

In reciprocal space, the refinement is carried out by software. Once the initial model is finished, a set of structure factors can be calculated using Fourier transformation (including phases, Equation 17). It is therefore able to calculate from the model a set of expected structure factor amplitudes in the condition under which the data was collected. This set of structure factor amplitudes |Fc|, is then compared with the experimentally measured structure factor amplitudes |Fo|. These programs use sophisticated statistical algorithms, such as maximum-likelyhood algorithm, to minimize the difference between |Fo| and |Fc|, by updating atom parameters in the model.

After the reciprocal refinement calculation is done, new phases are calculated and two difference maps are usually generated to guide a new round of real space refinement. One map is the difference map, or |Fo|-|Fc| map, which shows where the model should result in higher or lower density than the observed one. Fo-Fc density is particularly powerful in indicating the presence of ligands. The other map is the 2Fo-Fc map, which

uses 2|Fo|-|Fc| as the amplitude. Therefore the level of the map resembles that of the original experimental map, but exhibits both features of the experimental data and the model.

Refinement is carried out in real space followed by reciprocal space refinement for several rounds. In the later stage, small molecule ligands, if any, and waters are added to the model. Convergence of the model to the experimental data is monitored by many statistical values derived in the reciprocal space calculation. One important value is the R-factor, which describes the discrepancy between the model and the data. To avoid bias introduced by manipulating phases, typically 5% of the reflections are left out of refinement and the R-factor generated with these reflections, termed $R_{free}$, is a particular important indicator of the quality of the model. Crystallographic models of good quality generally aim at R-factors of 0.2 or below.

Other important critia include bond length deviation from the ideal value, bond angle deviation from the ideal value, and the Ramachandran diagram, which plots the the $\psi/\varphi$ angle (of the peptide bond) relationship of each residue. Most residues in a refined model shall be in the statistically favored regions.

# 4 MATERIALS AND METHODS

## 4.1 MATERIALS

### 4.1.1 Chemicals

Chemicals from the following companies were used: GE Healthcare (Freiburg), Baker (Deventer, Niederlande), Fluka (Neu-Ulm), GERBU (Gaiberg), Merck (Darmstadt), Pharma-Waldhof (Düsseldorf), Qiagen (Hilden), Riedel-de-Haen (Seelze), Roche (Mannheim), Roth (Karlsruhe), Serva (Heidelberg) und Sigma-Aldrich (Deisenhofen).

### 4.1.2 Enzymes

| Enzymes | Supplier |
|---|---|
| Phusion DNA polymerase | Finnzymes (Espoo, Finland) |
| Restriction enzymes | Fermentas (St.Leon-Rot) |
| T4 DNA ligase | Fermentas (St.Leon-Rot) |
| Thrombin | Sigma-Aldrich (Deisenhofen) |

### 4.1.3 Kits

| Kits | Supplier |
|---|---|
| QIAprep Spin Miniprep Kit | Qiagen (Hilden) |
| QIAquick PCR Purification Kit | Qiagen (Hilden) |
| QIAquick Gel Extraction Kit | Qiagen (Hilden) |
| RNeasy Mini Kit | Qiagen (Hilden) |
| BigDye Terminator Sequencing Kit | Fermentas (Langen) |
| GelStar Nucleic Acid Gel Stain | Lonza (Switzerland) |
| Perfect 1kb-DNA standard | Invitrogen (Karlsruhe) |
| Wide Range, SDS7 protein marker | Sigma (Deisenhofen) |

### 4.1.4 Microorganisms

| Bacterial Strains | Antibiotic Resistance | Supplier (Source) |
|---|---|---|
| *E. coli* BL21 (DE3) | / | Novagen |
| *E. coli* BL21 (DE3) pLysS | Chloramphenicol | Novagen |
| *E. coli* Rosetta2 | / | Novagen |
| *E. coli* Rosetta2 pLysS | Chloramphenicol | Novagen |
| *P. aeruginosa* PAO1 wildtype | / | Collaborator |
| *P. aeruginosa* PAO1 *ΔpqsE* | / | Collaborator |
| *P. aeruginosa* PAO1 pEw** | Ampicilin | This study |

**: Represents a series of strain, generated in this study by transforming the *ΔpqsE* strain with a pUCP20-pqsE plasmid. pEw: wild type PqsE, pE182: PqsE E182A mutant, pE273: PqsE S273 mutant, etc.**

### 4.1.5 Media and Antibiotics

| Culture Medium | Composition / Description |
|---|---|
| Luria-Bertani (LB) | 10 g/l Bactotryptone, 10 g/l NaCl, 5 mM NaOH, 5 g/l yeast extract |
| SOC | 1.55g Luria Broth, 250mM KCl, 2M $MgCl_2$, 1M Glucose |
| Terrific Broth (TB) | 12 g/l BactoTryptone, 24 g/l Bacto-yeast-extract, 4 g/l glycerol, 17 mM $KH_2PO_4$, 72 mM $K_2HPO_4$ |
| LeMaster | Prepared as described by Le Master *et al.* (Doublie, 1997) and http://structure.biochem.queensu.ca/protocols/lemaster.htm |

Antibiotics from GERBU (Gaiberg) were used at the concentration 100 mg/l for ampicillin, 50 mg/l for kanamycin and 34 mg/l for chloramphenicol unless where specified.

### 4.1.6 Buffers

| Buffer | Composition / Description |
|---|---|
| ***SDS-PAGE*** | |
| SDS Sample buffer | 50 mM Tris pH 8.9, 100 mM DTT, 2% (w/v) SDS, 0.25% (w/v) Bromophenol blue, 10% Glycerine |
| SDS Running buffer | 25 mM Tris pH 8.3, 192 mM Glycine, 0.1% (w/v) SDS |
| Coomassie Blue Staining solution | 0.25 % (w/v) Coomassie Brilliant Blue R 250, 45 % Ethanol, 10 % Acetic Acid |
| Destaining solution | 10% Acetic Acid, 5% Ethanol |
| ***Agarose Gel Electrophoresis*** | |
| TAE-Buffer | 40 mM Tris, 0.1% (v/v) Acetic acid, 1 mM EDTA pH 8.0 |
| Loading Buffer Orange | 6% Sucrose; 4% Glycerin; 0.04% Orange G; $H_2O$ |
| ***Purification*** | |
| Ni Column Buffer A | 50 mM $Na_2HPO_4$, pH 8.0, 500 mM NaCl in case of PqsE constructs with HisTag, and 300 mM NaCl in case of PA0803 |
| Ni Column Buffer B | Buffer A plus 500 mM Imidazol pH 8.0 |
| GST Column Buffer | 10 mM $Na_2HPO_4$ 1.8 mM $KH_2PO_4$ pH 7.3, 140 mM NaCl, 2.7 mM KCl |
| GST Elution Buffer | 50 mM Tris-HCl pH 8.0, 10 mM reduced glutathione |
| MBP Column Buffer | 20 mM Tris-HCl pH 7.4, 0.2 M NaCl; 1 mM DTT |
| MBP Elution Buffer | Column buffer plus 10 mM Maltose |
| Strep Column Buffer | 100 mM Tris-HCl pH 8.0, 150 mM NaCl |
| Strep Elution Buffer | Column buffer plus 2.5 mM Desthiobiotin |
| Dialysis Buffer | 50 mM Tris-HCl pH 8.0, 150 mM NaCl (0.5 to 2 mM DTT where specified) |
| Gel Filtration | 20 mM Tris-HCl pH 8.0, 150 mM NaCl (0.5 to 2 mM DTT where specified) |

**Table 4.1: List of Common Buffers.**

## 4.2 EQUIPMENTS

| Equipment | Model | Provider |
|---|---|---|
| SDS-PAGE Chamber | | BIO-RAD |
| Agarose Gel Chamber | Horizon 58 | Life Biotechnologies |
| Electroporation | Gene Pulser | BIO-RAD |
| Microfluidizer | M -110 S | Microfluidics |
| PCR Machine | PCR Sprint | Thermo Electron Corp. |
| Thermoblock | Thermomixer comfort | Eppendorf |
| FPLC system I | ÄKTA Prime | GE Healthcare |
| FPLC system II | 650E Advanced Protein Purification System | Waters |
| Minicentrifuges | 5415C / 5415D | Eppendorf |
| Table Centrifuge | 5804R | Eppendorf |
| Centrifuge | Avanti Centrifuge J-20 XP | Beckmann |
| Rotors | JLA 8.1000 / JA12 | Beckmann |
| Ultracentrifuge | OptimaTM L-70K | Beckmann |
| Rotors | Ti 45 | Beckmann |
| Chomatography Columns | HiTrap Chelating HP<br>Glutathion Fast Flow<br>MBPTrap HP<br>HiLoad 26/60 Superdex 75 prep grad | GE Healthcare |
| Strep-Tactin Column | Strep-Tactin Sepharose | IBA BioTAGnology |
| Spectrophotometer I | DU 650 | Beckmann |
| Spectrophotometer II | ND – 1000 | PeqLab |

## 4.3 ANALYTICAL METHODS

### 4.3.1 Determination of protein concentration

Determination of protein concentration was routinely carried out via Bradford assay (Bradford, 1976). Commercially available Bradford stock solution (Sigma Aldrich) was

diluted 1:5 freshly before a batch of purification using water pre-cooled to 4°C. A calibration curve was prepared using 2 mg/ml BSA standard (Sigma Aldrich). 800 µl of the 1× Bradford solution was placed in a plastic cuvette as blank. In another cuvette, the same solution was supplied with 2 µl of protein. Cuvettes were let to stand in room temperature for 5 min and then optical density was measured at 595 nm on a Beckmann DU650 spectrophotometer. The $OD_{595}$ is compared to the calibration curve to derive the concentration of the protein sample. If the protein was too concentrated, it was diluted before addition to the Bradford solution so that the $OD_{595}$ falls to the linear range of 0.1-0.6.

Alternatively, protein concentration was measured directly by UV absorption at 280 nm in a quartz cuvette on a Beckmann DU650 spectrophotometer. Absorption coefficient ε was calculated by Protparam (Gasteiger et al., 2003). For PqsE, ε of 64440 $M^{-1}cm^{-1}$ was used and for PA0803, ε of 25565 $M^{-1}cm^{-1}$ was used.

### 4.3.2 Agarose Gel Electrophoresis

Nucleic acid samples, mostly DNA and in some cases highly-concentrated RNA samples, were analyzed by agarose gel electrophoresis.

Agarose gel was prepared by adding appropriate amount of electrophoresis grade agarose (Invitrogen) into TAE buffer (Section 4.1.6). The mixture was heated in microwave oven till the agarose powder completely melted followed by adding of 0.5 µg/ml ethidium bromide or 1× GelStar stain (Lonza, 10,000× stock). The hot gel was then cast into a mold, with a comb placed at ~0.5 cm from one end to form the sample wells, and allowed to cool. The prepared gel was then placed in a horizontal electrophoresis apparatus and kept under 70V field to develope. The time required depends on the percentage of the gel. Upon finishing of the electrophoresis, the gel was taken to a UV light plate equipped with a camera to take a photo.

### 4.3.3 SDS-PAGE

Protein samples, for example obtained from chromatography fractions or from thrombin cleavage, were monitored by SDS-PAGE. They were loaded onto 15% SDS PAGE gels and electrophoresis was carried out according to Laemmli *et al*. ( 1970). The running gel was composed of 15% acrylamide, 0.4% bisacrylamide, 0.1% (w/v) SDS and 375 mM Tris, pH 8.8. The polymerisation of the gel material was initiated by adding 14 µM

/µl N,N,N,N -Tetramethyl-Ethylenediamine (TEMED) and 0.5 mg/ml ammonium persulphate (APS). The gel was cast by pouring it into the casting chamber and covering it with isopropanol/water 1:1. After polymerisation, the isopropanol/water mixture was replaced by the stacking gel: 5% acrylamide, 0.13% bisacrylamide, 0.1% (w/v) SDS, 125mM Tris, pH 6.8, 14 µM/µl TEMED and 0.5% mg/ml APS.

Prior to application on the gel, the protein samples were denatured by incubation for 5 minutes at 95°C in sample buffer (given below). The protein molecular weight marker (LMW-Standard, Amersham Biosciences) was composed of protein phosphorlylase b (97 kDa), albumin (67 kDa), ovalbumin (43 kDa), carboanhydrase (30 kDa), trypsin inhibitor (20.1 kDa) and lysozyme (14.4 kDa). The electrophoresis was carried out at 60 mA in SDS running buffer. The gels were stained with a Coomassie Blue solution and then destained with destaining solution to display the protein bands.

### 4.3.4 HPLC

High performance liquid chromatography (HPLC) analyses were carried out on a Waters system (Waters Corp.) equipped with an inline AF degasser, 600S controller, 717 plus autosampler, 2487 Dual λ Absorbance Detector and a ProntoSIL 120-5-C18-Aq 5 µm column (Bischoff Analysentechnik).

The flow rate was 1 ml/min, the solvents were usually (unless where specified) A: 0.1% trifluoroacetic acid in water; B: 0.1% trifluoroacetic acid in acetonitrile. The gradient applied was typically (unless where specified): 0-2 min 100% A, 2-27 min 0-100% B, 27-32 min 100% B, 32-37 min 100% A.

### 4.3.5 ESI-MS and HPLC-MS

Electro-Spray-Ionization Mass-Spectrometry (ESI-MS) was routinely used to control the quality of the protein preparation. Prior to loading the sample to the ESI-MS machine, the protein was applied to a NAP5 column to exchange the buffer either to a volatile buffer or water when appropriate. The final protein concentration was adjusted to 1~3 mg/ml.

Mass spectrometry was carried out in the positive ion detection mode. Data were collected at the m/z range of 700 - 2000. A protein sample typically gives multiple peaks, due to different number of charges it captures. These peaks were deconvoluted with the Bioworks Browser software (Thermo Electron Corp.) to give the mass in the desired range.

HPLC-MS was used to monitor small molecules, such as those tested as potential substrates of PqsE. Data were collected at the m/z range of 100 - 700. UV detectors were also used for compounds that have detectable UV absorption. The flow rate was 1 ml/min; solvent A was 0.1% formic acid in water, and solvent B, 0.1% formic acid in acetonitrile. The column was developed with the following gradient: 0-1 min 100% A, 1-15 min 0-100% B, 15-20 min 100% A. Mass spectroscopy was usually carried out in both positive and negative ion detection mode.

ESI-MS and HPLC-MS analyses were carried out on a FINNIGAN LCQ Advantage MAX mass spectrometer (Thermo Electron Corp.) coupled with an Agilent 1100 HPLC system (Agilent Technologies), using a Nucleodur C18 gravity 3 μm 125/4 column (Machery Nagel).

### 4.3.6 X-ray Fluorescence

X-ray fluorescence scanning was carried out on beamline X10SA of the SLS. Briefly, the crystal was mounted on the beamline equipped with a Ketek Si-drift fluorescence detector. Then an excitation scan was carried out, varying the X-ray source energy around a particular absorption edge of a particular metal.

## 4.4 PREPARATION AND TRANSFORMATION OF COMPETENT CELLS

### 4.4.1 Preparation and electro-transformation of *E. coli*

Sterile media and solutions were chilled prior to use unless otherwise indicated. Competent cells for plasmid amplification (*E. coli* XL1-Blue) were prepared as follows:

- 100 ml Luria Broth (LB) or SOC medium were inoculated with a single colony *Escherichia coli* XL1-Blue and grown overnight at 37°C with continuous shaking.
- The next day, 5 ml preculture was diluted with 500 ml SOC medium and grown further at 37°C to optical density $OD_{600}$ = 0.6. The cells were harvested by centrifugation at 3000 × g for 15 minutes.
- The pellet was washed with 500 ml sterile $H_2O$ at 4 °C twice.
- The pellet was then resuspended in 10 ml 10% glycerol (4 °C) and recentrifuged.

- The resulting cell pellet was finally resuspended in approximately 2.5 ml 10% glycerol (4 °C) and aliquoted into 75 µl portions.
- Aliquots were flash frozen in liquid nitrogen and stored at -80 °C till further use.
- For electro-transformation, 75 µl of the competent cells were incubated with approximately 1 ng of DNA, transformed by electroporation using a BioRad Gene Pulser apparatus.
- Cells were then resuspended in 1ml antibiotic free LB and incubated with shaking for 30-60 min at 37 °C.
- 100 µl of this suspension was then diluted 10 to 100 fold if necessary, plated on an agar selection medium containing the appropriate antibiotic.

### 4.4.2 Preparation and heat-shock transformation of *E. coli*

Competent cells for protein expression (*E. coli* BL21 (DE3), BL21 (DE3) pLysS, BL21 (DE3) RIL, Rosetta2, Rosetta2 pLysS) were prepared as follows:

- Start a 30 ml overnight culture in LB.
- The next morning inoculate in 100 ml LB with starting $OD_{600} = 0.2$
- Grow cells at 37 °C till $OD_{600} = 0.8$, put on ice to stop growing.
- Harvest cells by centrifugation for 15 min at 2000 × g at 4°C, discard supernatant.
- Resuspend the cells in 1/10 of original volume (10 ml) in filter-sterilized TSS medium.
- Make 100 µl aliquots, flash cooled in liquid $N_2$ and stored at -80 °C until further use.
- For heat-shock transformation, add plasmid DNA to 100 µl ice-cold competent cells (thawed first at first at 37 °C) and incubate on ice for 30 min.
- Heat-shock in a 42 °C water bath for 90 seconds.
- Chill on ice for 5 min.
- Add 900 µl LB medium, shake under 37 °C for 45 min.
- Plate bacteria on a LB plate with appropriate antibiotics for selection.

### 4.4.3 Preparation and transformation of *Pseudomonas aeruginosa*

Preparation of Electro-competent *Pseudomonas aeruginosa* (PAO1) and subsequent transformation with plasmids was carried out at room temperature as follows:

- Streak the bacteria tight on LB plates with a cotton swab. Two plates are required for each electroporation.
- Grow plates at 37 °C for 24 hours.

- Harvest cells with an inoculation loop and put cells from each plate into a separate 1.5 ml Eppendorf tube. Resuspend the cells in 1 ml MilliQ water.
- Centrifuge 2 min with a table centrifuge at 13000 rpm.
- Remove supernatant as well as the extracellular slime.
- Wash the cells 3 times with 1 ml of MilliQ water, which then result in a small pellet.
- Resuspend the cells with 50 µl MilliQ water and pool the 2 tubes.
- For electro-transformation, mix 50 µl of this with 100 ng of the plasmid and electroporate at 25 µF, 2.45 kV, 200 Ohm with time constant at about 5 sec.
- Regenerate in LB Medium at 37 °C for 1h.
- Plate bacteria on a LB plate with appropriate antibiotics for selection.

## 4.5 CLONING AND PLASMID CONSTRUCTION

### 4.5.1 Preparation of *Pseudomonas aeruginosa* Genomic DNA

Extraction of *P. aeruginosa* PAO1 genomic DNA was performed with the traditional phenol/chloroform method.

- Innoculate culture from freshly plated colonies of PAO1. Grow cells to $OD_{600}$ = 0.8 in 500 ml LB medium. Pellet cells by centrifugation, and resuspend in 25 ml 50 mM Tris (pH 8.0), 50 mM EDTA.
- Freeze cell suspension at -20 °C.
- Add 2.5 ml 250 mM Tris (pH 8.0), 10 mg/ml lysozyme to frozen suspension, and let thaw at room temperature. When thawed, place on ice for 45 min.
- Add 5 ml 0.5% SDS, 50 mM Tris (pH 7.5), 0.4 M EDTA, 1 mg/ml proteinase K. Place in 50°C water bath for 60 min.
- Extract with 30 ml Tris-equilibrated phenol and centrifuge at 10,000X g for 15 min. Transfer top layer to new tube (avoid interface).
- Add 0.1 vol 3 M Na acetate (mix gently), then add 2 vol 95% ethanol (mix by inverting).
- Spool out DNA and transfer to 25 ml 50 mM Tris (pH 7.5), 1 mM EDTA, 200 g/ml RNase. Dissolve overnight by rocking at 4 °C.

- Extract with equal volume chloroform (mix by inverting) and centrifuge at 10,000 × g for 5 min. Transfer top layer to a new tube.
- Add 0.1 vol 3M Na acetate (mix gently), then add 2 vol 95% ethanol (mix by inverting).
- Scoop out DNA and dissolve in 20 ml 50 mM Tris (pH 7.5), 1 mM EDTA.
- Check purity and integrity of DNA by electrophoresis and spectrophotometric analysis.

### 4.5.2 Cloning of *pqsE* and *PA0803* Gene from *P. aeruginosa* Genomic DNA

The genes of interest (*pqsE, PA0803*) were amplified by polymerase chain reaction (PCR, (Saiki et al., 1985), see Table 4.2) using *Phusion* Polymerase. *Pseudomonas aeruginosa* genomic DNA prepared as described in Section 4.2.1 was used as template. Primers were designed manually based on published gene sequences (Winsor et al., 2009). All primers were synthesized by MWG Biotech (Table 4.3).

| Cycle | Temperature | Time |
|---|---|---|
| **Mix:** | ~ 300 ng Template DNA<br>1 µl forward primer (25 pmol stock)<br>1 µl reverse primer (25 pmol stock)<br>1 µl dNTPs mix (10 mM stock)<br>10 µl 5× Phusion buffer<br>**Add** MilliQ water to 49.5 µl | |
| **Denature:** | 98°C | 5 min |
| | **On ice** | 5 min |
| | **Add** 0.5 µl Phusion Polymerase | |
| 1× | 98°C | 30 sec |
| | 98°C | 10 sec |
| 5× | 55°C (depending on primers) | 20 sec |
| | 72°C | 20 sec / kb |
| | 98°C | 10 sec |
| 30× | 60°C (depending on primers) | 20 sec |
| | 72°C | 20 sec / kb |
| 1× | 72°C | 5 min |
| | 4°C | keep |

**Table 4.2: Typical PCR protocol for amplification of genes from genomic DNA.**

PCR products were purified on agarose gels, digested with the corresponding pair of restriction enzymes (Fermentas) and ligated using T4 DNA Ligase (Fermentas) into the corresponding expression vectors (Novagen), which were also digested with the same pair of restriction enzymes (Table 4.4). Restriction digests, sticky-end DNA ligations, amplification and isolation of plasmids followed standard procedures using the appropriate Qiagen kit where necessary. Electrocompetent *E. coli* strain XL-1 Blue was routinely used for maintenance of plasmids. Upon ligation and amplification, the constructs were checked by restriction digestion and sequencing to ensure that they contain the desired gene fragment. These constructs were used for subsequent affinity purification of the proteins.

| Primer name | Primer sequence | Tm (°C) |
|---|---|---|
| pqsE-for | 5'-TGAACCGCATATGTTGAGGCTTTC-3' | |
| pqsE-rev | 5'- AATGGGGATCCCTTATCAGTCCAGAGGCAG -3' | |
| pqsE_NdeI_for | 5'-CCATATGTTGAGGCTTTCGGCTCCCGG-3' | 69.5 |
| pqsE_XhoI_rev | 5'-CGAATTCCTCGAGCTTATCAGTCCAGAGGCAG-3' | 70.8 |
| pa0803_for | 5'-GTATGCCATATGCACACGCCCGCCA-3' | 67.9 |
| pa0803_rev | 5'-AATGGATCCGTCATCATGCCCAGGGATC-3' | 68 |

**Table 4.3: List of primers used for cloning.**

| Plasmid Name | Restriction Sites | Plasmid Name | Restriction Sites |
|---|---|---|---|
| pET28a-pqsE | NdeI / BamHI | pMAL_TEV_pqsE | NdeI / XhoI |
| pGATEV_mod_pqsE | NdeI / XhoI | pET19Strep_pqsE | NdeI / XhoI |
| pET19m-0803 | NdeI / BamHI | pET19m-0803H49A | NdeI / BamHI |

**Table 4.4: List of constructs and corresponding restriction sites.**

## 4.6 VARIATIONS AND MUTAGENESIS

### 4.6.1 Construction of wildtype PqsE with different affinity tags

GST, MBP, and StrepTagII fusion proteins were generated from the pET28a-pqsE plasmid (Section 3.4.2), which encodes His-tagged PqsE. First the 906 bp *pqsE* gene was amplified via PCR (Table 4.5). Primers (pqsE_NdeI_for and pqsE_XhoI_rev, Table 4.3) were designed to use NdeI and XhoI restriction sites, which is suitable to the target vectors. The fragment was then digested with the corresponding restriction enzymes followed by ligation into the appropriate sites (NdeI/XhoI) of various vectors that were treated with the same pair of enzymes. These result in the plasmid of pGATEV_mod_pqsE, pMAL_TEV_pqsE and pET19Strep_pqsE that encode fusion proteins with a corresponding N-terminal affinity tag.

| Mix | Cycle | Temperature | Time |
|---|---|---|---|
| ~ 50 ng Template DNA<br>1 µl forward primer (25 pmol stock)<br>1 µl reverse primer (25 pmol stock)<br>1 µl dNTPs mix (10 mM stock)<br>10 µl 5× Phusion buffer<br>Add MilliQ water to 49 µl<br><br>Add 1 µl Phusion Polymerase | 1× | 98°C | 2 min |
| | 35× | 98°C | 15 sec |
| | | 65°C | 20 sec |
| | | 72°C | 50 sec |
| | 1× | 72°C | 7 min |
| | | 4°C | keep |

**Table 4.5: PCR protocol for amplification of pqsE from pET28-pqsE**

### 4.6.2 Site-directed Mutagenesis

Site-directed mutagenesis experiments were carried out as described in the manual of the QuikChange II XL system (Stratagene). The residues to mutate were manually chosen based on the determined X-ray structure of the wild type proteins. The procedures are summarized as follows:

- A PCR using primers containing the mutation was carried out (Table 4.6).
- Add 1 µl of restriction enzyme DpnI, which digest the template plasmid DNA of bacterial origin.
- Incubate at 37°C overnight.

- Transform into electrocompetent XL1-Blue cells, plate on agar.
- Incubate at 37°C overnight.
- Pick 5-6 colonies, shake 5 ml overnight culture in LB medium.
- Inoculate a fresh 1 ml culture to make glycerol stocks, use the rest of the overnight culture to prepare plasmid DNA.
- Carry out a sequencing to confirm mutation at desired position.

| Mix | Cycle | Temperature | Time |
|---|---|---|---|
| 50~ 200 ng Template DNA (plasmid extracted from XL1-Blue)<br>2 µl forward primer (10 pmol stock)<br>2 µl reverse primer (10 pmol stock)<br>2 µl dNTPs mix (10 mM stock)<br>10 µl 5× Phusion buffer<br>Add MilliQ water to 49 µl<br><br>Add 1 µl Phusion Polymerase | 1× | 98°C | 45 sec |
| | 16× | 98°C | 15 sec |
| | | 65°C* | 20 sec |
| | | 72°C | 40 sec / kb |
| | 1× | 72°C | 10 min |
| | | 4°C | keep |

**Table 4.6: PCR protocol for site-directed mutagenis. *Annealing temperature of each experiment depends on primers used in that particular case.**

| Primer name | Primer sequence | Tm (°C) |
|---|---|---|
| pqsE_E182A_for | 5'-ATGCCCTGGGCGCGTTCGACGAG-3' | 69.6 |
| pqsE_S273A_for | 5'-GGTGGGCAGGCCGTCGACTTC-3' | 67.6 |
| pqsE_H282A_for | 5'-GCGAACTGGCCCTGGGGAGCATG-3' | 69.6 |
| pqsE_S285A | 5'-ACTGCACCTGGGGGCCATGCGCCGGATG -3' | 78.0 |
| pqsE_R288A | 5'-TGGGGAGCATGCGCGCGATGCTGGAGATTC-3' | 78.3 |
| 0803_H49A_for | 5'-ACAGGTGCTCGCCGCCGAGTTGA-3' | 67.8 |

**Table 4.7: List of Mutagenesis primers. Only the sense-strand primers are listed; the anti-sense-strand primers have exactly the reverse-complement sequences of the corresponding sense-strand primers. PCR for S285A and R288A use 72°C as annealing temperature and therefore has only two temperature steps in each cycle.**

## 4.7 PROTEIN EXPRESSION AND PURIFICATION

### 4.7.1 Protein Expression

Proteins were expressed in various *E. coli* strains (Novagen). An overnight culture from a single colony was grown and diluted the next morning with fresh medium suspended with appropriate antibiotics. The cells were grown at 37°C with vigorous shaking until an $OD_{600}$ = 0.8. Protein expression was induced using 1 mM isopropyl-β-D-thiogalactoside (IPTG) for 3 hours at 37°C or alternatively using 0.5 mM IPTG for 16 hours at 20°C. The cells were harvested by centrifugation for 20 minutes at 6000×g. When not immediately used for protein purification, the pellets were flash frozen and stored at -80°C.

| Protein | *E.coli* Strain | IPTG (mM) | Temperature (°C) | Time (hrs) |
|---|---|---|---|---|
| PqsE wildtype (His) | Rosetta pLysS | 1 | 37 | 3 |
| SeMet-PqsE | BL21 (DE3) pLysS | 0.5 | 20 | 16 |
| PqsE E182A | Rosetta2 pLysS | 0.5 | 20 | 16 |
| PqsE S273A | Rosetta2 pLysS | 0.5 | 20 | 16 |
| PqsE H282A | Rosetta2 pLysS | 0.5 | 20 | 16 |
| GST-PqsE | BL21 (DE3) RIL | 0.5 | 20 | 16 |
| MAP-PqsE | BL21 (DE3) | 0.5 | 20 | 16 |
| StrepII-PqsE | Rosetta2 | 0.5 | 20 | 16 |
| PA0803 wildtype | Rosetta2 pLysS | 1 | 37 | 3 |
| SeMet-PA0803 | Rosetta2 pLysS | 0.6 | 20 | 16 |
| PA0803 H49A | Rosetta2 pLysS | 0.5 | 20 | 16 |

**Table 4.8: Expression strains and conditions of different proteins.**

### 4.7.2 Protein Purification

**Preparation of the Cell Lysate:** The cell pellet was resuspended in the appropriate column loading buffer (Table 4.1) containing 1 mM PMSF (Phenylmethylsulfonyl fluoride, protease inhibitor). The cells were lysed by passing three times through a microfluidizer (model 110S, Microfluidics Cooperation). The lysate was then ultracentrifuged at 150000×g

(Beckman ultracentrifuge model Optima L-70K, rotor Ti45) for 45 minutes and the resulting supernatant was filtered through a 0.2 μm filter.

**Ni-affinity Chromatography:** A pre-packed 5ml Hitrap column (GE Healthcare) was used to purify protein from up to 3 liters of culture. The column was charged with 100 mM nickel chloride and pre-equilibrated with Buffer A on an Äkta Prime FPLC system (GE Healthcare). The filtered supernatant was then injected into the system at a flow rate of 5 ml/min. The loaded column was washed with Buffer A until the $OD_{280}$ was constant. Non-specifically bound proteins were removed by washing with 8 - 10 column volumes of Buffer A containing 2 % Buffer B and then 5 column volumes of 5 % Buffer B, after which the bound protein of interest was eluted in an imidazole gradient of 5 to 100% Buffer B over a volume of 475 ml. Fractions containing pure target protein were identified by SDS-PAGE and desired fractions were pooled.

Protein concentration was determined with the Bradford assay. The pooled fractions were then supplied with 1 unit thrombin per 4 mg protein and dialyzed against a buffer (Dialysis Buffer, Section 3.1.6) which is compatible with both thrombin and TEV protease. The cleavage proceeded at room temperature for 2 hours and the dialysis system was then moved to 4°C overnight. The digestion removes the 6×His tag and leaves 3 additional residues (Gly-Ser-His) at the N-terminus of the expressed protein (Section 3.1). Completeness of cleavage was comfirmed with SDS-PAGE. The protein was filtered through a 0.2 μm filter to remove precipitate, concentrated to below 15 ml in an Ultrafiltration Chamber (Amicon) using a 10 kDa cut off membrane (Millipore) and further purified with gel filtration.

**Glutathion-affinity Chromatography:** Purifications of GST-tagged fusion proteins were carried out with an 80 ml Glutathion Sepharose Fast Flow Column (GE Healthcare) on an ÄKTA Prime FPLC System (GE Healthcare). The column was first equilibrated with the GST Column Buffer (Table 4.1) before applying lysate a 5 ml/min flow rate.

The column was washed with GST Column Buffer until the $OD_{280}$ of the flow through returned to baseline level, a gradient from 0% to 100% GST Elution Buffer over a volume of 80 ml was run with 2 ml/min flow rate. The column was kept under 100% elution buffer to allow complete elution of the fusion protein. 2 ml/tube fractions were collected, analyzed on SDS-PAGE and pooled.

**Maltose-affinity Chromatography:** Purifications were carried out with a 5 ml MBPTrap HP-Column (GE Healthcare) on an Advanced Protein Purification System (Waters 650E). The column was first equilibrated with the MBP Column Buffer (Table 4.1). Cell lysate was then applied at 4 ml/min flow rate. The column was washed with column buffer until the $OD_{280}$ of the flow through returned to baseline level, then the bound fusion protein was eluted with 60 ml of MBP Elution Buffer. 4 ml/tube fractions were collected, analyzed by SDS-PAGE and desired fractions were pooled.

Cleavage of the MBP-tag was first tried by adding TEV protease (m/m 1:40) to affinity-purified MBP-PqsE. After 16 hours of incubation at 4°C approximately 70% of the tag was cleaved-off, as analyzed by SDS-PAGE. A second maltose-affinity chromatography was performed to remove the MBP-tag and uncleaved fusion protein. However, the MBP-tag, cleaved and uncleaved protein could not be separated, even by treating with 5 mM DTT or passing through a Superdex G200 gel-filtration column. Therefore, on-column cleavage was carried out as an alternative strategy. Fresh lysate was loaded at a flow rate of 2.5 ml/min to the column and washed. 2.6 mg TEV protease was diluted in MBP-column buffer to final volume of 5 ml, loaded on to the column and incubated at 4°C overnight. The cleaved PqsE protein was eluted with 20 ml MBP-column buffer with flow rate of 2.5 ml/min.

**StrepTagII-affinity Chromatography:** The StrepTagII-fusion proteins were purified via a gravity flow Strep-Tactin Sepharose Column (IBA BioTAGnology). The StrepTagII is an eight amino acid peptide (sequence WSHPQFEK). It resembles the interaction of streptavidin to biotin, with reduced affinity.

In a typical purification, the column was first equilibrated with the Strep Column Buffer (Table 4.1). The cell lysate was then applied to the column, followed by washing with 25 ml of column buffer. Because the StrepTagII-Streptactin interaction is very specific, only the fusion protein was bound to the column. Elution was carried out with 6 times 2.5 ml Strep Elution Buffer. 5 ml/tube fractions were collected, analyzed with SDS-PAGE, and pooled. Due to the limited binding capacity, StrepTagII fusion proteins were purified in relatively small quantities. Therefore buffer of the purified protein was exchanged to gel filtration buffer on a NAP5 Column (GE Healthcare) and then concentrated in an Amicon Ultra-15 Ultracell (10 kDa Mw cut off).

## 4.8 GEL FILTRATION

A gel filtration step was used to carry out the final purification, buffer exchange and determination of the oligomeric state of the protein. Up to 15 ml of concentrated, filtered protein solution was injected to either a Superdex G75 HR 26/60 column (GE Healthcare) or a Superdex G200 HR 26/60 column (GE Healthcare) pre-equilibrated with Gel Filtration Buffer on a Waters 650E FPLC system. The protein was injected and eluted isocratically at a flow rate of 1.0 ml/min, with collection of 4 ml fractions. The protein fractions were analyzed with SDS-PAGE, pooled and concentrated via ultrafiltration for further crystallization experiments and activity tests. Molecular weight was calculated from retention time of the peaks against a standard calibration curve, obtained by applying a standard sample mixture of proteins of known molecular weight (Sigma Aldrich). Gel filtration of PqsE constructs were carried out at 4°C, while PA0803 constructs were carried out at room temperature.

## 4.9 PRODUCTION OF SELENOMETHIONINE LABELED PROTEINS

### 4.9.1 Production of SeMet-PqsE

As molecular replacement studies using coordinates of β-lactamases, which were predicted to be of similar fold, were unsuccessful, experimental phasing using anomalous dispersion methods was initiated. Seleno-L-methionine was incorporated into PqsE by using a minimum media as described by Le Master *et al* (Doublie, 1997). Good expression was achieved with *E. coli* BL21 (DE3) pLysS cells bearing pET28a with 6×His-tagged PqsE. 10 ml overnight culture was started with single colony in LB media supplemented with kanamycin and chloramphenicol, pelleted the next morning, and suspended in LeMaster media containing 50 mg/L seleno-L-methionine, 15 μg/ml kanamycin and 17 μg/ml chloramphenicol. The culture was grown at 37°C to mid-log phase ($OD_{600}$ of 0.7) and allowed to cool to 20°C before overnight induction with 0.5 mM IPTG. The labelled protein had purification properties identical to those of the native protein.

### 4.9.2 Production of SeMet-PA0803

As molecular replacement studies using coordinates of the protein *E.coli* glyoxalase-I, which might be of similar fold, were unsuccessful, experimental phasing using the anomalous dispersion method was initiated. Seleno-L-methionine was incorporated into PA0803 by inhibition of methionine biosynthesis in synthetic media (Doublie, 1997). *E. coli* Rosetta2 pLysS cells bearing pET-19mod with 6×His-tagged PA0803 were grown overnight in Luria Bertani media supplemented with ampicillin and chloramphenicol. They were pelleted the next morning with mild centrifugation and immediately resuspended in LeMaster media containing 50 mg/L seleno-L-methionine, 15 μg/ml kanamycin and 17 μg/ml chloramphenicol. The culture was grown at 37°C to mid-log phase ($OD_{600}$ of 0.7) and allowed to cool to 20°C before overnight induction with 0.6 mM IPTG. The labelled protein had purification properties identical to those of the native protein.

## 4.10 CRYSTALLIZATION

### 4.10.1 PqsE Crystallization

Initial crystallization conditions of pure PqsE were determined using Crystal Screen and Crystal Screen 2 (Hampton Research). The protein concentration was screened at 20, 10 and 5 mg/ml by dilution of the protein stock with gel filtration buffer. The screens were set up by sitting drop method, with drops consisting of 1 μl protein and 1 μl precipitant solution. All crystallization trials were carried out at 20°C.

Conditions that produced microcrystalline precipitates were optimized via the hanging drop method (1 μl + 1 μl drop size) with respect to precipitant concentration and pH to reduce the amount of nucleation, increase the size and improve the appearance of the crystals obtained. Diffraction-quality crystals were obtained in two different crystal forms. Crystal form 1 was generated with a protein concentration of 20 mg/ml and a reservoir consisting of 0.1 M sodium HEPES pH 7.6, 0.2 M magnesium chloride and 30 – 32 % (v/v) PEG 400. Se-Met labeled PqsE crystals, as well as crystals of PqsE E182A mutant were obtained at similar conditions. Crystal form 2 was generated with 0.1 M imidazole pH 6.5, and 0.6 M NaAc. For diffraction data collection, these crystals needed to be cryo-protected,

which was achieved by quick washing in reservoir solution supplemented with 15% (v/v) glycerol.

### 4.10.2 Crystallization of PqsE-ligand complexes

Apo-PqsE crystals were obtained at conditions described in the previous section (Crystal form 1). The drop is then supplied with 1µl of 20 mM M636 (for chemical structure see Section 5.9.2) solution, dissolved in the mother liquor. A few crystals were taken out in mounting loops and flash-cooled in liquid nitrogen after 1 hour and 2 hours respectively. Since the crystals showed neither apparent change in shape nor loss of integrity, they were left overnight in 20 °C for subsequent samples to be taken the next morning.

Similarly, apo-PqsE E182A crystals were generated in the same conditions and then the crystal drops were supplied with 1 µl of 5 mM bis-pNPP solution, dissolved in the mother liquor. Crystals were sampled after 1 hour, 2 hours and overnight.

### 4.10.3 Crystallization of PA0803

Initial crystallization conditions of purified PA0803 were determined using The Classics Suite and The Pegs Suite from Nextal (now Qiagen) with a Mosquito liquid handling robot (TTP Labtech). The protein concentration was screened at 40, 20 and 10 mg/ml by dilution of the protein stock with gel filtration buffer. The screens were set up by sitting drop method, with drops consisting of 1 µl protein and 1 µl precipitant solution. All crystallization trials were carried out at 20°C.

Conditions that produced microcrystalline precipitates were optimized via hanging drop method (1 µl + 1 µl drop size) with respect to precipitant concentration and pH to reduce the amount of nucleation and increase the size and appearance of crystals obtained. Diffraction-quality crystals were obtained with a protein concentration of 40 mg/ml and a reservoir consisting of 100 mM MES pH 6.5 and 36 – 40 % (v/v) PEG 200. Se-Met labeled PA0803 crystals, as well as crystals of PA0803 H49A mutant were obtained at similar conditions.

### 4.10.4 Generation of PA0803-PYO complex crystals

Apo-PA0803 crystals were generated with conditions described in the previous section. The drop is then supplied with 1µl of 1 mM PYO solution, dissolved in the mother liquor. The color of the crystals was inspected under a microscope. A few crystals were

taken out in mounting loops and flash-cooled in liquid nitrogen after 2 hours and tested on the X-ray beam. Since the crystals showed neither apparent change in shape nor loss of integrity, the drop was left in 20 °C for 24 hours before cryo-sampling.

## 4.11 DATA COLLECTION

The precipitant solutions in which the crystals were obtained are themselves cryo-protectants, which allow the crystals to be flash-cooled in liquid nitrogen without further cryo-protection. All data collections were carried out at 100 K. Collection strategies of the datasets used in this report are summarized as Table 4.8.

| Protein | | Beamline* | λ (Å) | Images | Oscillation (°) | Note |
|---|---|---|---|---|---|---|
| PqsE | Native | ESRF ID14-2 | 0.933 | 200 | 0.7 | 10 - 1.6 Å |
| PqsE | Native | ESRF ID14-2 | | 60 | 2.5 | 20 - 3.6 Å |
| PqsE | Native | SLS X10SA | 0.9786 | 140 | 1.0 | XF 2 |
| PqsE | *Se-Met | SLS X10SA | 0.9789 | 100 | 1.0 | *MAD(pk) |
| PqsE | *Se-Met | SLS X10SA | 0.9796 | 100 | 1.0 | *MAD(inf) |
| PqsE | *Se-Met | SLS X10SA | 0.9764 | 719 | 0.5 | *MAD(hr) |
| PqsE | PqsE-M636 | SLS X10SA | 1.0000 | 100 | 1.0 | 10 - 1.8 Å |
| PqsE | PqsE-M636 | SLS X10SA | 1.0000 | 100 | 1.0 | 20 - 2.4 Å |
| PqsE | E182A bis-pNPP | SLS X10SA | 0.9788 | 120 | 1.0 | |
| PA0803 | Native1 | In-house Rigaku | 1.5418 | 206 | 0.5 | 5 - 1.6 Å |
| PA0803 | Native2 | In-house Rigaku | 1.5418 | 480 | 1 | 14 - 3 Å |
| PA0803 | Native3 | In-house Rigaku | 1.5418 | 480 | 1 | 20 - 3.9 Å |
| PA0803 | Native4 | In-house Rigaku | 1.5418 | 500 | 1 | 12 - 3 Å |
| PA0803 | *Se-Met | SLS X10SA | 0.9792 | 270 | 1.0 | SAD |
| PA0803 | PYO | SLS X10SA | 0.9796 | 100 | 1.0 | |
| PA0803 | H49A | In-house Rigaku | 1.5418 | 105 | 0.5 | |

**Table 4.9: Summary of X-ray data collections. Beamline ID14-2 of the ESRF uses a ADSC Q4 CCD detector, while beamline X10SA of the SLS uses a MAR225 CCD detector, and the in-house Rigaku generator uses a MAR345**

**detector. *Abbreviations: Se-Met (seleno-L-methionine derivative protein used for phasing experiments); ESRF (European Radiation Facility, Grenoble, France); SLS (Swiss Light Source, Villigen, Switzerland); XF (Crystal form); MAD (multi-wavelength anomalous dispersion; pk, peak wavelength; inf, inflection wavelength; hr, high-engergy remote wavelength); SAD (single-wavelength anomalous dispersion).**

## 4.12 DATA PROCESSING

### 4.12.1 Data Integration

Integration and scaling of all data were done with the XDS package (Kabsch, 1993). 5% of the total reflections were labeled for calculation of Free-R values and remained the same throughout all datasets in the same space group. A final reflection file in mtz format for each dataset was generated, which was used in the refinement to improve corresponding models.

### 4.12.2 Phase determination

**MAD Phasing of PqsE:** Since phasing via various SAD experiments had not been successful, three data sets were collected at the peak-, inflection- and high energy remote wavelength of Se, to carry out a three-wavelength MAD experiment (Table 4.9). XPREP version 6.09 (Bruker Analytical X-ray Solutions, 2001) was used to extract anomalous differences and to prepare input files for SHELXD (Schneider and Sheldrick, 2002). Four out of five Se atoms were successfully located by SHELXD. The program SHARP (delaFortelle and Bricogne, 1997) was used to refine the position of these Se atoms and generate the initial phases for PqsE. The initial phases were improved by solvent flattening, using the program SOLOMON (Abrahams and Leslie, 1996) and DM (Cowtan, 1994) from the CCP4 suite (Bailey, 1994), as implemented in the SHARP-interface. This allowed for unambiguous determination of the correct hand. The resulting phase set was then transferred to the high resolution native data set and phases were extended to full resolution in DM (Cowtan, 1994).

**SAD Phasing of PA0803:** Sufficient phase information was successfully obtained via the SAD experiment at the peak wavelength: a high redundancy dataset of Se-Met labeled PA0803 was collected at the K-edge of Se (λ of the X-ray tuned to 0.97917Å).

XPREP version 6.09 (Bruker Analytical X-ray Solutions, 2001) was used to extract anomalous differences and to prepare input files for SHELXD (Schneider *et al.*, 2002). Se atoms were located by SHELXD. 13 out of 16 Se atoms, belonging to one of the four chains in the ASU, were successfully located. The program SHARP (delaFortelle *et al.*, 1997) was used to refine the position of these Se atoms and generate the initial phases for PA0803. The initial phases were improved by solvent flattening, using the program SOLOMON (Abrahams *et al.*, 1996) and DM (Cowtan, 1994) in the CCP4 suite (Bailey, 1994).

### 4.12.3 Model building and Refinement

**PqsE:** An initial model was built manually by remodeling a polyalanine version of PDB-entry 1SML, followed by alternating rounds of refinement with REFMAC5 (Murshudov et al., 1997) and manual correction in ONO and COOT. COOT was also used to locate water molecules in the final rounds of refinement. Using TLS-refinement in REFMAC5 the refinement converged at $R_{work}$ = 12.0% and $R_{free}$ = 16.9%. 96.6% of all residues lie in the favored regions of the Ramachandran plot as defined by MOLPROBITY.

A restraint library for bis-pNPP was constructed with the PRODRG server. The complex of the E182A mutant with bis-pNPP was refined to $R_{work}$ = 15.9% and $R_{free}$ = 19.6%, with 96.6% of all residues falling into the favored regions of the Ramachandran diagram.

When the data set for PqsE crystal form 2 became available, molecular replacement was done with the program PHASER from the CCP4 suite to locate the two PqsE monomers in the new ASU. The output PDB coordinates were then put to REFMAC5 for a round of rigid body refinement. This model was used as the starting model for further refinement. Refinement followed the same strategy as employed for crystal form 1, defining each monomer as a TLS-body in REFMAC5. The structure was refined to $R_{work}$ = 15.1% and $R_{free}$ = 21.1%, and 96.7% of all amino acids adopt favored backbone geometry in the Ramachandran plot.

**PA0803:** The electron density map after density modification was of sufficient quality to automatically build 540 residues out of 590 residues in the ASU. The model was refined one round against the high-resolution native dataset in rigid-body mode to generate initial 2fo-fc and fo-fc density maps. The model was then submitted to manual adjustment in

COOT. Combined with maximum-likelyhood refinement of atom positions and B-factors with the program REFMAC5, the model reached $R_{work}$ = 20.8% and $R_{free}$ = 23.6%.

An initial PA0803-PYO model was generated by rigid-body refinement using the coordinates of the apo-structure against the PYO dataset. When refinement converged, restraint libraries were constructed with the PRODRG server. Model of ligands was then incorporated to the apo-structure in further rounds of TLS, position and B-factor refinement until $R_{free}$ dropped to 20.5%.

The H49A mutant structure served the sole purpose of verifying the mutagenesis. A model carrying the mutation was therefore generated from the wildtype model and submitted to a few rounds of refinement against the H49A dataset.

### 4.12.4 Model Validations

The final models were validated by the programs PROCHECK (Laskowski et al., 1993) and ERRAT (Colovos and Yeates, 1993). Several refined structures have been deposited in the Protein Data Bank PDB, together with structure factor amplitudes (crystal form 1, wild type protein: access code 2Q0I; E182A mutant in complex with bis-pNPP: access code 3DH8; crystal form 2: access code 2Q0J).

Similar structures were identified using the Dali Server (Holm et al., 2008). Structure-based alignments (using PDB coordinates) between similar structures was performed using the online server COMPARER (Shindyalov and Bourne, 1998).

## 4.13 BIOCHEMICAL METHODS

### 4.13.1 Binding and turnover tests with potential substrates of PqsE

Various substances from the context of quorum sensing in *Pseudomonas aeruginosa* were tested for binding and turnover with PqsE. Typically, the compound was incubated with PqsE and then analyzed with HPLC and HPLC-MS, comparing to a control sample without PqsE supplement. Usually the control sample was injected first to obtain the rentention time of the compound alone. Then experiment samples were tested, followed by a final injection with the control sample, to ensure that the compound was stable at the

experimental conditions. Alternatively, when the compound had poor UV absorption or when HPLC-MS showed ambiguous results, ITC was used to test the binding.

PQS, pyochelin and cyclic-di-GMP were kind gifts of F. Bredenbruch and M. Mohr, other chemicals were purchased from Sigma, Alfa Aesar, Serva, Acros and Frontier Scientific.

### 4.13.2 Isothermal Titration Calorimetry (ITC)

ITC measurements were performed at 25°C on a MicroCalorimeter system (Microcal Inc.) to obtain the affinity between the protein and its respective ligand. In this study it was also used to probe whether a small molecule ligand can interact with a particular protein. These ligands usually have unfavorable spectrometric properties that make observation via UV/VIS or Fluorescence Spectroscopy difficult. In a typical measurement, the small molecule ligand was dissolved with MilliQ water or gel filtration buffer when appropriate and diluted with gel filtration buffer to a final concentration of 1 mM. For some hydrophobic ligands, DMSO was first used to dissolve the ligand to a high concentration (100 mM to 2M) and then dilute this stock solution with gel filtration buffer to 1 mM. The protein was treated with a buffer exchange with a NAP 5 or NAP 25 column (GE Healthcare) to ensure that it is in exactly the same buffer as the ligand, and then adjusted to a final concentration of 100 µM.

All solutions were degassed prior to loading into the apparatus. The system was allowed to equilibrate for at least 30 minutes and measurements were started with an initial 2 µl injection, followed by injections of 8 µl at 4 minute intervals. Data were analyzed with Origin (OriginLab Corporation).

### 4.13.3 Enzymatic Activity Screen (EAS)

Hydrolases in a particular family usually have detectable activity towards general substrates, which contain the core reaction moiety that the enzyme is able to chemically modify. Utilizing this phenomenon the activity of PqsE was tested against a set of general chromogenic substrates to assess PqsE's hydrolytic capacity. This method was adapted according to Kuznetsova *et al* (Kuznetsova et al., 2005) in attempts to classify PqsE into the family of phosphatases, phosphodiesterases, proteases or esterases. In addition, nitrocefin was included to test PqsE for β-lactamase activity. PqsE was applied at 40 µM concentration

and assays were performed at 25°C to avoid precipitation of the protein. The screens were allowed to react for several hours and then inspected by eye or in a spectrophotometer.

| Enzyme Class | Test Compound | Reaction Conditions |
|---|---|---|
| β-lactamase | 1 mM nitrocefin | 50 mM Phosphate (pH 7.4), 10% Glycerol |
| Phosphatase | 4 mM pNPP | 50 mM HEPES (pH 7.5), 5 mM $Mg^{2+}$, 0.5 mM $Mn^{2+}$ |
| PDE/Nuclease | 0.83 mM bis-pNPP | 50 mM Tricine (pH 8.5), 5 mM $Mg^{2+}$, 0.5 mM $Mn^{2+}$ |
| Esterase | 1 mM pNP-palmitate | 50 mM Tris (pH 8.0), 0.4% Triton X-100 |
| Esterase | 1mM palmitoyl-CoA | 50 mM HEPES (pH 7.5), 0.4% Triton X-100, 1mM DTNB |
| Protease | 0.2 mM BAPNA<br>0.1 mM Leu-pNA | 50 mM HEPES (pH 7.5), 0.5mM $Ca^{2+}$, 0.5 mM $Zn^{2+}$, 1mM DTT |

**Table 4.10: Reactions for classifying enzymatic activities.**

### 4.13.4 Characterization of the PDE activity

Optimum conditions for bis-pNPP hydrolysis were determined by varying pH and metal composition. As a result, subsequent tests were performed in 50 mM Tricine pH 8.5, 2 mM $MnCl_2$. UV-VIS spectroscopy experiments were performed either with a Beckman DU-600 spectrophotometer or a NanoDrop ND-1000 spectrometer. Substances were dissolved to their maximum concentration in $H_2O$ or DMSO, and then diluted with the desired measuring buffer to the final concentration.

**Enzyme kinetics of bis-pNPP hydrolysis:** Enzymatic parameters (the Michaelis-Menten constant $K_M$, turnover number $k_{cat}$ and inhibitions constant $K_i$) for bis-pNPP hydrolysis were determined by varying the substrate concentration (100 µM, 200µM, 500µM, 1 mM, 2mM and 5 mM) and following the absorption of para-nitrophenolate at 405 nm. 10 µM concentration of PqsE protein (wild type with various tags or E182A mutant) was applied at the beginning of each measurement and the reactions were followed for 2 hours with a data point each 45 seconds. The $K_M$ and $k_{cat}$ values were derived from fitting the data with Grafit 5 (Erithacus Software).

**Inhibition assays:** Kinetic parameters for inhibition of PqsE activity by ATP or anthranilate were determined by applying a fixed concentration of inhibitor to a series of

reaction with different substrate concentrations. The reaction set-up was the same as in the hydrolysis assays, with addition of inhibitors. Determination of the inhibition type was carried out by repeating the experiments with a different inhibitor concentration.

**DNA hydrolysis assay:** Potential phosphodiester substrates of PqsE were tested by following the reaction with HPLC, HPLC-coupled ESI mass spectrometry or agarose gel electrophoresis where appropriate. Particularly, hydrolysis of DNA was analyzed by following PqsE digestion of λ phage DNA on agarose gels. Each 20 µl reaction contains 5 µl λ-DNA in 50 mM Tricine buffer pH8.5 and 2mM $MnCl_2$. The reaction was started by adding 1 µl of PqsE protein. Negative controls of this DNA degradation included incubation with reaction buffer only, reaction buffer supplemented with 0.5 mM $FeSO_4$ but excluding PqsE (to exclude DNA degradation due to Fenton chemistry), and reactions including PqsE and EDTA or ATP to inhibit the enzyme.

## 4.14 ANALYSIS OF METAL IN PQSE

### 4.14.1 ICP-MS

Inductively coupled plasma mass spectrometry (ICP-MS) was used to measure the metal content of recombinant PqsE before crystallization. Samples were analyzed on an Element2 instrument from Thermo Electron Corporation equipped with a pneumatic nebuliser (Micromist, Omaha, USA) operating at a sample flow rate of 200 µL/min.

PqsE was applied as concentration of 533 µM, and contents of Mg, Ca, Mn, Fe, Ni, Cu and Zn were measured.

### 4.14.2 Electron Paramagnetic Resonance (EPR)

Recombinant protein (approx. 300 µM) was transferred into 2-mm EPR suprasil quartz tubes, degassed by several freeze−pump−thaw cycles on a vacuum line and sealed under vacuum. X-band (9-10 GHz) continuous wave EPR spectra were recorded on a Bruker Biospin Elexsys E680 EPR spectrometer fitted with a 3-mm split-ring (ER4118X-MS-3-W1) resonator. Calibration of the magnetic field and the microwave frequency were achieved by a Bruker ER035M teslameter and a Bruker microwave frequency counter, respectively. Low temperature measurements were performed in an

Oxford CF-935 helium gas-flow cryostat. The temperature was regulated to +/– 0.1 K by an Oxford Instruments ITC-503 temperature controller. Calibration of the magnetic field for precise g-value determination was performed with a Li:LiF standard.

### 4.14.3 Phenathroline assay

The amount and oxidation state of Fe in a sample solution was also investigated with 1,10-phenanthroline. This compound specifically forms a colored Fe(II)-complex that can be quantified spectrometrically at 512 nm. Calibration with inorganic $Fe(II)(NH4)_2(SO4)_2$ (Mohr's salt) showed very good linear correlation between $OD_{512}$ and Fe concentrations. Protein in 50 mM Tricine pH 8.5 were incubated with 1 mM 1,10-phenanthronline from a 100 mM stock in DMSO in the presence or absenceof 6 M urea to release iron by unfolding, and the absorption at 512 nm was monitored in a UV/Vis-spectrophotometer for 20 – 60 minutes.When the $OD_{512}$ reached a plateau, 2 mM $Na_2S_2O_4$ was added to the sample to reduce Fe(III) to Fe(II). The Fe(III) concentration was obtained by subtracting the Fe(II) concentration from the total Fe concentration.

For PqsE, the Fe(II)/Fe(II) bound form is not stable. Therefore addition of $Na_2S_2O_4$ without urea was sufficient to denature the protein and resulted in the chromogenic reaction. However, this process take about 25 min to reach completion.

### 4.14.4 Metal reconsitution assays

Reconstitution experiments were performed with the E182A-mutant of PqsE, using the bis-pNPP-based PDE test for monitoring activity since this provided the most robust assay. Three different methods were employed to produce reconstituted enzyme.

First, Fe free apo enzyme was prepared by incubation of 100 µM protein with 2 mM $Na_2S_2O_4$ and 1 mM 1,10-phenanthroline, followed by removal of excess reagents with a NAP5 gel filtration column in 50 mM Tricine pH 8.5. The protein was then incubated with 1 mM of various salts, ($CoCl_2$, $CaCl_2$, $MgCl_2$, $CuSO_4$, $CdCl_2$, $ZnSO_4$, $MnCl_2$, $Fe(II)(NH4)_2(SO4)_2$; $Fe(III)(NH4)_3(SO4)_3$), either applied alone or in combination.

Second, 1 – 5 µM of protein in 50 mM Tricine pH 8.5 were carefully titrated with EDTA until the PDE activity was significantly reduced. The required EDTA concentration was 50 µM. For reactivation, the deactivated protein was incubated with 1 mM of the metal ions listed above and PDE activity was reassessed.

Third, 1 – 5 μM of protein in 50 mM Tricine pH 8.5 were incubated with increasing concentrations of $CoCl_2$, $MnCl_2$ or $Fe(II)(NH4)_2(SO4)_2$ and phosphodiesterase activity at saturating bis-pNPP concentration (1 mM) was measured to derive concentration-dependent activation profiles. In order to determine the residual Fe concentration of the $Co^{2+}$-activated enzyme, 100 μM of protein were first incubated with 10 mM $CoCl_2$ on ice for 30 minutes and then passed through a NAP5 column. The Fe content was quantified with 1,10-phenanthroline as described above. In addition, phosphodiesterase activity with and without reincubation with $CoCl_2$ was determined to investigate whether $Co^{2+}$ bound in the initial activation experiment was lost in the reagent removal step.

## 4.15 ANALYSIS OF PYOCYANIN IN MUTANT PAO1 STRAINS

As an *in vivo* test of the PqsE mutants, a plasmid containing wildtype *pqsE* was constructed using the pUCP20 vector as described in Section 4.5.2. Using this plasmid as template, plasmids containing the *pqsE* gene that carry E182A, S273A, H282A, S285A or R288A single mutation were constructed as described in Section 4.6.2. These plasmids were transformed into the *P. aeurginosa* PAO1 *ΔpqsE* mutant to generate the PAO1 pE strains.

Three parallel 5 ml cultures of each strain (*ΔpqsE*, pEw, pE182, pE273, pE282, pE285, pE288) were started from a corresponding overnight culture. In order to obtain reproducible quantification, cultures were placed in identical 25 ml flasks, all started with an $OD_{600}$ of 0.05, and kept in the same 37 °C incubator with 175 rpm of shaking.

After 18 hours of incubation, cultures were centrifuged to remove bacterial cells and supernatants were analyzed as described in the literature (Farrow, III *et al.*, 2008). Briefly, 500 μl aliquots of the supernantants were extracted with 300 μl chloroform. The organic phase was then extracted with 100 μl 0.2 N HCl to give a pink solution containing pyocyanin. The $OD_{520}$ was measured using a NanoDrop ND-1000 spectrophotometer, and the amount of pyocyanin present was calculated by comparison to a calibration curve, generated by measuring solutions with known quantities of pyocyanin (Colour Your Enzyme, Bath, Ontario, Canada). This assay can detect pyocyanin concentration in the range of 10 μM to 300 μM.

## 4.16 TRANCRIPTOME ANALYSIS

GeneChip hybridization and analysis were performed by the Microarray facility of the Helmholtz Institute for Infection Research (Braunschweig). Experiments follow the Affimetrix guidelines and conformed to the MIAME requirements (Minimum Information About a Microarray Experiment). Data were combined with the latest annotation from the website of the *P. aeruginosa* PAO1 sequence and the community annotation project provided at http://www.pseudomonas.com . Preparation of samples for Microarray analysis is described below.

### 4.16.1 Cell preparation

2 ml pre-cultures of *Pseudomonas aeruginosa* PAO1 *ΔpqsE* mutant and the PAO1 pEw strain were started from colonies on freshly spread LB plates. Three 5 ml overnight cultures in LB were started for both strains from these pre-cultures with starting $OD_{600}$ of 0.05.

After 16 hours, the optical density was measured again for each culture. $10^9$ bacteria ($OD_{600}$=1) were then pipetted to a fresh tube and mixed with the same volume of RNA protect buffer (Section 4.1.6), followed by 5 minutes, 8000 rpm centrifugation at room temperature. Supernatant was carefully and thoroughly removed, and pellets were then stored at -80 $^{o}$C for (maximum) overnight.

### 4.16.2 RNA Extration

RNA Extration was performed according to the manuals of Qiashredder column and RNeasy Kit (Qiagen), with some modifications.

- After thawing the bacterial pellets, centrifuge at 8000rpm for 5min and remove any supernatant left.
- Add 200 µL of TE with 800 µg/mL Lysozyme (8 µL of a 20 mg/mL Stock + 192 µL TE pH = 8.0), resuspend the pellet and vortex for 30s. Afterwards incubate for 10min at RT, vortex 2-3 times while incubating.
- Add 700 µL of RTL Buffer with Mercaptoethanol (10 µL Mercaptoethanol + 1 mL RTL Buffer).
- Store at -80°C (maximum overnight, minimum 30min).

- Thaw samples and load onto a Qiashredder column and centrifuge for 2 min at 14.000 rpm (one column per tube).
- Place flow through to a new tube and add 500 µL 96% ethanol.
- Pool tubes originating from one bacteria culture, and load the RNeasy column with 700 µL at the maximum each time and centrifuge each time for 20 s at 14.000 rpm; discard flow through.
- Load column with 700 µL RW1 buffer, incubate for 3 min at room temperatue, then centrifuge for 20 s at 14.000 rpm.
- Place column into a new 2 mL tube and add 500 µl RPE buffer, centrifuge for 20 s at 14.000 rpm.
- Add 500 µL RPE buffer, centrifuge for 2 min at 14.000 rpm, and discard flow through.
- Then centrifuge for 2 min at 14.000 rpm, let column stand for 5 min at room temperature to dry the column.
- Take column to a new 1.5mL tube and add 50 µL of RNase free water, incubate for 5 min and centrifuge for 1 min at 14.000 rpm. Add another 50 µL, incubate and centrifuge again.
- For DNase digestion take 100 µL sample, add 80 µL RNA storage buffer (Section 4.1.6), 20µL DNase buffer (10×), 40 U DNase (4 µL). Mix carefully and incubate for 30 min at 37°C.
- Add 700 µL of RTL Buffer with Mercaptoethanol (10µL Mercaptoethanol + 1mL RTL Buffer).
- Add 500 µL 96% ethanol.
- Purify the RNA again (steps colored blue above), using new RNeasy columns.
- Mix 3 µl sample and 77 µl H2O, measure the RNA concentration using a spectrophotometer (store samples at -80°C). Successful purification gives A260/280 around 1.8 to 2, with expected quantity of 500 ng/µl to1 µg/µl. For cDNA synthesis, combine 2 × 5 µg (from each purification) and adjust with RNase free water up to 20-23 µL.

### 4.16.3 cDNA synthesis

- Combine together 2 different RNA species (obtained out of different columns) in equal quantity in one PCR tube (adjust the quantity of each without adding water). The final volume should be 20 to 23 µL.
- Two to three PCR reactions are enough to yield 10 µg cDNA (out of 10 µg RNA, ideally).
- Prepare a control PCR without enzyme.

| | |
|---|---|
| Total RNA volume | 20µL |
| Random hexamer primers (300ng/µL) | 4µL |

Thermocycler temperature paused at 70°C

***Annealing step:***

| | | |
|---|---|---|
| 70°C | 10 min | (denaturation of RNA secondary structures) |
| 25°C | 10 min | (primers annealing) |

Place immediately on ice

Thermocycler temperature paused at 25°C

| **Master Mix** | **1 rxn** | **3 rxn** | **4 rxn** |
|---|---|---|---|
| 5 × 1st Strand Buffer | 10 µL | 30 µL | 40 µL |
| 100 mM DTT | 5 µL | 15 µL | 20 µL |
| 10 mM dNTP(each) | 3 µL | 9 µL | 12 µL |
| RNase free H2O | 3 µL | 9 µL | 12 µL |
| SuperScript II (Invitrogen) | 5 µL | 15 µL | 20 µL |
| pre-mix total vol. (without RNA template) | 26 µL | | |

Carefully added to each sample (Final rxn volume: 50 µL)

***Reverse transcription step:***

| | |
|---|---|
| 25°C | 10 min |
| 37°C | 60 min |
| 42°C | 60 min |
| 70°C | 15 min |

- Add 10 µL H2O to the cDNA samples.
- Add 20 µL 1N NaOH and incubate for 30min at 65°C in a Thermocycler to denature the RNA.
- Neutralize with 20 µL 1N HCl and purify with Qiagen PCR purification Kit.
- Pool the reactions into one tube and add 500 µL of PB buffer, mix carefully.

- Load the column with the sample (the control reaction goes to an extra column) and centrifuge at 13.000rpm for 1min.
- Discard flow through and add 750 µL PE buffer, centrifuge for 1min at 13.000 rpm.
- Discard flow through and centrifuge for 2 min at 13.000 rpm.
- Take column to another tube and let it dry for 5 min at room temperature.
- Add 45 µL of water to the column and let it stand for 5 min, then centrifuge for 2 min at 13.000 rpm.
- Repeat the previous step once more.
- Photometric measurement of cDNA quantity: A260/230 should be around 2; and A260/280 around 1.7-1.8.

### 4.16.4 cDNA fragmentation

- Run first a test fragmentation reaction using 10 µL of cDNA.
- The quantity of enzyme can be adjusted btween 0.35 U/µg cDNA and 0.45 U/µg cDNA.
- Pre-heat Thermocycler to 37°C and pipette the DNase just before putting the tube(s) in the block.
- Incubate 9 min 37°C, 10 min 98°C and keep at 4°C.
- Check the fragmentation by performing a 2% agarose gel electrophoresis using 50 bp marker.
- Fragment size should be between 200 und 50 bp.
- The main fragmentation reaction will be performed with 40 µl cDNA + 5 µl Buffer and DNase.

### 4.16.5 Terminal Labeling

| ***Mix*** | |
|---|---|
| 5 ×Reaction Buffer | 12 µl |
| 10 × $CoCl_2$ | 6 µl |
| Biotin-ddUTP | 1 µl |
| Fragmentation Product | 39 µl |
| $H_2O$ | 1 µl |
| Terminal Deoxynucleotide Transferase | 1 µl |

- Incubate 60 min at 37°C.
- Stop the reaction by adding 2µl of a 0.5 M EDTA pH 8.0 solution.
- Mix 5 µl of the biotin labeled DNA fragments with 5 µl NeutrAvidin solution (400 µg in 100 µl 50 mM Tris pH 7.0).
- Leave at room temperature for 5min.
- Check the labeling by running the NeutrAvidin coupled DNA in a 2% agarose gel.

## 4.17 FIGURE PREPARATION

Figures of structural models were prepared using the program PYMOL (DeLano Scientific). Chemical structures and related reactions/schemes were made with ChemDraw Ultra 10.0 (Cambridgesoft). Schemes of biological systems were drawn with CORELDRAW (Corel Corporation). The anomolous Patterson map was generated using XPREP. Topology diagrams were drawn with TOPDRAW from the CCP4 suite (Bailey, 1994) and edited in CORELDRAW. Contacting amino acids in the PA0803 dimer interface were identified using the CCP4 program CONTACT.

Final figures were adjusted for printing with PHOTOSHOP CS3 (Adobe).

# 5 RESULTS AND DISCUSSION

Given that two unrelated proteins, PqsE and PA0803, were studied in this work, the results are organized into 3 parts. The first part presents the experimental results from structure determination of both proteins; the second part presents and discusses the results from analyzing the PqsE structure and biochemical assays; and the third part presents and discusses the results from structural and biochemical analysis of PA0803.

# PART I

# STRUCTURE DETERMINATIONS

## 5.1 SEQUENCE ANALYSIS

### 5.1.1 General analysis

At the beginning of this research, the only available information was the primary sequence of PqsE and PA0803, retrieved from the *Pseudomonas* sequence database (Winsor *et al.*, 2009). It was deduced that PqsE is a cytoplasmic protein (Nakai and Kanehisa, 1991) with molecular weight of 34306.2 Da and theoretical pI of 5.34 (Gasteiger *et al.*, 2003); whereas PA0803 is a protein with molecular weight of 15863.7 Da, theoretical pI of 5.03 but unknown cellular location. PqsE has five methionine residues out of a total of 301, while PA0803 has four methionines out of 146, suggesting that seleno-methionine substitution is the method of choice for heavy-atom phasing.

### 5.1.2 Threading

The fold of a protein often provides insights to its functions or properties. It is therefore interesting to predict the folding prior to purification and crystallization trials. Sequences of PqsE and PA0803 were submitted to a fold recognition server (Kelley and

Sternberg, 2009), which analyzes the sequences for secondary structure elements and then search as the PDB for proteins that have similar arrangement of secondary structures. The best hits are listed as Table 5.1, indicating that PqsE belongs to the metallo-β-lactamase type fold, while PA0803 belongs to the Glyoxalase/bleomycin resistance protein type fold.

| PDB ID | Description | E-Score | Sequence identity |
|---|---|---|---|
| ***PqsE*** | | | |
| 1K07 | Zn metallo-β-lactamase | 3.3e-22 | 10% |
| 2QMN | Zn metallo-β-lactamase | 3.7e-22 | 10% |
| 1SML | Zn metallo-β-lactamase | 4.4e-22 | 13% |
| 2OBW | Glyoxalase II | 2e-19 | 16% |
| 1XM8 | Glyoxalase II | 2.5e-19 | 15% |
| ***PA0803*** | | | |
| 2P25 | Glyoxalase family protein | 1.7e-13 | 13% |
| 1QIP | Human Glyoxalase I | 5.7e-13 | 13% |
| 2QNT | Structural Genomics, unknown function | 8.7e-13 | 17% |
| 1KLL | Antibiotic resistance protein | 1.2e-12 | 16% |
| 2PJS | bleomycin resistance protein | 1.4e-12 | 18% |

**Table 5.1: Results from Phyre server, for PqsE/PA0803 each, five top hits (predicted most similar fold) are listed, sorted descending from top by the Phyre server E-score (a score for prediction accuracy, falls between 0 and 1; an E-score of 0.05, e.g., indicates a 5% probability that the prediction is wrong).**

## 5.2 PROTEIN EXPRESSION AND PURIFICATION

### 5.2.1 Purification of PqsE

The 301-amino-acid full length PqsE was expressed as various fusions with N-terminal affinity tags. In a typical purification via affinity chromatography and gel filtration at least 95% pure protein could be obtained. Among various methods, nickel affinity purification gives the best yield of > 30mg per liter of culture. (Figure 5.1).

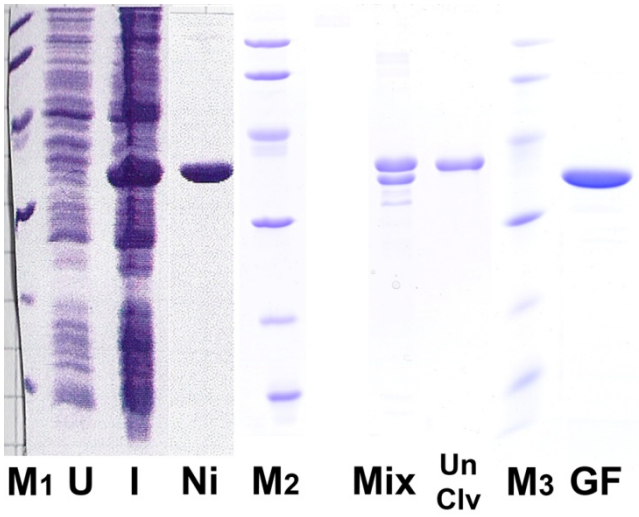


**Figure 5.1: PqsE was expressed in *E. coli* as a His-Tag fusion protein and purified using affinity chromatography. $M_1$: Marker1; U: Un-induced culture; I: Induced culture; Ni: After $Ni^{2+}$ affinity column; $M_2$: Marker2; Mix: 1 to 1 mixture of cleaved PqsE and Uncleaved PqsE; UnClv: Un-cleaved PqsE; $M_3$: Marker3; GF: After gel filtration.**

### 5.2.2 Purification of PA0803

The 146-amino-acid full length PA0803 was expressed with an N-terminal His-tag. In a typical purification via Ni-affinity chromatography and gel filtration at least 95% pure protein could be obtained with yield of > 50mg per liter of culture. (Figure 5.2).

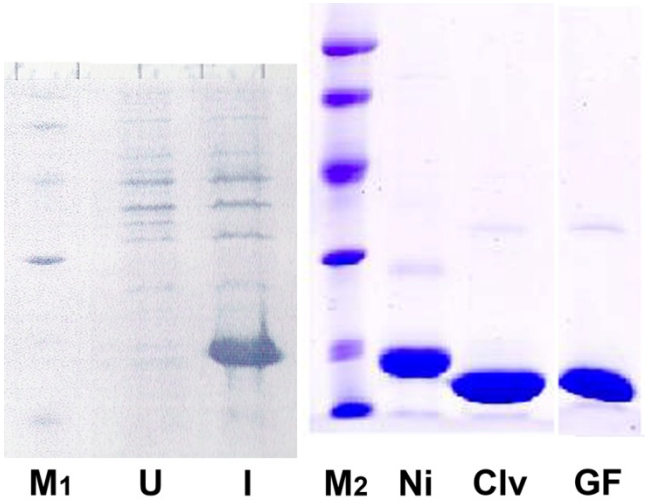


**Figure 5.2: PA0803 was expressed in *E. coli* as a His-Tag fusion protein and purified using affinity chromatography. $M_1$: Marker1; U: Un-induced culture; I: Induced culture; $M_2$: Marker2; Ni: After $Ni^{2+}$ affinity column; Clv: After TEV-cleavage and the 2nd Ni column; GF: After gel filtration.**

## 5.3 GEL FILTRATION

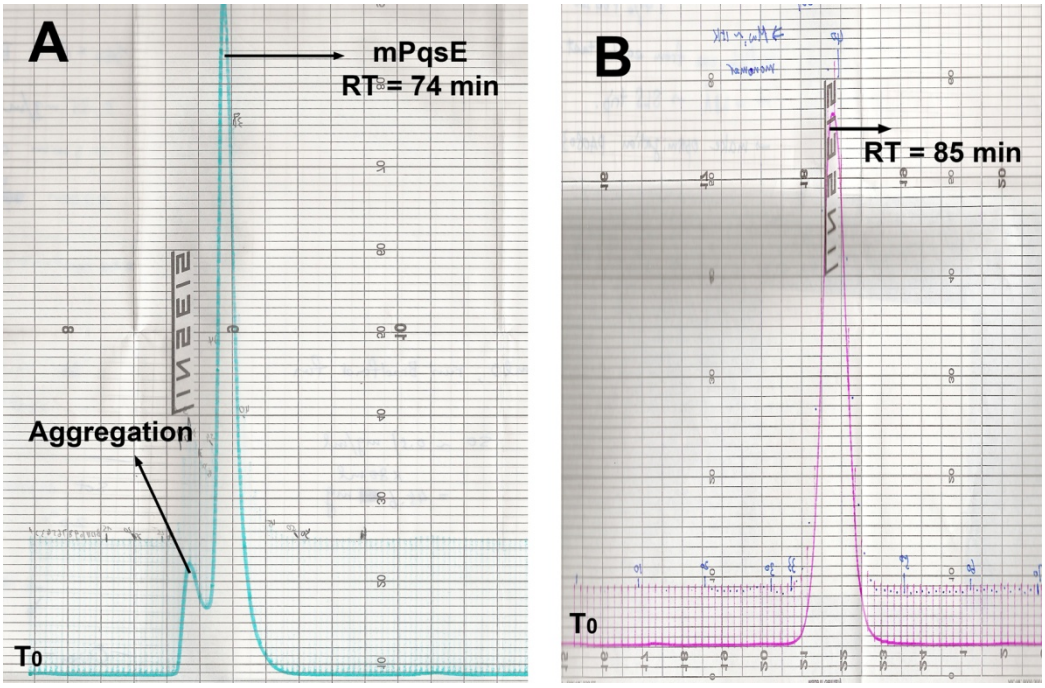


**Figure 5.3: Gel filtration chromatogram of PqsE (a) and PA0803 (b). $T_0$: starting time. RT: retention time (converted to 2 ml/min flowrate).**

The PqsE peak eluted with a retention time (RT) of 74 min (Figure 5.3A) on a Superdex G75 HR (26/60) column (GE Healthcare). The corresponding molecular weight is 45 kDa, estimated from the calibration curve. It is close to 1.5 times the molecular weight of the PqsE monomer (35 kDa). This indicates that PqsE is a monomer in solution.

The PA0803 peak eluted with a retention time of 85 min (Figure 5.3B) on an analytical Superdex G75 HR (26/60) column (GE Healthcare). The corresponding molecular weight is 30 kDa, estimated from the calibration curve. It is close to twice the molecular weight of the PA0803 monomer (14 kDa). This indicates that PA0803 is a dimer in solution.

## 5.4 CRYSTALLIZATION

### 5.4.1 Crystallization of PqsE

From the initial screen, a condition containing PEG400 as precipitant (0.1 M HEPES buffer pH7.5, 0.2 M $MgCl_2$, 30% v/v PEG400) yielded hexagonal-shaped crystals (crystal from 1) that looked most promising and was therefore selected for further optimization. The size and shape of the crystals was improved by varying pH and PEG concentration of this condition (Figure 5.4A). These crystals were flash cooled in liquid nitrogen and exposed to X-rays at 100K. Crystals (XF1) diffract to 2.1 Å in house and were sent to the synchrotron for data collection.

In the process of optimizing crystal form 1, decay of the diffraction quality was observed. Crystals diffracted to ~2.1 Å in the first 3 days, 2.6~2.8 Å after a week, dropping to about 4 Å after 2-3 weeks. Addition of 1mM TCEP to purified protein slowed the decay process to some extend. The cause of the decay might be sensitivity to oxygen, as it is later found out that PqsE possesses a di-nuclear Fe center. This hypothesis is supported with observations that PqsE stored at -80 °C for a long period also gave poor crystals. Therefore, fresh purifications of the protein were typically carried out for activity tests and further crystallization experiments.

As the PqsE structure determined in space group $P3_221$ has an unexpected bound ligand, it is plausible to assume that the protein is in a closed conformation. Additional crystallization trials were therefore setup, in search for alternative space groups that might trap PqsE in a different conformation. Plate-shaped crystals were found using sodium acetate (NaAc) as a precipitant. Optimization of the condition led to thicker plate shaped crystals which diffracted to approximately 2.5 Å on a home-source rotating anode and 2.1 Å at the synchrotron.

Because the PqsE E182A mutant catalyzes the hydrolysis of bis-pNPP, incubation of PqsE with bis-pNPP resulted in turn-over of the substrate molecule as indicated by the color change of the drop (from colorless to yellow). Therefore the soaking method was chosen to obtain a complex structure of PqsE with the bis-pNPP substrate, taking advantage of the slow kinetics of the hydrolysis. Using the condition yielding crystal form 1, fresh PqsE crystals were prepared and soaked with a mother liquor containing bis-pNPP. These crystals

diffracted to 1.8 Å at the synchrotron. The PqsE-M636 complex was obtained in similar manner, because M636 dissolves relatively well in water (~20 mM).

Selenomethionine-labeled PqsE was crystallized for phasing by the Multi-wavelength Anomalous Dispersion method and crystallized using the same conditions as the native protein, crystal form 1. These crystals diffracted to 3.0 Å in house and 2.5 Å at the synchrotron.

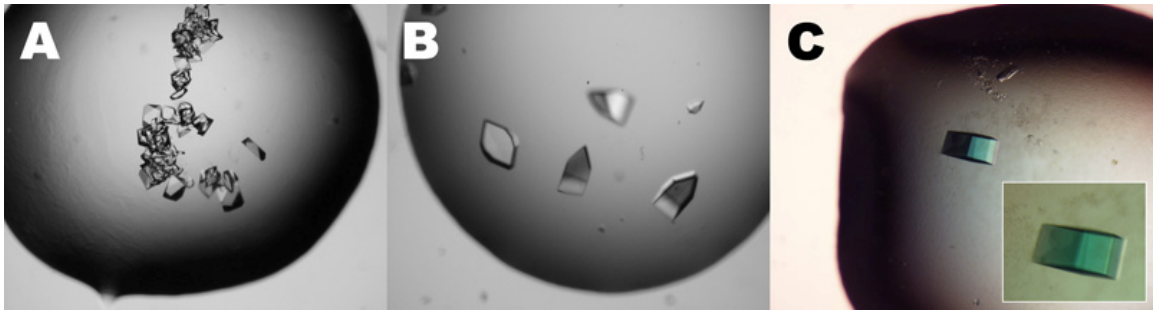


**Figure 5.4: Photos of crystals presented in this report. A) Crystal of wildtype PqsE, XF1 B) Crystal of wildtype PA0803 C) A PA0803 crystal soaked in 1mM pyocyanin and washed in a back-soak solution which contains no pyocyanin, an enlarged view is shown in the box. The crystal was visibly blue.**

### 5.4.2 Crystallization of PA0803

In the initial screen, a condition with PEG200 as precipitant (0.1 M MES buffer pH 6.5, 40% v/v PEG200) yielded promising orthorhombic-shaped crystals. Optimization by varying the pH and PEG concentration reduced number of nucleation and generated large crystals with smooth surfaces (Figure 5.4B). These crystals were tested for diffraction in house. They were flash cooled in liquid nitrogen and exposed to X-rays at 100K. Crystals diffract to 1.6 Å in house and a native dataset were collected.

After the structure of the wild-type protein was determined, a site-directed mutagenesis experiment was carried out. Residue H49 was mutated to alanine and crystals were grown under similar conditions.

Selenomethionine-labeled PA0803 was crystallized for phasing by the Single-wavelength Anomalous Dispersion method using the same condition as the native protein. These crystals diffract to 3.0 Å in house and 2.5 Å at the synchrotron.

To obtain crystals of pyocyanin-bound PA0803, both the co-crystallization and soaking method were tried. Co-crystallization of PYO-PA0803 did not give crystals in the condition described above, neither in a new round of screening. On the other hand, soaking

apo-PA0803 crystals overnight in a mother liquer supplied with 1 mM PYO produced blue-colored crystals after back-soaking for 30 seconds in a drop without PYO (Figure 5.4C). The crystals diffracted to 2.2 Å in house and were sent to synchrotron for data collection.

## 5.5 STRUCTURE DETERMINATION

### 5.5.1 Data Collection Statistics

The native crystals of PqsE diffracted to a maximum resolution of 1.6 Å at ESRF and belong to the trigonal space group $P3_221$ with unit cell dimensions of 61.06 Å, 61.06 Å, 145.51 Å; 90°, 90°, 120°. A Matthew's coefficient (Matthews, 1968) of 2.24 $Å^3$/Da was calculated, which corresponds to only one molecule in the asymmetric unit (ASU) with approximately 45% solvent content.

The Se-Met labeled PqsE crystals, PqsE E182A crystals, PqsE-M636 complex and PqsE E182A-bispNPP complex all have almost identical cell dimensions as above.

The $P2_1$ crystal form has unit cell dimensions of 44.76 Å, 66.09 Å, 110.26 Å; 90°, 97.19°, 90°. Matthew's coefficient (Matthews, 1968) calculations of 1 – 3 molecules per ASU were performed. Only that of two molecules per ASU, 2.31 $Å^3$/Da, corresponds to a reasonable value of 46.8% solvent content.

The native crystals of PA0803 diffracted to a maximum resolution of 1.6 Å in house and have an orthogonal space group $P2_12_12$ with unit cell dimensions of 84.9×101.4×92.6 $Å^3$. The Matthew's coefficient (Matthews, 1968) corresponding to 1 – 10 molecules per ASU was calculated. Those of 4-6 molecules per ASU, 3.14-2.09 $Å^3$/Da, correspond to reasonable values of 60.8%-41.3% solvent content. The Se-Met labeled PA0803 crystals have almost identical cell dimensions.

PA0803 H49A crystals are in another space group $P4_32_12$, with a unit cell dimension of 96.6×96.6×84.0 $Å^3$. Matthew's coefficient (Matthews, 1968) corresponding to 1 – 5 molecules per ASU was calculated. Those of 2 or 3 molecules per ASU, 3.09 or 2.09 $Å^3$/Da, correspond to reasonable values of 60.2% or 40.3% solvent content.

Data collection statistics for all crystals reported here are summarized in Table 5.2.

**Table 5.2**

| Nr. | Resolution (Å) | High-res Shell (Å) | R-merge % | Reflections | Completeness (%) | Redundancy | <I/σ(I)> | B ($Å^2$) | Note |
|---|---|---|---|---|---|---|---|---|---|
| PqsE_1 | 20-1.57 | 1.67-1.57 | 4.1 (21.4) | 372797 | 98.6 (92) | 8.4 | 23.9 (6.5) | 27.1 | Native, XF1 |
| PqsE_2 | 20-2.1 | 2.2-2.1 | 11.2 (21.4) | 109061 | 97.8 (97.5) | 3.0 | 13.7 (4.9) | 32.2 | XF2 |
| PqsE_3 | 20-2.5 | 2.6-2.5 | 9.7 (38.5) | 66938 | 99.8 (99.9) | 3.2 | 13.2 (3.8) | 47.3 | Se-Met (pk) |
| PqsE_4 | 20-2.5 | 2.6-2.5 | 9.8 (38.9) | 66942 | 99.8 (100) | 3.2 | 12.8 (3.7) | 47.4 | Se-Met (inf) |
| PqsE_5 | 20-2.45 | 2.5-2.45 | 7.3 (39.3) | 256583 | 99.8 (100) | 11.7 | 25.5 (7.3) | 46.7 | Se-Met (hr) |
| PqsE_6 | 20-1.8 | 1.9-1.8 | 5.6 (36.1) | 245922 | 99.5 (99.6) | 8.1 | 19.5 (4.7) | 37.1 | PqsE-M636 |
| PqsE_7 | 20-1.8 | 1.9-1.8 | 6.3 (37.7) | 206108 | 99.5 (100) | 6.9 | 17.1 (4.5) | 33.8 | E182A:bis-pNPP |
| PA0803_1 | 20-1.6 | 1.7-1.6 | 7.2 (32.6) | 1125803 | 98.4 (92.9) | 10.7 | 18.1 (3.6) | 25.5 | Native |
| PA0803_2 | 20-1.7 | 1.8-1.7 | 6.5 (39.8) | 795912 | 86.7 (49.8) | 5.4 | 15.7 (2.8) | 27.9 | Se-Met (pk) |
| PA0803_3 | 20-1.7 | 1.8-1.7 | 6.8 (38.5) | 353094 | 99.5 (99.8) | 4.0 | 15.5 (3.4) | 30.1 | PA0803:PYO |
| PA0803_4 | 20-2.2 | 2.3-2.2 | 9.4 (14.2) | 79432 | 97.0 (81.7) | 3.94 | 17.3 (8.4) | 22.4 | H49A |

**Table 5.2: Data collection statistics. For the SeMet data Friedel pairs were treated as separate observations. High-res Shell: highest resolution shell.** $R_{sym} = \Sigma \mid I(h)j - \langle I(h)\rangle \mid / \Sigma I(h)j$ where I(h)j is the scaled observed intensity of the i-th symmetry related observation of reflection h and <I(h)> is the mean value

### 5.5.2 Phasing Statistics for PqsE

A Patterson map was calculated using the anomalous differences of the derivative data to find Se atoms. The Harker sections showed clear peaks above 1.5σ (Figure 5.5B), indicating the presence of at least four Se atoms in each ASU.

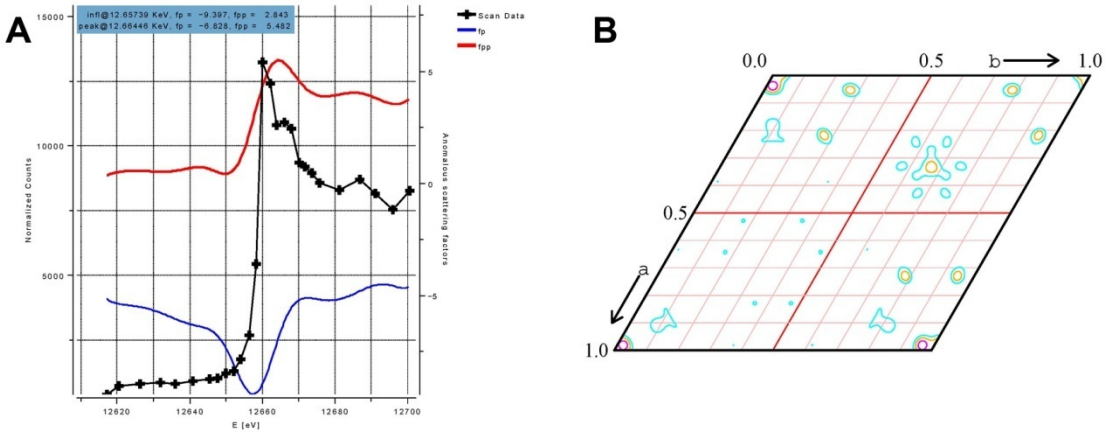


**Figure 5.5: Phasing of PqsE. A) X-ray fluoresence scan of the Se-Met crystal. Experimental f' and f'' values are measured. B) Patterson section Z=0.333 for SAD delta (F): Space group $P3_221$; +Y down; +Z cross; 256 × 256 Grid; contour level 1.5 sigma.**

A heavy atom search was then carried out with SHELXD. It successfully located all five selenium atoms with Patterson figure of merit (PATFOM) of 25.92 and correlation coefficient (CC) of 51.61/40.99 for all and weak reflections, respectively. These statistics suggested that the substructure of Se atoms was successfully determined with high probability. Based on the coordinates of the Se atoms, initial protein phases were calculated with the program SHARP, using experimentally determined f' and f'' values (Figure 5.5A). MAD data was used from 20 – 2.5 Å. The initial phase, which has an overall FOM of 0.533, was then improved by solvent flattening using the programs SOLOMON and DM. The solvent content was set to 43%. Statistics of the first cycle of solvent flattening clearly indicated that the inverted hand was the correct one, whose overall correlation was significantly higher than that of the other hand (0.2849 vesus 0.1052). Phasing statistics are summarized in Table 5.3.

***Fluorescence Scan*** (Figure 5.5A)

| | E (eV) | f' | f'' |
|---|---|---|---|
| Remote | 12697.61 | -5.13 | 3.67 |
| Inflection | 12657.25 | -7.95 | 1.21 |
| Peak | 12665.00 | -6.25 | 3.37 |

***Phasing Statistics of the last SHARP cycle***

| | | |
|---|---|---|
| FOM | | 0.5381 |
| Highest resolution shell (2.05-2.00Å) | | 0.2798 |
| Phasing power (acentrics) anomalous of HR dataset | | 1.989 |
| Highest resolution shell (2.05-2.00Å) | | 0.528 |
| Phasing power (acentrics) anomalous of PK dataset | | 0.929 |
| Phasing power (acentrics) isoomorphous of INF dataset | | 0.868 |
| Phasing power (centrics) isoomorphous of INF dataset | | 0.747 |
| Cullis R-factor (acentrics) anomalous of HR dataset | | 0.647 |
| Highest resolution shell (2.56-2.50Å) | | 0.951 |
| Cullis R-factor (acentrics) anomalous of PK dataset | | 0.808 |
| Cullis R-factor (acentrics) isomorphous of PK dataset | | 0.856 |
| Cullis R-factor (centrics) isomorphous of PK dataset | | 0.846 |
| Cullis R-factor (acentrics) anomalous of INF dataset | | 0.910 |
| Cullis R-factor (acentrics) isomorphous of INF dataset | | 0.809 |
| Cullis R-factor (centrics) isomorphous of INF dataset | | 0.783 |
| ***Statistics from the first solvent flattening cycle*** | Uninverted hand | Inverted hand |
| Contrast | 0.6448 | 0.7354 |
| Overall R-factor R0 | 0.4858 | 0.5426 |
| R-factor | 0.4860 | 0.5420 |
| Overall Correlation | 0.2849 | 0.1052 |

**Table 5.3: Phasing statistics of PqsE.**

### 5.5.3 Phasing Statistics for PA0803

Like in the case of phasing PqsE, a Patterson map was calculated using the anomalous differences of the derivative data to find Se atoms. The Harker sections showed clear peaks above 2σ (Figure 5.6B), which were used subsequently to locate heavy atom positions.

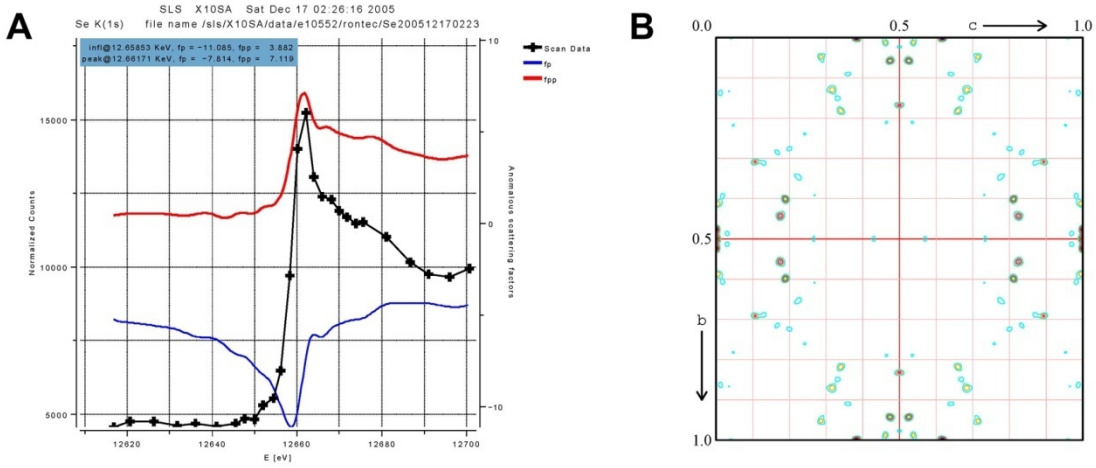


**Figure 5.6: Phasing of PA0803. A) X-ray fluoresence scan of the Se-Met crystal. Experimental f' and f'' values are measured. B) Patterson section X=0.5 for SAD delta (F): Space group $P2_12_12$; +Y down; +Z cross; 256 × 256 Grid; contour level 2 sigma.**

A heavy atom search was then carried out with SHELXD. It successfully located 13 out of 16 expected selenium atoms with Patterson figure of merit (PATFOM) of 11.8 and correlation coefficient (CC) of 51.7/33.3 for all and weak reflections, respectively. These statistics suggested that the Se-atom substructure was determined successfully with high likelyhood. Based on the coordinates of the Se atoms, initial protein phases were calculated using program SHARP, using experimentally determined f' and f'' values (Figure 5.6A). SAD data was used from 20 – 2 Å. The initial phase, which has an overall FOM of 0.533, was then improved by solvent flattening using the programs SOLOMON and DM. The solvent content was set to 60%. Statistics of the first cycle of solvent flattening clearly indicated that the inverted hand was the correct one, whose overall correlation was significantly higher than that of the other hand (0.4107 vesus 0.2061). Phasing statistics are summarized in Table 5.4.

| | | | |
|---|---|---|---|
| ***Fluorescence Scan*** (Figure 5.6A) | | | |
| | E (eV) | f' | f'' |
| Inflection | 12658.53 | -11.085 | 3.882 |
| Peak | 12662.51 | -7.814 | 7.119 |
| ***Phasing Statistics of the last SHARP cycle*** | | | |
| FOM | | | 0.5330 |
| Highest resolution shell (2.05-2.00Å) | | | 0.4045 |
| Phasing power (acentrics) anomalous | | | 3.133 |
| Highest resolution shell (2.05-2.00Å) | | | 1.641 |
| Cullis R-factor (acentrics) anomalous | | | 0.440 |
| Highest resolution shell (2.05-2.00Å) | | | 0.719 |
| ***Statistics from the first solvent flattening cycle*** | | Uninverted hand | Inverted hand |
| Contrast | | 0.6656 | 0.6020 |
| Overall R-factor R0 | | 0.5021 | 0.4376 |
| R-factor | | 0.4980 | 0.4350 |
| Overall Correlation | | 0.2061 | 0.4107 |

**Table 5.4: Phasing statistics of PA0803.**

### 5.5.4 Refinement Statistics for PqsE

Determination of the correct hand was confirmed by inspection of the electron density maps after solvent flattening. The electron density of the correct hand is well connected and showed a clearly defined protein molecule from the N-terminal to L298, with only 3 residues at the C-terminal invisible. A serine and a histine residue, originating from the expression vector, were also observed in the electron density at the N-terminus. Refinement was carried out using the program REFMAC5. After a round of initial rigid body refinement, the model was improved by several rounds of TLS (translation, libration,

screw-rotation displacement), individual B-factor (temperature factor, showing flexibility of the atom) and positional refinement together with manual adjustment. Then the model of the co-purified ligand (benzoate, Figure 5.14) and waters were added to the model, followed by a few rounds of refinement. At last, alternative conformations, which can be observed at this resolution, were built manually where necessary. The wildtype PqsE XF1 structure was refined to $R_{work}$ = 12.0% and $R_{free}$ = 16.9%. 96.6% of all residues lie in the favored regions of the Ramachandran plot. XF 2 was phased by molecular replacement using the protein model of crystal form 1. The structure was refined to $R_{work}$ = 15.1% and $R_{free}$ = 21.1%, and 96.7% of all amino acids adopt favored backbone geometry in the Ramachandran plot (Figure 5.7).

For protein-ligand complex structures, a round of rigid-body refinement with the model for apo-wildtype PqsE was sufficient to give interpretable 2fo-fc and fo-fc densities, on which further refinement of each structure was based. After a few rounds of manual adjustment, the ligand and waters were incorporated into the electron density and the model was submitted for B-factor and positional refinement. The complex of PqsE with synthetic ligand M636 was refined to $R_{work}$ = 17.8% and $R_{free}$ = 21.9%, with 96.6% of all residues falling into the favored regions of the Ramachandran diagram. The complex of the E182A mutant with bis-pNPP was refined to $R_{work}$ = 15.9% and $R_{free}$ = 19.6%, with 96.6% of all residues falling into the favored regions of the Ramachandran diagram (Figure 5.7).

Refinement statistics of PqsE are summarised in Table 5.5.

| | wt XF1 | wt XF2 | E182A-bispNPP | M636 |
|---|---|---|---|---|
| Resolution (Å) | 52.7 – 1.57 | 20 – 2.1 | 20 – 1.8 | 20 – 1.8 |
| Unique reflections | 44378 | 36641 | 28614 | 28767 |
| Test set reflections | 2236 | 1854 | 1495 | 1472 |
| Amino acids | 303 | 611 | 303 | 298 |
| Protein atoms | 2458 | 4854 | 2411 | 2372 |
| Ligand molecule (atoms) | 1 (9) | 2(18) | 1 (23) | 1 (17) |
| Metal ions | 2 | 4 | 2 | 2 |
| Total non-H atoms | 2469 | 4876 | 2661 | 2566 |
| $H_2O$ | 346 | 376 | 224 | 175 |
| ***R Value*** | | | | |
| Working set (%) | 12.2 | 15.1 | 15.6 | 17.8 |
| Working+Test set (%) | 12.0 | 15.4 | 15.8 | 18.0 |
| Test set ($R_{free}$, %) | 16.9 | 21.1 | 19.6 | 21.9 |
| Highest Resolution Shell (Å) | 1.57 – 1.61 | 2.15 – 2.1 | 1.85 – 1.8 | 1.85 – 1.8 |
| $R_{work}$ (%) | 10.8 | 16.1 | 16.0 | 17.4 |
| $R_{free}$ (%) | 20.4 | 23.6 | 25.8 | 24.5 |
| Mean B value (Overall, $Å^2$) | 18.03 | 25.76 | 25.65 | 27.29 |
| ***RMSD from ideal values*** | | | | |
| Bond length (Å) | 0.027 | 0.019 | 0.027 | 0.026 |
| Bond angle (°) | 2.089 | 1.731 | 2.207 | 2.160 |

**Table 5.5: Refinement statistics of the PqsE models.**

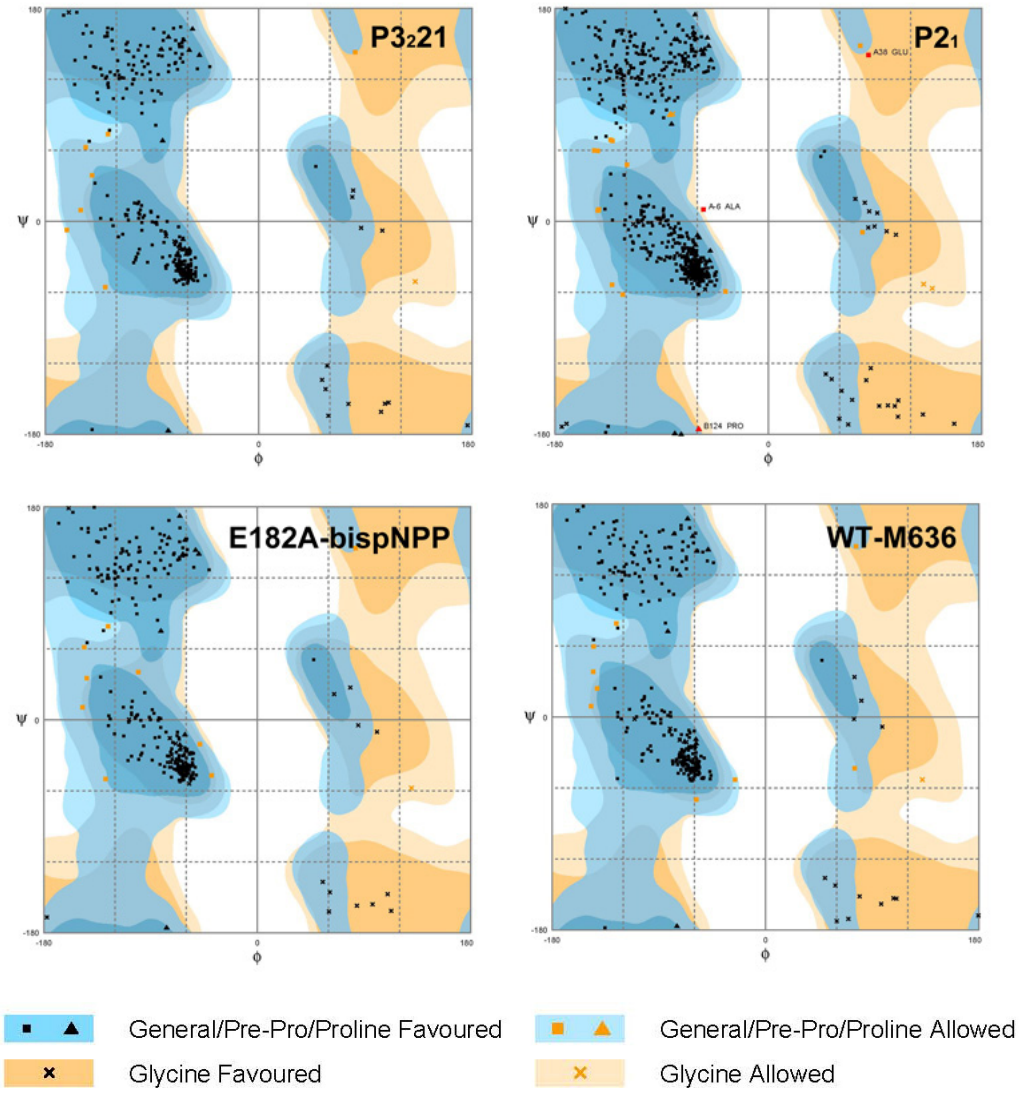


**Figure 5.7: Ramachandran plot showing the torsion angles of all peptide bonds of the major conformations of the PqsE models used in this report. More than 96.5% of all amino acids have torsion angles in the most favoured region in all models. Only 3 residues (0.5%) in the relative low resolution XF2 model are in the outlier region. The plot was generated using the program RAMPAGE from the CCP4 suite.**

### 5.5.5 Refinement Statistics for PA0803

Determination of the correct hand was confirmed by inspection of the electron density maps after solvent flattening. The electron density of the correct hand is well connected and showed clearly defined four polypeptide chains , with only a flexible loop $G_{42}$-$E_{43}$-$D_{44}$-$G_{45}$ not visible on the density. Refinement was carried out using the program REFMAC 5. After a few rounds of initial rigid body refinement, the model was improved by several rounds of TLS (translation, libration, screw-rotation displacement), individual B-factor (temperature factor, showing flexibility of the atom) and positional refinement together with manual adjustment. The binding sites were identified because electron density showed binding of PEG200 to the protein. These ligands and waters were added to the model, followed by a few rounds of refinements. At last, alternative conformations were then built manually where necessary. The final model has an $R_{work}$ of 16% and an $R_{free}$ of 20%.The Ramachandran plot shows no residues in the disallowed region (Figure 5.8).

For the pyocyanin complex structure, a round of rigid-body refinement with the model of apo-PA0803 (PEG200 molecules removed) was sufficient to give interpretable 2fo-fc and fo-fc densities, which further refinement was based on. After a few rounds of manual adjustment and REFMAC 5 refinement, density at the active site was inspected. Only 1 out of 4 sites showed density that resembles the shape of pyocyanin, while the others remained as PEG200. Ligands were then incorporated into the model, followed by a few further rounds of refinement. The final model has an $R_{work}$ of 17% and an $R_{free}$ of 20.5%. The Ramachandran plot shows no residues in the disallowed region (Figure 5.8).

For the mutant H49A structure, a round of rigid-body refinement with the model for wildtype PA0803 was sufficient to give interpretable 2fo-fc and fo-fc densities, which further refinement was based on. Waters were incorporated into the electron density and the model was submitted for B-factor and positional refinement. Refinement statistics of PqsE are summarised in Table 5.6.

| | Wild Type | PYO | H49A |
|---|---|---|---|
| Resolution (Å) | 20 – 1.66 | 20 – 1.7 | 20 – 2.3 |
| Unique reflections | 90486 | 83500 | 17172 |
| Test set reflections | 4818 | 4447 | 889 |
| Amino acids | 574 | 578 | 286 |
| Protein atoms | 4425 | 4531 | 2186 |
| Ligand molecule (atoms) | 4 (52) | 8 (107) | 3 (39) |
| Total non-H atoms | 5201 | 5109 | 2415 |
| $H_2O$ | 724 | 471 | 190 |
| ***R Value*** | | | |
| Working set (%) | 15.8 | 16.6 | 17.8 |
| Working+Test set (%) | 16.0 | 16.8 | 18.1 |
| Test set ($R_{free}$, %) | 20.2 | 20.5 | 23.5 |
| Highest Resolution Shell (Å) | 1.70 – 1.66 | 1.74 – 1.70 | 2.36-2.3 |
| $R_{work}$ (%) | 16.8 | 23.0 | 24.1 |
| $R_{free}$ (%) | 23.0 | 28.7 | 31.4 |
| Mean B value (Overall, $Å^2$) | 18.69 | 18.37 | 16.60 |
| ***RMSD from ideal values*** | | | |
| Bond length (Å) | 0.026 | 0.029 | 0.019 |
| Bond angle (°) | 2.237 | 2.396 | 1.808 |

**Table 5.6: Refinement statistics of the PA0803 models.**

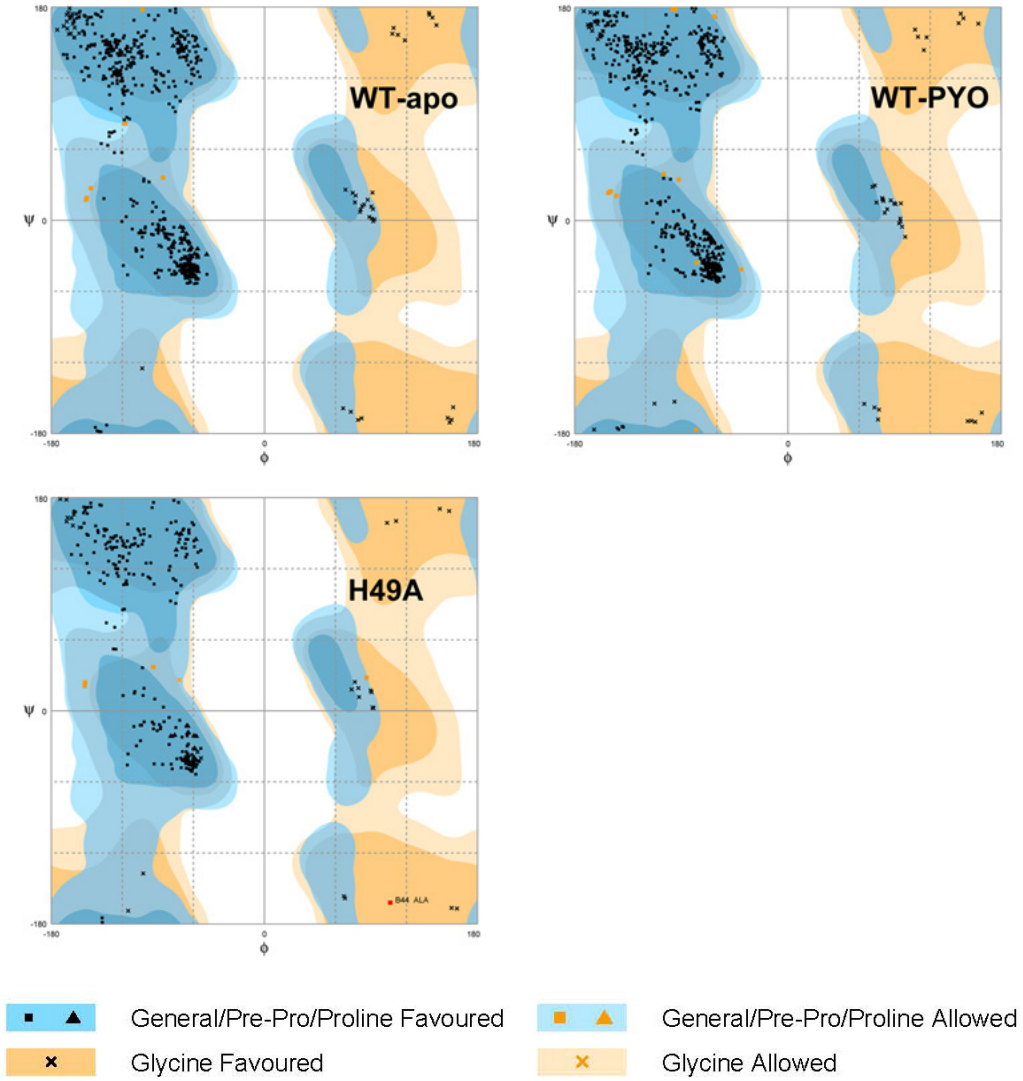


**Figure 5.8: Ramachandran plot showing the torsion angles of all peptide bonds of the major conformations of the PA0803 models used in this report. More than 97.9% of all amino acids have torsion angles in the most favoured region in all models. Only 1 residue (0.4%) in the relative low resolution H49A model is in the outlier region. The plot was generated using the program RAMPAGE from the CCP4 suite.**

# PART II

## STRUCTURAL AND FUNCTIONAL ANALYSIS OF PQSE

In the following section the crystal structures of PqsE determined in this study are analyzed, together with biochemical data, to obtain insight into its physiological function.

## 5.6 COMPARISON BETWEEN THE TWO CRYSTAL FORMS

As two different crystal forms of PqsE have been obtained, it is interesting to check whether any difference can be observed.

### 5.6.1 Crystal Packing of Crystal form 2 (XF2)

Crystal packing in XF2 was examined as it has two PqsE molecules in an ASU (Figure 5.9). From the coordinates, it can be observed that contacts between the two molecules in an ASU involve residues from the C-terminal helices only. The active sites are well separated and therefore there is no indication that the crystallographic dimer of PqsE is a functional dimer. Together with gel filtration results, PqsE is most likely functioning in monomeric form; the packing of two PqsE molecules in an ASU in XF2 is due to the crystallization process and is not likely to be the functional unit of PqsE.

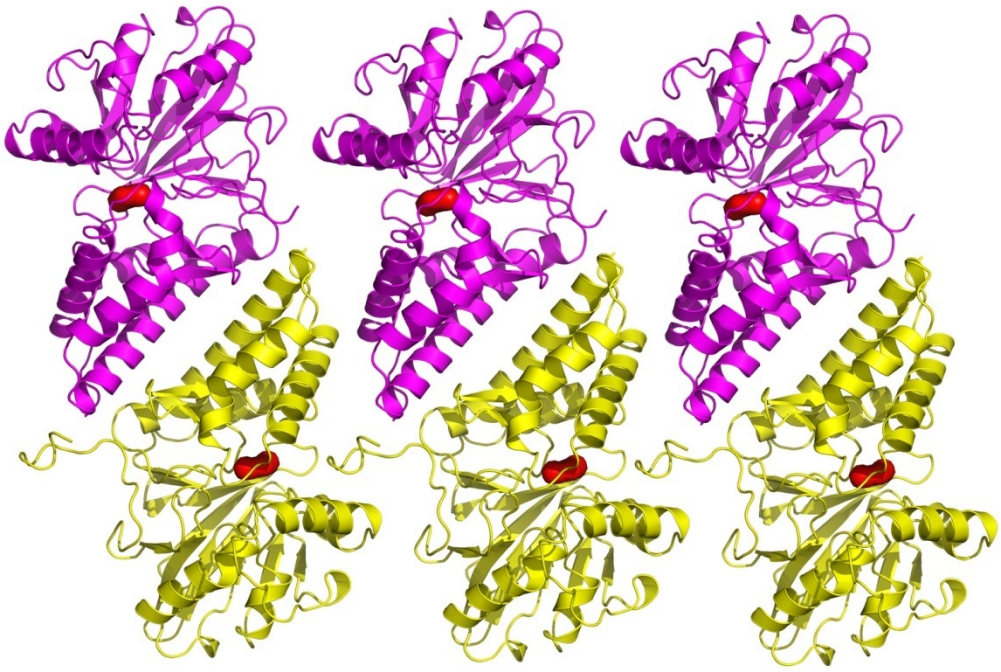

**Figure 5.9: Crystal packing of PqsE XF2. Two chains in an ASU are shown as yellow and magenta cartoons, respectively. Active sites, each consists of two Fe atoms and a water molecule, are shown in red, surface presentation.**

### 5.6.2 Comparison of PqsE structures in XF1 and XF2

First, the two chains of PqsE molecule in the ASU of XF2 were compared, using Superpose from the CCP4 suite with the secondary structure matching (SSM) algorithm. The two chains overlay well except for a slight difference at the loop L117-Q121 (Figure 5.10A). The two structures have an RMSD of 0.350 Å.

Then, chain A of XF2 is compared with the PqsE molecule in the XF1 structure using the same method. The two chains overlay well except for a slight difference at the loop L117-L123 and the loop P278-E280 (Figure 5.10B), but none of the loops is involved in ligand binding. The two structures have an RMSD of 0.498 Å.

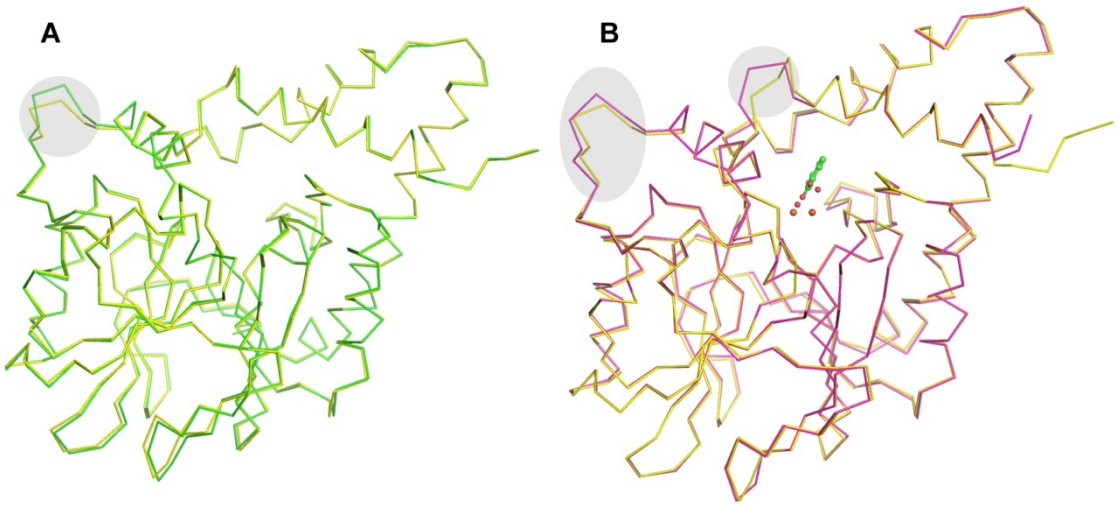


**Figure 5.10: Comparison of PqsE structures in two XFs. A) Overlay of chain A (yellow) and B in XF2 (green). B) Overlay of XF1 (magenta) and chain A of XF2 (yellow). Structures are shown in Cα ribbon presentations, except the ligand and metal ions/active site waters are shown as balls-and-sticks, to point out the binding site. Gray shades indicate the loops that have differences.**

It can be therefore concluded that the two crystal forms do not have significant differences regarding to the protein structure. As XF1 has higher resolution, the atom coordinates of PqsE in XF1 structure are used throughout the following discussion, unless where specified.

## 5.7 OVERALL TOPOLOGY OF PQSE

### 5.7.1 Topology of PqsE

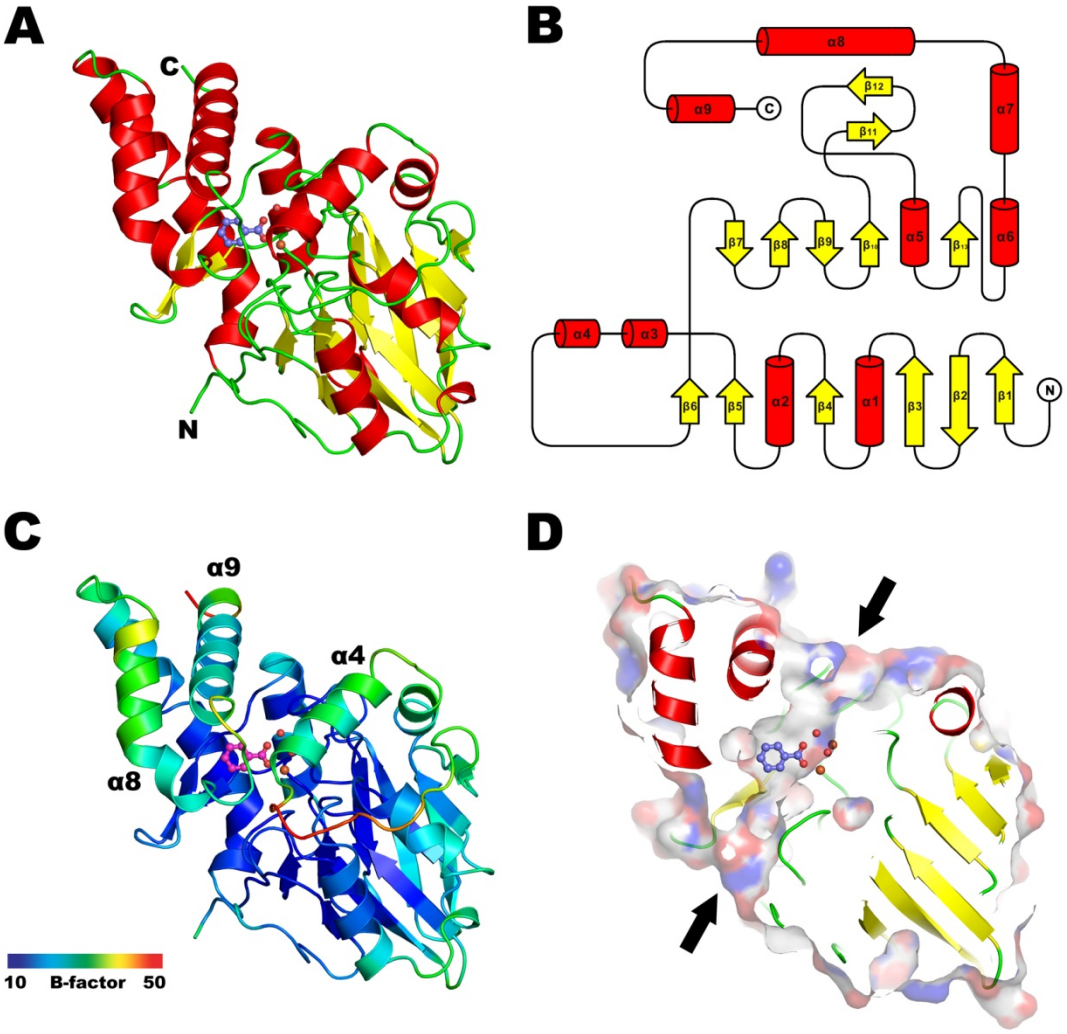


**Figure 5.11: Crystal structure of PqsE. A) Cartoon representation. Helices colored in red, strands in yellow. B) Topology diagram of PqsE, with α-helices depicted as red cylinders and β-strands as yellow arrows with orientation according to their direction in the β-sheet. C) PqsE structure colored by Cα B-factor. The bound ligand was colored magenta. D) Surface representation of PqsE. Black arrows indicate tunnels to the active site.**

The overall structure of PqsE is presented in various formats. Secondary structure elements were numbered sequentially (α1-α9, β1-β13), starting from the N-terminus (Figure 5.11A, B). PqsE folds into only one domain, which consists of an αβ/αβ sandwich core that

resembles proteins in the metallo-β-lactamase superfamily extended by three additional α-helices (α7-α9) at its C-terminus that form a lid-like structure and limit the access to the di-nucleic active site. B-factors in α4, α8 and α9 are significantly higher than the surrounding (Figure 5.11C), indicating the possibility of movement of these helices, which might facilitate entry or exit of the native ligands. In the surface presentation (Figure 5.11D), it became obvious that two channels approach the active center from opposite sides of the molecule, suggesting that the natural substrate of PqsE could be an extended molecule.

### 5.7.2 Comparison of fold with structural neighbors

Structural neighbors of PqsE were identified with the DALI server, using wild type PqsE XF1 PDB coordinates. The largest group of proteins that define this structural superfamily are indeed metallo-β-lactamases, as the threading predicted in Section 5.1.1. However, proteins of this fold also exhitbit large functional diversity (Table 5.7), which makes the annotation of PqsE function challenging. Comparison of the overall structure of PqsE and similar proteins are shown in Figure 5.12.

| PDB ID/Chain | RMSD | %id | Description |
|---|---|---|---|
| 1E5D/A | 2.8 | 19 | Rubredoxin:oxygen oxidoreductase |
| 1VME/A | 2.7 | 19 | Flavoprotein |
| 1K07/A | 2.7 | 15 | FEZ-1 β-lactamase |
| 1YCG/A | 3.3 | 19 | Nitric oxide reductase |
| 2FHX/A | 2.7 | 17 | SPM-1β-lactamase from *P. aeruginosa* |
| 1XM8/A | 2.4 | 22 | Glyoxalase II |
| 1P9E/A | 2.7 | 21 | Methyl Parathion Hydrolase |
| 3DHA/A | 2.7 | 20 | N-acyl HSL Hydrolase |
| 2FK6/A | 3.3 | 20 | Ribonuclease Z |
| 1WRA/A | 3.5 | 15 | Phosphorylcholine esterase |
| 1QHW/A | 4.1 | 7 | Purple acid phosphatase |

**Table 5.7: Strutural neighbors of PqsE and their functions. Only one protein from each functional family is listed here.**

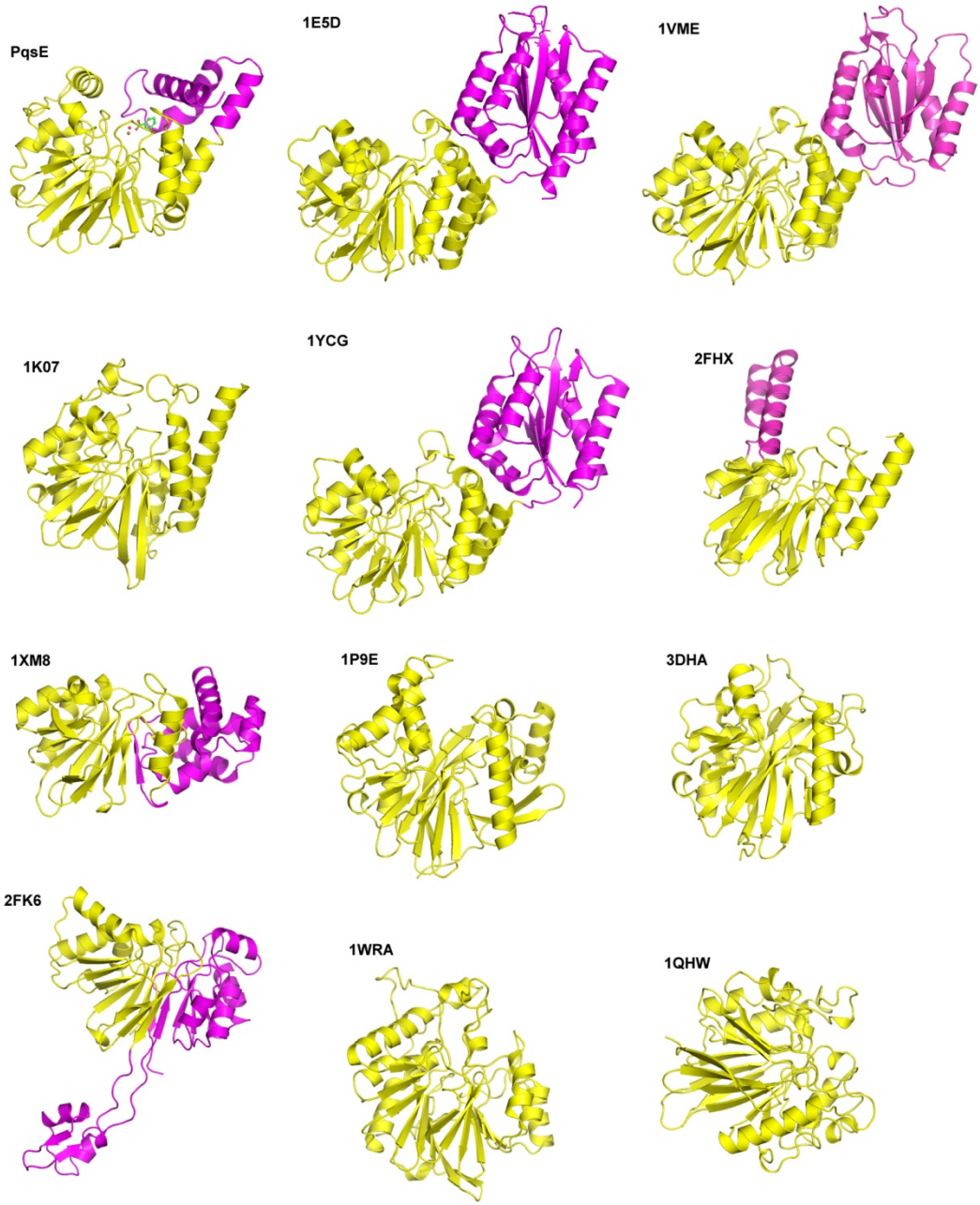


**Figure 5.12: Comparison of PqsE and its structural neighbors. Structures are shown in cartoon representation. The metallo-β-lactamase domain is colored yellow, whereas additional structural elements are colored magenta.**

## 5.8 THE ACTIVE CENTER OF PQSE

### 5.8.1 Identification of the metal atoms

The active center of PqsE was identified both by comparing its structure to other similar proteins and through the presence of a co-purified ligand. There are two metal ions at the active center, which are octahedrally coordinated. As the metal ions are usually critical for the function of proteins in this fold, they were carefully examined by a variety of methods.

First, ICP-MS measurements were carried out to quantify the total metal content in the protein. The protein was applied at a concentration of 533 µM, determined by measuring sulfur in the solution in a 1:200 dilution (14 S / PqsE molecule). The concentrations of divalent metals are determined as listed in Table 5.8.

| Isotope | $[M^{2+}]$ (µg/l) | $[M^{2+}]$ (µM) | $[M^{2+}]$:[Protein] |
|---|---|---|---|
| Mg26 | 109 | 4 | 0.01 |
| Ca44 | 1868 | 47 | 0.09 |
| Mn55 | 389 | 7 | 0.01 |
| Fe56 | 36472 | 654 | 1.23 |
| Ni58 | 3169 | 54 | 0.10 |
| Ni60 | 3252 | 55 | 0.10 |
| Cu63 | 791 | 12 | 0.02 |
| Cu65 | 330 | 5 | 0.01 |
| Zn64 | 2631 | 40 | 0.08 |
| Zn66 | 3341 | 51 | 0.10 |
| S32(1:200) | 1194 | 37.3 | 14/200 |

**Table 5.8: Results of ICP-MS of PqsE.**

It is clear that in the sample only the amount of iron is significant. However, the metal to protein ratio is lower than the expected ratio of 2:1. This may be explained by a loss of iron during purification, which is also supported by phenanthroline assays described later.

Second, X-ray fluorescence of PqsE crystals was measured at the Swiss Light Source synchrotron. X-rays are high energy photons that are sufficient to excite atomic electrons to move from low energy shells to high energy shells. When such events take place, electrons on other shells will fall to the lower energy orbitals to fill the vacancy, and emit energy via fluorescent X-rays. Due to the characteristic distribution of electron orbitals, each metal has special absorption edges where, e.g., K shell electrons get excited. Placing an X-ray detector perpendicular to the excitation beam, an excitation scan that covers a certain energy range can reveal the nature of the metal, because X-ray fluorescence emission will rise sharply when the increase of X-ray energy passes an absorption edge of the metal. In the experiments using PqsE crystals, strong emission is only observed near the K-absorption edge of Fe (Figure 5.13A).

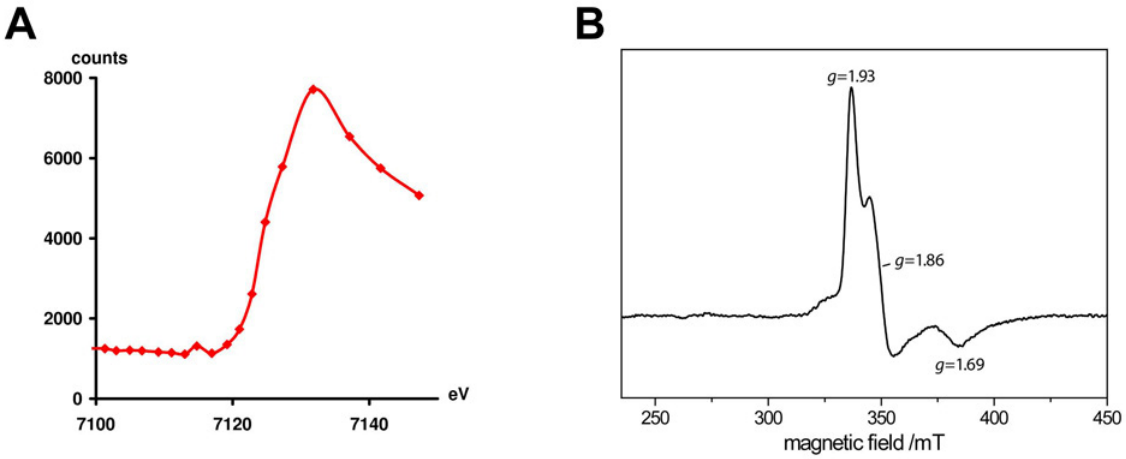


**Figure 5.13: A) X-ray fluorescence spectrum of a PqsE crystal at the iron K-absorption edge (tabulated value: 7111 eV). B) X-band continuous wave EPR frozen-solution spectra of *P. aeruginosa* PqsE in protonated buffer. The spectrum was recorded at 10 K with a microwave power 2 mW, a microwave frequency 9.120 GHz, and a magnetic-field modulation amplitude of 0.5 mT (100 kHz field modulation).**

Last, EPR experiments were carried out to determine the oxidation state of the Fe atoms. The experiment was set up under conditions typical for studying this type of systems. The obtained spectrum was complex, with three signals with g-factor of 1.93, 1.86 and 1.69 (Figure 5.13B). This result matches very well with the reported values (g=1.93, 1.87 and 1.73) from a study on a similar protein *Arabidopsis* mitochondrial glyoxalase II (Marasinghe et al., 2005), revealing that PqsE has a mixed Fe(III)/Fe(II) active center.

### 5.8.2 Active center of PqsE

The bi-nucleic active center of PqsE consists of two Fe atoms that are 3.5 Å away from each other, bridged by a water molecule and by the side chain of D178. The remaining residues through which PqsE coordinates the iron atoms consist of a conserved sequence motif 69HXHXDH74~H159~H221 (Daiyasu et al., 2001). H69, H71, H159 together with a water watermolecule coordinate Fe1, while Fe2 is interacting with D73, H74 and H221. A protein (PDB ID 1XM8) that has a Fe(III)/Zn(II) center has a similar structure to PqsE (Section 5.7.2). In the 1XM8 structure it is clear that the Fe(III) ion binds to the metal binding site equivalent to Fe2 in PqsE, because Fe and Zn has different coordination geometry. This suggests the Fe(III) atom in PqsE is also more likely to bind at the Fe2 site. This hypothesis is supported by docking calculations with benzoate to PqsE. Despite from the docking score affinity cannot be trustably deduced, the scores implies that Fe(III) in the Fe2 site is energictively more favorable than Fe(III) in the Fe1 site.

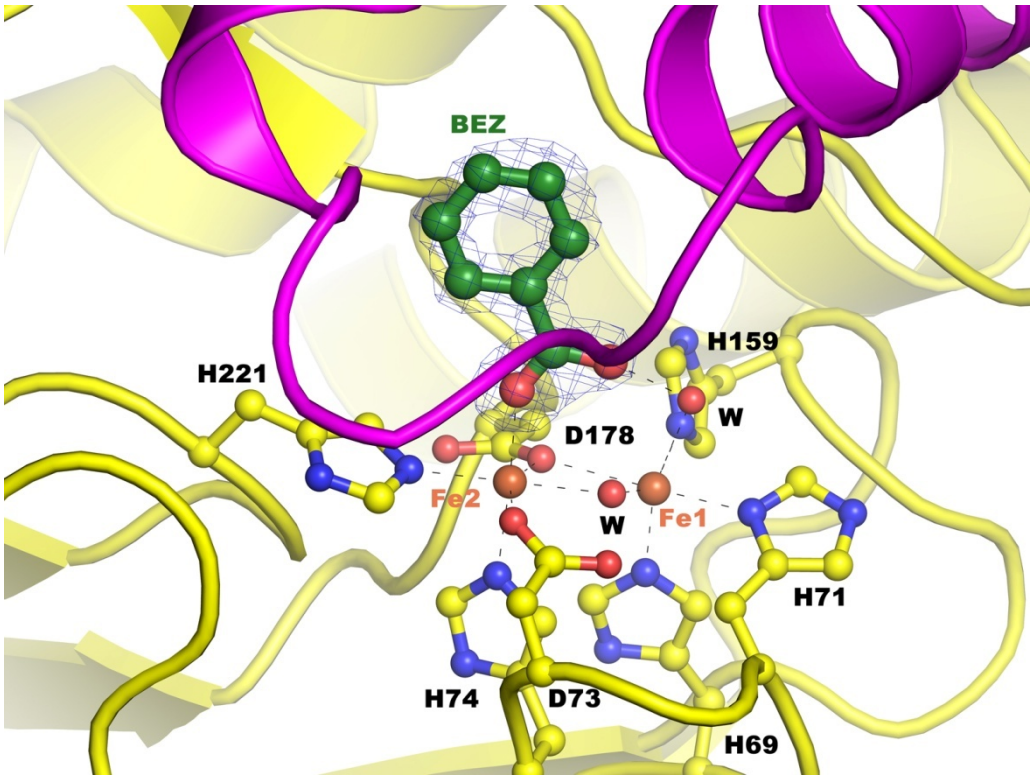


**Figure 5.14: Active site of PqsE, indicated by binding of an unexpected ligand interpreted as benzoic acid. The ligand and side chain of binding site residues are shown in balls-and-sticks presentation. The rest of the protein is shown as cartoon, with C-terminal helices colored magenta. Two Fe atoms are shown as orange spheres. Fo-Fc density is shown as blue mesh at sigma level 2.5.**

The active center of PqsE places the protein into the relatively small number of proteins with bi-nuclear-Fe centers within this fold family whose structures have been determined. Other members of this group include rubredoxin:oxygen oxidoreductase ROO from *Desulfovibrio gigas* (Frazao et al., 2000), the FprA enzymes from *Moorella thermoacetica* (Silaghi-Dumitrescu et al., 2005) and *Methanothermobacter marburgensis* (Seedorf et al., 2007), and also certain phosphatases like pig allantoic fluid purple acid phosphatase PPAP (Guddat et al., 1999) or the phosphorylcholine esterase domain of choline binding protein E from *Streptococcus pneumoniae* Pce (Garau et al., 2005). ROO and FprA are from anaerobic bacteria and both contain a second, flavin-binding domain that is involved in the redox reactions that these enzymes catalyze. As this domain is absent in PqsE, it is unlikely that PqsE has oxidoreductase function but belongs to the large hydrolase group within the metallo-β-lactamase family instead.

Interestingly, the wider and longer of the two channels leading to the active center binds a co-purified ligand with approximately 70% occupancy in both crystal forms. This ligand was assigned as benzoate from the shape of its electron density (Figure 5.14). Its location coincides with the substrate binding site in related enzymes and its carboxylate group participates in coordinating Fe2. This finding may hint towards natural substrates of PqsE.

### 5.8.3 Comparison of active site with structural neighbors

As described in previous sections, the three C-terminal helices shelter the active site of PqsE, making the proximity of a redox-active cofactor impossible. Therefore, it is most likely that PqsE utilizes its bi-nuclear-Fe center to hydrolyze its substrate(s). Hydrolases that are similar to PqsE includes phosphorylcholine esterases, purple acid phosphatases, β-lactamases, and the recently characterized AHL-lactonases. The later two are reported to have zinc activity centers. However, given the high degree of reservation of metal-ion binding residues (Figure 5.15) and the biological relavence of the AHL-lactonases, they are nevertheless compared below.

Structural coordinates of PqsE, two β-lactamases (1K07 and 2FHX), a lactonase (3DHA), an esterase (1WRA) and a purple acid phosphatase (1QHW) were superimposed using the pairwise align function on Dali server, taking PqsE as reference. Then a structure based sequence alignment was analyzed with program ClustalX2 (Larkin et al., 2007).

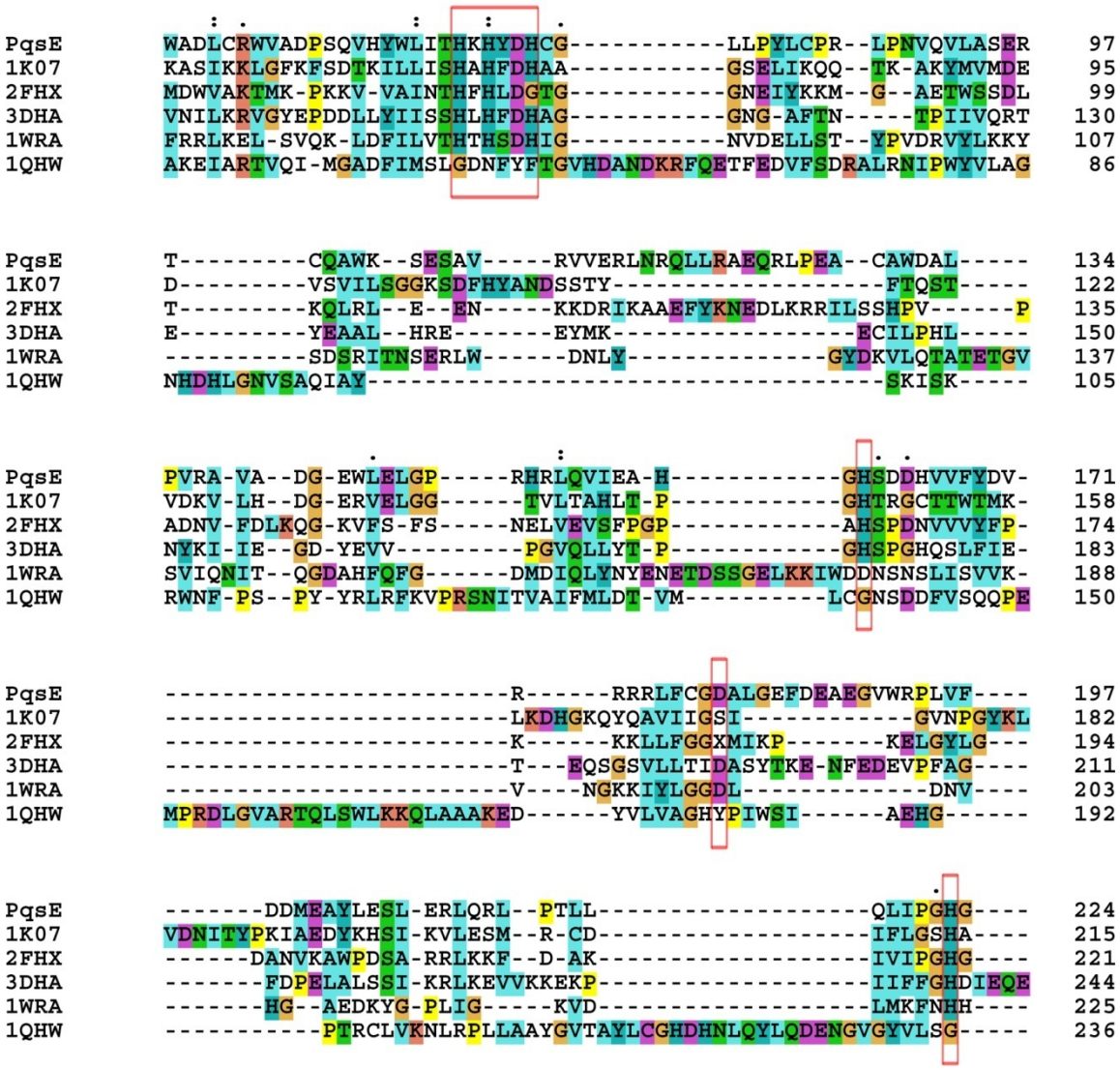


**Figure 5.15: Structure-based sequence alignment of PqsE and related hydrolases. Only the metal coordinating segments are shown, with the metal binding histidines and aspartates pointed out by red boxes.**

The alignment indicates that PqsE and the lactonase share completely conserved (HXHXDH~H~D~H) set of metal coordination residues, whereas the two lactamases lack the bridging D178, the phosphorylcholine esterase lacks the H159 and the phosphatase does not have the HXHXDH motif at all.

However, the lactonase active site uses the same set of residues to coordinate two zinc atoms. The nature of these two metal ions was confirmed both by ICP-MS (Thomas et al., 2005) and the square pyramidal coordination of the atoms (Figure 5.16). Zn1 atom was coordinated by H113, H239, D112; Zn2 was coordinated by H108, H110 and H173; the two Zn atoms are 3.3 Å apart, bridged by OD1 atom of D195 and a water molecule. In the

product complex (PDB ID: 3DHB), the bridging water was replaced by an oxygen atom from the carbonyl moiety of the ring-opened product N-hexanoyl-homoserine, maintaining the zinc atoms in their preferred five-ligand coordination geometry.

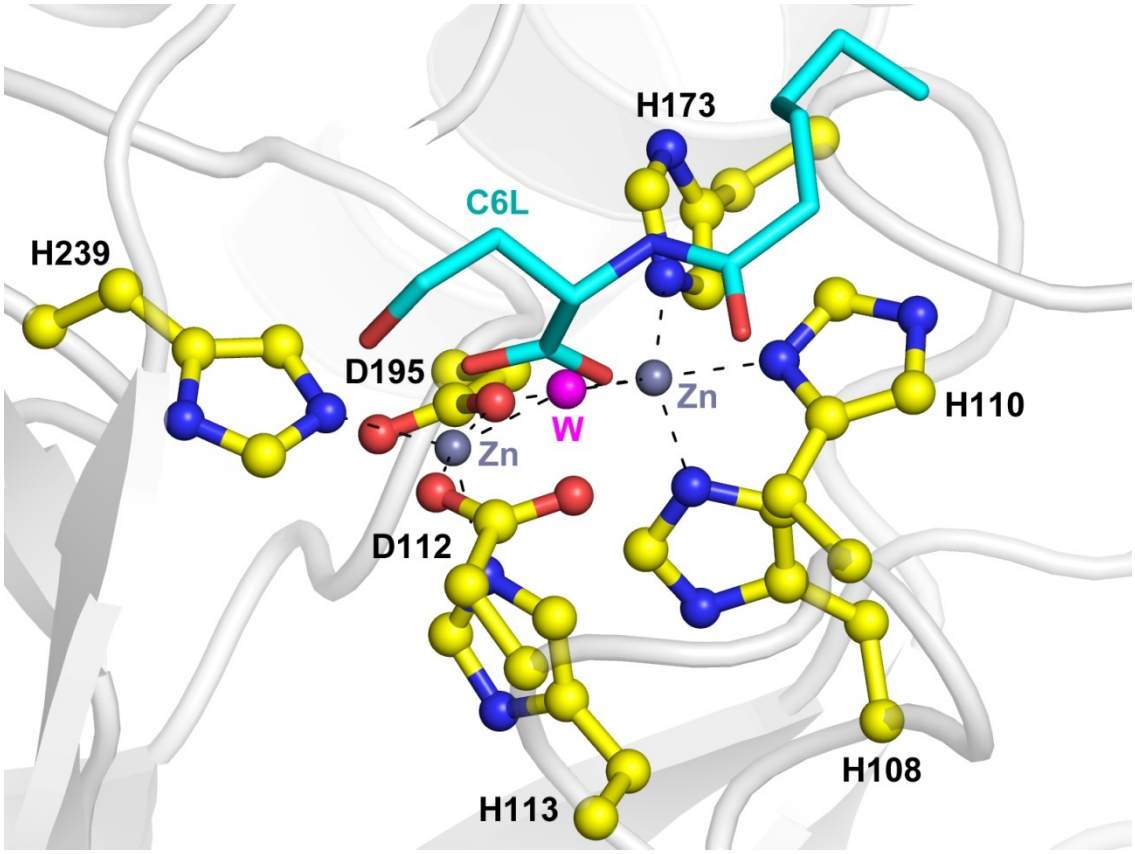


**Figure 5.16: Active site of a homoserine-lactone hydrolase active site. Figure generated by overlaying the apo form (PDB ID: 3DHA) structure and complex with the product (PDB ID: 3DHB). The protein backbone is shown as white cartoon, with active site residues highlighted as yellow balls-and-sticks. The bridging water in the apo structure is shown as a magenta sphere. The water bridging the two Zn atoms is shown as the magenta sphere W.**

The comparison shows that PqsE has some similarity at the sequence level to other proteins in the metallo-β-lactamase superfamily. Nevertheless, given the different nature of metal center and the diversity of function among proteins of this fold, it is not possible to deduce the exact molecular function of PqsE from the comparison. The search of the function has to be approached biochemically.

## 5.9 ACTIVITY TESTS OF PQSE WITH VARIOUS LIGANDS

### 5.9.1 PqsE with various available compounds

In order to determine which chemical reaction PqsE catalyzes, a selection of compounds were assayed with HPLC, HPLC-MS or ITC for binding and turnover. The results of these tests were summarized in Table 5.9.

| Compound | Analysis method | Activity/Binding |
|---|---|---|
| PQS | (HPLC, LC-MS, ITC) | - |
| ***Pyochelin related compounds*** | | |
| Pyochelin | (LC-MS) | - |
| Isochorismate | (LC-MS) | - |
| Salicyclic-AMP | (LC-MS) | - |
| ***Compounds that have a benzoyl (or nicotineamide) moiety*** | | |
| Benzoic acid | (LC-MS, ITC) | + ($K_D$ = 32.1 ± 1.8 µM) |
| Nicotinamide | (LC-MS, ITC) | - |
| Salicylic acid | (HPLC, LC-MS, ITC) | - |
| Acetyl-salicylic acid | (HPLC, LC-MS) | - |
| Ethyl-salicylic acid | (HPLC, LC-MS) | - |
| Anthranilic acid | (ITC) | + ($K_D$ = 24.1 ± 1.2 µM) |
| ***Compounds that have a homoserinelactone moiety*** | | |
| L-HSL hydrochloride | (ITC) | - |
| N-(β-ketocaproyl)-L-HSL | (LC-MS) | - |
| N-3-oxo-octanoyl-L-HSL | (LC-MS) | - |
| Phthalide | (LC-MS) | - |
| Phthalimide | (LC-MS) | - |
| ***Thioesters*** | | |
| S-hydroxymethylthiobenzoate | (LC-MS) | - |
| S-(4-nitrobenzoyl)-mercaptoethane | (LC-MS) | + ($K_M$ = 14 µM, $k_{cat}$ = 7.2 $min^{-1}$) |
| Parathion / methylparathion | (LC-MS) | - |

**Table 5.9: Commercially available compounds tested for binding or activity with PqsE.**

PQS was chosen because the binding site of PqsE seems perfectly suited for a PQS-shaped molecule. In addition, PqsE was originally reported to be a "PQS response

protein". However, neither binding nor turnover was observed, implicating that PqsE functions independently of PQS *in vitro*. This result is supported by recent *in vivo* observations (Farrow, III *et al.*, 2008) as well as the finding that PQS functions by binding and activating the transcription factor PqsR/MvfR (Xiao *et al.*, 2006a).

Homoserine lactones were tested because of the structural similarity between PqsE and the quorum quenching lactonases that have been described in the literature (Thomas *et al.*, 2005;Momb et al., 2008;Liu et al., 2008), despite the different nature of the metal ions.

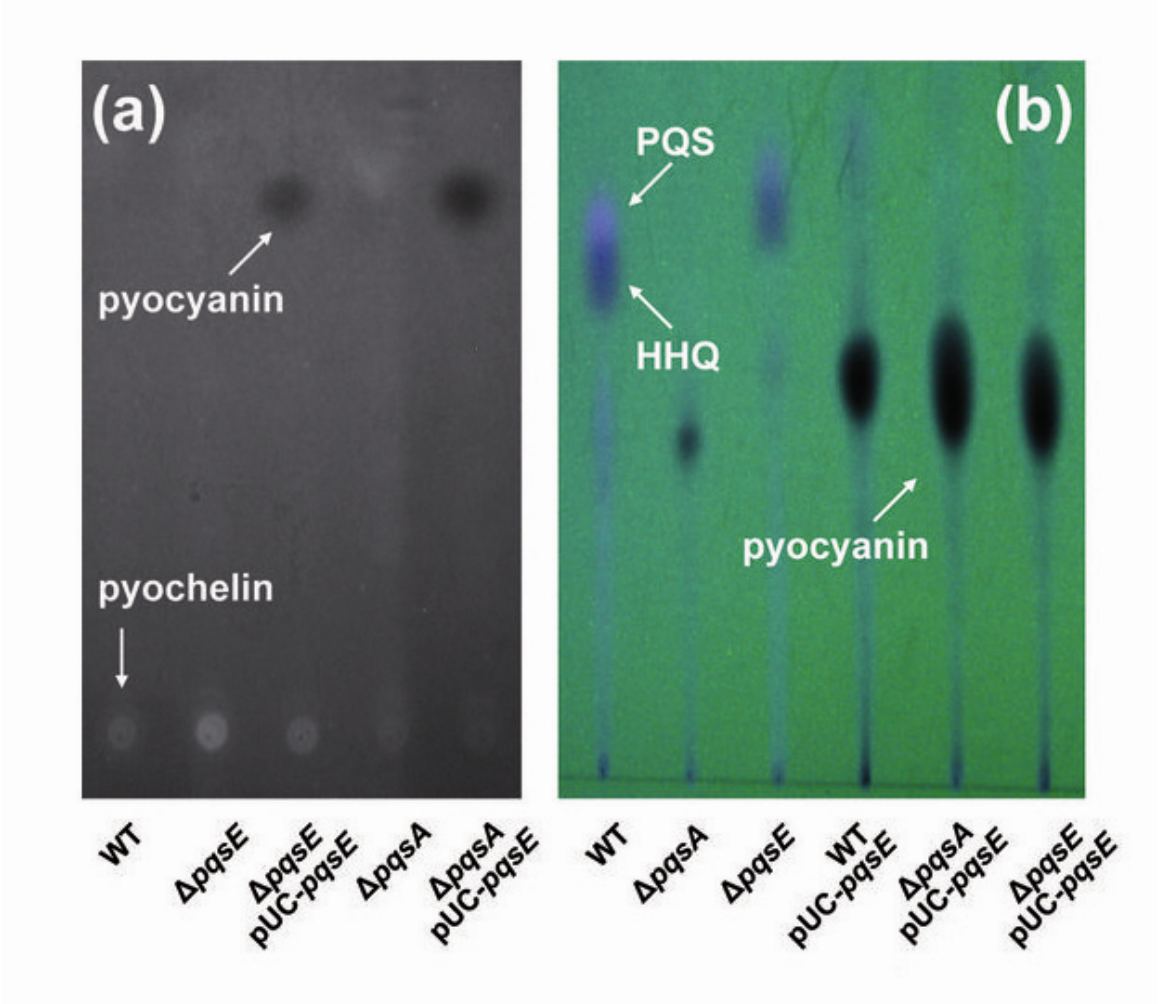


**Figure 5.17: Thin layer chromatographic analysis of PQS, pyochelin and pyocyanin in wild type *P. aeruginosa*, a *ΔpqsE* mutant and a *ΔpqsA* mutant constitutively overexpressing PqsE from a pUC-plasmid.**

The siderophore pyochelin was selected because a *pqsE*-deficient strain of *P. aeruginosa* was found in the laboratory of our collaborators to produce high levels of pyochelin but only small quantities of the PqsE-regulated pyocyanin, whereas

overproduction of PqsE lead to less pyochelin but copious amounts of pyocyanin (Figure 5.17A). Since pyochelin autoinduces its own biosynthesis (Serino et al., 1997;Reimmann et al., 1998) there may be a direct competition between these two pathways, which make use of the same precursor chorismic acid and which may shift towards pyocyanin biosynthesis if PqsE hydrolyses pyochelin or one of its precursors. A similar metabolic competition is also expected between pyocyanin and PQS biosynthesis itself, and indeed, overproduction of PqsE in wild type *P. aeruginosa* also reduced PQS and its precursor HHQ in favor of pyocyanin (Figure 5.17B). Based on this hypothesis, pyochelin was incubated with PqsE, analyzed on HPLC-MS but showed no turnover. Two of its precursors, isochorismate and salicylic-AMP were not commercially available. The responsible synthetic genes were therefore cloned, expressed and purified to produce these compounds experimentally. However, coupled enzyme assays monitored with HPLC-MS showed also no turnover.

Of the molecules tested for binding to PqsE, only benzoate and anthranilate showed binding with moderate affinity, with affinity constants in the micromolar range (Figure 5.18).

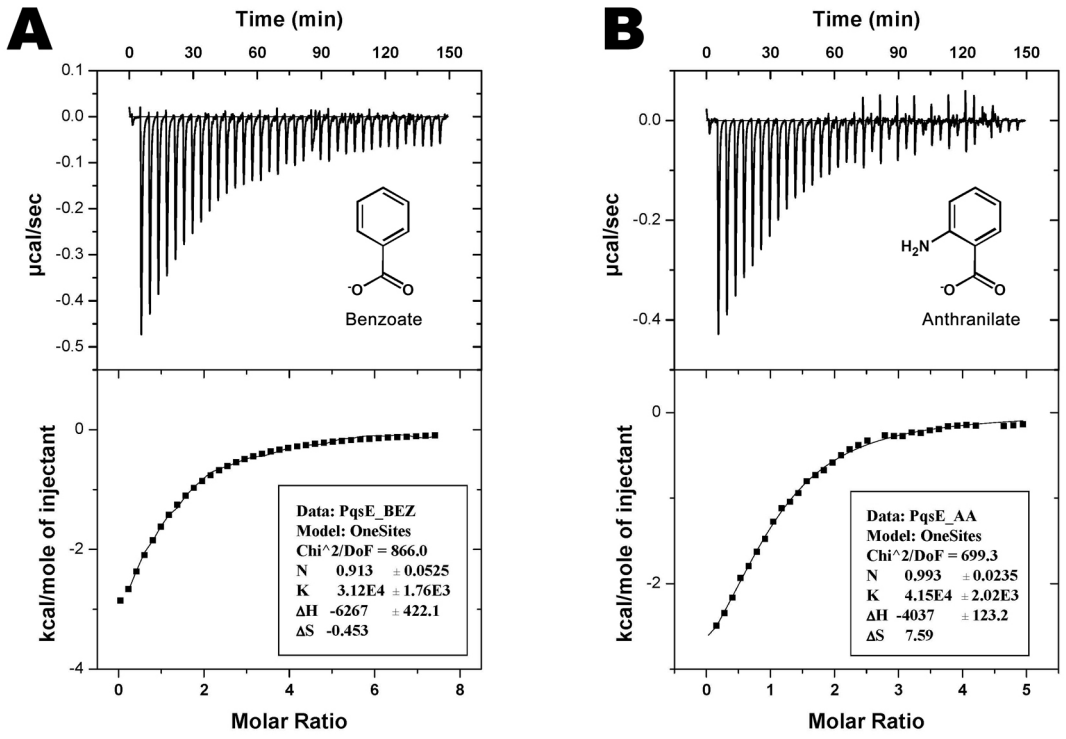


**Figure 5.18: ITC of PqsE with A) benzoic acid and B) anthranilic acid.**

### 5.9.2 Active center of PqsE in complex with M636

The fact that benzoate as well as anthranilate can bind to PqsE suggested binding tests with synthetic compounds that possess an anthranilate moiety. Available are compounds synthesized by Matthias Mentel for probing the phenazine biosynthesis pathway (Ahuja *et al.*, 2008). Inspection of the PqsE active site led to the decision of choosing piperidyl anthranilates for ITC experiments.

Significant binding was only found when titrating PqsE with the enantiomerically pure (R)-5-bromo-2-(piperidin-3-ylamino)benzoic acid compound (named M636) with $K_D$ of 41±7 µM (Figure 5.19). Titration with the non-bromide-substituted compound showed no detectable binding.

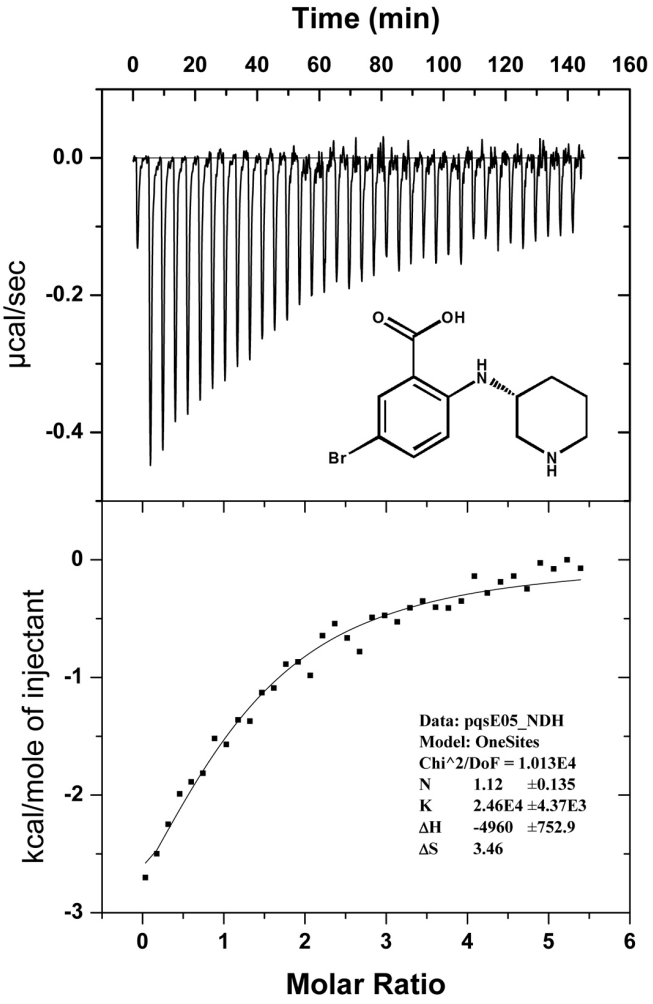


**Figure 5.19: ITC of PqsE and the M636 compound.**

The crystal structure of this protein-ligand complex was subsequently determined by soaking native PqsE crystals with a mother liquor drop containing the M636 ligand. Fo-Fc density at 2.5 σ level clearly indicated the presence of the ligand (Figure 5.20). Examination of the active site reviewed the mode of binding. Briefly, the side chain of R288 residue forms H-bonds with the nitrogen atom of the piperidyl moiety of the ligand, while the bromide atom of the ligand is coordinated by the carboxyl oxygens of E182 and one NE atom of the H282 side chain. The two carboxy oxygens of the benzoate moiety of M636 are directly coordinated by the Fe atoms of PqsE (Figure 5.20), unlike the benzoic acid found in the native structure where one of the carboxy oxygen is bridged by a water molecule to one Fe atom (Figure 5.14).

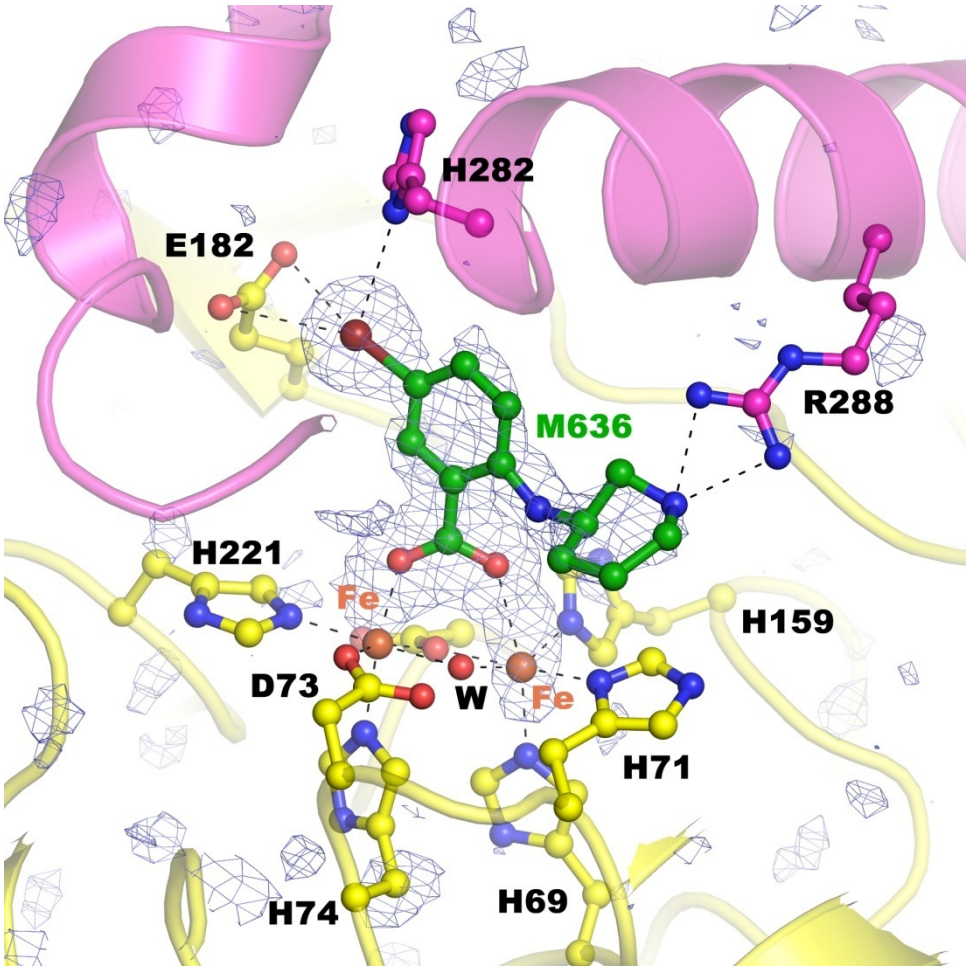


**Figure 5.20: Crystal structure of PqsE in complex with synthetic ligand M636. The ligand and side chain of binding site residues are shown in ball-and-stick. The rest of the protein is shown as cartoon, with C-terminal helices colored magenta. Two Fe atoms are shown as orange spheres. Fo-Fc density that indicates the presence of ligand is shown at 2.5 sigma level.**

Despite mutagenesis data (Section 5.12.3) suggesting that the natural substrate is not likely to be sequestered by PqsE via R288, M636 is the first synthetic small molecule found to bind PqsE. It may serve as a starting point for designing inhibitors targeting PqsE.

## 5.10 ENZYMATIC ACTIVITY SCREEN

Since neither genetic experiments reported in the literature nor the structural data obtained in this study revealed the molecular role of PqsE, an enzymatic activity screen using chromogenic general substrates was carried out to classify PqsE into one of the hydrolase families (Figure 5.21). For β-lactamases, a yellow substrate Nitrocefin is expected to be turned over to a red product. For phosphatases, phosphodiesterases, esterases and proteases, a para-nitro-phenol / para-nitro-aniline moiety is cleaved off to give a yellow color that can be quantified spectrometrically at 405 nm. For thio-esterases, a coenzyme A moiety is cleaved off and the resulting free thiol can be quantified spectrometrically at 412 nm with Ellman's reagent (5, 5'-dithiobis-(2-nitrobenzoic acid) or DTNB).

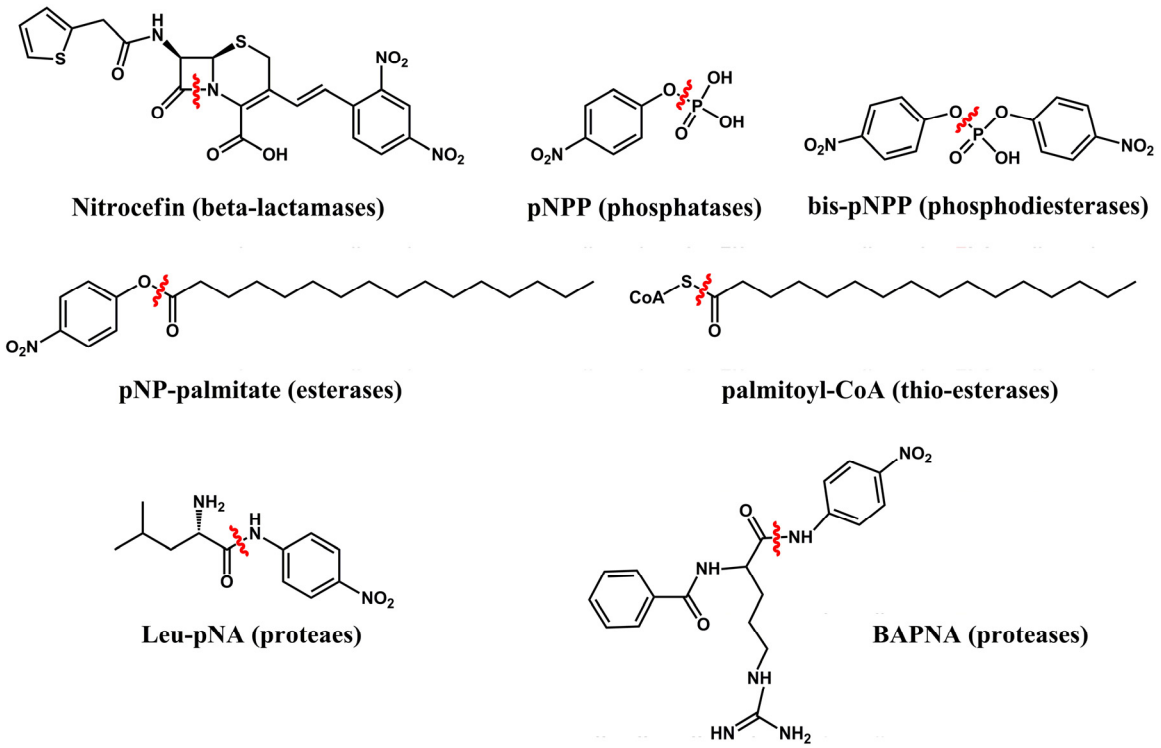


**Figure 5.21: Scheme for screening enzymatic activity.**

Among all the compounds tested, bis-pNPP was hydrolyzed at a very slow rate. The palmitoyl-CoA/DTNB mixture also turned yellow but the control with only DTNB and PqsE gave yellow color as well, probably due to the ability of DTNB to react with the thiol moieties on the protein. HPLC and careful spectrophotometric assays confirmed that PqsE has also thioesterase activity. These activities were examined by further experiments described in the following sections.

## 5.11 CHARACTERIZATION OF HYDROLYTIC ACTIVITIES

### 5.11.1 Enzyme kinetics of bis-pNPP hydrolysis

To obtain kinetic parameters of PqsE hydrolyzing the bis-pNPP substrate, a series of experiments with various bis-pNPP concentrations were carried out. To assess whether the low activity is caused by some impurities introduced during purification and whether there is loss of activity due to the Ni-NTA affinity purification (the usage of imidazol may compete with the active site histidines for the iron atoms), activities of PqsE protein from different tags/purification strategies were also measured. The results are summarized in Figure 5.22 and the derived $K_M$ and $k_{cat}$ values are listed in Table 5.10.

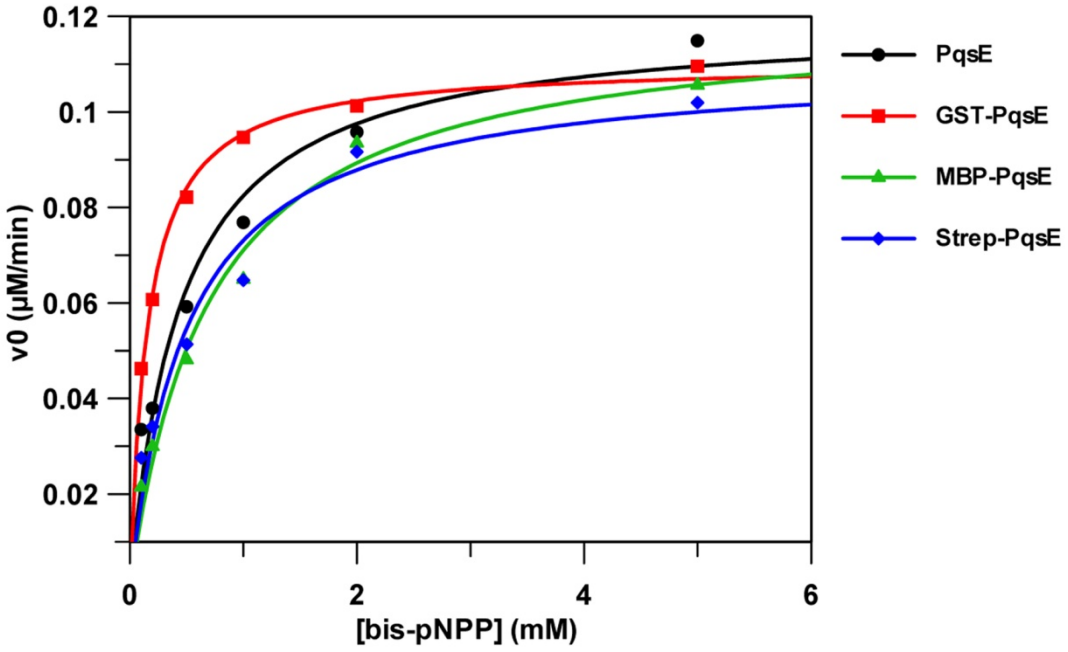


**Figure 5.22: Measurement of bis-pNPP hydrolysis kinetic parameters for various PqsE wild type construct.**

| Protein | $K_M$ (µM) | kcat ($min^{-1}$) |
|---|---|---|
| PqsE (Ni-NTA purification) | 124 | 0.011 |
| MBP-PqsE (with Tag) | 346 | 0.009 |
| MBP-PqsE (Tag removed) | 405 | 0.011 |
| GST-PqsE | 156 | 0.011 |
| Strep-PqsE | 507 | 0.011 |

**Table 5.10: Enzymatic parameters of various PqsE wild type constructs.**

It can be concluded from Table 5.10 that Ni-affinity chromatography yields protein that has similar activity to proteins purified via other strategies. Therefore in further experiments the protein was always purified with a Ni-column due to its superior loading capacity. Because the PqsE constructs used in these kinetic assays were expressed in different bacterial strains and were purified by fundamentally different chromatographies, the results also provided additional support that the PDE activity could be attributed to PqsE instead of contaminating PDEs.

### 5.11.2 Activity tests with natural phosphodiesters

Most phosphodiesterases (PDEs) hydrolyze the general substrate bis-pNPP. However, hydrolyzing this chromogenic substrate does not provide insights to the potential biological function of PqsE. Some phosphodiesters that occur in nature were therefore tested. The results of this group of experiments are summarized in Table 5.11 below.

Of all natural phosphodiesters tested, only nucleic acids (DNA/RNA) were shown to be hydrolyzed. pNP-phosphocholine is also hydrolyzed but at an extremely slow rate. However, the rather slow PDE activity of PqsE raised the concern that this activity might be due to the contamination with small amount of fast PDEs. Especially, DNase I was routinely used when disrupting the bacteria cells, to reduce the viscosity of the cell suspension liquid of the Rosetta pLysS strains used in the purification. It was hence important to carry out controls of nuclease activity to demonstrate that the low activity really can be attributed to PqsE.

| Phosphodiesters and related compounds | | Activity |
|---|---|---|
| cAMP / cGMP | (HPLC) | - |
| ADP / ATP | (HPLC) | - |
| NMPs / dNMPs | (HPLC) | - |
| cyclic-di-GMP | (LC-MS) | - |
| pNP-phosphocholine | (UV-VIS spec / LC-MS) | + (extremely slow) |
| sn-Glycero-3-Phosphocholine | (LC-MS) | - |
| 1-Caproyl-sn-Glycero-3-Phosphocholine | (LC-MS) | - |
| DNA | (Agarose gel with EB) | + |
| RNA | (Agarose gel with EB) | + |

**Table 5.11: Common phosphodiesters tested in this study.**

### 5.11.3 Controls of nuclease activity

In order to examine the slow nuclease activity, several controls were made and the results are summarized as follows. First, hydrolysis of λ-DNA was followed over time in comparison with a control adding equal amounts of gel filtration buffer to the reaction mixture instead of the PqsE protein (Figure 5.23A). It can be concluded that PqsE hydrolyzes double stranded λ-DNA in a time-dependent, non-specific manner.

It is well known that free iron ions in solution have the ability to cleave DNA molecules under certain conditions. This phenomenon is termed as Fenton chemistry. As high concentrations of the unstable PqsE protein were applied in the assays, there might be free iron ions released into the protein solution when a proportion of PqsE denatures. Therefore, a second control experiement was carried out, with both single stranded and double stranded DNA tested for digestion by PqsE. For comparison, 5-fold molar concentration of Fe ions was added instead of the PqsE solution, to rule out the possibility of degradation due to Fenton reaction in the assay conditions. The agarose gel clearly showed that PqsE but not Fe cleaved both single and double stranded DNA (Figure 5.23B). The gel

also suggested that the cleavage of dsDNA by PqsE might actually occur in succession to spontaneous unpairing of the end of dsDNA molecules.

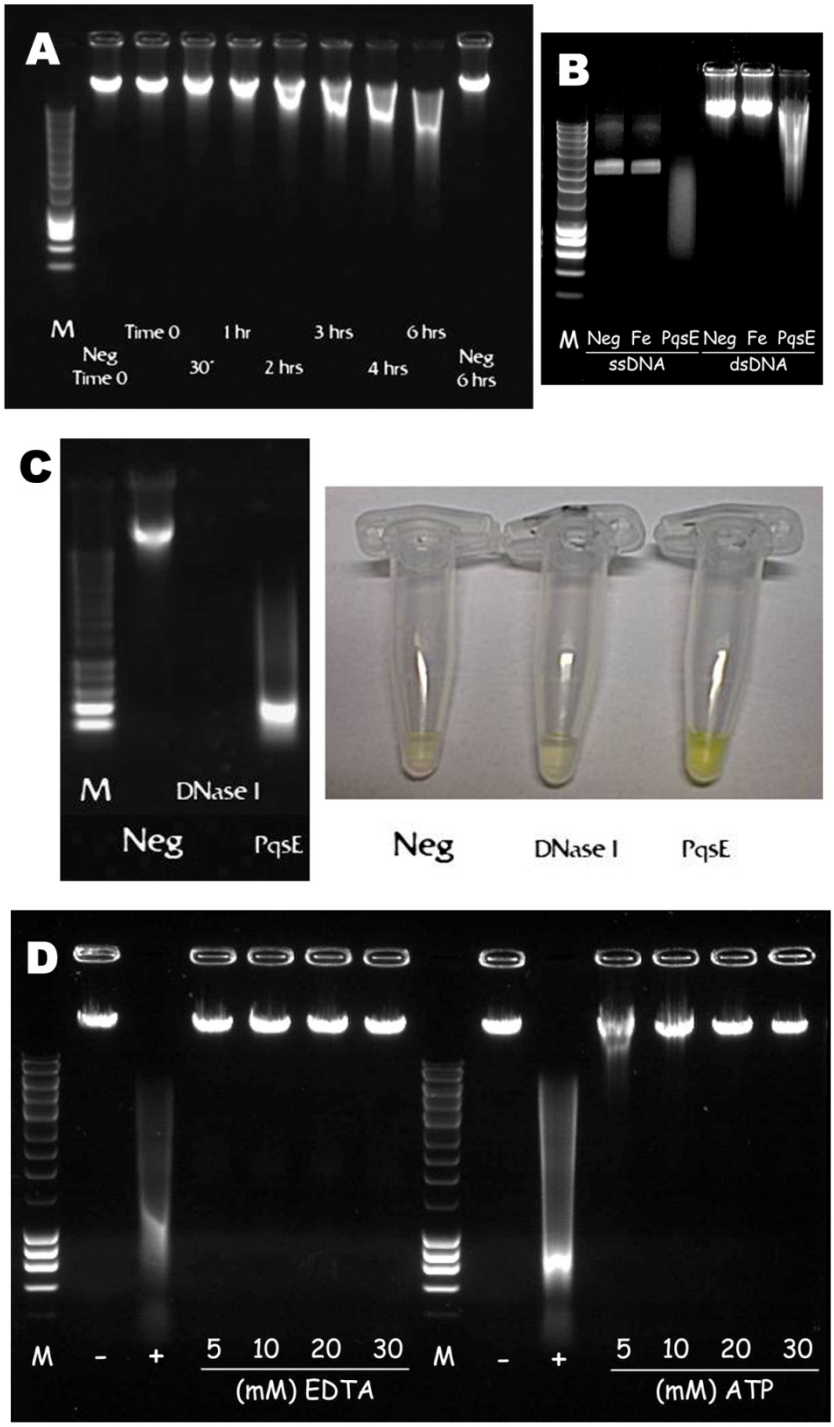


**Figure 5.23: Controls of PqsE nuclease activity. A) Hydrolysis of λ-DNA over time. B) Hydrolysis of ssDNA and dsDNA, in comparison to 5-fold of Fe. C) Comparison of PDE activity of PqsE and Dnase I, with λ-DNA and bis-pNPP under the same conditions. D) Inhibition of PqsE with EDTA and ATP.**

Next, the PDE activities of PqsE were compared with those of DNase I. Hydrolysis of λ-DNA and bis-pNPP were tested under the same conditions. It can be seen that DNase I hydrolyzes DNA faster, but bis-pNPP slower, than PqsE (Figure 5.23C). This implied that the PDE activity observed in previous experiments was not a result of DNase I addition in PqsE purification procedures.

Last, hydrolysis reactions of λ-DNA by PqsE were tested under conditions that contain typical PDE inhibitors. The presence of 5 mM or more EDTA in the reaction mixture totally abolished PqsE activity (Figure 5.23D). Another inhibitor tested was ATP, which is a competitive inhibitor of most PDEs at high concentrations. Presence of 5 mM ATP left only residual activity of PqsE and 10 mM or above completely abolished the PqsE hydrolysis (Figure 5.23D).

With these controls it can be concluded that the nuclease (DNase) activity described in previous sections can be attributed to PqsE.

### 5.11.4 Characterization of thioesterase activity

In the enzymatic activity screen assays, it was indicated that PqsE may have thioesterase activity as well. However, the usage of DTNB always caused a high background in the control reaction, which made it ambiguous to judge whether a slow hydrolysis is a genuine reaction or just some artifact.

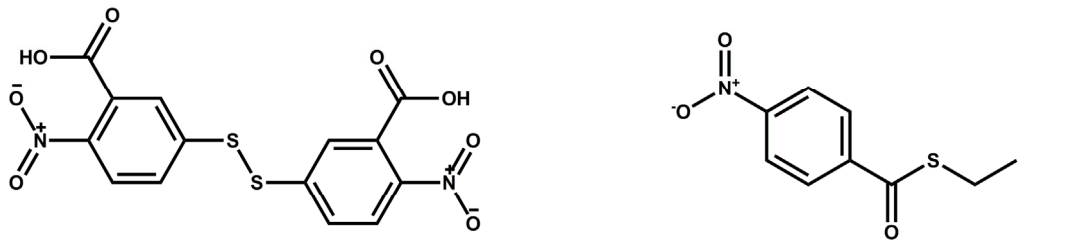


Dithionitrobenzoic acid (DTNB) S-(4-nitrobenzoyl)-mercaptoethane (S-4NB-ME)

**Figure 5.24: Chemical Structure of DTNB and S-4NB-ME.**

Additional support of thioesterase activity was obtained by investigated benzoate derivatives. Since benzoate was co-purified from the active center, one hypothesis was that benzoate is a product or product analogue which was resulted in by over-expressing PqsE in *E. coli*. In light of this, commercially available benzoate derivatives were incubated with PqsE and analyzed with HPLC method. Tested compounds include esters, thioesters and

amides. Of the compounds examined, only S-(4-nitrobenzoyl)-mercaptoethane (S-4NB-ME) was hydrolyzed. The hydrolytic activity of this compound was confirmed by DTNB assay and kinetic parameters of $K_M$ of 14 μM and $k_{cat}$ of 7.2 $min^{-1}$ (in presence of 2 mM $MnCl_2$) was obtained. The hydrolysis product, p-nitrobenzoic acid was tested with PqsE in ITC, but the affinity fell beyond the detection limit ($K_D$ > 100 μM).

In nature, coenzyme-A (CoA) derivatives are the most abundant family of thioesters. They are also physiologically very important. Several commercially available CoA-compounds, including acetyl-CoA, benzoyl-CoA, malonyl-CoA, succinyl-CoA and glutaryl-CoA were tested with PqsE in HPLC but none of them was hydrolyzed.

## 5.12 SITE-DIRECTED MUTAGENESIS

### 5.12.1 In vitro properties of PqsE mutants

It well known that the metal ions are essential for the activity of this enzyme superfamily. Loss of metal ions directly leads to the loss of activity (Section 5.13). Therefore mutagenesis of residues that coordinate the iron atoms will most likely result in dead mutants that are incapable of binding iron. These mutants may not provide information for obtaining insights into the *in vitro* function of PqsE. Mutagenesis was hence carried out to alter residues that compose the active site but are located on the opposite site to the iron atoms. Besides, since polar residues have greater possibility to participate in catalysis or to form hydrogen bonds with the substrate, their mutations should have stronger effect in changing substrate binding properties than mutation of non-polar residues. Five single residue mutants were therefore generated: E182A, S273A, H282A, S285A and R288A and ligated to pET28a vector for recombinant expression and to pUCP20 for *in vivo* characterization.

Two of the mutants, E182A and S273A were successfully expressed and purifed. H282A could be overexpressed but 90% protein fell into inclusion bodies, suggesting that this mutant may not fold properly. Hydrolytic activities of purified mutant protein were then examined in comparison with the wild type PqsE.

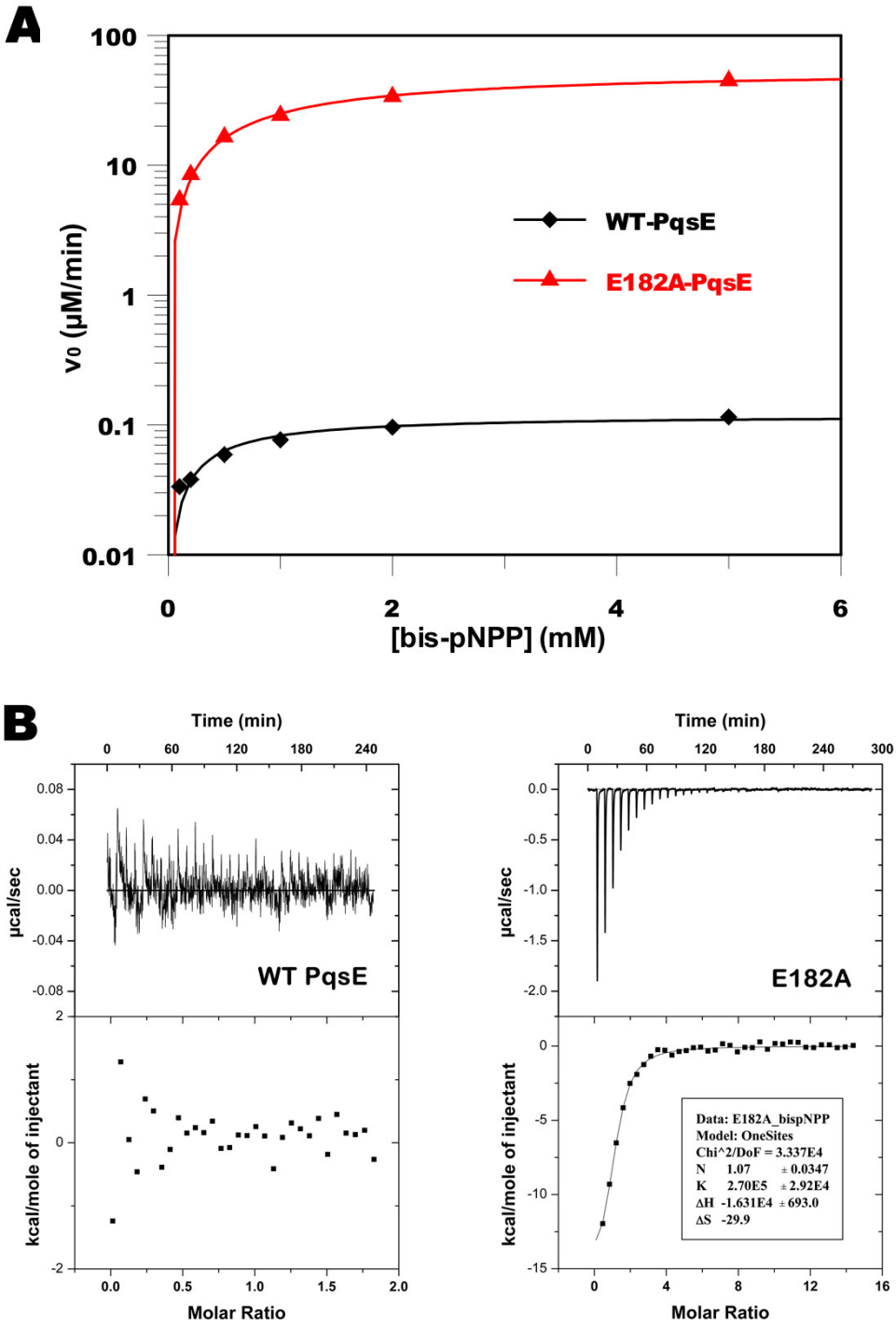


**Figure 5.25: A) Bis-pNPP hydrolysis activity of PqsE E182A mutant in comparison with wild type PqsE, purified with Ni-NTA chromatography. B) Determination of the binding affinity of E182A and bis-pNPP, in absence of $Mn^{2+}$.**

Surprisingly, hydrolysis of bis-pNPP was greatly enhanced in the E182A mutant. Kinetic measurement indicated an increment of ~1000 fold in turnover (Figure 5.25A $K_M$ =

208 µM, $k_{cat}$ = 12.4 $min^{-1}$). This can be explained by increased ligand affinity determined via ITC ($K_D$ = 3.5 ± 0.4 µM, while the affinity between wild type PqsE and bis-pNPP is beyond the detection limit of ITC, Figure 5.25B).

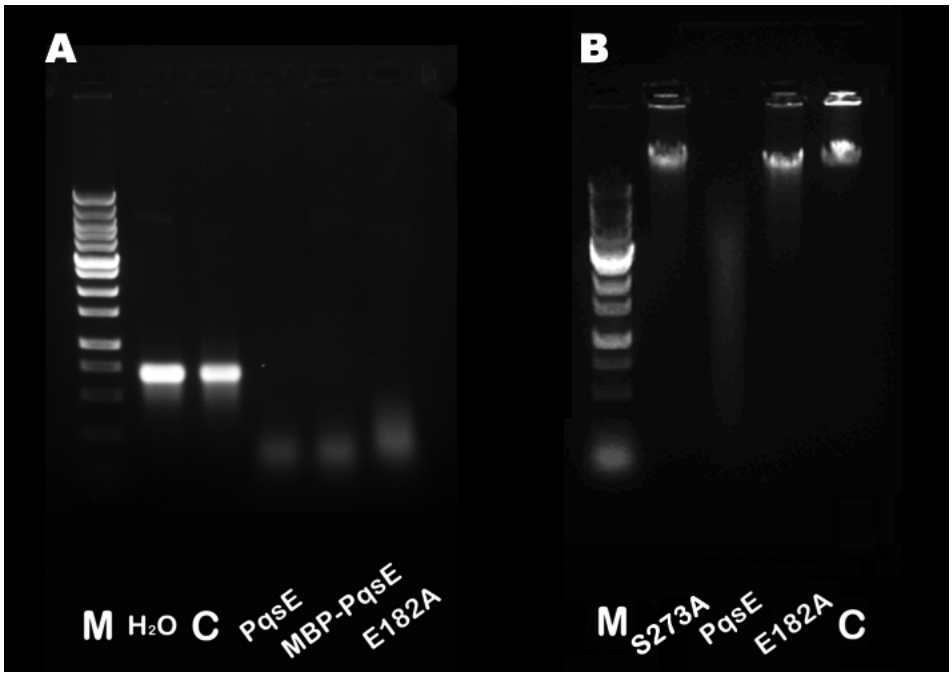


**Figure 5.26: Comparison of wild type PqsE and E182A mutant. A) RNase activity against a mRNA fragment. B) Dnase activity against λ-DNA.**

Hydrolysis of nucleic acids and S-4NB-ME thioester also showed altered activity. However, contrary to hydrolysis of bis-pNPP, the E182A mutant hydrolyzed S-4NB-ME, DNA and RNA slower than the wild type protein ($K_M$ = 13µM, $k_{cat}$ = 0.18 $min^{-1}$ for S-4NB-ME, DNA and RNA see Figure 5.26).

Thus, *in vitro* examination of the mutant protein provided evidence that the hydrolytic activities of PqsE can be altered by a single mutation, but for the same E182A mutant hydrolysis of bis-pNPP shifted towards different direction from that of S-4NB-ME and nucleic acids. Futher experiments were therefore required to identify the reason for this discrepancy between different *in vitro* assays.

### 5.12.2 Active center of PqsE E182A in complex with bispNPP

Site-directed mutagenesis created a PqsE mutant E182A that showed enhanced bis-pNPP hydrolysis *in vitro*. ITC experiments revealed that this increase in activity can be

attributed to increase of the affinity between the protein and the substrate. A crystal structure of the E182A-substrate complex was therefore determined, using the soaking method (Figure 5.27).

The structure revealed that removal of the glutamate side chain of E182 increases the space available for substrate binding, explaining the increase in affinity and hence activity. The phosphate group of bis-pNPP coordinates both iron atoms such that the bridging water molecule is positioned for an $S_N2$-reaction at the phosphorus atom. However, potential catalytic residues seem to require rearrangements within the active center to be able to protonate the expected oxyanion intermediate.

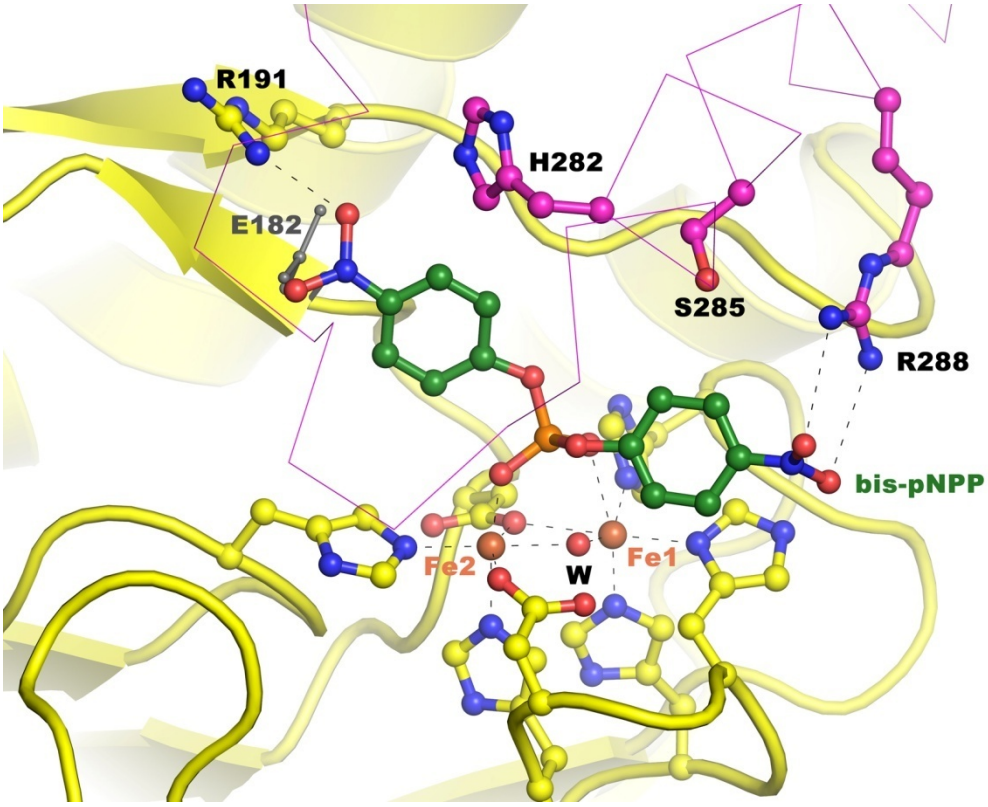


**Figure 5.27: Crystal structure of the PqsE E182A mutant in complex with bis-pNPP substrate. The ligand and side chain of binding site residues are shown in ball-and-stick. The rest of the protein is shown as cartoon, with C-terminal helices colored magenta. Two Fe atoms are shown as orange spheres. The side chain of E182 is shown in thinner, gray lines. The water molecule bridging the two iron atoms is ideally positioned for attack of the phosphate group.**

### 5.12.3 In vivo test of PqsE mutants

The wild type *Pseudomonas aeruginosa* PAO1 strain produces about 50 µM pyocyanin after overnight incubation under typical culture conditions described in Section

4.15. In frame deletion of the *pqsE* gene abolished the pyocyanin production under the same conditions. To examine the PqsE mutants, the PAO1 *ΔpqsE* strain was transformed with a plasmid pUCP20-*pqsE*, where the *pqsE* gene was either the wild type or a mutated gene. The resulting series of PAO1 strains were cultured under the same conditions and their pyocyanin production was quantified and compared.

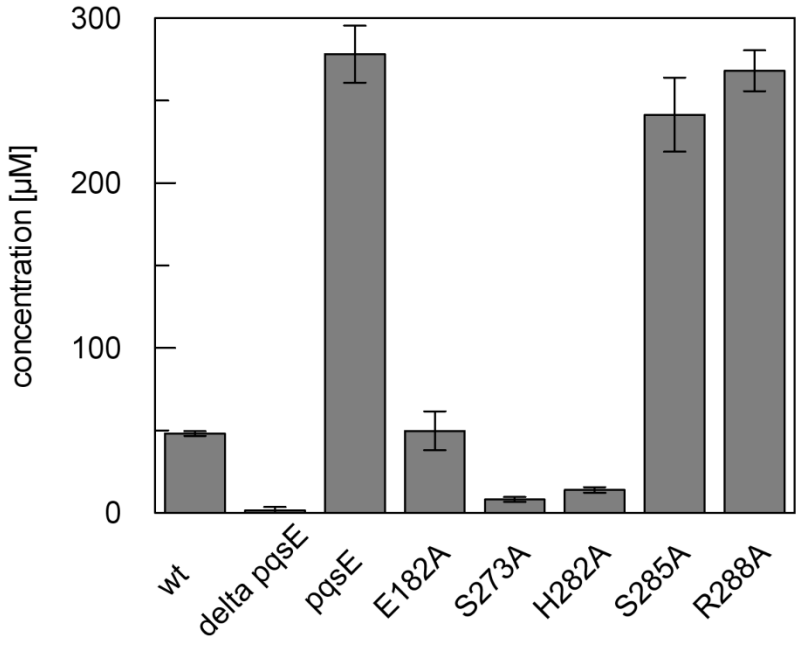


**Figure 5.28: Pyocyanin production in various PAO1 strains. *wt: PAO1 wild type stain; delta pqsE: pqsE in-frame deletion mutant; pqsE: delta pqsE transformed with pUCP20-pqsE; E182A: delta pqsE transformed with pUCP20-pqsE_E182A mutant; S273A, H282A, S285A, R288A: delta pqsE transformed pUCP20-pqsE plasmids carrying corresponding mutations. Error bars indicate the standard deviation of three parallel expriments.**

As shown in Figure 5.28, PAO1 ΔpqsE + pUCP20-pqsE_wt strain produced more than 5 fold of pyocyanin than the PAO1 wild type strain, probably because PqsE expression in this strain is not regulated as in the wild type PAO1. When transformed with plasmid carrying *pqsE* mutants, pyocyanin production in E182A, S273A and S282A are greatly reduced, with E182A dropping back to wild type PAO1 level and the other two even lower. Mutation of S285A and R288A seems to have no effect on pyocyanin production.

## 5.13 PHENANTHROLINE-BASED ASSAYS

Despite having characterized the enzymatic properties of wildtype PqsE and mutants from various aspects, conclusions are hard to be drawn and questions remain. It has been

observed that kinetic parameters vary between different batches of purifications and the proteins decay rather quickly, even when kept at -80 °C. As indicated by the 1.2:1 ratio from ICP-MS measurements, one possible explaination for these observations is that one or more Fe atoms may be lost during and after purification, resulting in loss of activities. Therefore, phenanthroline-based assays were developed both as a quick and simple quantification method of Fe and to address some further issues.

Phenanthroline is a heterocyclic organic compound. Due to structural similarities to 2,2'-bipyridine, phenanthroline also forms strong six-coordinated, octahedral complexes with most metal ions (Figure 5.29). However, only the complex $[Fe(phen)_3]^{2+}$, called "ferroin", exhibits a dark red color and can be quantified photometrically at 512 nm. Quantifications were carried out according to a calibration curve generated with inorganic Fe salt. Using UV-Vis scans, it was confirmed that complexes with other metal ions, including $Co^{2+}$ and $Fe^{3+}$, cause nearly no absorption at 512 nm.

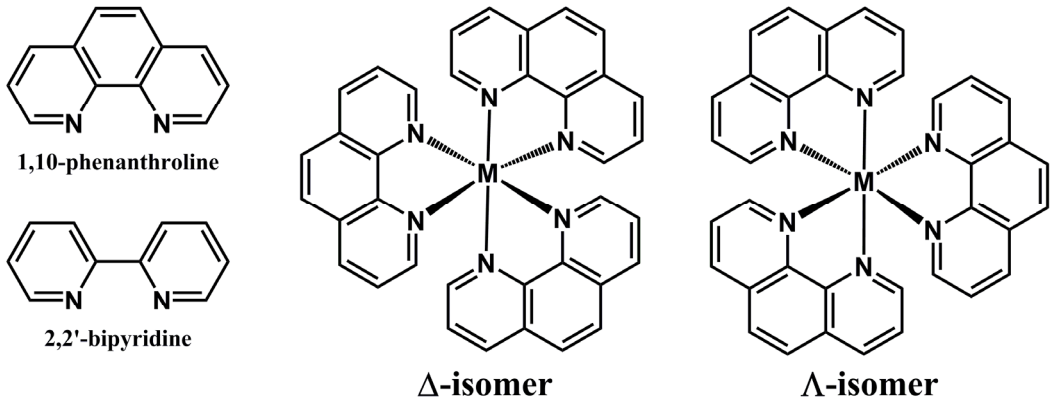


**Figure 5.29: Chemical structure of phenanthroline and its metal complexes.**

In addition, the Fe(III) form of the phenanthroline complex has a standard potential of +1.06V, which means that it can be easily reduced to the Fe(II) form and develop the red color. Therefore, by simply adding reducing agents after a stable plateau of $OD_{512}$ is formed, Fe(III) and Fe(II) concentration can be quantified in one experiment. Utilizing phenanthroline to quantify the Fe content, assays with wildtype PqsE and E182A were carried out to investigate the relationship between metal content and hydrolytic activity.

### 5.13.1 Measurement of Fe(II) and Fe(III) content in PqsE protein

The detailed protocol for these measurements is described in Section 4.14.3. In brief, PqsE sample was diluted to a solution containing 6M urea, and then phenanthroline was

added. The solution was monitored at 512 nm in a spectrophotometer. The $OD_{512}$ indicates the Fe(II) concentration. $Na_2S_2O_4$ was added when the $OD_{512}$ reaches a plateau, the difference between the second plateau and the first one indicated the Fe(III) concentration.

From results with different batches of protein it was clear that Fe is not always at full occupancy. For example, one batch of wildtype PqsE crystallized well but behaved poorly in the kinetics measurement. When assayed with phenanthroline, it showed over 95% occupancy of Fe ([Fe] / [Protein] = 1.9) with a nearly 1:1 Fe(II) to Fe(III) ratio (Figure 5.30, blue line).

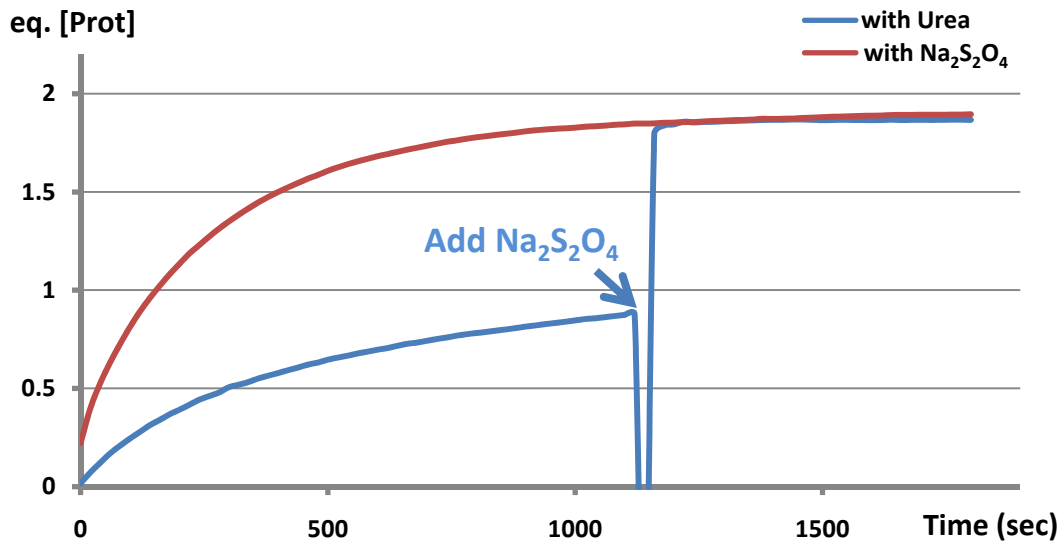


**Figure 5.30: Measurement of Fe(II) and Fe(III) in a batch of wildtype PqsE, using phenanthroline. Measured absorption readings at 512 nm wavelength were normalized to equivalent protein concentration.**

It was also observed in the experiments using urea as denaturation agent that the first stage is a curve, while after adding sodium dithionite the absorption jumped up instantly to the level of final readout. This is most likely due to the fact that urea only gradually denatures the protein. Parallel experiments with 4/5/6 M urea in the solution showed no difference in the final OD, but the time required to reach equilibrium showed clear dependence on urea concentration (data not shown). When $Na_2S_2O_4$ was added, all free Fe ions in the solution were reduced to Fe(II), and it has been reported that the fully reduced Fe(II)/Fe(II) form of a similar mixed-valent active center was not stable (Merkx and Averill, 1998). To examine whether this is also the case for PqsE, the protein was diluted to a solution with only phenanthroline in buffer (no urea), and monitored immediately after

addition of $Na_2S_2O_4$. The result indeed suggests that Fe(II) rapidly dissociates from the protein and formed complex with phenanthroline (Figure 5.30, brown line).

Analyzing the numbers from the urea experiment carefully, the Fe(II) and Fe(III) contents are not exactly 1:1. The concentration of Fe(III) was calculated to be 37.54 μM while Fe(II) was 33.41 μM. This small difference may be an artifact because the addition point of $Na_2S_2O_4$ seemed to be a bit too early for the OD to fully reach a very flat plateau, but considering the fact that Fe(III)/Fe(II) bound to the protein while Fe(II)/Fe(II) did not, the difference may also be an indication that Fe(III) binds more tightly to PqsE. This hypothesis was examined by metal exchange experiments described in the following section.

### 5.13.2 Metal exchange experiments

A batch of E182A showed reduced bis-pNPP hydrolysis activity ($K_M$ = 582 μM, $k_{cat}$ = 2.19; in contrast to $K_M$ = 208 μM, $k_{cat}$ = 12.4 before). The Fe content of this batch of protein was analyzed via phenanthroline assay (Figure 5.31A). The [Fe] / [Protein] ratio was determined to be 1.2:1. Interestingly, the [Fe(III)] / [Fe (II)] ratio was 3.29, which means that in this batch of protein the Fe(III) occupancy was about 92% while the Fe(II) occupancy was only 28%.

By applying EDTA at 50 μM concentration, the bis-pNPP hydrolysis activity can be fully abolished (not measurable in previous conditions). Addition of different divalent metals restored the activity to different extent (Figure 5.31B). As expected, addition of Fe(III) did not restored the PDE activity, which means that the hydrolysis of bis-pNPP requires a divalent metal.

Co(II) improved the efficiency almost 10 fold, even better than Fe(II), but it is unclear whether Co(II) binds to E182A with higher affinity than Fe(II). Therefore it is not possible to predict whether Co(II) can displace the more tightly bound Fe(III) or not. A following experiment was carried out to answer this question. The same E182A protein as depicted by the blue line in Figure 5.31A was incubated with 50-fold excess of Co(II), then passed through a gel-filtration column to remove the excess Co(II). Fe content and bis-pNPP hydrolysis activity was then analyzed and compared to the untreated E182A.

As depicted by the brown line in Figure 5.31A, after the Co(II) incubation, the total [Fe] / [Protein] ratio dropped to 1.04, and the [Fe(III)] / [Fe(II)] ratio rose to 7.00. This indicates that the Fe(III) occupancy is still 91% (from 92%) while the Fe(II) occupancy

dropped to 13% (from 28%). To test whether there is Co(II) bound at all, bis-pNPP hydrolysis of this preparation was measured at saturating 1 mM substrate concentration, in parallel with the untreated protein. The $V_0$ of the Co(II)-treated E182A was about 2.6 fold of the $V_0$ of the untreated protein (Figure 5.32A).

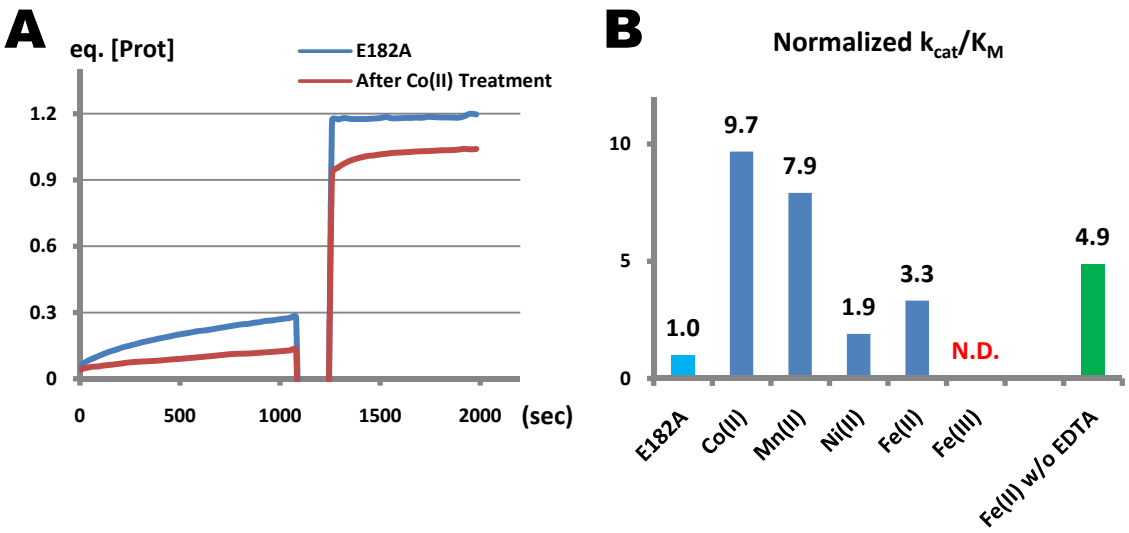


**Figure 5.31: A) Fe analysis of a batch of E182A before (blue line) and after (brown line) incubation with Co(II). B) Efficiency for bis-pNPP analysis in presence of 50 µM EDTA and different metals. Shown as $k_{cat}/K_M$ value normalized to that of untreated E182A (cyan). For contrast, a sample with Fe(II) addition without EDTA was also measured (green). N.D.: not detectable.**

### 5.13.3 Dependence of PqsE activity on metal concentration

Despite Co(II) treated E182A described in the previous section exhibited enhanced bis-pNPP hydrolysis comparing to the untreated protein, the hydrolysis can be further improved by addition of Co(II) in the reaction for both treated and untreated E182A (Figure 5.32A).

A series of reactions was therefore set up, using 1 mM of bis-pNPP and varying the Co(II) concentration in the hydrolysis reaction mixture. Untreated E182A was used at 1 µM concentration. As shown in Figure 5.32B, the reaction rate reached a maximum when Co(II) was added at very high concentration. Half-maximum rate was reached at Co(II) concentration of approximately 280 µM.

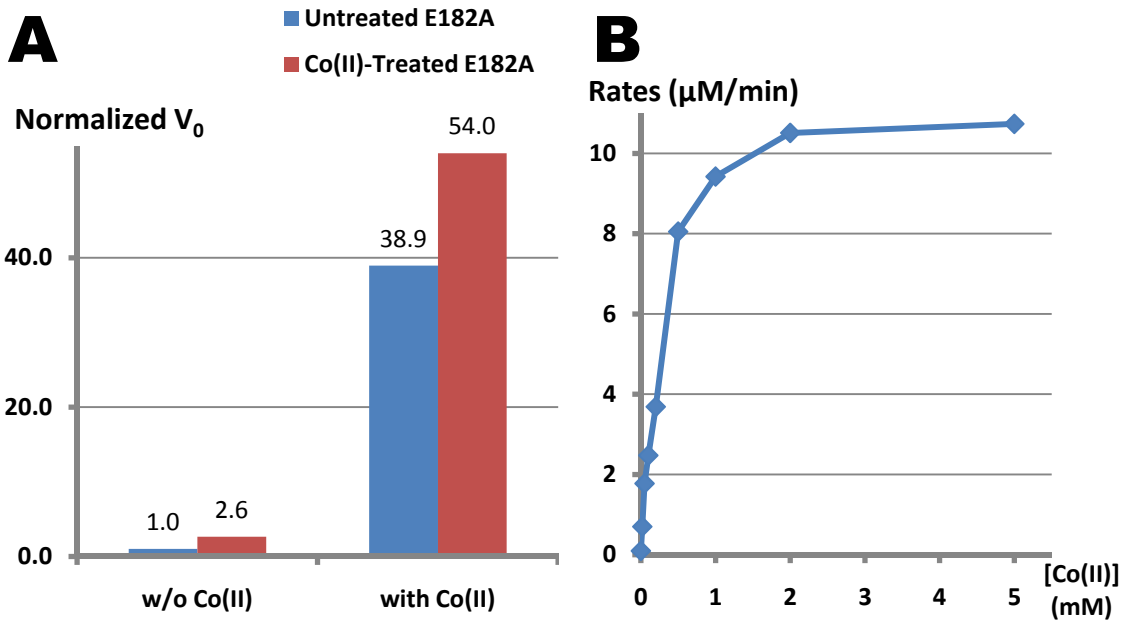


**Figure 5.32: Dependence of bis-pNPP hydrolysis activity on added Co(II) in the reaction mixture. A) Hydrolysis of bis-pNPP by untreated and Co(II)-treated E182A, with or without additional Co(II) in reaction mixtures. $V_0$ values are normalized to that of untreated E182A without addition of Co(II). B) Dependence of hydrolysis rate on the concentration of additional Co(II).**

## 5.14 TRANSCRIPTOME ANALYSIS

To obtain insights to the natural substrate of PqsE and to show the content of the PqsE-regulon, genome-wide transcription profiles of a *P. aeruginosa* PAO1 *ΔpqsE* mutant and the PAO1 *ΔpqsE*+pUCpqsE strain (over-producer) were analyzed as described in Section 4.16. 162 genes that have significant difference in their transcription level between these mutants were identified, out of which 122 were strongly up-regulated and 40 were strongly down-regulated in the over-producer. The complete list is attached in the appendices of this thesis (Table 8.1).

As reported by Farrow et al, the function of PqsE requires the presence of the Rhl-QS system. Indeed, the transcriptome analysis showed that PqsE activates the *rhl* genes but not the *las* genes. The list of 162 genes was compared to that reported by Schuster et al to remove Rhl-controled genes. 100 genes are controlled by PqsE but not RhlR. These are listed in Table 5.12.

| Identifier | Ratio | Gene Name | Annotation |
|---|---|---|---|
| ***Genes with Known Functions*** | | | |
| PA0140 | 3.5 | ahpF | alkyl hydroperoxide reductase subunit F |
| PA0282 | 2.32 | cysT | sulfate transport protein CysT |
| PA0849 | 3.29 | trxB2 | thioredoxin reductase 2 |
| PA0865 | 3.07 | hpd | 4-hydroxyphenylpyruvate dioxygenase |
| PA0931 | 2.53 | | siderophore receptor protein |
| PA0997 | -2.09 | pqsB | Homologous to β-keto-acyl-acyl-carrier protein synthase |
| PA1001 | -2.38 | phnA | anthranilate synthase component I |
| PA1097 | -2.08 | fleQ | transcriptional regulator FleQ |
| PA1180 | -2.31 | phoQ | two-component sensor PhoQ |
| PA1480 | 2.38 | ccmF | cytochrome C-type biogenesis protein CcmF |
| PA1483 | 2.38 | cycH | cytochrome c-type biogenesis protein |
| PA1901 | 5.16 | phzC2 | phenazine biosynthesis protein PhzC |
| PA1902 | 5.07 | phzD2 | phenazine biosynthesis protein PhzD |
| PA1903 | 4.68 | phzE2 | phenazine biosynthesis protein PhzE |
| PA1904 | 5.09 | phzF2 | probable phenazine biosynthesis protein |
| PA1905 | 5.53 | phzG2 | probable pyridoxamine 5'-phosphate oxidase |
| PA1927 | 2.48 | metE | 5-methyltetrahydropteroyltriglutamate-homocysteine S-methyltransferase |
| PA2008 | 2.4 | fahA | fumarylacetoacetase |
| PA2016 | -2.44 | gnyR | Regulatory gene of gnyRDBHAL cluster, GnyR |
| PA2259 | 2.04 | ptxS | transcriptional regulator PtxS |
| PA2413 | 2.69 | pvdH | L-2,4-diaminobutyrate:2-ketoglutarate 4-aminotransferase, PvdH |
| PA2493 | 4.55 | mexE | multidrug efflux membrane fusion protein MexE precursor |
| PA2494 | 3.42 | mexF | multidrug efflux transporter MexF |
| PA2495 | 2.91 | oprN | multidrug efflux outer membrane protein OprN precursor |
| PA2507 | 2.64 | catA | catechol 1,2-dioxygenase |
| PA2508 | 5.01 | catC | muconolactone delta-isomerase |
| PA2509 | 3.63 | catB | muconate cycloisomerase I |
| PA2647 | 2.01 | nuoL | NADH dehydrogenase I chain L |
| PA3126 | -2.41 | ibpA | heat-shock protein IbpA |
| PA3186 | 3.76 | oprB | Glucose/carbohydrate outer membrane porin OprB precursor |
| PA3192 | 2.21 | gltR | two-component response regulator GltR |
| PA3193 | 2.27 | glk | glucokinase |
| PA3477 | 2.87 | rhlR | transcriptional regulator RhlR |
| PA3478 | 3.61 | rhlB | rhamnosyltransferase chain B |
| PA3479 | 3.34 | rhlA | rhamnosyltransferase chain A |

| | | | |
|---|---|---|---|
| PA3811 | -2.38 | hscB | heat shock protein HscB |
| PA3812 | -2.03 | iscA | probable iron-binding protein IscA |
| PA3813 | -2.05 | iscU | probable iron-binding protein IscU |
| PA3814 | -2.2 | iscS | L-cysteine desulfurase (pyridoxal phosphate-dependent) |
| PA4309 | -3.57 | pctA | chemotactic transducer PctA |
| PA4310 | -3.26 | pctB | chemotactic transducer PctB |
| PA4443 | 2.25 | cysD | ATP sulfurylase small subunit |
| PA4236 | 2.74 | katA | catalase |
| PA4613 | 4.49 | katB | catalase |
| PA4934 | 2.42 | rpsR | 30S ribosomal protein S18 |
| PA5100 | 3.16 | hutU | urocanase |
| PA5128 | 2.62 | secB | secretion protein SecB |
| PA5163 | 2.21 | rmlA | glucose-1-phosphate thymidylyltransferase |
| PA5499 | -2.09 | np20 | transcriptional regulator np20 |

### *Functionally Unannotated Genes*

| | | |
|---|---|---|
| PA0227 | 3.18 | probable CoA transferase, subunit B |
| PA0271 | 2.18 | hypothetical protein |
| PA0541 | 2.96 | hypothetical protein |
| PA0737 | -2.11 | hypothetical protein |
| PA0848 | 4.55 | probable alkyl hydroperoxide reductase |
| PA0938 | 2.96 | hypothetical protein |
| PA1095 | -2 | hypothetical protein |
| PA1123 | 3 | hypothetical protein |
| PA1297 | -4.36 | probable metal transporter |
| PA1298 | -2.05 | conserved hypothetical protein |
| PA1423 | -2.81 | probable chemotaxis transducer |
| PA1463 | -2.78 | hypothetical protein |
| PA1545 | -2.6 | hypothetical protein |
| PA1555 | 2.19 | probable cytochrome c |
| PA2112 | 2.91 | conserved hypothetical protein |
| PA2114 | 2.46 | probable major facilitator superfamily (MFS) transporter |
| PA2126 | 2.04 | conserved hypothetical protein |
| PA2260 | 2.1 | hypothetical protein |
| PA2384 | 2.03 | hypothetical protein |
| PA2393 | 2.35 | probable dipeptidase precursor |
| PA2411 | 2.89 | probable thioesterase |
| PA2481 | -2.55 | hypothetical protein |
| PA2482 | -2.66 | probable cytochrome c |
| PA2634 | -2.36 | probable isocitrate lyase |
| PA2654 | -2.05 | probable chemotaxis transducer |
| PA2868 | 2.07 | hypothetical protein |

| | | |
|---|---|---|
| PA2992 | 2.31 | hypothetical protein |
| PA3187 | 5.13 | probable ATP-binding component of ABC transporter |
| PA3237 | 4.14 | hypothetical protein |
| PA3287 | 4.89 | conserved hypothetical protein |
| PA3307 | -2.33 | hypothetical protein |
| PA3351 | -2.03 | hypothetical protein |
| PA3600 | -2.91 | conserved hypothetical protein |
| PA3601 | -2.65 | conserved hypothetical protein |
| PA3690 | 2.27 | probable metal-transporting P-type ATPase |
| PA3729 | -2.01 | conserved hypothetical protein |
| PA3730 | -2.51 | hypothetical protein |
| PA3731 | -2.75 | conserved hypothetical protein |
| PA3732 | -2.65 | conserved hypothetical protein |
| PA3815 | -2.23 | conserved hypothetical protein |
| PA3865 | -2.48 | probable amino acid binding protein |
| PA4311 | -2.08 | conserved hypothetical protein |
| PA4357 | 3.78 | conserved hypothetical protein |
| PA4421 | -2.04 | conserved hypothetical protein |
| PA4507 | -2.09 | hypothetical protein |
| PA4520 | -2.1 | probable chemotaxis transducer |
| PA4630 | -2.08 | hypothetical protein |
| PA4674 | -2.22 | conserved hypothetical protein |
| PA4881 | 2.59 | hypothetical protein |
| PA5219 | 2.1 | hypothetical protein |
| PA5460 | 2.84 | hypothetical protein |

**Table 5.12: List of PqsE controlled genes. Orange boxes: PqsE-activated gene clusters. Blue boxes: PqsE-suppressed gene clusters. Gray shades show that the Rhl-QS genes were indeed up-regulated.**

When mapped to the metabolic pathways using the KEGG database tools (Kanehisa and Goto, 2000;Kanehisa et al., 2006;Kanehisa et al., 2008), 51 out of the PqsE-controlled genes appear to be not well studied as "hypothetical proteins". From those annotated several observations can be made.

PqsE-suppressed genes seem to have links to iron uptake. For example, gene cluster PA3811-PA3815 encodes potential iron-binding proteins. PA5499 (*np20*) encodes a transcription factor predicted to be a Fur-like iron/zinc uptake regulator. HHQ biosynthesis genes (*pqsB, phnA*) are also down regulated. Considering the auto-inductive nature of the *pqsA-D-pqsR* QS system, PqsE may serve as an off-switch when enough HHQ molecules are present in the quorum. It is however interesting to note that *pqsH*, the gene converting

HHQ to PQS (PA2587, data shown in Table 8.1), is up-regulated in presence of PqsE. This implies that *P. aeruginosa* discriminates the HHQ and PQS molecules and the yet poorly understood biological roles of these metabolites are very important for the bacteria.

Besides, two chemotactic transducer genes, *pctA and pctB*, were also suppressed by the presence of PqsE. The two encoded proteins share 81% sequence identity and had been reported to be responsible for the chemotaxis of *P. aeruginosa* to L-amino acids (Kuroda et al., 1995;Taguchi et al., 1997).

As reviewed in Section 1.4.6, PqsE controls the expression of many virulence related genes. Indeed, in the presence of PqsE, genes for phenazine biosynthesis (both copies of the *phz* operon), protease production (*lasA, lasB*) and hydrogen cyanide biosynthesis (*hcnA/B*) are among the most activated ones (data shown in Table 8.1). From the literature it is known that the function of PqsE is closely connected to active Rhl-QS system (Farrow, III *et al.*, 2008). It has been reported that the *phz1* operon (PA4209-PA4217), *las* and *hcn* genes are controlled by Rhl-QS (Schuster *et al.*, 2003). It is therefore difficult to judge whether the up-regulation of these genes are solely the result of Rhl activation or PqsE also directly active them. Nevertheless, at least the *phz2* operon (PA1899-PA1905), consists of *phzA-G*, is directly active by PqsE.

Meanwhile, in addition to the expected virulence / QS genes, a group of genes which are involved in tryptophan metabolism / anthranilate metabolism are highly up-regulated (*kynB, antA-C, catA-C, katA/B*). Since kynU is co-regulated with kynB, it is likely to be up-regulated as well. As shown in Figure 5.33, the biosynthesis of aromatic amino acids proceeds from chorismate, down-stream to the skikimate pathway. In particular, the biosynthesis of tryptophan uses anthranilate as an intermediate. Interestingly, the biosynthesis of phenazines branches off from chorismate and the biosynthesis of HHQ/PQS branches off from anthranilate. Therefore, the biological function of PqsE seems to be linked to anthranilate homeostasis in the cell but with complications: Rhl-QS is known to activate *kynB* and *antA-C*, but not *catA-C* and *katA-B* (Schuster *et al.*, 2003). Anthranilate is either synthesized from chorismate or degraded from tryptophan. It was observed that genes for degradation of tryptophan were more strongly transcribed in presence of PqsE, as well as the genes for degradation of anthranilate/catechol. However, the biosynthesis of HHQ/PQS is reduced. It is not clear yet whether the overall level of anthranilate is changed or not, because

despite the fact that transcription levels of the anthranilate synthase phnA/B are significantly reduced, there is at least one more copy of anthranilate synthase trpE/G in the cell.

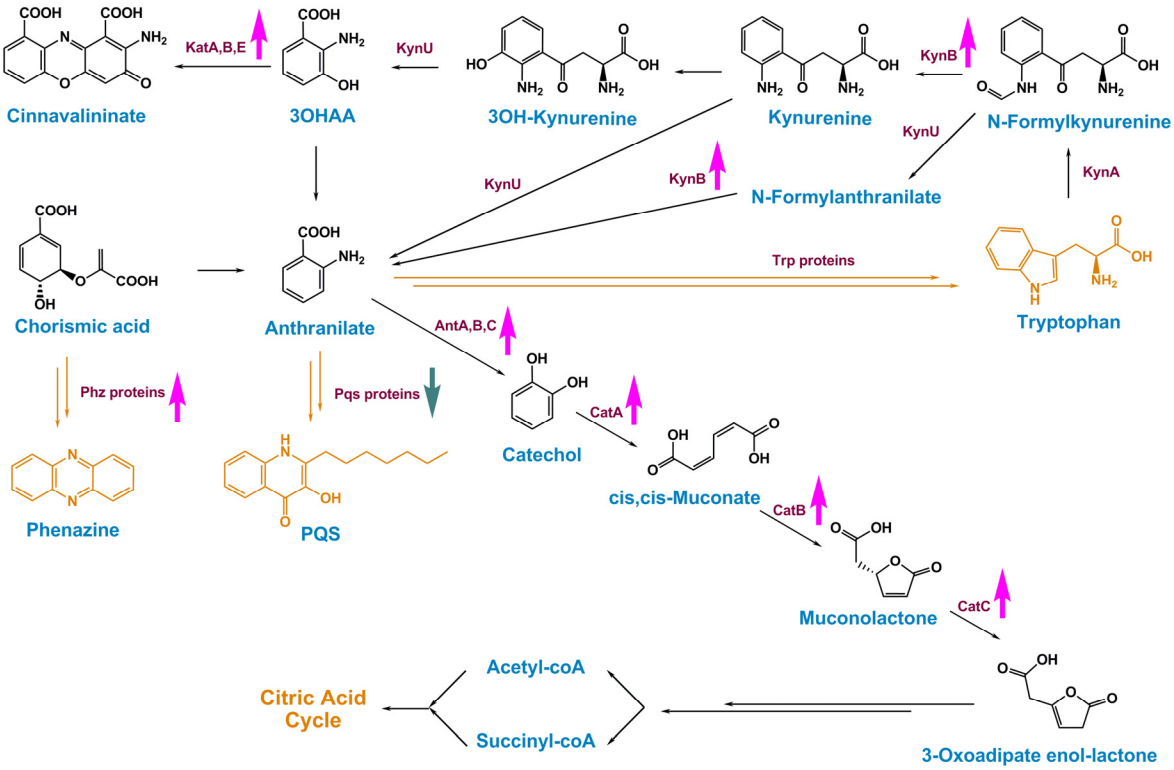


**Figure 5.33: Scheme of changes in gene expression in anthranilate-connected metabolites. Pink arrow, significant up-regulation in presence of PqsE; green arrow, significant down regulation in presence of PqsE.**

In summary, the transcriptome data strongly suggests that PqsE controls expression of virulence genes as well as genes in primary metabolic pathways. The flow of chorismate is shifted towards phenazine biosynthesis and the bacteria actively degrade anthranilate, via the catechol intermediate, into the citric acid cyle. The anthranilate level may be maintained by degrading tryptophan, which is not required for cell growth anymore at that stage. However, because the scheme involves many proteins of which the regulation mechanisms have not been well established, it is not obvious how PqsE achieves this at the molecular level.

# PART III
# STRUCTURAL AND FUNCTIONAL ANALYSIS OF PA0803

As described in Section 5.1, it was predicted that PA0803 shares the same fold as EhpR (a phenazine binding protein that has the glyoxalase/bleomycin resistant protein fold) and therefore may be able to bind phenazines. In this chapter, crystal structures of PA0803 determined in this study are presented, together with biochemical data to support this hypothesis.

## 5.15 COMPARISON OF THE PA0803 STRUCTURES

Structures of wild type apo-PA0803, the PA0803-PYO complex and the H49A mutant were compared to assess whether significant structural changes occur upon binding of pyocyanin or mutation of a binding site residue.

The protein was crystallized in two space groups: the H49A mutant in the high symmetry $P4_32_12$ space group with one dimer per ASU; and the wild type PA0803 structures in $P2_12_12$ containing four monomers per ASU, two of which (chain A and B) forming a dimer, while chain C and D each forming a dimer with the same chain from the neighbouring ASUs, as shown in Figure 5.34.

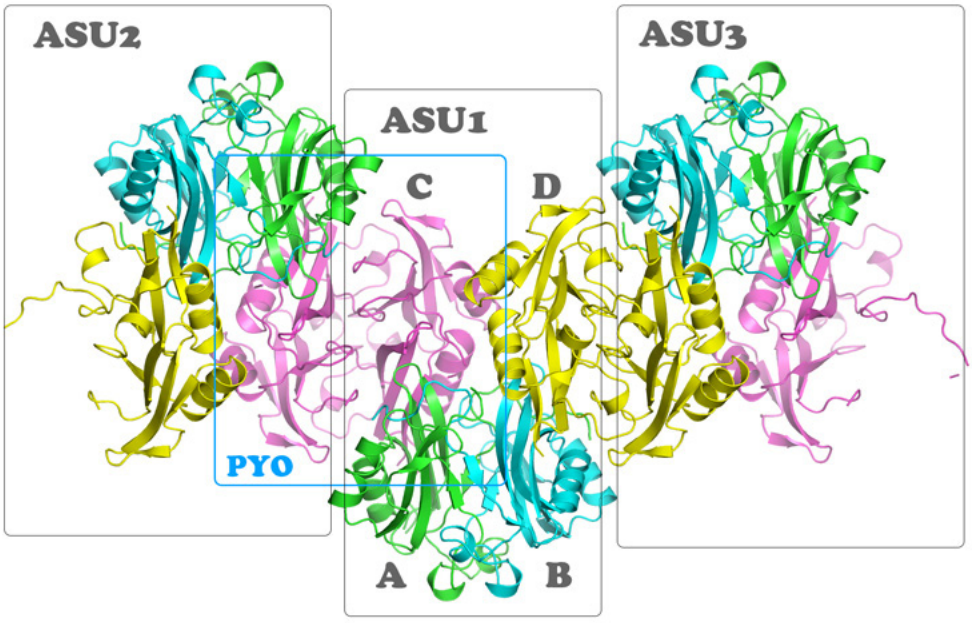


**Figure 5.34: Crystal packing of PA0803 in the $P2_12_12$ space group. ASU: asymmetric unit; A, B, C, D indicate the chains. Blue box and PYO label indicate the dimer that has pyocyanin bound.**

In the PA0803-PYO structure, pyocyanin is only observed at the two binding sites of the Chain C ─ Chain C dimer, which gives an overall occupancy of 25%.

Next, the structure of chain C in the PA0803-PYO structure is pairwisely compared to all other chains in all obtained structures, using the program SUPERPOSE in the CCP4 suite. RMSD differences are listed below:

| Moving Structure | | Overall RMSD (Å) |
|---|---|---|
| Structure | Chain | |
| PA0803-PYO | A | 0.368 |
| PA0803-PYO | B | 0.361 |
| PA0803-PYO | D | 0.333 |
| apo_PA0803 | A | 0.434 |
| apo_PA0803 | B | 0.314 |
| apo_PA0803 | C | 0.178 |
| apo_PA0803 | D | 0.388 |
| H49A | A | 0.471 |
| H49A | B | 0.473 |

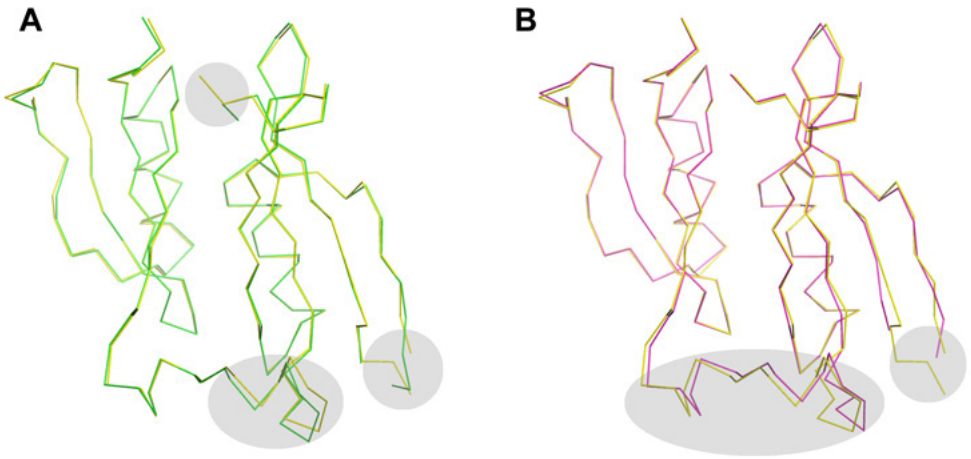


**Figure 5.35: Comparison of obtained PA0803 structures with largest RMSD. A) Overlay of chain C in PYO-structure (yellow) and chain A in apo-structure (green). B) Overlay of chain B in H49A structure (magenta) and chain C in PYO-structure (yellow). Structures are shown in Cα ribbon presentations. Gray shades indicate the loops that have differences.**

Inspection of the structures with the highest RMSD values revealed that the differences are mostly in the hinge loop (A71-G85) and a flexible G42EDG45 loop which is poorly defined by the electron density (Figure 5.35). Since no significant structural change is observed, the structures of PA0803 described below all refer to the C-C dimer in the $P2_12_12$

structures unless where specified. This dimer is formed by chain C in ASU1 and chain C from the neighboring unit cell (Figure 5.34), to avoid confusion, chain C in ASU 1 will be referred as **chain 1** and chain C in ASU2 as **chain 2** in the following discussions.

## 5.16 OVERALL TOPOLOGY OF PA0803

PA0803 has the fold of Glyoxalase I/Bleomycin Resistance Protein superfamily (Pfam accession number PF00903) as shown in Figure 5.36A, B. Secondary structure elements were numbered sequentially (α1-α4, β1-β9), starting from the N-terminus. Each PA0803 monomer consists of two α-helices and two β-sheets. It folds into two similar domains, hinged by a long loop (Ala71 to Gly84) that contains two very short α-helices. The first four strands β1 to β4 form one β-sheet in which β1/β4 are in a parallel configuration, while β2/β3 and β3/β4 are anti-parallel (Figure 5.36B). The second domain consists of the α2 helix and five β-strands. The β-strands form a β-sheet, which is similar to that in the first domain, except that the strand corresponding to β2 is broken into two shorter β-strands (β6 and β7) by a loop in the middle. All components are connected by short or long loops. While most of the loops are well defined, the A71-G85 hinge loop, the very short E120 to G123 loop and loop G42 to Q46 have higher temperature factors (B-factors, see Figure 5.36C), indicating increased flexibilities. Residues E43-G45 are in fact so flexible that the electron density in the region is not ordered enough to allow building of a reliable model.

It can also be observed that the β-sheet region is rather hydrophobic (Figure 5.36D), suggesting that this region should be buried in the protein interior. The N-terminus is positively charged, while the cleft near the C-terminus is negatively charged. These observations further support that the functional unit of PA0803 is a dimer.

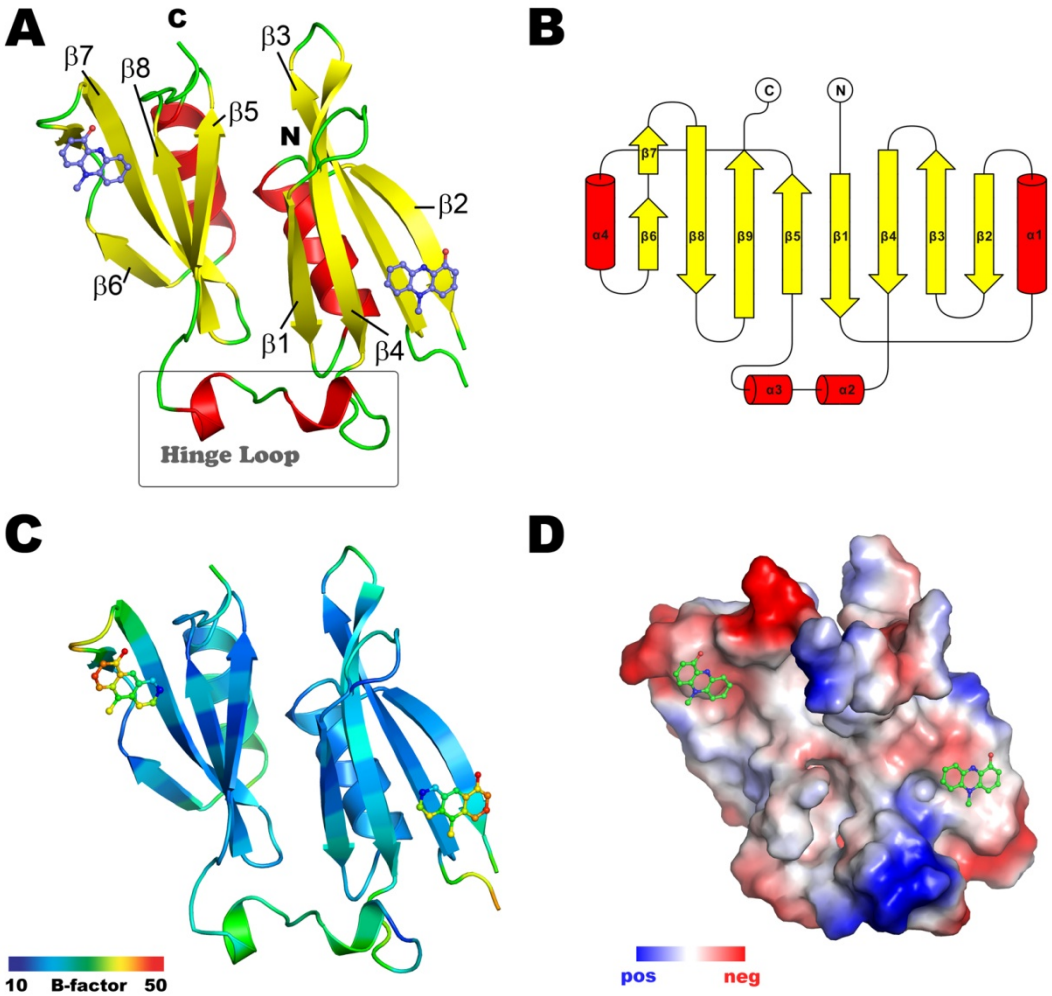


**Figure 5.36: Crystal structure of a PA0803 monomer. A) Cartoon representation. Helices colored in red, strands in yellow. B) Topology diagram of PA0803, with α-helices depicted as red cylinders and β-strands as yellow arrows with orientation according to their direction in the β-sheet. C) PA0803 structure colored by B-factor. D) Surface charge representation of PA0803.**

## 5.17 THE FUNCTIONAL UNIT AS A DIMER

### 5.17.1 Mode of dimerization

All known proteins in this superfamily (PF00903) function as dimers. Dimer formation is also critical for their functions because two ligand binding sites form at the monomer/monomer interface. Proteins may dimerize in different ways. The manner in which the glyoxalase-like proteins form dimers has either one or both of the following characteristics: “arm exchange” (Bergdoll et al., 1997) and “domain swapping”.

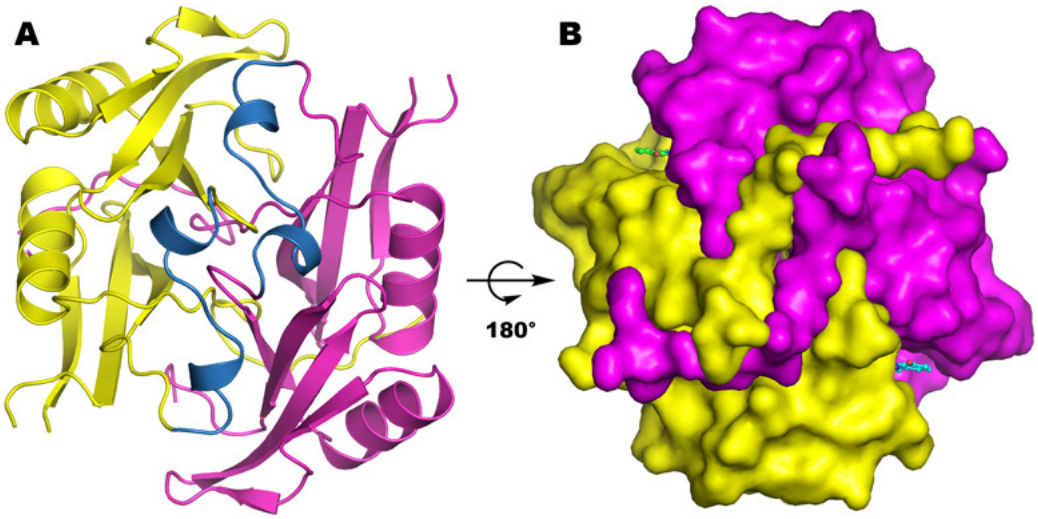


**Figure 5.37: Two views of the PA0803 functional dimer. (A) Ribbon model of the dimer, with ligand removed and the hinge loops colored blue. (B) Surface presentation from the opposite orientation, chain 1 and 2 are colored yellow and magenta, respectively.**

From the determined crystal structures, it is clear that PA0803 forms a dimer by a twisted form of arm exchange (Figure 5.37). The N-terminal loop consisting of five amino acid residues from Ala5 to Val9 of one PA0803 monomer is buried in a cleft formed by the β3-β4 connecting loop and the C-terminal loop of the other monomer, while the loop Val9 to Pro14 is sandwiched between the β4 and β5-strand of the other chain by hydrogen bonds (Figure 5.39). The arm-exchange form of dimer formation results in two large concavities at the dimer interface where the pyocyanin molecules are bound.

On the other hand, despite domain-swapping was observed in some similar proteins, the electron density is clear that this is not the case in PA0803. Therefore the binding pockets can not be formed by a single chain alone, but only at the dimer interface.

In order to swap domains, regions on two polypeptide chains have to proximate each other in an anti-parallel fashion. An example is the Mitomycin C binding protein MRD (PDB ID 1KLL), for which the domain swapping occurs at P67-T68 site (Martin *et al.*, 2002). As illustrated in Figure 5.38B, the Cα atom of P67 of one chain is 5.0Å apart from the Cα atom of T68 of the other chain. Since proline is able to adopt both *trans*- and *cis*-conformation, the loops can connect in another way to form two 180° turns so that the N- and C-terminus of each polypeptide chain is "swapped" (Figure 5.38A, taken from the original publication: Martin *et al.*, 2002).

There are two places on the hinge loop of PA0803 that are close to the same residues of the other chain of the dimer: A85-G86 and N88-T89. Since they locate at the junction of N- and C-terminal domains, they are possible locations for domain swapping. In particular, location of A85-G86 in PA0803 is similar to that of P67-T68 in MRD (Figure 5.38C). The flexibility of glycine also makes it possible to adopt wider range of torsion angles. However, the spatial distance between the Cα atom of A85 of one chain and the Cα of G86 of the other chain are 6.4 Å, significantly larger than in MRD. In addition, in the MRD protein the residues involved in swapping align as anti-parallel loops, while in the case of PA0803 A85-G86, neighbouring residues form helical structures, which in fact strongly limit the direction of the carbonyl moiety of these two residues.

The other location where anti-parallel loops come into proximity is N88-T89 (Figure 5.38D). However, it is also not likely for domain swapping to occur for two reasons. First, there is no proline or glycine residue which can adopt a *cis*- conformation to allow a 180° turn. Second, although the distance (5.8Å) is shorter than A85-G86, it is still two large to make a reasonable connection without strongly affecting the neighboring residues.

To confirm that domain swapping does not occur in PA0803 the high resolution electron density map was examined. At all these sites, the loops are clearly defined and show no ambiguity between the chains. To rule out the possibility of over-fitting during refinement, omit maps with the corresponding residues removed were calculated. The omit maps also showed clearly defined fo-fc density that allow unambiguous modeling of these loops.

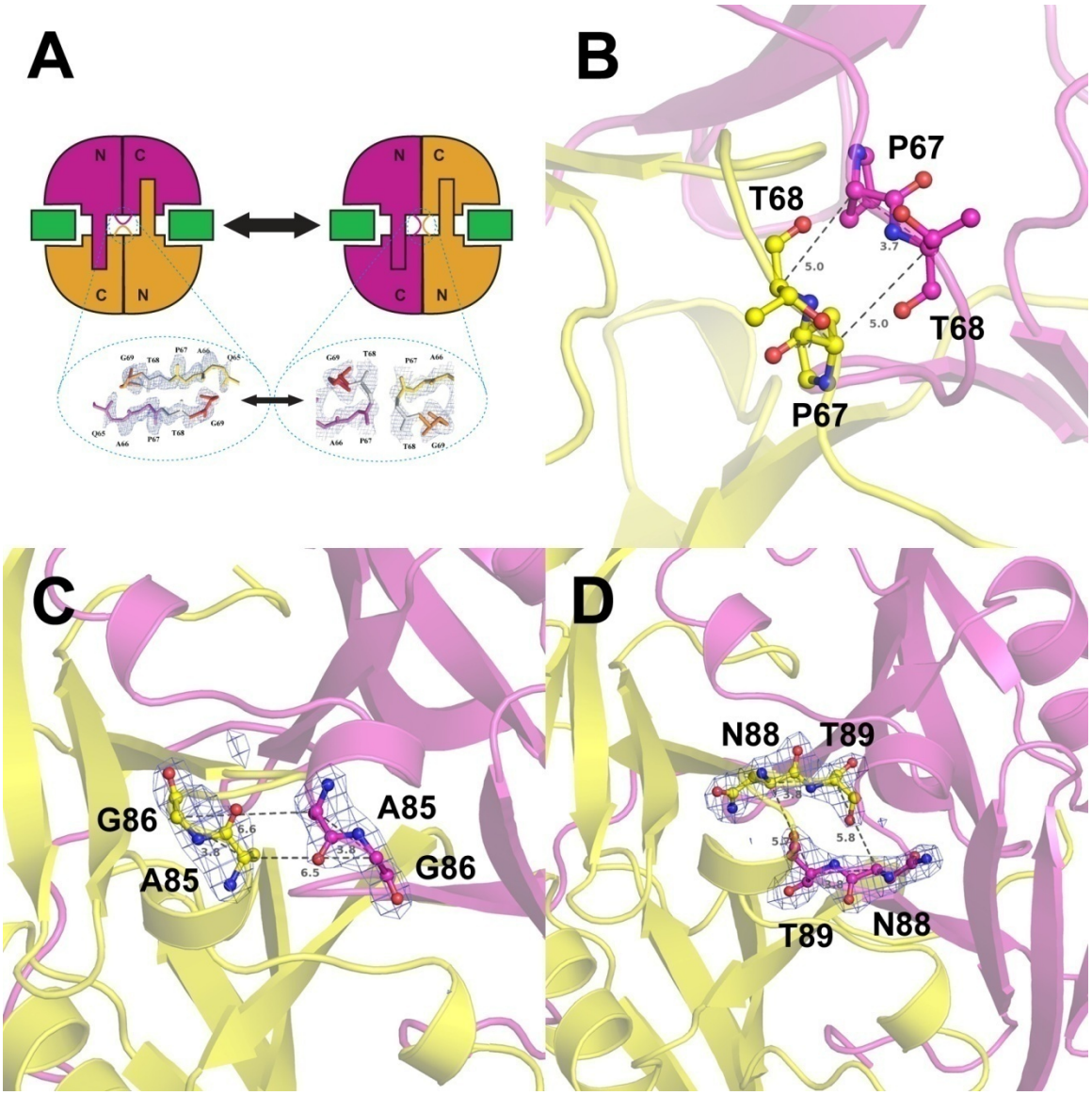


**Figure 5.38: Domain swapping is not observed in PA0803. A) Scheme and electron density of a domain-swapping protein MRD. Eletron density is taken from the original publication. B) Cartoon representation of the MRD protein (PDB ID 1KLL) at the P67-T68 swapping site, showing the distances between the Cα atoms of the residues. C) PA0803 near residue A85 and G86, Fo-Fc density of the omit-map is shown at contour level 2.5 sigma. (D) PA0803 near residue N88 and T89, Fo-Fc density of the omit-map is shown at contour level 2.5 sigma.**

### 5.17.2 Interactions at dimer interface

The size of the dimer interface (Figure 5.41) was determined with the program NACCESS (S.Hubbard and J. Thornton, 1992) and AREAIMOL of the CCP4 suite, using

1.4 Å as solvent/probe radius. Each monomer possesses an accessible surface of 9020 $Å^2$, while the dimer has an overall accessible surface of 11896 $Å^2$, therefore the dimer interface is 3072 $Å^2$ (~30%), which is at the high end of the typical range of oligomeric protein interfaces (Jones et al., 2000). Abundant interactions are found at strands β1/β5 and several loops, especially the hinge loop (Figure 5.41). Part of β3, β4, β6 also involve in dimerization, forming the ligand binding site at the interface. Approximately 1/3 of the amino acids are located at the interface (Table 5.13), mostly hydrophobic residues, with polar amino acids involved in the periphery. The percentage of polar residues (37%) is also within the normal range of oligomeric domain-domain interfaces.

| | |
|---|---|
| **Hydrophobic Residues** | |
| Non-polar | Pro4, Ala5, Val9, Ala10, Val12, Ile13, Pro14, Cys15, Leu16, Gly33, Ala55, Pro57, Ala60, Gly62, Met63, Met65, Leu78, Met79, Ala85, Gly86, Gly87, Leu92, Leu94, Val95, Val96, Ala97, V114, Pro144 |
| Aromatic | Phe32, Tyr54, Tyr75, Tyr93, Tyr142, Trp145 |
| **Polar Residues** | |
| Polar | Thr3, Ser6, Asn7, Thr8, Ser11, Gln35, Thr53, Ser56, Asn58, Asn61, Asn88, Thr89, Gln90, Ser91 |
| Charged | His2, Lys37, Glu51, Arg80, His135, Asp143 |

**Table 5.13: Residues at PA0803 dimer interface.**

From the composition of interface residues, it is obvious that hydrophobic interactions play a critical role in holding the dimer together. Plenty of hydrogen bonds are also observed. Residues on β1 strand of one monomer form hydrogen bonds with residues on β5 strand of the complementary monomer (Figure 5.39A). Ser6/Ser11 from each chain also form a ring-like "interlock" system with Asn61/Val95 residues of the other chain (Figure 5.39B).

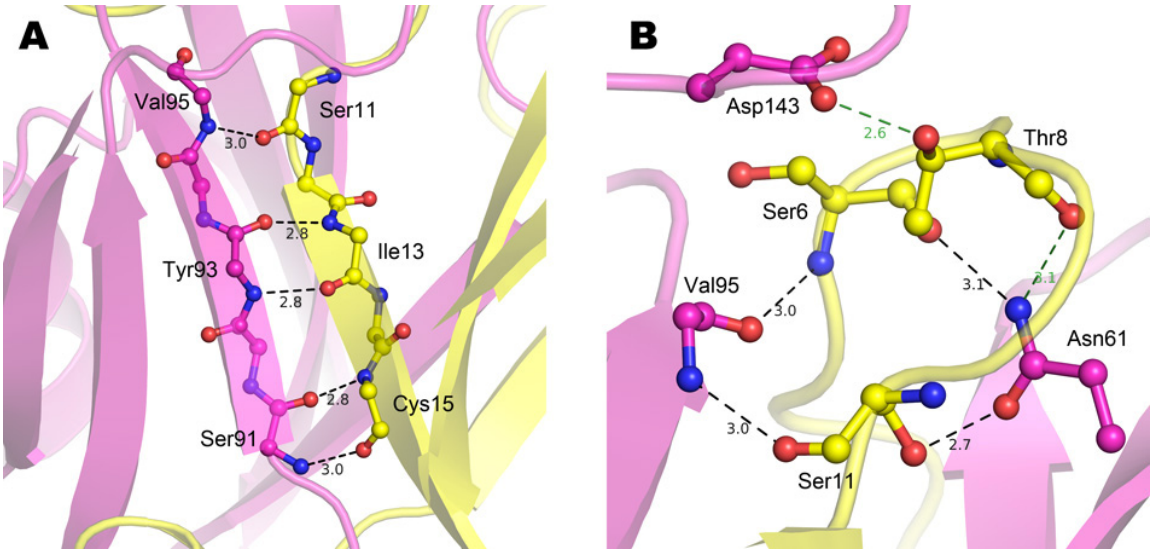


**Figure 5.39: Strong inter-chain hydrogen bond networks. Residues from chain 1 are colored in yellow and chain 2 in magenta. A) H-bonds between main chain atoms of β1 of chain 1 (Ser11-Cys15) and β5 of chain 2 (Ser91-Val95). B) The "inter-lock" (black dashes): consists of Ser6, Ser11 from one chain and Asn61, Val95 from the other chain. N61 is also connected to Thr8-Asp143 via an H-bond (green dashes). For clarity of the figure only the main chain atoms of V95 and side chains of N61/D143 are shown.**

### 5.17.3 Water molecules contributing to dimerization

Some water molecules are trapped inside the dimer, spreading along the two-fold axis and separated by the side chains of Pro14/Gln90 into solvent-shielded compartments. Near Pro14, four water molecules are enclosed in a hydrophobic pocket formed by Ala10-Pro14, Asn61-Met63 of each chain. One pair of waters (Figure 5.40A, upper pair) stabilizes the N and O atoms of V12 via two hydrogen bonds. The other pair of waters (Figure 5.40A, lower pair) binds the N and C atoms of M63 to the O atom of V12 of the same chain. The last pair of structural waters is found near Q90. They are separated by the T89-Q90 loops in to two separate vincinities (Figure 5.40B). Each water molecule has five surrounding protein residues that are in the distance of forming hydrogen bonds, namely the NE2 atom of Q90, OG1 atom of T89 of one chain and the O atom of Q90, ND2 atom of N88, ND1 atom of H135 of the other chain.

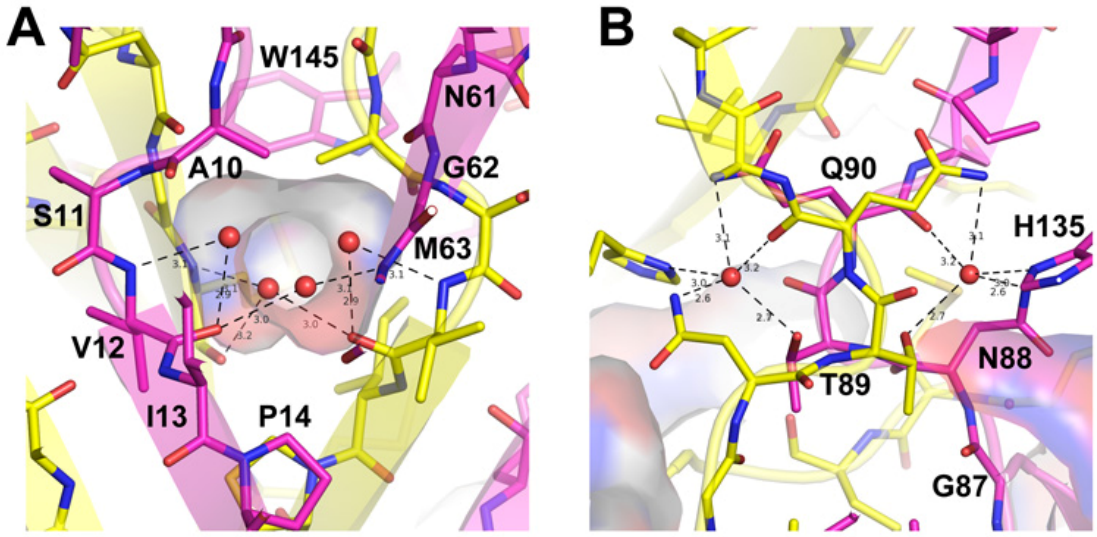


**Figure 5.40: Structural waters at the dimer interface. Black dashes show the distances between the water molecules and neighboring polar atoms.**

The presence of these structural waters provides bridging interactions via intra- and inter- chain hydrogen bonds with surrounding residues, enhancing the strength and complexity of the interaction network that links strands β1- and β5 of the two monomers.

### 5.17.4 Key residues at the interface

Dimer formation is likely to play an essential role for PA0803 to function, as indicated in the cases of bleomycin resistance proteins for which failure in dimerization abolishes their function (Bergdoll *et al.*, 1997;Kumagai et al., 1999). Key residues summarized in this section are illustrated with Figure 5.41.

Ser11 serves as the link between the N-terminal loop and strand β1. It forms various hydrogen bonds with surrounding residues. Typically a proline residue serves this function in other arm-exchange proteins, such as Pro9 in Bleomycin-binding protein ShBle (1BYL) and BLMA (1QTO); Pro12 in tumor necrosis factor TNF (1TNF); Pro19 in Bovine seminale ribonuclease A (1BSR); Pro27 in Methylamine dehydrogenase (2MTA); Pro81 in tomato bushy stunt virus TBSV (2TBV) and Pro11 in another phenazine-binding protein EhpR. This type of proline dependent arm-exchange was previously reviewed (Bergdoll *et al.*, 1997). As proline is often found in turning loops, the reason for which a serine instead of a proline is present in PA0803 needs to be investigated by further experiments. One possibility

is that despite serine and proline are quite isosteric, the side chain of Ser11 is required for a hydrogen bond with Val95 of the other chain, which will be lost if a proline is in this position. This hydrogen bond is a part of the interlocking hydrogen bonds (Figure 5.39B).

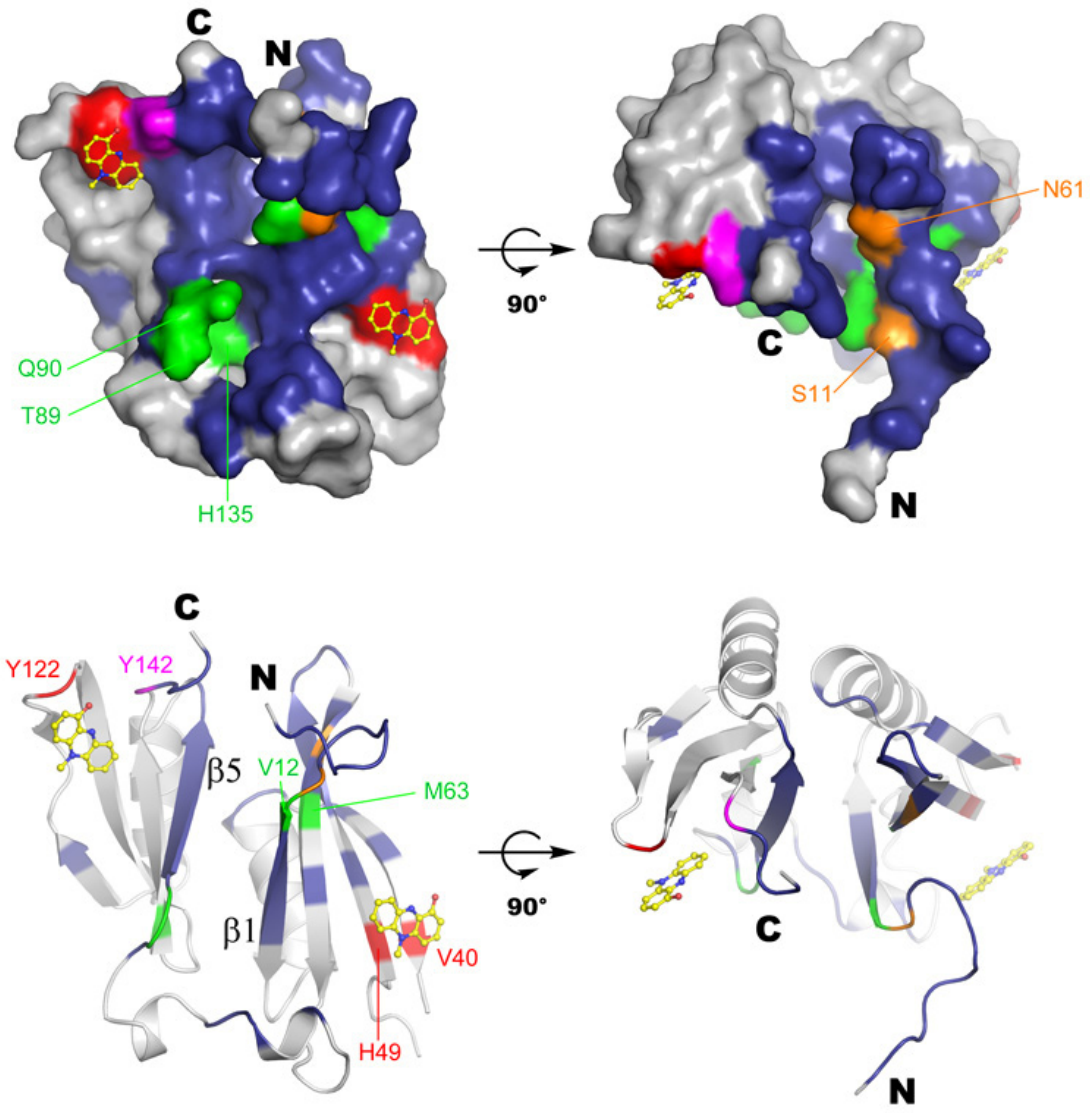


**Figure 5.41: The PA0803 dimer interface from two orientations by surface representation and the corresponding cartoon presentation. Bound PYO is shown as ball-and-stick, colored by atoms. All surface exposed residues of chain 1 that are involved in the interface are colored in blue. Residues involved in forming ligand binding pockets are colored in red. Tyr142, which involves in both, is colored in magenta. Residues that involve in binding structural waters are colored green. Two residues, Ser11 and Asn61, which are likely key residues of dimer formation, are colored in orange.**

Asn 61 is located at the center of the interaction network and has extensive interactions with neighboring residues. Together with Ser6, Thr8, Ser11 and Val95, it forms the "interlock" system, stabilizing a sharp turn that orients the N-terminal loop (Figure 5.39B).

Tyr142 participates both in dimerization and in ligand sequestering. However, it does not form interactions that seem to be essential for dimerization. Its interaction partner is Glu51 of the complementary chain, which is on the β3 strand. It functions together with Val40, His49 and Tyr122, all of which are involved in ligand binding only and will be discussed in Section 5.19.

## 5.18 ANALYSIS OF THE PA0803 LIGAND BINDING SITE

Support to the hypothesis that PA0803 can bind pyocyanin was obtained by determination of a PA0803-PYO complex crystal structure via soaking experiments. The 1.7 Å resolution structure (Figure 5.42A) also revealed how pyocyanin is sequestered by the protein.

Examining the structure of the complex, it becomes obvious that the π-stacking interaction between the aromatic rings of H49 of one chain, Y122 of the other chain and the phenazine backbone of PYO is a key interaction. The aromatic rings of both residues are 3.5Å apart from the phenazine ring. The Y122 side chain is able to adopt two possible conformations (Figure 5.42A, B). Upon binding of pyocyanin only the one shown in was observed (Figure 5.42A). The orientation of the PYO molecule could be determined by its hydroxy oxygen, which is 3.8 Å apart from the OH moiety of Tyr142, in the range of a weak hydrogen bond. In addition, the H49 residue is stabilized in this conformation by a water molecule. Further to the periphery, side-chains of residue Leu38, Val40, Leu48, Met65 (chain 1) and Tyr93 (chain 2) provide more stabilizing forces via hydrophobic interactions; the OE2 atom of Glu51 (chain 1) stabilizes the OH atom of Tyr142 via a strong hydrogen bond (length ~2.6Å).

The active sites of apo-PA0803 were found to be occupied by PEG200 molecules (Figure 5.42B), which were present at an overwhelming concentration (~ 40% w/v) in the crystallization solution. It could therefore compete PYO out of the binding sites, since PYO can only be dissolved to a maximum concentration of 1 mM in water.

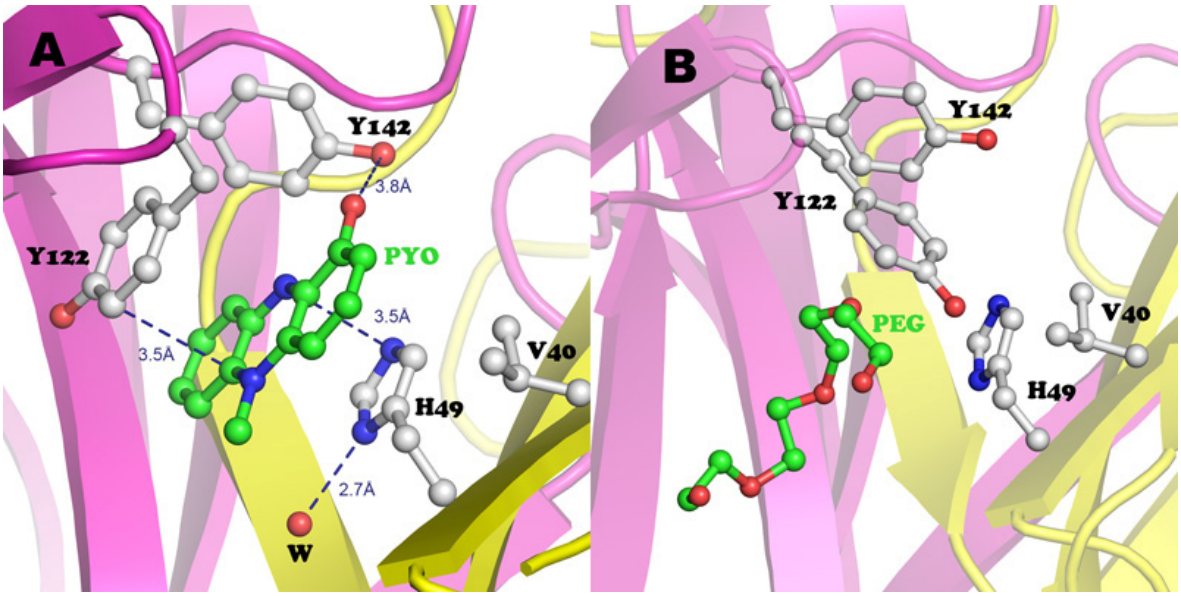


**Figure 5.42: The active site of PA0803. A) PA0803:PYO complex. Dark blue dashes show key distances: between the OH atom of Tyr 142 and O17 atom of the hydroxyl group in PYO; plane distances between the side chain of H49/Y122 and the phenazine ring of PYO. B) Apo-PA0803 structure with active site occupied by PEG200 molecules from the crystallization solution.**

## 5.19 PHENAZINE-BINDING ACTIVITIES OF PA0803

The affinity between PA0803 and pyocyanin was experimentally determined via isothermal titration calorimetry (ITC). This indicated that PA0803 bound pyocyanin with a low-micromolar affinity ($K_D = 3.92 \pm 0.23$ μM, Figure 5.43A). To prove that the affinity was indeed attributed by the protein and the ligand, a mutant protein H49A was later investigated under the same conditions as shown in Figure 5.43B. The $K_D$ dropped an order of magnitude with this mutation ($38.0 \pm 11.5$ μM).

Although this shows that PA0803 indeed can bind pyocyanin, the binding affinity is rather moderate. From the PA0803:PYO crystal structure, the interactions also seemed scarce. Figure 5.42 showed that the only interaction that might confer specificity is the weak hydrogen bond between the hydroxy oxygen of PYO and the OH atom of Y142, which raised questions whether PA0803 specifically binds pyocyanin or can also bind other phenazine compounds.

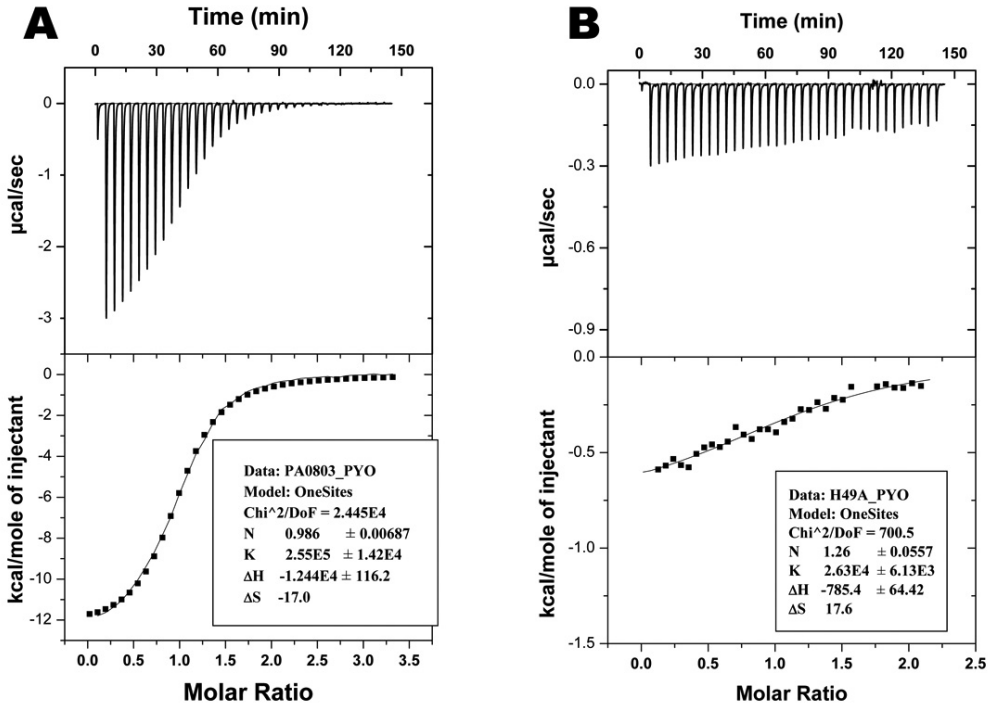


**Figure 5.43: ITC of PA0803 (100 µM in measurement cell) against pyocyanin (PYO, 1 mM in syringe). A) Wild type protein B) H49A mutant.**

Therefore, preliminary assessments of the specificity was carried out experimentally via ITC using a handful of available phenazine compounds. The measurements were conducted on an ITC machine that operates with a much lower sample volume (~ 300 µl protein). Therefore, the binding of PYO complex was reassessed and a $K_D$ of 1.48 ± 0.11 µM was obtained, confirming the results with the previous measurement.

The first compound investigated was the pyocyanin precursor phenazine-1-carboxylic acid (PCA), which should be present in *P. aeruginosa* cells. Only very weak binding was detected. When tested with a 1-hydroxy-phenazine derivative lomofungin, however, an affinity in the same range as pyocyanin was observed with $K_D$ = 9.21 ± 3.1 µM. These measurements indicated that the polarity of the hydroxy moiety of Y142 indeed favor 1-hydroxylated phenazines.

## 5.20 COMPARISON OF PA0803 WITH SIMILAR PROTEINS

### 5.20.1 Structural neighbors of PA0803

The refined model of PA0803 was submitted to the DALI server to find similar structures in the PDB database. The result coincides with that of threading (Section 5.1.2). Most of the similar proteins fall into the category of either glyoxalases I or antibiotic resistance/binding proteins. There are also a large number of hypothetical proteins of unknown function from structural genomics initiatives (PDB ID 2RBB, 3E5D, 2Q48, 2RKO, 2QNT, 1SS4, etc.). Many of these are bacterial proteins. However, there are also eukaryotic proteins like 1XY7 from *Arabidoposis thaliana*. Interestingly, a functionally unassigned gene product PA1353 from *P. aeruginosa* PAO1 (PDB ID 1U6L) was identified as a protein of this fold as well. This may be due to gene duplication in bacterial species, which will be discussed in Section 6.1. Another notable protein is one from *Salmonella typhimurium* (PDB ID 3HNQ), which has been reported to be part of a three-component operon that is predicted to have functions involving biosynthesis and modification of the peptidoglycan layer of the *Salmonella* cell wall (Shi et al., 2006). Similar proteins of known and unknown functions are listed in Table 5.14.

| PDB ID/Chain | RMSD | %id | Description |
|---|---|---|---|
| ***Function Known*** | | | |
| 1F9Z/A | 3.2 | 13 | Glyoxalase I from *E. coli* |
| 1QIP/C | 3.7 | 15 | Human Glyoxalase I |
| 2P7M/C | 2.7 | 11 | FosX, fosfomycin hydrolase |
| 1EWJ/B | 2.6 | 19 | Bleomycin binding protein BLMT |
| 1KLL/A | 3.2 | 14 | Mytomycin binding protein MRD |
| ***Function Unknown*** | | | |
| 1XY7/B | 2.4 | 21 | From eukaryote *A. thaliana* |
| 1U6L/A | 2.3 | 15 | PA1353 from *P. aeruginosa* |
| 3HNQ/A | 2.9 | 14 | Virulence protein from *S. typhimurium* |

**Table 5.14: Strutural neighbors of PA0803 and their functions. Only the most representative protein from each functional group is listed.**

PDB coordinates of PA0803, EhpR and similar structures listed in Table 5.14 were superimposed and a sequence alignment based on the superimposition was generated (Figure 5.44).

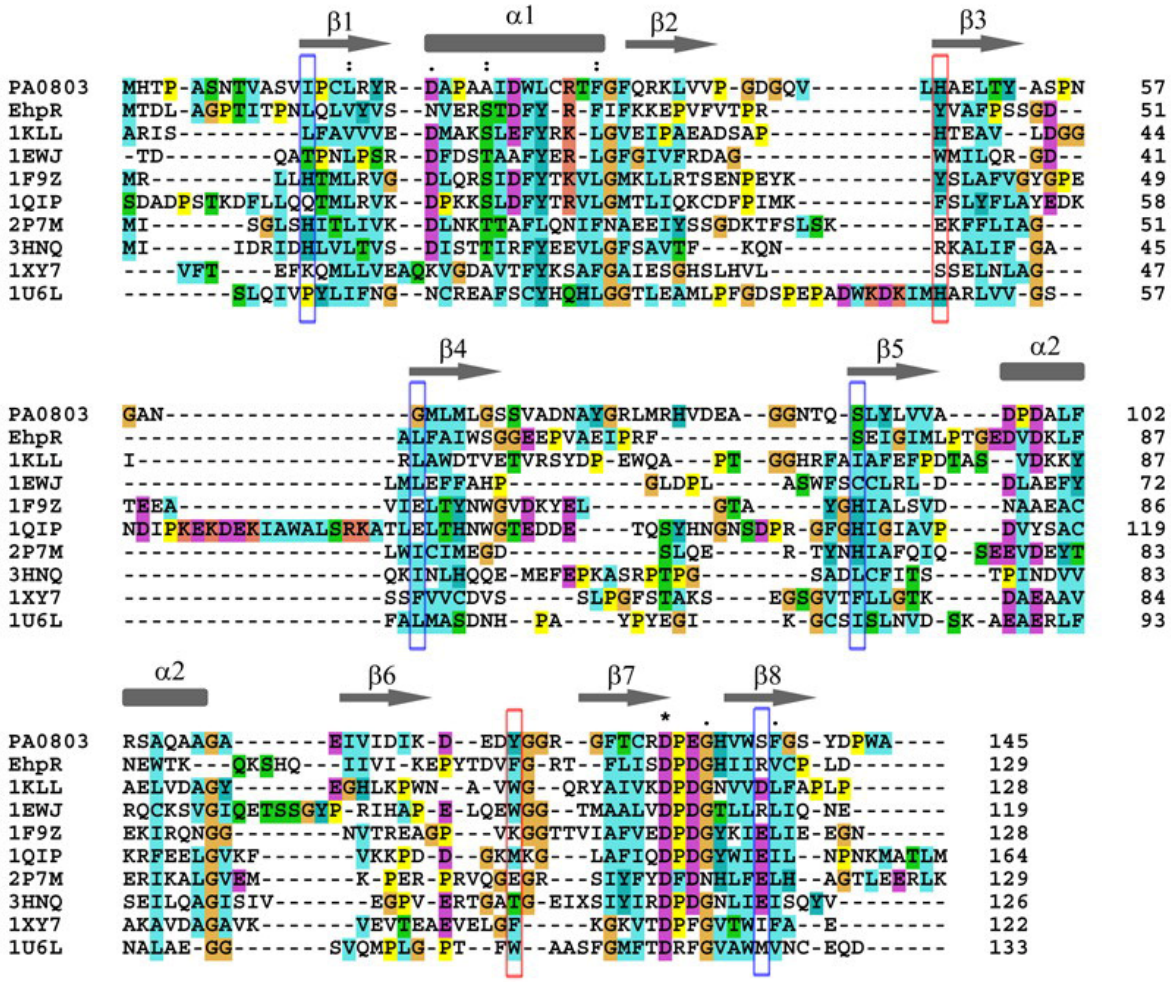


**Figure 5.44: Sequence alignment of PA0803 and similar structures. Conserved secondary structures for this superfamily are shown above the sequences. Some proteins lack some of these elements (such as EhpR does not have a β6 but a long loop instead). Residues that are crucial for antibiotic binding are boxed in red. Residues that are required for catalysis in cases of glyoxalases (1F9Z, 1QIP, 2P7M) are boxed in blue.**

These comparisons indicate that the βαβββ motif is conserved among the glyoxalase/bleomycin resistance superfamily proteins. However, these proteins clearly fall into two functional groups: antibiotic-binding proteins (PA0803, EhpR, 1KLL, 1EWJ) and hydrolases (1F9Z, 1QIP, 2P7M).

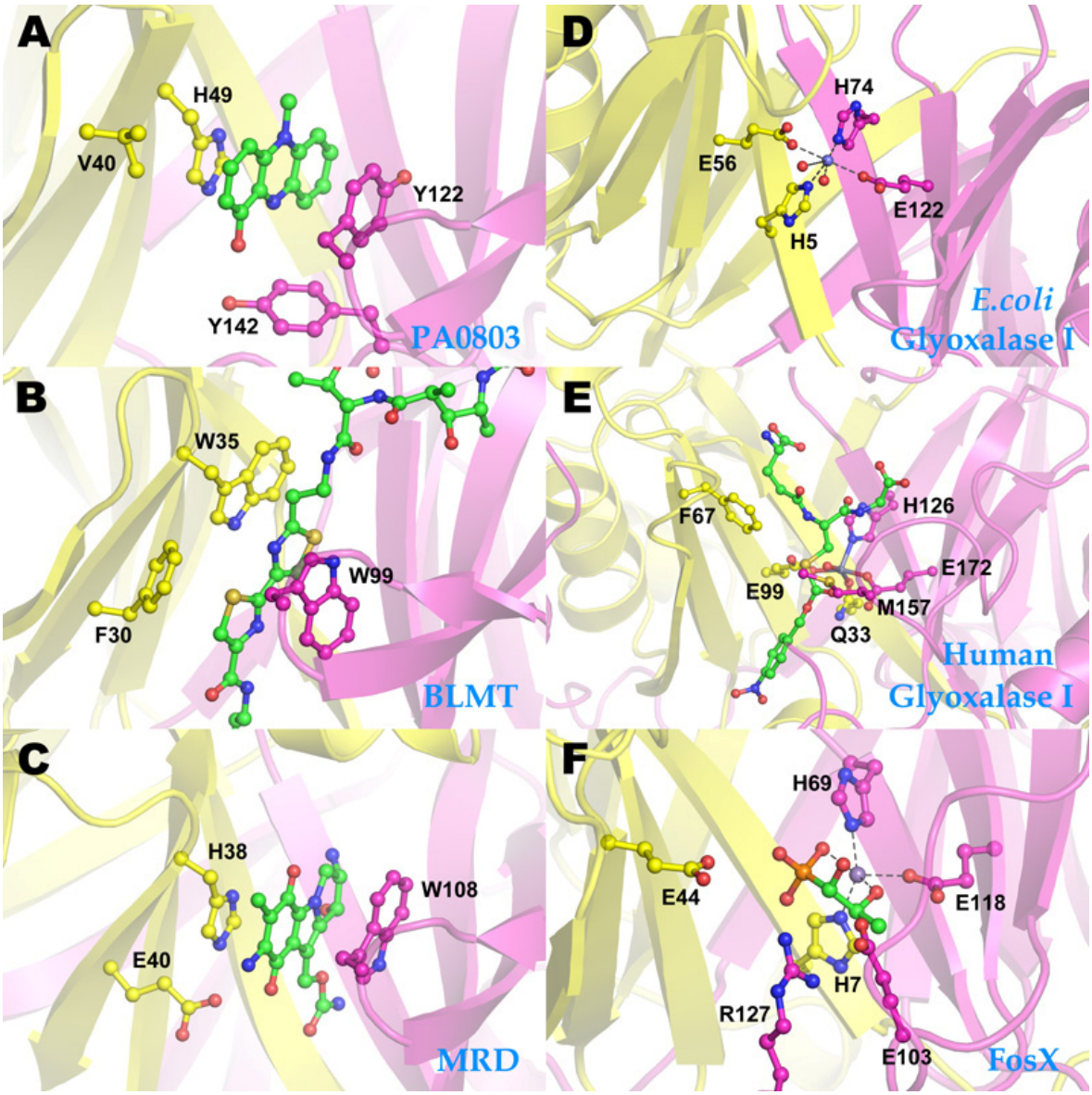


**Figure 5.45: Comparison of the binding sites of PA0803 and similar proteins, shown in ball-and-stick presentation with backbone of the proteins shown in cartoon. Chain one is colored by atom with carbon in yellow and chain two is colored by atom with carbon in magenta. Ligands are colored with carbon atoms in green. A) PA0803 B) Bleomycin binding protein BLMT C) the Mitomycin C binding protein MRD D) *E.coli* glyoxalase I E) Human glyoxalase I F) Fosfomycin hydrolase FosX, using the product-bound structure 2P7Q.**

A similarity between these two functional groups is that the binding sites locate at a similar position on the dimer interface: the β1-β4 strands from one polypeptide chain form a cleft with β5-β8 strands from the other chain to accommodate the ligand, while additional boundaries of the binding sites are defined by neighboring loops, such as the C-terminal

residues. However, the antibiotic-binding proteins have an aromatic amino acid residue at the beginning of the β3 strand and another aromatic residue at the loop between β6 and β7 (indicated by red boxes in Figure 5.44) to sandwich the aromatic moieties of the ligands. Interestingly, the hydrolases also have residues with bulky side chains at equivalent positions, suggesting that these residues might also be important for substrate binding. On the other hand, the hydrolases possess additional conserved residues to bind a catalytical metal ion (Four residues in glyoxalases and three in the case of 2P7M, blue boxes in Figure 5.44). PA0803 and EhpR apparently lack polar residues at these positions, supporting the hypothesis that they are binding proteins but not hydrolases of phenazines. For comparison, the active sites of PA0803, BLMT, MRD, FosX, *E. coli* and human glyoxalase I are shown together in Figure 5.45. Comparison of PA0803 and EhpR is addressed in the next section due to the fact that they both can bind phenazines.

### 5.20.2 Comparison of PA0803-PYO and EhpR-GA complexes

In a previous project carried out by the author, the phenazine resistance protein EhpR was characterized by crystallographic and biochemical means. Despite the physiological role of PA0803 remaining to be clarified, comparison of these two protein-ligand complexes reveals some common features of their phenazine-binding modes.

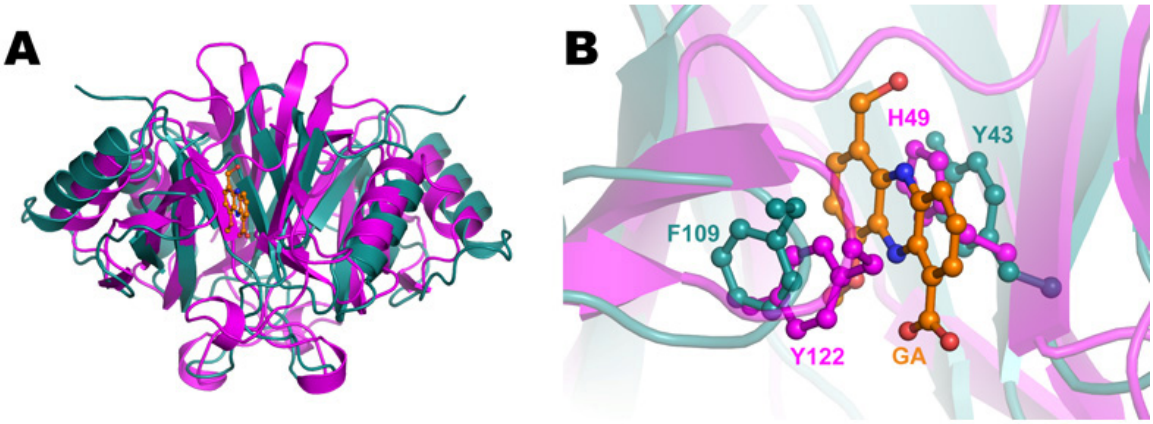


**Figure 5.46: Comparison of PA0803 and EhpR. A) Superimposition of the two dimers by individual chains. Shown in cartoon presentation with the EhpR dimer colored dark cyan and the PA0803 dimer colored magenta. B) Comparison of the active site. PA0803 chains were separately superimposed to the corresponding chain of the EhpR dimer. π-stacking residues are shown as sticks.**

First, both proteins are dimeric glyoxalase superfamily proteins that form two ligand binding sites at the dimer interface. Despite low sequence homology (19% sequence identity), the folds of these two proteins are highly conserved. Superimposition of the two protein resulted in an RMSD of 4.24 Å for Cα atoms on one chain (Figure 5.46A).

When superimposed, the active sites also showed high level of similarity and they follow identical mechanisms to sequester the target compound (Figure 5.46B). GA is a precursor of the potential actual ligand AGA and binds rather weakly to EhpR. This resulted in a not very ideal geometry of the EhpR-GA complex (Figure 5.46B). However, in the PA0803:PYO structure, three aromatic rings are parallel with equal distances of 3.5 Å (Figure 5.42A). This clearly shows that the proteins utilize the two aromatic amino acids to sandwich the phenazine ring by π-stacking interaction. It is not yet clear whether different aromatic amino acids at these positions will cause changes in affinity or specificity. Further experiments, such as mutagenesis, can be designed based on the structural findings reported in this study.

# 6 CONCLUSIONS AND OUTLOOK

## 6.1 GENE DUPLICATIONS

It is well known that bacteria cluster their genes into operons to regulate expression of functionally related genes simulateously. To ensure the presence of functional proteins at times when needed, bacteria often include two or more copies of some genes in their genome, placed under different genetic controls. In *Pseudomonas aeruginosa*, e.g., there are at least two copies of anthranilate synthases genes. One copy exists in the tryptophan biosynthesis pathway (*trpE/G*), the other copy locates immediately downstream to the *pqs* operon (*phnA/B*). They have high sequence similarity (38% identical between trpE/phnA and 47% between trpG/phnB) but are separately regulated. At the on-set of stationary phase, the biosynthesis of tryptophan is not active but the bacteria start to make large amounts of PQS which utilizes anthranilate as a precursor. Therefore, the purpose for the bacteria to encode a copy of anthranilate synthases next to the *pqs* operon is very clear: to ensure sufficient supply of the precursor during PQS biosynthesis.

Similar duplications are not rare in *P. aeruginosa*. There are also two copies of the entire *phzA-G* operon. The difference between these two operons has not been thoroughly studied. However, it is apparent they are not equal because one operon (*phz2*) has the phenazine modifying genes *phzM* and *phzS* in its neighborhood while the other has none.

For this reason, *in vivo* data obtained from *P. aeruginosa* should be viewed with the fact in mind that the bacteria may have another gene located elsewhere in the genome, which can carry out the same function under stressful situations.

### 6.1.1 Examination for duplication of PqsE

The PqsE knock-out mutant strain fails to produce pyocyanin (Gallagher *et al.*, 2002), suggesting that there is no redundant copy of *pqsE* in the *P. aeruginosa* PAO1 genome. To confirm this, a search for similar proteins was carried out with PqsE amino acid sequence using the fold-recognition algorithm PSI-BLAST. However, no ORF has significant sequence homology to PqsE. Only three ORFs (PA3614, PA5487, PA1415), products of which are annotated as hypothetical proteins, exhibit moderate similarity to fragments of PqsE (all shorter than 100 residues). In addition, PA1415 has higher sequence

similarity to a protein SPM-1, a metallo-β-lactamase from a clinically isolated *P. aeruginosa* strain. The sequence of SPM-1, whose structure is available with PDB ID 2FHX, was aligned to PqsE but was found to differ in its metal-binding residues (Figure 5.15). Indeed, SPM-1 was reported to bind zinc and its β-lactamase activity was biochemically confirmed (Murphy et al., 2003;Murphy et al., 2006). In the PAO1 genome there is no clear annotation of a metallo-β-lactamase. Whether PA1415 carries out this function requires further investigations. Nevertheless, it is not likely to carry out the same function as PqsE.

### 6.1.2 Examination for duplication of PA0803

With PA0803 the same similarity search as carried out for PqsE was also performed. No ORF with high sequence similarity was found. However, the structure of another hypothetical protein PA1353 was determined by Min *et al.* (PDB ID 1U6L) but its function has not yet been determined. PA1353 was identified by the Dali server to have the same fold as PA0803. A structure-based sequence alignment clearly shows that the 149-amino-acid PA1353 does not possess catalytic residues conserved in glyoxalases (Figure 5.44). On the contrary, the pyocyanin-binding residues in PA0803 (H49 and Y122) have exact counterparts in PA1353 (H53 and W114). Therefore, PA1353 could be another protein in the PAO1 genome that can bind pyocyanin or other phenazines.

Preliminary experiments with a PA0803 deletion mutant in *P. aeruginosa* PA14 displayed no difference in growth and pyocyanin production under the conditions investigated (Dietrich *et al.*, unpublished personal communications). This suggested functional redundancy of PA0803, if at all this protein is involved in phenazine metabolism.

A similarity search using the sequence of PA1353 identified further similar ORFs. Most notably PA4641 and PA1358, both hypothetical proteins, showed high full-length sequence homology (43% identical for PA4641 and 27% identical for PA1358). Therefore, multiple ORFs in the *P. aeruginosa* PAO1 genome encode proteins that may be able to bind phenazines. These gene products need to be examined by future studies.

## 6.2 CONCLUSIONS AND OUTLOOK

Despite significant structural and functional insights into both PqsE and PA0803 have been obtained, the physiological roles of them are yet to be determined. For PqsE, the natural substrate remains to be discovered, in spite of exhaustive trials carried out in this study. Evidences point out two possible directions, phosphodiesters and thioesters, which are both abundant in the cell. For PA0803, it is not yet clear whether phenazines are its natural ligands, given the moderate affinity.

### 6.2.1 Future studies on PqsE

**Challenges for finding natural substrates**

First, PqsE has a unique active site structure. The reaction mechanisms of many structurally related proteins have been described in the literature (Daiyasu *et al.*, 2001;Mitic et al., 2006). However, the active center of PqsE has significant differences from all of them. The additional helices at the C-terminus of PqsE render its active center relatively buried in comparison to similar proteins (Figure 5.12). This suggests that desolvation makes an important contribution to substrate activation in PqsE. Indeed no water molecules other than those coordinating the metal ions are found in the immediate vicinity of the active center.

Second, catalysis in metallohydrolases is carried out by two metal ions, the nature of which varies widely among this group of hydrolases. Without knowledge about the molecular function of PqsE, it is not possible to assign its natural metal composition from the reconstitution experiments described in Section 5.13.2. However, it is clear that recombinant PqsE contained a redox-stable Fe(III)/Fe(II) center. Besides glyoxalase II, only purple acid phosphatases (PAPs) are known to have Fe(III)/M(II) mix-valent activity centers, where M(II) can either be Fe, Mn or Zn. Considering high homology in metal-coordinating residues, it is clear that in this protein family not only the immediate metal binding residues determine the composition of the active center metals. In both PqsE and PAPs, the Fe(III) is tightly bound but the divalent cation is exchangeable. Taking into account that PqsE is a regulatory protein that responds to growth phase or growth conditions, its native active center metal composition is likely determined by metal availability within the cell. The rather weak M(II) metal also requires delicate handling of the protein and careful design of control experiments for all activity assays.

Next, the crystal complex of E182A-PqsE with bis-pNPP provides mechanistic insight into the hydrolytic activity of PqsE but no clue for natural substrate. Similar to findings in other metallohydrolases, the bridging water molecule is perfectly positioned for hydrolytic attack of the substrate, and the positive charge of the neighboring metal ions will increase its nucleophilicity (Figure 5.27). In agreement to mechanistic studies performed with other binuclear metallohydrolases, the emerging negative charge of the transition state in hydrolysis is expected to be stabilized through coordination with the dimetal center (Mitic *et al.*, 2006), and it is conceivable that the phosphate moiety of the bis-pNPP complex mimics the corresponding tetrahedral intermediate in thioester hydrolysis. However, unlike many other metallohydrolases, the active center of PqsE lacks a protonating residue in the immediate vicinity of the metal ions. Related enzymes utilize such a residue (generally a conserved histidine) to stabilize the negatively charged leaving group, which may explain why hydrolysis could only be observed towards substrates with very good leaving groups such as paranitro-substituted phenolates or benzoates.

**Future investigations based on structural/biochemical data**

Phosphodiesterase activity towards DNA and RNA was observed, but this activity seems too low to be meaningful, even if metallo-β-lactamases that play physiological roles in DNA- or RNA-processing are known (Dominski, 2007) and many other binuclear metallohydrolases have been assigned as phosphoesterases (Guddat *et al.*, 1999;Garau *et al.*, 2005). More promising seems the finding of slightly higher levels of thioesterase activity toward a para-substituted benzoate derivative S-4NB-ME, which is in accordance with the copurified benzoate-shaped ligand. However, S-4NB-ME showed no detectable affinity with PqsE in ITC (data not shown) and the p-nitro moiety seems too large for the small pocket formed by S273, H282 and E182 at the meta- or para- position of the benzoate ring (Figure 5.11D). Nevertheless, since mutagenesis data (Figure 5.28) suggested that these polar residues are required for the physiological function of PqsE *in vivo*, it is possible that the natural substrate of PqsE is an m- or p-substituted benzoate derivative.

Thioesters play important roles in countless degradative and biosynthetic pathways, e.g. in fatty acid metabolism or in polyketide and non-ribosomal peptide biosynthesis and also in the turnover of phenylalanine to benzoate. In these pathways the carboxylic acid is linked to a phosphopantetheine moiety, which in turn is either bound to a carrier protein or to

3-phospho-AMP in coenzyme A. The phosphopantetheine group itself is an extended arm, which seems to make it ideally suited to bind to the longer tunnel leading to the active site of PqsE. Docking calculations predicted that the CoA moiety would fit well into the PqsE active site if it adopted a bent conformation (Figure 6.1A). Even if none of the tested CoA derivatives was hydrolyzed, it is still tempting to speculate that PqsE functions by interfering with one of these pathways, i.e. by sending a metabolic rather than a transcriptional signal like in other quorum sensing systems.

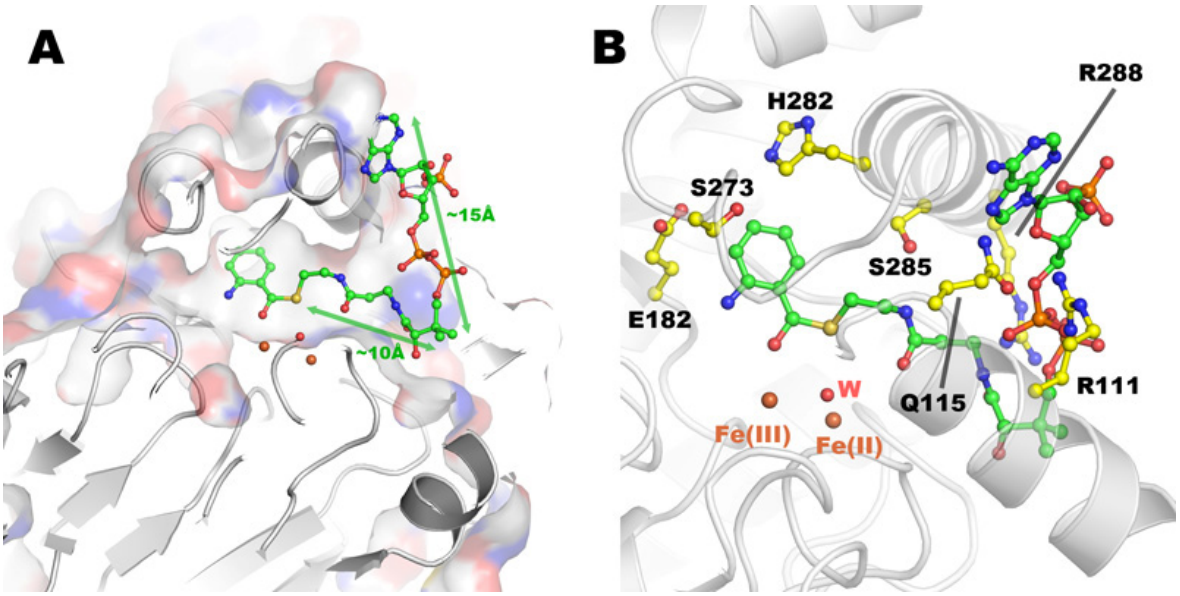


**Figure 6.1: Docking calculation of anthranilyl-CoA binding to PqsE. A) Protein in surface representation showing that the compound fits the tunnel well. B) Residues in polor contact with the substrate (not E182, S273, H282). These three residues are shown because their importance in vivo, which also suggest that the natural substrate may have a meta- or para-position substitution on the benzoyl-moiety).**

The observation of a copurified benzoate-shaped ligand in the active center indicates that the regulatory effect of PqsE may be mediated through a chorismate-derived molecule. Docking (Figure 6.1) and virtual screening (Table 6.1) with PqsE structure also points into the same direction.

In microorganisms and plants, chorismate is a central metabolite that is distributed into numerous tightly regulated pathways (Dosselaere and Vanderleyden, 2001), and several of its derivatives have regulatory roles either as activators of specific transcription factors in

a manner similar to PQS, or by acting as allosteric feedback inhibitors like e.g. the aromatic amino acids, which inhibit the first step of chorismate biosynthesis in the shikimate pathway (Herrmann, 1995). The fact that many of the pathways that utilize chorismate are conserved across different microorganisms could explain why Farrow et al. observed PqsE-dependent coactivation of a RhlR/rhlA'-lacZ reporter system in the heterologous host *E. coli*, which does not possess a *pqs*-operon itself (Farrow, III *et al.*, 2008).

| Ranking | Compound Name | G-Score |
|---|---|---|
| 2 | Indoleglycerol phosphate | -10.6 |
| 3 | Sulfathalidine | -10.5 |
| 5 | 1-(2-Carboxyphenylamino)-1'-deoxy-D-ribulose 5'-phosphate | -10.0 |
| 22 | 6-Hydroxynicotinate | -9.0 |
| 24 | 2,3-Dihydroxybenzoate | -8.9 |
| 31 | Urocanate | -8.7 |
| 32 | 4-Hydroxyhydratropate | -8.7 |
| 35 | Aminosalicylate sodium anhydrous | -8.6 |
| 36 | 4-Aminosalicylate | -8.6 |
| 37 | Vanillate | -8.4 |
| 38 | 4-Hydroxyphenylglyoxylate | -8.4 |
| 39 | 4-Hydroxybenzoate | -8.4 |
| 43 | Phthalylamide | -8.3 |
| 44 | 4-Hydroxyphenylacetate | -8.3 |
| 45 | 2,5-Dihydroxybenzoate | -8.2 |
| 46 | Nicotinate | -8.2 |
| 48 | Isonicotinic acid | -8.2 |
| 49 | 6-Methylsalicylate | -8.1 |
| 53 | 4-Aminobenzoate | -8.1 |
| 54 | Salicylate | -8.0 |
| 55 | N-Methylnicotinate | -8.0 |
| 56 | Phthalate | -7.8 |
| 58 | 4-Hydroxyphthalate | -7.8 |
| 63 | Sodium thiosalicylate | -7.7 |
| 64 | N-Methylanthranilate | -7.7 |
| 65 | 2-Carboxybenzaldehyde | -7.6 |
| 67 | 3-Fluorobenzoate | -7.5 |
| 69 | 2-Fluorobenzoate | -7.4 |
| 70 | Benzoate | -7.4 |
| 72 | Pyrrole-2-carboxylate | -7.4 |

| | | |
|---|---|---|
| 73 | 4-Fluorobenzoate | -7.4 |
| 76 | 2,4-Dinitrophenol | -7.3 |
| 78 | 3-Methoxyanthranilate | -7.2 |
| 80 | 1,2-Didehydropiperidine-2-carboxylate | -7.1 |
| 81 | delta1-Piperideine-2-carboxylate | -7.1 |
| 83 | Anthranilate | -7.1 |
| 84 | 2-Nitrophenol | -7.0 |
| 85 | 2-Chlorobenzoate | -7.0 |
| 90 | 3-Hydroxyanthranilate | -6.8 |
| 94 | N-Methyl-4-aminobenzoate | -6.3 |

**Table 6.1: Compounds with a benzoyl-shaped moiety from top 100 hits in a virtual screen. The PqsE wt structure was used as receptor and the ligand database was the KEGG compounds (the best collection of known metabolites). Anthranilate and benzoate, which have experimentally determined binding, are indicated by shades. G-scores are results from the GLIDE algorithm, lower G-score suggests better binding.**

One hypothesis formed from the virtual screening shown in Table 6.1 is that PqsE prevents the conversion from anthranilate to tryptophan by degrading one of the products of the tryptophan biosynthesis (Trp) proteins, sinces hit 2 and 5 are both products of Trp proteins. This also fits the PDE activity of PqsE because 5-Phosphoribosyl diphosphate (PRPP) is utilized to activate the anthranilate in the first step of this pathway. A preliminary experiment was carried out by incubating anthranilate, PRPP and the Trp proteins with and without PqsE. The small molecule composition showed no significant difference under HPLC-MS. This however does not rule out the possibility that one of the compounds listed in Table 6.1 is the natural substrate of PqsE. Coupled-enzymatic systems are known to have drawbacks. For example, the product small molecules may remain bound to the Trp proteins and were not accessible to PqsE. A better way to assay these compounds is to chemically synthesize them and incubate directly with PqsE.

**Future investigations based on transcriptome data**

Transcriptome analysis described in Section 5.14 has provided insights to the physiological function of PqsE. However, a clear picture can not be drawn because PqsE is weaved into a very complicated signaling network. In a recent report, it has been shown that expression of only a portion of the QS-controlled genes can be advanced by early expression of LasR and RhlR (Schuster *et al.*, 2007). This means that "QS-controlled genes" are not

only controlled by "quorum (cell density)", but also by other factors like growth phase and media composition.

Therefore, the gene expression patterns observed in Section 5.14 as well as those described in the literature (Schuster *et al.*, 2003;Schuster et al., 2004a;Deziel *et al.*, 2005;Schuster *et al.*, 2007) may all be sums of multiple factors that are difficult to separate. In light of this, *P. aeruginosa* cultures should be grown in media with more precise composition than LB and TB, e.g. a rich synthetic media LeMaster. If PqsE indeed functions by altering metabolic pathways, monitoring gene expressions in *P. aeruginosa* grown in different media may provide additional clues for the natural substrate of PqsE.

In addition, transcriptome data should be supplemented with the expression of all key transcription regulators monitored by real-time PCR. Another interesting experiment would be to generate mutants with multiple key regulators (PqsE, LasR, RhlR, MvfR, RpoS) deleted. Monitoring gene expressions in these mutants would help to dissect the complex transcriptome data.

It also has become obvious that to understand the molecular function of PqsE and ultimately the signalling network involving PqsE, metabolism in *P. aeruginosa* has to be revisited. Metabolomics techniques can be applied to obtain metabolic profiles or to follow key metabolites like anthranilate or catechol.

There are also alternatives to monitor cellular anthranilate/catechol levels. It has been reported that PA2511 encodes an anthranilate-dependent transcription regulator termed AntR (Oglesby *et al.*, 2008). In principle, it should be possible to create a bio-sensor with a reporter gene placed under control of an *ant*-promoter. Despite not experimentally proven, the *cat* operon also has a *catR* gene (PA2510) which can potentially be used to construct a bio-sensor for catechol.

### 6.2.2 Future studies on PA0803

The crystal structure of the PA0803:PYO complex and ITC data showed that PA0803 can bind PYO. PA0803 is structurally similar to phenazine-resistance protein EhpR from *P. agglomerans*. However, EhpR is co-transcribed with the phenazine biosynthesis operon of this organism and was shown to confer resistance to the phenazine antibiotic AGA to *E.coli* (Giddens *et al.*, 2002), while deletion of PA0803 is not lethal to *P. aeruginosa*

PA14. It is possible that PYO is not really as toxic to *Pseudomonas* as AGA to *P. agglomerans* and *E.coli*, but it is nevertheless also possible that nature designed this protein to bind other ligands rather than phenazines. In fact, the active site of PA0803 is very large and accessible, raising doubt whether PYO is the natural ligand (Figure 6.2). Many metabolites have aromatic moieties that might also be able to be sandwiched by PA0803, when the metabolite sterically fits the binding pocket.

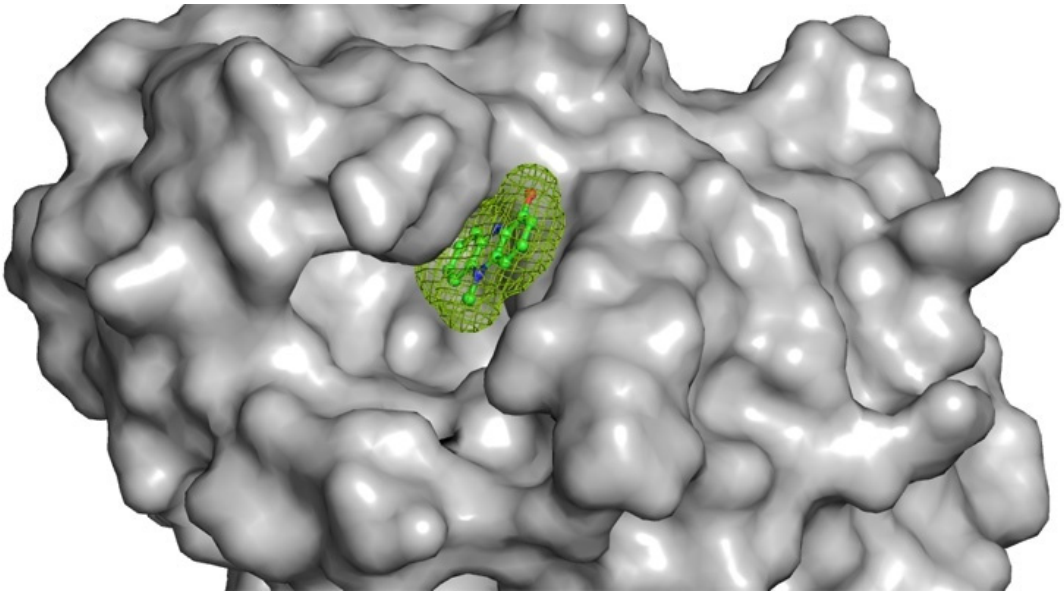

**Figure 6.2: Pyocyanin in the PA0803 active site cavity. The protein is depicted by surface; PYO is shown as ball-and-stick covered by mesh indicating the space it occupies.**

In spite of the unclear function *in vivo*, the lack of polar residues at the active site suggests that PA0803 is unlikely to have catalytic function and therefore most probably is a binding protein. In the study of a structurally similar protein, the Mitomycin C resistance protein MRD, a membrane transporter protein encoded by gene *mct* was found in the same cluster to function together with MRD (Sheldon *et al.*, 1999). The gene product of *mct* is predicted to be a MFS (major facilitator superfamily)-transporter. It was therefore proposed that MRD involves in transport of the antibiotic molecules. In the vincinity of the PA0803 gene, there are three hypothetical proteins predicted as membrane proteins (PA0800-PA0802) and a predicted aldo/keto reductase (PA0804). PA0804 is co-transcribed with PA0803, but due to a non-coding gap between PA0802 and PA0803 is not clear whether or not PA0800-PA0802 is transcribed together with PA0803-PA0804.

Therefore, further investigations are required to obtain an explaination for the interesting observation that PA0803 can bind PYO. It could be helpful to monitor with real-time PCR the transcription of the PA0803 gene in *P. aeruginosa* during its growth, so that the timing of PA0803 expression and pyocyanin production can be compared. Mutagenesis of more residues, such as Y142F has to be carried out in order to gain further mechanistic insights to the protein.

### 6.2.3 Development of research tools

**Model database for hypothetical proteins**

In both PqsE and PA0803 projects there exists a major difficulty of lacking research tools. As shown in the result sections, a large portion of the ORFs in the *P. aeruginosa* genome has not been studied. Annotations were made by analyzing primary sequences and many gene products were tagged as "(conserved) hypothetical proteins". This makes the interpretation of data difficult, e.g. the transcriptome data shown in Table 5.12.

In recent years, homology modeling has become a mature technique in bioinformatics. Algorithms provide good prediction of the fold of a given amino acid sequence, as shown by the threading of both PqsE and PA0803 (Section 5.1.2). Therefore, establishing a database with homology models of all "hypothetical proteins" will be a powerful tool to interpret transcriptome data as well as to investigate gene duplications.

**Metabolite library**

Both PqsE and PA0803 projects are in essence trying to discover the molecular functions of a protein. However, the available *in vitro* assays as well as *in silico* virtual screening libraries are still limited.

Combinatorial chemical synthesis has made available small molecule libraries. They play important role in modern drug discoveries. However, there is no comprehensive small molecule library of biologically relavent metabolites, not to speak e.g. *Pseudomonas* metabolites. Developing such chemical and virtual libraries would great help in the functional annotation of proteins.

# 7 SUMMARY

*Pseudomonas aeruginosa* is an antibiotic resistant opportunistic bacterial pathogen that remains one of the leading causes of death in immunocompromised patients. *P. aeruginosa* synthesizes an arsenal of virulence factors, one of which is the bluish phenazine derivative pyocyanin. The Latin name "aeruginosa", meaning "copper rust", was given to this species because of its characteristic blue-green color, mostly resulting from the combined execretion of pyocyanin and the yellow metabolite pyoverdine. The physiological function of pyocyanin seems to be complex: it is a respiratory pigment, an antibiotic against other microbials, a signal for *P. aeruginosa* and a prominent virulence factor in pathogenesis as well.

In this work, two proteins with unknown molecular function, PqsE and PA0803 were studied *in vitro* and *in vivo*, using a broad spectrum of techniques. Crystal structures of both proteins alone and in complex with ligands/substrates were determined at high resolution. Together with other methods, potential molecular functions of both proteins were investigated. The structural and functional insights gained here will guide further studies in search for the natural ligands/substrates.

**Molecular Function of PqsE**

The first project studies one of the molecular mechanisms through which *P. aeruginosa* controls the biosynthesis of pyocyanin as well as some other virulence factors, via a specific signaling molecule termed *Pseudomonas* quinolone signal (PQS). Specifically, the gene product of *pqsE*, a member of the PQS biosynthetic *pqsABCDE* operon, was characterized. Previous studies showed that *pqsE* is not required for the biosynthesis of PQS, but deletion of its gene leads to loss of virulence production, including pyocyanin. This suggested that *pqsE* is a potential target for therapeutic intervention against *P. aeruginosa* infections. It is therefore compelling to understand the gene product at molecular level.

Since its discovery in 1999, PqsE has drawn extensive attention in bacteriallogy research. Many reports in the literature demonstrated the importance of PqsE as a critical link between quorum sensing and virulence, yet despite recent progress providing significant insight into the PQS system, the molecular function of PqsE remains a mystery. In this study, recombinant PqsE was cloned, expressed, purified and characterized.

Surprisingly, PqsE does not interact with PQS at all and is therefore not a PQS signal response protein. Since previous findings, mostly obtained by genetic experiments, did not provide a comprehensive starting point, the crystal structure of PqsE was first determined to 1.6 Å resolution, expecting the three dimensional structure to point out directions of possible molecular mechanisms.

PqsE is a binuclear metallohydrolase with an Fe(III)M(II) mixed-valent activity center. A copurified ligand was assigned as benzoate and may indicate that PqsE exerts its regulatory effect by converting a chorismate-derived molecule. Further, PqsE was found to slowly hydrolyze phosphodiesters including single- and double-stranded DNA as well as mRNA and also the thioester S-(4-nitrobenzoyl)mercaptoethane. Higher activity was observed after incubation with $Co^{2+}$ and, to lesser entent, $Mn^{2+}$, suggesting that the Fe(II)Fe(III) center of recombinant PqsE may be an artifact of heterologous expression. A crystal complex of the E182A mutant with bis-pNPP was obtained and suggests a catalytic mechanism for hydrolysis. Transcriptome analysis of PqsE deletion mutant and a complement strain was carried out. Data suggested that the PqsE natural substrate may be related to anthranilate or catechol.

**Pyocyanin-Binding Activity of a Hypothetical Protein PA0803**

The 6 mega base-pair *Pseudomonas aeruginosa* genome contains about 5500 ORFs, many of which have never been studied and are annotated as hypothetical proteins. However, lack of apparent connection to known pathways does not mean that they play less important roles for the bacteria.

In the second project reported here, a gene with locus ID PA0803 was investigated. PA0803 has low sequence similarity to a known phenazine resistance protein EhpR from *P. agglomerans* but is not located near either of the two phenazine-biosynthesis gene clusters of *P. aeruginosa*. To clarify whether it can bind phenazines or not, recombinant PA0803 was cloned, expressed, purified and characterized. Crystal structure of PA0803 was determined to 1.6 Å resolution. ITC experiments and the determination of PA0803:PYO complex structure confirmed that PA0803 can bind pyocyanin with low micromolar affinity. This protein, among a few other gene products, may serve as escort proteins of aromatic small molecules.

# 8 APPENDICES

## 8.1 FULL TABLE OF PQSE TRANSCRIPTOME RESULTS

| Identifier | Ratio* | Gene Name | Annotation |
|---|---|---|---|
| ***Genes Up-regulated in over-producer (PqsE-activated)*** | | | |
| PA1871 | 6.68 | lasA | LasA protease precursor |
| PA2513 | 6.43 | antB | anthranilate dioxygenase small subunit |
| PA2300 | 5.94 | chiC | chitinase |
| PA4211 | 5.70 | phzB1 | probable phenazine biosynthesis protein |
| PA3190 | 5.55 | | probable binding protein component of ABC sugar transporter |
| PA0852 | 5.55 | cbpD | chitin-binding protein CbpD precursor |
| PA1905 | 5.53 | phzG2 | probable pyridoxamine 5'-phosphate oxidase |
| PA2069 | 5.35 | | probable carbamoyl transferase |
| PA1901 | 5.16 | phzC2 | phenazine biosynthesis protein PhzC |
| PA3187 | 5.13 | | probable ATP-binding component of ABC transporter |
| PA4217 | 5.11 | phzS | flavin-containing monooxygenase |
| PA1904 | 5.09 | phzF2 | probable phenazine biosynthesis protein |
| PA1902 | 5.07 | phzD2 | phenazine biosynthesis protein PhzD |
| PA4209 | 5.07 | phzM | probable phenazine-specific methyltransferase |
| PA2508 | 5.01 | catC | muconolactone delta-isomerase |
| PA2512 | 4.96 | antA | anthranilate dioxygenase large subunit |
| PA2194 | 4.92 | hcnB | hydrogen cyanide synthase HcnB |
| PA3287 | 4.89 | | conserved hypothetical protein |
| PA1903 | 4.68 | phzE2 | phenazine biosynthesis protein PhzE |
| PA2493 | 4.55 | mexE | multidrug efflux membrane fusion protein MexE precursor |
| PA2514 | 4.55 | antC | anthranilate dioxygenase reductase |
| PA0848 | 4.55 | | probable alkyl hydroperoxide reductase |
| PA4613 | 4.49 | katB | catalase |
| PA2193 | 4.32 | hcnA | hydrogen cyanide synthase HcnA |
| PA3790 | 4.16 | oprC | putative copper transport outer membrane porin OprC precursor |
| PA2204 | 4.16 | | probable binding protein component of ABC transporter |
| PA3237 | 4.14 | | hypothetical protein |
| PA3188 | 4.14 | | probable permease of ABC sugar transporter |
| PA4357 | 3.78 | | conserved hypothetical protein |
| PA3186 | 3.76 | oprB | Glucose/carbohydrate outer membrane porin OprB precursor |
| PA2509 | 3.63 | catB | muconate cycloisomerase I |
| ig_4713795 _4713098 | 3.61 | | promoter region of the phz1 operon |
| PA3478 | 3.61 | rhlB | rhamnosyltransferase chain B |
| PA3183 | 3.59 | zwf | glucose-6-phosphate 1-dehydrogenase |
| PA3189 | 3.58 | | probable permease of ABC sugar transporter |
| PA2195 | 3.54 | hcnC | hydrogen cyanide synthase HcnC |

| | | | |
|---|---|---|---|
| PA0140 | 3.50 | ahpF | alkyl hydroperoxide reductase subunit F |
| PA4078 | 3.43 | | probable nonribosomal peptide synthetase |
| PA2494 | 3.42 | mexF | multidrug efflux transporter MexF |
| PA2067 | 3.34 | | probable hydrolase |
| PA3479 | 3.34 | rhlA | rhamnosyltransferase chain A |
| PA3181 | 3.31 | | 2-keto-3-deoxy-6-phosphogluconate aldolase |
| PA4205 | 3.31 | mexG | hypothetical protein |
| PA4134 | 3.30 | | hypothetical protein |
| PA0849 | 3.29 | trxB2 | thioredoxin reductase 2 |
| PA3520 | 3.28 | | hypothetical protein |
| PA0227 | 3.18 | | probable CoA transferase, subunit B |
| PA5100 | 3.16 | hutU | urocanase |
| PA2274 | 3.10 | | hypothetical protein |
| PA0122 | 3.08 | | conserved hypothetical protein |
| PA0865 | 3.07 | hpd | 4-hydroxyphenylpyruvate dioxygenase |
| PA4210 | 3.07 | phzA1 | probable phenazine biosynthesis protein |
| PA4141 | 3.02 | | hypothetical protein |
| PA3361 | 3.00 | lecB | fucose-binding lectin PA-IIL |
| PA1123 | 3.00 | | hypothetical protein |
| PA1869 | 2.99 | | probable acyl carrier protein |
| PA2587 | 2.99 | pqsH | probable FAD-dependent monooxygenase |
| PA0938 | 2.96 | | hypothetical protein |
| PA0541 | 2.96 | | hypothetical protein |
| PA5220 | 2.94 | | hypothetical protein |
| PA3182 | 2.94 | pgl | 6-phosphogluconolactonase |
| PA2112 | 2.91 | | conserved hypothetical protein |
| PA2495 | 2.91 | oprN | multidrug efflux outer membrane protein OprN precursor |
| PA3195 | 2.91 | gapA | glyceraldehyde 3-phosphate dehydrogenase |
| PA2411 | 2.89 | | probable thioesterase |
| PA1245 | 2.87 | | hypothetical protein |
| PA3477 | 2.87 | rhlR | transcriptional regulator RhlR |
| PA2303 | 2.85 | | hypothetical protein |
| PA5460 | 2.84 | | hypothetical protein |
| PA2331 | 2.79 | | hypothetical protein |
| PA0284 | 2.76 | | hypothetical protein |
| PA4236 | 2.74 | katA | catalase |
| PA3724 | 2.73 | lasB | elastase LasB |
| PA2068 | 2.70 | | probable major facilitator superfamily (MFS) transporter |
| PA4208 | 2.69 | opmD | probable outer membrane protein precursor |
| PA2413 | 2.69 | pvdH | L-2,4-diaminobutyrate:2-ketoglutarate 4-aminotransferase, PvdH |
| PA2081 | 2.68 | kynB | kynurenine formamidase, KynB |
| PA4206 | 2.68 | mexH | probable efflux membrane fusion protein precursor |
| PA1556 | 2.66 | | probable cytochrome c oxidase subunit |
| PA2507 | 2.64 | catA | catechol 1,2-dioxygenase |
| PA2327 | 2.63 | | probable permease of ABC transporter |

| | | | |
|---|---|---|---|
| PA5128 | 2.62 | secB | secretion protein SecB |
| PA2329 | 2.60 | | probable ATP-binding component of ABC transporter |
| PA4881 | 2.59 | | hypothetical protein |
| PA2330 | 2.57 | | hypothetical protein |
| PA0931 | 2.53 | | siderophore receptor protein |
| PA2564 | 2.51 | | hypothetical protein |
| PA4207 | 2.50 | mexI | probable Resistance-Nodulation-Cell Division (RND) efflux transporter |
| PA1927 | 2.48 | metE | 5-methyltetrahydropteroyltriglutamate-homocysteine S-methyltransferase |
| PA2030 | 2.48 | | hypothetical protein |
| PA2588 | 2.46 | | probable transcriptional regulator |
| PA2114 | 2.46 | | probable major facilitator superfamily (MFS) transporter |
| PA4934 | 2.42 | rpsR | 30S ribosomal protein S18 |
| PA2008 | 2.40 | fahA | fumarylacetoacetase |
| PA4738 | 2.39 | | conserved hypothetical protein |
| PA3334 | 2.38 | | probable acyl carrier protein |
| PA1480 | 2.38 | ccmF | cytochrome C-type biogenesis protein CcmF |
| PA1483 | 2.38 | cycH | cytochrome c-type biogenesis protein |
| PA2393 | 2.35 | | probable dipeptidase precursor |
| PA0282 | 2.32 | cysT | sulfate transport protein CysT |
| PA2992 | 2.31 | | hypothetical protein |
| PA2304 | 2.29 | | hypothetical protein |
| PA3193 | 2.27 | glk | glucokinase |
| PA3690 | 2.27 | | probable metal-transporting P-type ATPase |
| PA4443 | 2.25 | cysD | ATP sulfurylase small subunit |
| PA2066 | 2.25 | | hypothetical protein |
| PA5163 | 2.21 | rmlA | glucose-1-phosphate thymidylyltransferase |
| PA3192 | 2.21 | gltR | two-component response regulator GltR |
| PA1555 | 2.19 | | probable cytochrome c |
| PA0271 | 2.18 | | hypothetical protein |
| PA5219 | 2.10 | | hypothetical protein |
| PA2260 | 2.10 | | hypothetical protein |
| PA2868 | 2.07 | | hypothetical protein |
| PA4131 | 2.07 | | probable iron-sulfur protein |
| PA2305 | 2.07 | | probable non-ribosomal peptide synthetase |
| PA3331 | 2.06 | | cytochrome P450 |
| PA2031 | 2.04 | | hypothetical protein |
| PA2259 | 2.04 | ptxS | transcriptional regulator PtxS |
| PA2126 | 2.04 | | conserved hypothetical protein |
| PA2384 | 2.03 | | hypothetical protein |
| PA3734 | 2.02 | | hypothetical protein |
| PA2647 | 2.01 | nuoL | NADH dehydrogenase I chain L |
| PA4133 | 2.00 | | cytochrome c oxidase subunit (cbb3-type) |

### *Genes Down-regulated in over-producer (PqsE-suppressed)*

| | | | |
|---|---|---|---|
| PA1297 | -4.36 | | probable metal transporter |

| | | | |
|---|---|---|---|
| PA4309 | -3.57 | pctA | chemotactic transducer PctA |
| PA4310 | -3.26 | pctB | chemotactic transducer PctB |
| PA3600 | -2.91 | | conserved hypothetical protein |
| PA1423 | -2.81 | | probable chemotaxis transducer |
| PA1463 | -2.78 | | hypothetical protein |
| PA3731 | -2.75 | | conserved hypothetical protein |
| PA2482 | -2.66 | | probable cytochrome c |
| PA3601 | -2.65 | | conserved hypothetical protein |
| PA3732 | -2.65 | | conserved hypothetical protein |
| PA1545 | -2.60 | | hypothetical protein |
| PA2481 | -2.55 | | hypothetical protein |
| PA3730 | -2.51 | | hypothetical protein |
| PA3865 | -2.48 | | probable amino acid binding protein |
| PA2016 | -2.44 | gnyR | Regulatory gene of gnyRDBHAL cluster, GnyR |
| PA3126 | -2.41 | ibpA | heat-shock protein IbpA |
| PA1001 | -2.38 | phnA | anthranilate synthase component I |
| PA3811 | -2.38 | hscB | heat shock protein HscB |
| PA2634 | -2.36 | | probable isocitrate lyase |
| PA3307 | -2.33 | | hypothetical protein |
| PA1180 | -2.31 | phoQ | two-component sensor PhoQ |
| PA3815 | -2.23 | | conserved hypothetical protein |
| PA4674 | -2.22 | | conserved hypothetical protein |
| PA3814 | -2.20 | iscS | L-cysteine desulfurase (pyridoxal phosphate-dependent) |
| PA0737 | -2.11 | | hypothetical protein |
| PA4520 | -2.10 | | probable chemotaxis transducer |
| PA0997 | -2.09 | pqsB | Homologous to β-keto-acyl-acyl-carrier protein synthase |
| PA5499 | -2.09 | np20 | transcriptional regulator np20 |
| PA4507 | -2.09 | | hypothetical protein |
| PA4630 | -2.08 | | hypothetical protein |
| PA1097 | -2.08 | fleQ | transcriptional regulator FleQ |
| PA4311 | -2.08 | | conserved hypothetical protein |
| PA2654 | -2.05 | | probable chemotaxis transducer |
| PA3813 | -2.05 | iscU | probable iron-binding protein IscU |
| PA1298 | -2.05 | | conserved hypothetical protein |
| PA4421 | -2.04 | | conserved hypothetical protein |
| PA3351 | -2.03 | | hypothetical protein |
| PA3812 | -2.03 | iscA | probable iron-binding protein IscA |
| PA3729 | -2.01 | | conserved hypothetical protein |
| PA1095 | -2.00 | | hypothetical protein |

**Table 8.1: List of genes whose expressions are significantly different in PAO1 ΔpqsE mutant and PAO1 ΔpqsE+pUCpqsE mutant.**

## 8.2 SYMBOLS AND ABBREVIATIONS

### Amino Acids

| | | | | | |
|---|---|---|---|---|---|
| A | Ala | Alanine | M | Met | Methionine |
| C | Cys | Cystine | N | Asn | Asparagine |
| D | Asp | Asparatate | P | Pro | Proline |
| E | Glu | Glutamate | Q | Gln | Glutamine |
| F | Phe | Phenylalanine | R | Arg | Arginine |
| G | Gly | Glycine | S | Ser | Serine |
| H | His | Histidine | T | Thr | Threonine |
| I | Ile | Isoleucine | W | Trp | Tryptophan |
| K | Lys | Lysine | V | Val | Valine |
| L | Leu | Leucine | Y | Tyr | Tyrosine |

### Physical Scales and Symbols

| | | | |
|---|---|---|---|
| kDa | Kilodalton | mM | millimolar |
| rpm | rounds per minute | µM | micromolar |
| l | liter | × g | gravitational acceleration fields |
| ml | milliliter | Å | Ångstrom |
| µl | microliter | ºC | degree centigrade |
| M | molar | º | degree (angle) |

### Abbreviations

| | |
|---|---|
| APS | Ammonium persulfate |
| ATP | Adenosine 5'-triphosphate |
| cAMP | Cyclic adenosine 5' -monophosphate |
| cGMP | Cyclic guanosine 5' -monophosphate |
| CCD | Charge-coupled devices |
| DNA | Deoxyribonucleic acid |
| C-terminal | Carboxy terminal |
| DTT | Dithiothreitol |
| EDTA | Ethilendiaminetetraacetic acid |

| | |
|---|---|
| ESRF | European Synchrotron Radiation Facility |
| FPLC | Fast Performance Liquid Chromatography |
| HEPES | 4-(2-hydroxyethyl)-1-piperazineethanesulfonic acid |
| IPTG | Isopropyl β D thiogalactoside |
| ITC | Isothermal Titration Calorimetry |
| MAD | Multi-wavelength anomalous dispersion |
| MES | 2-(N-morpholino)ethanesulfonic acid |
| MS | Mass-spectrometry |
| NCS | Non-crystallographic symmetry |
| N-terminal | Amino terminal |
| PAGE | Polyacrylamide gel electrophoresis |
| PCA | Phenazine-1-carboxylate acid |
| PCR | Polymerase chain reaction |
| PDC | Phenazine-1,6-dicarboxylate acid |
| PDE | Phosphodiesterase |
| PEG | Polyethylene glycol |
| PMSF | Phenylmethylsulfonyl fluoride |
| PYO | Pyocyanin |
| RNA | Ribonucleic acid |
| SAD/SAS | Single-wavelength anomalous dispersion/scattering |
| SDS | Sodium Dodecyl Sulphate |
| SOD | Superoxide dismutase |
| TEMED | N,N,N,N -Tetramethyl-Ethylenediamine |
| TLS | Translation, libration, screw-rotation displacement |
| Tris | Tris[hydroxymethyl] amino methane |

# REFERENCES

REFERENCES

1. Abrahams,J.P. and Leslie,A.G.W. (1996). Methods used in the structure determination of bovine mitochondrial F-1 ATPase. *Acta Crystallographica Section D-Biological Crystallography,* **52,** 30-42.

2. Ahuja,E.G., Janning,P., Mentel,M., Graebsch,A., Breinbauer,R., Hiller,W., Costisella,B., Thomashow,L.S., Mavrodi,D.V., and Blankenfeldt,W. (2008). PhzA/B catalyzes the formation of the tricycle in phenazine biosynthesis. *J. Am. Chem. Soc.,* **130,** 17053-17061.

3. Allesen-Holm,M., Barken,K.B., Yang,L., Klausen,M., Webb,J.S., Kjelleberg,S., Molin,S., Givskov,M., and Tolker-Nielsen,T. (2006). A characterization of DNA release in Pseudomonas aeruginosa cultures and biofilms. *Mol. Microbiol.,* **59,** 1114-1128.

4. Audenaert,K., Pattery,T., Cornelis,P., and Hofte,M. (2002). Induction of systemic resistance to Botrytis cinerea in tomato by Pseudomonas aeruginosa 7NSK2: role of salicylic acid, pyochelin, and pyocyanin. *Mol. Plant Microbe Interact.,* **15,** 1147-1156.

5. Bailey,S. (1994). The Ccp4 Suite - Programs for Protein Crystallography. *Acta Crystallographica Section D-Biological Crystallography,* **50,** 760-763.

6. Baron,S.S. and Rowe,J.J. (1981). Antibiotic Action of Pyocyanin. *Antimicrobial Agents and Chemotherapy,* **20,** 814-820.

7. Bera,A.K., Atanasova,V., Robinson,H., Eisenstein,E., Coleman,J.P., Pesci,E.C., and Parsons,J.F. (2009). Structure of PqsD, a Pseudomonas quinolone signal biosynthetic enzyme, in complex with anthranilate. *Biochemistry,* **48,** 8644-8655.

8. Bergdoll,M., Remy,M.H., Cagnon,C., Masson,J.M., and Dumas,P. (1997). Proline-dependent oligomerization with arm exchange. *Structure,* **5,** 391-401.

9. Blankenfeldt,W., Kuzin,A.P., Skarina,T., Korniyenko,Y., Tong,L., Bayer,P., Janning,P., Thomashow,L.S., and Mavrodi,D.V. (2004). Structure and function of the phenazine biosynthetic protein PhzF from Pseudomonas fluorescens. *Proc. Natl. Acad. Sci. U. S. A,* **101,** 16431-16436.

10. Bottomley,M.J., Muraglia,E., Bazzo,R., and Carfi,A. (2007). Molecular insights into quorum sensing in the human pathogen Pseudomonas aeruginosa from the structure of the virulence regulator LasR bound to its autoinducer. *J. Biol. Chem.,* **282,** 13592-13600.

11. Bradford,M.M. (1976). A rapid and sensitive method for the quantitation of microgram quantities of protein utilizing the principle of protein-dye binding. *Anal. Biochem.,* **72,** 248-254.

12. Bredenbruch,F., Geffers,R., Nimtz,M., Buer,J., and Haussler,S. (2006). The Pseudomonas aeruginosa quinolone signal (PQS) has an iron-chelating activity. *Environmental Microbiology,* **8,** 1318-1329.

13. Brint,J.M. and Ohman,D.E. (1995). Synthesis of multiple exoproducts in Pseudomonas aeruginosa is under the control of RhlR-RhlI, another set of regulators in strain PAO1 with homology to the autoinducer-responsive LuxR-LuxI family. *J. Bacteriol.,* **177,** 7155-7163.

14. BU'LOCK,J.D. (1961). Intermediary metabolism and antibiotic synthesis. *Adv. Appl. Microbiol.,* **3,** 293-342.

15. Byng,G.S., Eustice,D.C., and Jensen,R.A. (1979). Biosynthesis of phenazine pigments in mutant and wild-type cultures of Pseudomonas aeruginosa. *J. Bacteriol.,* **138,** 846-852.

16. Calfee,M.W., Shelton,J.G., McCubrey,J.A., and Pesci,E.C. (2005). Solubility and bioactivity of the Pseudomonas quinolone signal are increased by a Pseudomonas aeruginosa-produced surfactant. *Infection and Immunity,* **73,** 878-882.

17. Cao,H., Krishnan,G., Goumnerov,B., Tsongalis,J., Tompkins,R., and Rahme,L.G. (2001). A quorum sensing-associated virulence gene of Pseudomonas aeruginosa encodes a LysR-like transcription regulator with a unique self-regulatory mechanism. *Proceedings of the National Academy of Sciences of the United States of America,* **98,** 14613-14618.

18. Chin,A.W.T., van den,B.D., de Voer,G., van der Drift,K.M., Tuinman,S., Thomas-Oates,J.E., Lugtenberg,B.J., and Bloemberg,G.V. (2001). Phenazine-1-carboxamide production in the biocontrol strain Pseudomonas chlororaphis PCL1391 is regulated by multiple factors secreted into the growth medium. *Mol. Plant Microbe Interact.,* **14,** 969-979.

19. Chugani,S.A., Whiteley,M., Lee,K.M., D'Argenio,D., Manoil,C., and Greenberg,E.P. (2001). QscR, a modulator of quorum-sensing signal synthesis and virulence in Pseudomonas aeruginosa. *Proc. Natl. Acad. Sci. U. S. A,* **98,** 2752-2757.

20. Coleman,J.P., Hudson,L.L., McKnight,S.L., Farrow,J.M., Calfee,M.W., Lindsey,C.A., and Pesci,E.C. (2008). Pseudomonas aeruginosa PqsA is an anthranilate-coenzyme a ligase. *Journal of Bacteriology,* **190,** 1247-1255.

21. Colovos,C. and Yeates,T.O. (1993). Verification of Protein Structures - Patterns of Nonbonded Atomic Interactions. *Protein Science,* **2,** 1511-1519.

22. Cowtan,K. (1994). 'dm': An automated procedure for phase improvement by density modification. *Joint CCP4 and ESF-EACBM Newsletter on Protein Crystallography,* **31,** 34-38.

23. D'Argenio,D.A., Calfee,M.W., Rainey,P.B., and Pesci,E.C. (2002). Autolysis and autoaggregation in Pseudomonas aeruginosa colony morphology mutants. *Journal of Bacteriology,* **184,** 6481-6489.

24. D'Argenio,D.A., Gallagher,L.A., Berg,C.A., and Manoil,C. (2001). Drosophila as a model host for Pseudomonas aeruginosa infection. *J. Bacteriol.,* **183,** 1466-1471.

25. Daiyasu,H., Osaka,K., Ishino,Y., and Toh,H. (2001). Expansion of the zinc metallo-hydrolase family of the beta-lactamase fold. *FEBS Lett.,* **503,** 1-6.

26. delaFortelle,E. and Bricogne,G. (1997). Maximum-likelihood heavy-atom parameter refinement for multiple isomorphous replacement and multiwavelength anomalous diffraction methods. *Macromolecular Crystallography, Pt A,* **276,** 472-494.

27. Delaney,S.M., Mavrodi,D.V., Bonsall,R.F., and Thomashow,L.S. (2001). phzO, a gene for biosynthesis of 2-hydroxylated phenazine compounds in Pseudomonas aureofaciens 30-84. *J. Bacteriol.,* **183,** 318-327.

28. DeWitte,J.J., Cox,C.D., Rasmussen,G.T., and Britigan,B.E. (2001). Assessment of structural features of the pseudomonas siderophore pyochelin required for its ability to promote oxidant-mediated endothelial cell injury. *Arch. Biochem. Biophys.,* **393,** 236-244.

29. Deziel,E., Gopalan,S., Tampakaki,A.P., Lepine,F., Padfield,K.E., Saucier,M., Xiao,G.P., and Rahme,L.G. (2005). The contribution of MvfR to Pseudomonas aeruginosa pathogenesis and quorum sensing circuitry regulation: multiple quorum sensing-regulated genes are modulated without affecting lasRI, rhlRI or the production of N-acyl-L-homoserine lactones. *Molecular Microbiology,* **55,** 998-1014.

30. Deziel,E., Lepine,F., Milot,S., He,J.X., Mindrinos,M.N., Tompkins,R.G., and Rahme,L.G. (2004). Analysis of Pseudomonas aeruginosa 4-hydroxy-2-alkylquinolines (HAQs) reveals a role for 4-hydroxy-2-heptylquinoline in cell-to-cell communication. *Proceedings of the National Academy of Sciences of the United States of America,* **101,** 1339-1344.

31. Dietrich,L.E., Price-Whelan,A., Petersen,A., Whiteley,M., and Newman,D.K. (2006). The phenazine pyocyanin is a terminal signalling factor in the quorum sensing network of Pseudomonas aeruginosa. *Mol. Microbiol.,* **61,** 1308-1321.

32. Dietrich,L.E., Teal,T.K., Price-Whelan,A., and Newman,D.K. (2008). Redox-active antibiotics control gene expression and community behavior in divergent bacteria. *Science,* **321,** 1203-1206.

33. Diggle,S.P., Matthijs,S., Wright,V.J., Fletcher,M.P., Chhabra,S.R., Lamont,I.L., Kong,X.L., Hider,R.C., Cornelis,P., Camara,M., and Williams,P. (2007). The Pseudomonas aeruginosa 4-quinolone signal molecules HHQ and PQS play multifunctional roles in quorum sensing and iron entrapment. *Chemistry & Biology,* **14,** 87-94.

34. Diggle,S.P., Winzer,K., Chhabra,S.R., Chhabra,S.R., Worrall,K.E., Camara,M., and Williams,P. (2003). The Pseudomonas aeruginosa quinolone signal molecule overcomes the cell density-dependency of the quorum sensing hierarchy, regulates rhl-dependent genes at the onset of stationary phase and can be produced in the absence of LasR. *Molecular Microbiology,* **50,** 29-43.

35. Dominski,Z. (2007). Nucleases of the metallo-beta-lactamase family and their role in DNA and RNA metabolism. *Crit Rev. Biochem. Mol. Biol.,* **42,** 67-93.

36. Dong,Y.H., Gusti,A.R., Zhang,Q., Xu,J.L., and Zhang,L.H. (2002). Identification of quorum-quenching N-acyl homoserine lactonases from Bacillus species. *Appl. Environ. Microbiol.,* **68,** 1754-1759.

37. Dosselaere,F. and Vanderleyden,J. (2001). A metabolic node in action: chorismate-utilizing enzymes in microorganisms. *Crit Rev. Microbiol.,* **27,** 75-131.

38. Doublie,S. (1997). Preparation of selenomethionyl proteins for phase determination. *Macromolecular Crystallography, Pt A,* **276,** 523-530.

39. Duan,K. and Surette,M.G. (2007). Environmental regulation of Pseudomonas aeruginosa PAO1 Las and Rhl quorum-sensing systems. *J. Bacteriol.,* **189,** 4827-4836.

40. Dubern,J.F. and Diggle,S.P. (2008). Quorum sensing by 2-alkyl-4-quinolones in Pseudomonas aeruginosa and other bacterial species. *Mol. Biosyst.,* **4,** 882-888.

41. Farrow,J.M., III, Sund,Z.M., Ellison,M.L., Wade,D.S., Coleman,J.P., and Pesci,E.C. (2008). PqsE functions independently of PqsR-Pseudomonas quinolone signal and enhances the rhl quorum-sensing system. *J. Bacteriol.,* **190,** 7043-7051.

42. Flood,M.E., Herbert,R.B., and Holliman,F.G. (1972). Pigments of Pseudomonas species. V. Biosynthesis of pyocyanin and the pigments of Ps. aureoaciens. *J. Chem. Soc. [Perkin 1],* **4,** 622-626.

43. Frazao,C., Silva,G., Gomes,C.M., Matias,P., Coelho,R., Sieker,L., Macedo,S., Liu,M.Y., Oliveira,S., Teixeira,M., Xavier,A.V., Rodrigues-Pousada,C., Carrondo,M.A., and Le Gall,J. (2000). Structure of a dioxygen reduction enzyme from Desulfovibrio gigas. *Nat. Struct. Biol.,* **7,** 1041-1045.

44. Fuqua,W.C., Winans,S.C., and Greenberg,E.P. (1994). Quorum sensing in bacteria: the LuxR-LuxI family of cell density-responsive transcriptional regulators. *J. Bacteriol.,* **176,** 269-275.

45. Galbraith,M.D., Giddens,S.R., Mahanty,H.K., and Clark,B. (2004). Role of glutamine synthetase in phenazine antibiotic production by Pantoea agglomerans Eh1087. *Can. J. Microbiol.,* **50,** 877-881.

46. Gallagher,L.A., McKnight,S.L., Kuznetsova,M.S., Pesci,E.C., and Manoil,C. (2002). Functions required for extracellular quinolone signaling by Pseudomonas aeruginosa. *Journal of Bacteriology,* **184,** 6472-6480.

47. Gambello,M.J. and Iglewski,B.H. (1991). Cloning and characterization of the Pseudomonas aeruginosa lasR gene, a transcriptional activator of elastase expression. *J. Bacteriol.,* **173,** 3000-3009.

48. Garau,G., Lemaire,D., Vernet,T., Dideberg,O., and Di Guilmi,A.M. (2005). Crystal structure of phosphorylcholine esterase domain of the virulence factor choline-binding protein e from streptococcus pneumoniae: new structural features among the metallo-beta-lactamase superfamily. *J. Biol. Chem.,* **280,** 28591-28600.

49. Gasteiger,E., Gattiker,A., Hoogland,C., Ivanyi,I., Appel,R.D., and Bairoch,A. (2003). ExPASy: the proteomics server for in-depth protein knowledge and analysis. *Nucleic Acids Research,* **31,** 3784-3788.

50. Giddens,S.R., Feng,Y., and Mahanty,H.K. (2002). Characterization of a novel phenazine antibiotic gene cluster in Erwinia herbicola Eh1087. *Mol. Microbiol.,* **45,** 769-783.

51. Guddat,L.W., McAlpine,A.S., Hume,D., Hamilton,S., de Jersey,J., and Martin,J.L. (1999). Crystal structure of mammalian purple acid phosphatase. *Structure.,* **7,** 757-767.

52. Hassan,H.M. and Fridovich,I. (1980). Mechanism of the antibiotic action pyocyanine. *J. Bacteriol.,* **141,** 156-163.

53. Hassett,D.J., Charniga,L., Bean,K., Ohman,D.E., and Cohen,M.S. (1992). Response of Pseudomonas aeruginosa to pyocyanin: mechanisms of resistance, antioxidant defenses, and demonstration of a manganese-cofactored superoxide dismutase. *Infect. Immun.,* **60,** 328-336.

54. Hassett,D.J., Ma,J.F., Elkins,J.G., McDermott,T.R., Ochsner,U.A., West,S.E., Huang,C.T., Fredericks,J., Burnett,S., Stewart,P.S., McFeters,G., Passador,L., and Iglewski,B.H. (1999). Quorum sensing in Pseudomonas aeruginosa controls expression of catalase and superoxide dismutase genes and mediates biofilm susceptibility to hydrogen peroxide. *Mol. Microbiol.,* **34,** 1082-1093.

55. Hassett,D.J., Schweizer,H.P., and Ohman,D.E. (1995). Pseudomonas aeruginosa sodA and sodB mutants defective in manganese- and iron-cofactored superoxide dismutase activity demonstrate the importance of the iron-cofactored form in aerobic metabolism. *J. Bacteriol.,* **177,** 6330-6337.

56. Haussler,S., Becker,T., Zaoui,C., Musken,M., and Bredenbruch,F. (2007). The Pseudomonas quinolone siganl (PQS) balances life and death in Pseudomonas aeruginosa populations. *International Journal of Medical Microbiology,* **297,** 140.

57. Herbert,R.B. and Holliman,F.G. (1969). Pigments of pseudomonas species. II. Structure of aeruginosin B. *J. Chem. Soc. [Perkin 1],* **18,** 2517-2520.

58. Herrmann,K.M. (1995). The Shikimate Pathway: Early Steps in the Biosynthesis of Aromatic Compounds. *Plant Cell,* **7,** 907-919.

59. Holliman,F.G. (1969). Pigments of pseudomonas species. I. Structure and synthesis of aeruginosin A. *J. Chem. Soc. [Perkin 1],* **18,** 2514-2516.

60. Hollstein,U. and McCamey,D.A. (1973). Biosynthesis of phenazines. II. Incorporation of (6-14C)-D-shikimic acid into phenazine-1-carboxylic acid and iodinin. *J. Org. Chem.,* **38,** 3415-3417.

61. Holm,L., Kaariainen,S., Rosenstrom,P., and Schenkel,A. (2008). Searching protein structure databases with DaliLite v.3. *Bioinformatics.,* **24,** 2780-2781.

62. Huang,J.J., Petersen,A., Whiteley,M., and Leadbetter,J.R. (2006). Identification of QuiP, the product of gene PA1032, as the second acyl-homoserine lactone acylase of Pseudomonas aeruginosa PAO1. *Appl. Environ. Microbiol.,* **72,** 1190-1197.

63. Jones,S., Marin,A., and Thornton,J.M. (2000). Protein domain interfaces: characterization and comparison with oligomeric protein interfaces. *Protein Engineering,* **13,** 77-82.

64. Juhas,M., Wiehlmann,L., Huber,B., Jordan,D., Lauber,J., Salunkhe,P., Limpert,A.S., von Gotz,F., Steinmetz,I., Eberl,L., and Tummler,B. (2004). Global regulation of quorum sensing and virulence by VqsR in Pseudomonas aeruginosa. *Microbiology,* **150,** 831-841.

65. Juhas,M., Wiehlmann,L., Salunkhe,P., Lauber,J., Buer,J., and Tummler,B. (2005). GeneChip expression analysis of the VqsR regulon of Pseudomonas aeruginosa TB. *FEMS Microbiol. Lett.,* **242,** 287-295.

66. Kabsch,W. (1993). Automatic Processing of Rotation Diffraction Data from Crystals of Initially Unknown Symmetry and Cell Constants. *Journal of Applied Crystallography,* **26,** 795-800.

67. Kanehisa,M., Araki,M., Goto,S., Hattori,M., Hirakawa,M., Itoh,M., Katayama,T., Kawashima,S., Okuda,S., Tokimatsu,T., and Yamanishi,Y. (2008). KEGG for linking genomes to life and the environment. *Nucleic Acids Research,* **36,** D480-D484.

68. Kanehisa,M. and Goto,S. (2000). KEGG: Kyoto Encyclopedia of Genes and Genomes. *Nucleic Acids Research,* **28,** 27-30.

69. Kanehisa,M., Goto,S., Hattori,M., Aoki-Kinoshita,K.F., Itoh,M., Kawashima,S., Katayama,T., Araki,M., and Hirakawa,M. (2006). From genomics to chemical genomics: new developments in KEGG. *Nucleic Acids Research,* **34,** D354-D357.

70. Kaplan,H.B. and Greenberg,E.P. (1985). Diffusion of autoinducer is involved in regulation of the Vibrio fischeri luminescence system. *J. Bacteriol.,* **163,** 1210-1214.

71. Kaplan,H.B. and Greenberg,E.P. (1987). Overproduction and purification of the luxR gene product: Transcriptional activator of the Vibrio fischeri luminescence system. *Proc. Natl. Acad. Sci. U. S. A,* **84,** 6639-6643.

72. Kawano,Y., Kumagai,T., Muta,K., Matoba,Y., Davies,J., and Sugiyama,M. (2000). The 1.5 angstrom crystal structure of a bleomycin resistance determinant from bleomycin-producing Streptomyces verticillus. *Journal of Molecular Biology,* **295,** 915-925.

73. Kelley,L.A. and Sternberg,M.J.E. (2009). Protein structure prediction on the Web: a case study using the Phyre server. *Nature Protocols,* **4,** 363-371.

74. Kerr,J.R. (2000). Phenazine Pigments: antibiotics and virulence factors. *Infect Dis Rev,* **2,** 184-194.

75. Klar,T.A., Jakobs,S., Dyba,M., Egner,A., and Hell,S.W. (2000). Fluorescence microscopy with diffraction resolution barrier broken by stimulated emission. *Proc. Natl. Acad. Sci. U. S. A,* **97,** 8206-8210.

76. Kumagai,T., Hibino,R., Kawano,Y., and Sugiyama,M. (1999). Mutation of the N-terminal proline 9 of BLMA from Streptomyces verticillus abolishes the binding affinity for bleomycin. *Febs Letters,* **450,** 227-230.

77. Kuroda,A., Kumano,T., Taguchi,K., Nikata,T., Kato,J., and Ohtake,H. (1995). Molecular cloning and characterization of a chemotactic transducer gene in Pseudomonas aeruginosa. *J. Bacteriol.,* **177,** 7019-7025.

78. Kuznetsova,E., Proudfoot,M., Sanders,S.A., Reinking,J., Savchenko,A., Arrowsmith,C.H., Edwards,A.M., and Yakunin,A.F. (2005). Enzyme genomics: Application of general enzymatic screens to discover new enzymes. *FEMS Microbiol. Rev.,* **29,** 263-279.

79. Laemmli,U.K. (1970). Cleavage of structural proteins during the assembly of the head of bacteriophage T4. *Nature,* **227,** 680-685.

80. Larkin,M.A., Blackshields,G., Brown,N.P., Chenna,R., McGettigan,P.A., McWilliam,H., Valentin,F., Wallace,I.M., Wilm,A., Lopez,R., Thompson,J.D., Gibson,T.J., and Higgins,D.G. (2007). Clustal W and Clustal X version 2.0. *Bioinformatics,* **23,** 2947-2948.

81. Laskowski,R.A., Macarthur,M.W., Moss,D.S., and Thornton,J.M. (1993). Procheck - A Program to Check the Stereochemical Quality of Protein Structures. *Journal of Applied Crystallography,* **26,** 283-291.

82. Latifi,A., Foglino,M., Tanaka,K., Williams,P., and Lazdunski,A. (1996). A hierarchical quorum-sensing cascade in Pseudomonas aeruginosa links the transcriptional activators LasR and RhIR (VsmR) to expression of the stationary-phase sigma factor RpoS. *Mol. Microbiol.,* **21,** 1137-1146.

83. Lau,G.W., Goumnerov,B.C., Walendziewicz,C.L., Hewitson,J., Xiao,W.Z., Mahajan-Miklos,S., Tompkins,R.G., Perkins,L.A., and Rahme,L.G. (2003). The Drosophila melanogaster toll pathway participates in resistance to infection by the gram-negative human pathogen Pseudomonas aeruginosa. *Infection and Immunity,* **71,** 4059-4066.

84. Lau,G.W., Ran,H., Kong,F., Hassett,D.J., and Mavrodi,D. (2004a). Pseudomonas aeruginosa pyocyanin is critical for lung infection in mice. *Infect. Immun.,* **72,** 4275-4278.

85. Lau,G.W., Ran,H.M., Kong,F.S., Hassett,D.J., and Mavrodi,D. (2004b). Pseudomonas aeruginosa pyocyanin is critical for lung infection in mice. *Infection and Immunity,* **72,** 4275-4278.

86. Laursen,J.B. and Nielsen,J. (2004). Phenazine natural products: biosynthesis, synthetic analogues, and biological activity. *Chem. Rev.,* **104,** 1663-1686.

87. Ledgham,F., Ventre,I., Soscia,C., Foglino,M., Sturgis,J.N., and Lazdunski,A. (2003). Interactions of the quorum sensing regulator QscR: interaction with itself and the other regulators of Pseudomonas aeruginosa LasR and RhlR. *Mol. Microbiol.,* **48,** 199-210.

88. Lepine,F., Milot,S., Deziel,E., He,J.X., and Rahme,L.G. (2004). electrospray/mass spectrometric identification and analysis of 4-hydroxy-2-alkylquinolines (HAQs) produced by Pseudomonas aeruginosa. *Journal of the American Society for Mass Spectrometry,* **15,** 862-869.

89. Lequette,Y., Lee,J.H., Ledgham,F., Lazdunski,A., and Greenberg,E.P. (2006). A distinct QscR regulon in the Pseudomonas aeruginosa quorum-sensing circuit. *J. Bacteriol.,* **188,** 3365-3370.

90. Liu,D., Momb,J., Thomas,P.W., Moulin,A., Petsko,G.A., Fast,W., and Ringe,D. (2008). Mechanism of the quorum-quenching lactonase (AiiA) from Bacillus thuringiensis. 1. Product-bound structures. *Biochemistry,* **47,** 7706-7714.

91. Longley,R.P., Halliwell,J.E., Campbell,J.J., and Ingledew,W.M. (1972). The branchpoint of pyocyanine biosynthesis. *Can. J. Microbiol.,* **18,** 1357-1363.

92. Mahajan-Miklos,S., Tan,M.W., Rahme,L.G., and Ausubel,F.M. (1999a). Molecular mechanisms of bacterial virulence elucidated using a Pseudomonas aeruginosa Caenorhabditis elegans pathogenesis model. *Cell,* **96,** 47-56.

93. Mahajan-Miklos,S., Tan,M.W., Rahme,L.G., and Ausubel,F.M. (1999b). Molecular mechanisms of bacterial virulence elucidated using a Pseudomonas aeruginosa-Caenorhabditis elegans pathogenesis model. *Cell,* **96,** 47-56.

94. Marasinghe,G.P.K., Sander,I.M., Bennett,B., Periyannan,G., Yang,K.W., Makaroff,C.A., and Crowder,M.W. (2005). Structural studies on a mitochondrial glyoxalase II. *Journal of Biological Chemistry,* **280,** 40668-40675.

95. Martin,T.W., Dauter,Z., Devedjiev,Y., Sheffield,P., Jelen,F., He,M., Sherman,D.H., Otlewski,J., Derewenda,Z.S., and Derewenda,U. (2002). Molecular basis of mitomycin C resistance in Streptomyces: Structure and function of the MRD protein. *Structure,* **10,** 933-942.

96. Maruyama,M., Kumagai,T., Matoba,Y., Hayashida,M., Fujii,T., Hata,Y., and Sugiyama,M. (2001). Crystal structures of the transposon Tn5-carried bleomycin resistance determinant uncomplexed and complexed with bleomycin. *Journal of Biological Chemistry,* **276,** 9992-9999.

97. Mashburn,L.M. and Whiteley,M. (2005). Membrane vesicles traffic signals and facilitate group activities in a prokaryote. *Nature,* **437,** 422-425.

98. Mashburn-Warren,L., Howe,J., Garidel,P., Richter,W., Steiniger,F., Roessle,M., Brandenburg,K., and Whiteley,M. (2008). Interaction of quorum signals with outer membrane lipids: insights into prokaryotic membrane vesicle formation. *Molecular Microbiology,* **69,** 491-502.

99. Matthews,B.W. (1968). Solvent Content of Protein Crystals. *Journal of Molecular Biology,* **33,** 491-&.

100. Mavrodi,D.V., Blankenfeldt,W., and Thomashow,L.S. (2006). Phenazine compounds in fluorescent Pseudomonas spp. biosynthesis and regulation. *Annu. Rev. Phytopathol.,* **44,** 417-445.

101. Mavrodi,D.V., Bonsall,R.F., Delaney,S.M., Soule,M.J., Phillips,G., and Thomashow,L.S. (2001). Functional analysis of genes for biosynthesis of pyocyanin and phenazine-1-carboxamide from Pseudomonas aeruginosa PAO1. *J. Bacteriol.,* **183,** 6454-6465.

102. Mavrodi,D.V., Ksenzenko,V.N., Bonsall,R.F., Cook,R.J., Boronin,A.M., and Thomashow,L.S. (1998). A seven-gene locus for synthesis of phenazine-1-carboxylic acid by Pseudomonas fluorescens 2-79. *J. Bacteriol.,* **180,** 2541-2548.

103. McDonald,M., Wilkinson,B., Van't Land,C.W., Mocek,U., Lee,S., and Floss,H.G. (1999). Biosynthesis of phenazine antibiotics in Streptomyces antibioticus: Stereochemistry of methyl transfer from carbon-2 of acetate. *Journal of the American Chemical Society,* **121,** 5619-5624.

104. McKnight,S.L., Iglewski,B.H., and Pesci,E.C. (2000). The Pseudomonas quinolone signal regulates rhl quorum sensing in Pseudomonas aeruginosa. *Journal of Bacteriology,* **182,** 2702-2708.

105. Merkx,M. and Averill,B.A. (1998). Ga3+ as a functional substitute for Fe3+: Preparation and characterization of the Ga3+Fe2+ and Ga3+Zn2+ forms of bovine spleen purple acid phosphatase. *Biochemistry,* **37,** 8490-8497.

106. Messenger,A.J. and Turner,J.M. (1978). Phenazine-1,6-dicarboxylate as the common precursor of other bacterial phenazines [proceedings]. *Biochem. Soc. Trans.,* **6,** 1326-1328.

107. Mitic,N., Smith,S.J., Neves,A., Guddat,L.W., Gahan,L.R., and Schenk,G. (2006). The catalytic mechanisms of binuclear metallohydrolases. *Chem. Rev.,* **106,** 3338-3363.

108. Momb,J., Wang,C., Liu,D., Thomas,P.W., Petsko,G.A., Guo,H., Ringe,D., and Fast,W. (2008). Mechanism of the quorum-quenching lactonase (AiiA) from Bacillus thuringiensis. 2. Substrate modeling and active site mutations. *Biochemistry,* **47,** 7715-7725.

109. Murphy,T.A., Catto,L.E., Halford,S.E., Hadfield,A.T., Minor,W., Walsh,T.R., and Spencer,J. (2006). Crystal structure of Pseudomonas aeruginosa SPM-1 provides insights into variable zinc affinity of metallo-beta-lactamases. *J. Mol. Biol.,* **357,** 890-903.

110. Murphy,T.A., Simm,A.M., Toleman,M.A., Jones,R.N., and Walsh,T.R. (2003). Biochemical characterization of the acquired metallo-beta-lactamase SPM-1 from Pseudomonas aeruginosa. *Antimicrob. Agents Chemother.,* **47,** 582-587.

111. Murshudov,G.N., Vagin,A.A., and Dodson,E.J. (1997). Refinement of macromolecular structures by the maximum-likelihood method. *Acta Crystallographica Section D-Biological Crystallography,* **53,** 240-255.

112. Nakai,K. and Kanehisa,M. (1991). Expert System for Predicting Protein Localization Sites in Gram-Negative Bacteria. *Proteins-Structure Function and Genetics,* **11,** 95-110.

113. Oglesby,A.G., Iii,J.M.F., Lee,J.H., Tomaras,A.P., Greenberg,E.P., Pesci,E.C., and Vasil,M.L. (2008). The influence of iron on Pseudomonas aeruginosa physiology - A regulatory link between iron and quorum sensing. *Journal of Biological Chemistry,* **283,** 15558-15567.

114. Park,S.Y., Kang,H.O., Jang,H.S., Lee,J.K., Koo,B.T., and Yum,D.Y. (2005). Identification of extracellular N-acylhomoserine lactone acylase from a Streptomyces sp. and its application to quorum quenching. *Appl. Environ. Microbiol.,* **71,** 2632-2641.

115. Parsons,J.F., Song,F., Parsons,L., Calabrese,K., Eisenstein,E., and Ladner,J.E. (2004). Structure and function of the phenazine biosynthesis protein PhzF from Pseudomonas fluorescens 2-79. *Biochemistry,* **43,** 12427-12435.

116. Pesci,E.C., Milbank,J.B.J., Pearson,J.P., McKnight,S., Kende,A.S., Greenberg,E.P., and Iglewski,B.H. (1999). Quinolone signaling in the cell-to-cell communication system of Pseudomonas aeruginosa. *Proceedings of the National Academy of Sciences of the United States of America,* **96,** 11229-11234.

117. Price-Whelan,A., Dietrich,L.E., and Newman,D.K. (2007). Pyocyanin alters redox homeostasis and carbon flux through central metabolic pathways in Pseudomonas aeruginosa PA14. *J. Bacteriol.,* **189,** 6372-6381.

118. Rahme,L.G., Ausubel,F.M., Cao,H., Drenkard,E., Goumnerov,B.C., Lau,G.W., Mahajan-Miklos,S., Plotnikova,J., Tan,M.W., Tsongalis,J., Walendziewicz,C.L., and Tompkins,R.G. (2000). Plants and animals share functionally common bacterial virulence factors. *Proc. Natl. Acad. Sci. U. S. A,* **97,** 8815-8821.

119. Rahme,L.G., Stevens,E.J., Wolfort,S.F., Shao,J., Tompkins,R.G., and Ausubel,F.M. (1995). Common virulence factors for bacterial pathogenicity in plants and animals. *Science,* **268,** 1899-1902.

120. Rampioni,G., Schuster,M., Greenberg,E.P., Bertani,I., Grasso,M., Venturi,V., Zennaro,E., and Leoni,L. (2007). RsaL provides quorum sensing homeostasis and functions as a global regulator of gene expression in Pseudomonas aeruginosa. *Mol. Microbiol.,* **66,** 1557-1565.

121. Ran,H.M., Hassett,D.J., and Lau,G.W. (2003). Human targets of Pseudomonas aeruginosa pyocyanin. *Proceedings of the National Academy of Sciences of the United States of America,* **100,** 14315-14320.

122. Reimmann,C., Serino,L., Beyeler,M., and Haas,D. (1998). Dihydroaeruginoic acid synthetase and pyochelin synthetase, products of the pchEF genes, are induced by extracellular pyochelin in Pseudomonas aeruginosa. *Microbiology,* **144 ( Pt 11),** 3135-3148.

123. Reszka,K.J., O'Malley,Y., McCormick,M.L., Denning,G.M., and Britigan,B.E. (2004). Oxidation of pyocyanin, a cytotoxic product from Pseudomonas aeruginosa, by microperoxidase 11 and hydrogen peroxide. *Free Radic. Biol. Med.,* **36,** 1448-1459.

124. Saiki,R.K., Scharf,S., Faloona,F., Mullis,K.B., Horn,G.T., Erlich,H.A., and Arnheim,N. (1985). Enzymatic amplification of beta-globin genomic sequences and restriction site analysis for diagnosis of sickle cell anemia. *Science,* **230,** 1350-1354.

125. Schneider,T.R. and Sheldrick,G.M. (2002). Substructure solution with SHELXD. *Acta Crystallographica Section D-Biological Crystallography,* **58,** 1772-1779.

126. Schuster,M. and Greenberg,E.P. (2006). A network of networks: quorum-sensing gene regulation in Pseudomonas aeruginosa. *Int. J. Med. Microbiol.,* **296,** 73-81.

127. Schuster,M. and Greenberg,E.P. (2007). Early activation of quorum sensing in Pseudomonas aeruginosa reveals the architecture of a complex regulon. *BMC. Genomics,* **8,** 287.

128. Schuster,M., Hawkins,A.C., Harwood,C.S., and Greenberg,E.P. (2004a). The Pseudomonas aeruginosa RpoS regulon and its relationship to quorum sensing. *Mol. Microbiol.,* **51,** 973-985.

129. Schuster,M., Lostroh,C.P., Ogi,T., and Greenberg,E.P. (2003). Identification, timing, and signal specificity of Pseudomonas aeruginosa quorum-controlled genes: a transcriptome analysis. *J. Bacteriol.,* **185,** 2066-2079.

130. Schuster,M., Urbanowski,M.L., and Greenberg,E.P. (2004b). Promoter specificity in Pseudomonas aeruginosa quorum sensing revealed by DNA binding of purified LasR. *Proc. Natl. Acad. Sci. U. S. A,* **101,** 15833-15839.

131. Seedorf,H., Hagemeier,C.H., Shima,S., Thauer,R.K., Warkentin,E., and Ermler,U. (2007). Structure of coenzyme F420H2 oxidase (FprA), a di-iron flavoprotein from methanogenic Archaea catalyzing the reduction of O2 to H2O. *FEBS J.,* **274,** 1588-1599.

132. Serino,L., Reimmann,C., Visca,P., Beyeler,M., Chiesa,V.D., and Haas,D. (1997). Biosynthesis of pyochelin and dihydroaeruginoic acid requires the iron-regulated pchDCBA operon in Pseudomonas aeruginosa. *J. Bacteriol.,* **179,** 248-257.

133. Sheldon,P.J., Johnson,D.A., August,P.R., Liu,H.W., and Sherman,D.H. (1997). Characterization of a mitomycin-binding drug resistance mechanism from the producing organism, Streptomyces lavendulae. *Journal of Bacteriology,* **179,** 1796-1804.

134. Sheldon,P.J., Mao,Y.Q., He,M., and Sherman,D.H. (1999). Mitomycin resistance in Streptomyces lavendulae includes a novel drug-binding-protein-dependent export system. *Journal of Bacteriology,* **181,** 2507-2512.

135. Shi,L., Adkins,J.N., Coleman,J.R., Schepmoes,A.A., Dohnkova,A., Mottaz,H.M., Norbeck,A.D., Purvine,S.O., Manes,N.P., Smallwood,H.S., Wang,H.X., Forbes,J., Gros,P., Uzzau,S., Rodland,K.D., Heffron,F., Smith,R.D., and Squier,T.C. (2006). Proteomic analysis of Salmonella enterica serovar Typhimurium isolated from RAW 264.7 macrophages - Identification of a novel protein that contributes to the replication of serovar Typhimurium inside macrophages. *Journal of Biological Chemistry,* **281,** 29131-29140.

136. Shindyalov,I.N. and Bourne,P.E. (1998). Protein structure alignment by incremental combinatorial extension (CE) of the optimal path. *Protein Engineering,* **11,** 739-747.

137. Silaghi-Dumitrescu,R., Kurtz,D.M., Jr., Ljungdahl,L.G., and Lanzilotta,W.N. (2005). X-ray crystal structures of Moorella thermoacetica FprA. Novel diiron site structure and mechanistic insights into a scavenging nitric oxide reductase. *Biochemistry,* **44,** 6492-6501.

138. Sio,C.F., Otten,L.G., Cool,R.H., Diggle,S.P., Braun,P.G., Bos,R., Daykin,M., Camara,M., Williams,P., and Quax,W.J. (2006). Quorum quenching by an N-acyl-homoserine lactone acylase from Pseudomonas aeruginosa PAO1. *Infect. Immun.,* **74,** 1673-1682.

139. Smith,R.S. and Iglewski,B.H. (2003). P. aeruginosa quorum-sensing systems and virulence. *Curr. Opin. Microbiol.,* **6,** 56-60.

140. Sugiyama,M., Kumagai,T., Hayashida,M., Maruyama,M., and Matoba,Y. (2002). The 1.6-A crystal structure of the copper(II)-bound bleomycin complexed with the bleomycin-binding protein from bleomycin-producing Streptomyces verticillus. *Journal of Biological Chemistry,* **277,** 2311-2320.

141. Taguchi,K., Fukutomi,H., Kuroda,A., Kato,J., and Ohtake,H. (1997). Genetic identification of chemotactic transducers for amino acids in Pseudomonas aeruginosa. *Microbiology,* **143 ( Pt 10),** 3223-3229.

142. Tan,M.W., Mahajan-Miklos,S., and Ausubel,F.M. (1999). Killing of Caenorhabditis elegans by Pseudomonas aeruginosa used to model mammalian bacterial pathogenesis. *Proceedings of the National Academy of Sciences of the United States of America,* **96,** 715-720.

143. Thomas,P.W., Stone,E.M., Costello,A.L., Tierney,D.L., and Fast,W. (2005). The quorum-quenching lactonase from Bacillus thuringiensis is a metalloprotein. *Biochemistry,* **44,** 7559-7569.

144. Timms-Wilson,T.M., Ellis,R.J., Renwick,A., Rhodes,D.J., Mavrodi,D.V., Weller,D.M., Thomashow,L.S., and Bailey,M.J. (2000). Chromosomal insertion of phenazine-1-carboxylic acid biosynthetic pathway enhances efficacy of damping-off disease control by Pseudomonas fluorescens. *Mol. Plant Microbe Interact.,* **13,** 1293-1300.

145. Turner,J.M. and Messenger,A.J. (1986). Occurrence, biochemistry and physiology of phenazine pigment production. *Adv. Microb. Physiol,* **27,** 211-275.

146. Ulrich,R.L. (2004). Quorum quenching: enzymatic disruption of N-acylhomoserine lactone-mediated bacterial communication in Burkholderia thailandensis. *Appl. Environ. Microbiol.,* **70,** 6173-6180.

147. Vannini,A., Volpari,C., Gargioli,C., Muraglia,E., Cortese,R., De Francesco,R., Neddermann,P., and Marco,S.D. (2002). The crystal structure of the quorum sensing protein TraR bound to its autoinducer and target DNA. *EMBO J.,* **21,** 4393-4401.

148. Vantland,C.W., Mocek,U., and Floss,H.G. (1993). Biosynthesis of the Phenazine Antibiotics, the Saphenamycins and Esmeraldins, in Streptomyces-Antibioticus. *Journal of Organic Chemistry,* **58,** 6576-6582.

149. Walker,T.S., Bais,H.P., Deziel,E., Schweizer,H.P., Rahme,L.G., Fall,R., and Vivanco,J.M. (2004). Pseudomonas aeruginosa-plant root interactions. Pathogenicity, biofilm formation, and root exudation. *Plant Physiol,* **134,** 320-331.

150. Winsor,G.L., Van Rossum,T., Lo,R., Khaira,B., Whiteside,M.D., Hancock,R.E., and Brinkman,F.S. (2009). Pseudomonas Genome Database: facilitating user-friendly, comprehensive comparisons of microbial genomes. *Nucleic Acids Res.,* **37,** D483-D488.

151. Xiao,G.P., Deziel,E., He,J.X., Lepine,F., Lesic,B., Castonguay,M.H., Milot,S., Tampakaki,A.P., Stachel,S.E., and Rahme,L.G. (2006a). MvfR, a key Pseudomonas aeruginosa pathogenicity LTTR-class regulatory protein, has dual ligands. *Molecular Microbiology,* **62,** 1689-1699.

152. Xiao,G.P., He,J.X., and Rahme,L.G. (2006b). Mutation analysis of the Pseudomonas aeruginosa mvfR and pqsABCDE gene promoters demonstrates complex quorum-sensing circuitry. *Microbiology-Sgm,* **152,** 1679-1686.

153. Yang,L., Barken,K.B., Skindersoe,M.E., Christensen,A.B., Givskov,M., and Tolker-Nielsen,T. (2007). Effects of iron on DNA release and biofilm development by Pseudomonas aeruginosa. *Microbiology-Sgm,* **153,** 1318-1328.

154. Zhang,Y.M., Frank,M.W., Zhu,K., Mayasundari,A., and Rock,C.O. (2008). PqsD is responsible for the synthesis of 2,4-dihydroxyquinoline, an extracellular metabolite produced by Pseudomonas aeruginosa. *J. Biol. Chem.,* **283,** 28788-28794.

# ZUSAMMENFASSUNG

*Pseudomonas aeruginosa* ist ein opportunistisches bakterielles Pathogen, das durch seine intrinsische Antibiotikaresistenz heute immer noch für eine hohe Sterblichkeit bei immunkompromitierten Patienten veranwortlich ist. *P. aeruginosa* produziert eine große Anzahl verschiedener Virulenzfaktoren, unter denen sich auch das blaue Phenazinderivat Pyocyanin befindet. Der lateinische Name "aeruginosa", übersetzt Grünspan, wurde wegen der charakteristischen blau-grünen Färbung von *P. aeruginosa*-Kulturen gewählt, die aus der Sekretion von Pyocyanin und dem gelben Metaboliten Pyoverdin resultiert. Die physiologische Bedeutung von Pyocyanin erscheint dabei äußerst komplex: es dient als respiratorisches Pigment, besitzt antibiotische Eigenschaften gegen andere Mikroorganismen, vermittelt transkriptorische Signale innerhalb von *P. aeruginosa* und ist zudem ein prominenter Virulenzfaktor in der Pathogenese.

In dieser Arbeit wurden PqsE und PA0803, zwei Proteine aus *P. aeruginosa* mit unbekannter molekularer Funktion, auf der in-vivo- und in-vitro-Ebene mit einem breiten Spektrum von Arbeitstechniken untersucht. Kristallstrukturen beider Proteine allein und im Komplex mit Liganden oder Substraten wurden bei hoher Auflösung bestimmt und zusammen mit anderen Methoden auf mögliche molekulare Funktionen untersucht. Die dabei gewonnenen strukturellen und funktionellen Erkenntnisse legen eine Basis für die zukünftige Suche nach den nativen Liganden bzw. Substraten beider Proteine.

**Molekulare Funktion von PqsE**

Im ersten Projekt wurde ein molekularer Mechanismus untersucht, mit dem *P. aeruginosa* die Biosynthese von Pyocyanin und einige andere Virulenzfaktoren durch das spezifische Signalmolekül *Pseudomonas*-Chinolon-Signal (PQS) kontrolliert. Dafür wurde im Besonderen das Genprodukt von *pqsE*, einem Teil des PQS-Biosyntheseoperons *pqsABCDE*, näher betrachtet, da vorhergehende Studien gezeigt hatten, dass *pqsE* für die PQS-Biosynthese nicht gebraucht wird, seine Deletion aber trotzdem zum Verlust der Virulenzproduktion einschließlich von Pyocyanin führt. Dies legt nahe, dass *pqsE* einen potentiellen Angriffspunkt für die Therapie von *P. aeruginosa*-Infektionen darstellt. Es ist daher interessant, sich mit der Funktion des Genprodukts auf der molekularen Ebene zu beschäftigen.

Seit seiner Enteckung 1999 hat PqsE viel Aufmerksamkeit in der bakteriologischen Forschung auf sich gezogen. Viele Arbeiten in der Literatur haben gezeigt, dass PqsE eine kritische Verbindung zwischen Quorum Sensing und der Virulenz herstellt. Dennoch ist es trotz allen Forschritts zum Verständnis des PQS-Systems bisher nicht gelungen, die molekulare Funktion von PqsE zu bestimmen. In dieser Arbeit wurde rekombinantes PqsE kloniert, exprimiert, gereinigt und schließlich charakterisiert. Überraschenderweise interagiert PqsE nicht mit PQS und ist deswegen kein PQS-Antwort-Protein, wie es ursprünglich in der Literatur vorgeschlagen wurde. Da vorausgehende, vorwiegend mit genetischen Methoden durchgeführte Arbeiten keinen offensichtlichen Startpunkt lieferten, wurde zunächst die Kristallstruktur von PqsE bei 1.6 Å Auflösung in der Hoffnung bestimmt, dass sich hieraus Hinweise für einen molekularen Mechanismus ableiten lassen.

PqsE ist eine binukleare Metallohydrolase mit einem gemischten Fe(III)M(II)-Aktivitätszentrum. Ein aus der Aufreinigung stammender Ligand wurde als Benzoat identifiziert und könnte anzeigen, dass PqsE seinen regulatorischen Effekt durch Umwandlung eines von Chorismat abgeleiteten Moleküls ausübt. Weiterhin wurde beobachtet, dass PqsE Phosphodiester einschließlich ein- und zweisträngiger DNA und RNA ebenso wie den Thioester S-(4-Nitrobenzyl)-mercaptoethan sehr langsam hydrolisieren kann. Höhere Aktivität wurde nach der Inkubation mit $Co^{2+}$ und, zu einem niedrigeren Grad, $Mn^{2+}$ beobachtet, was darauf hinweist, dass es sich bei dem zunächst in rekombinantem PqsE gefundenen Fe(III)/Fe(II)-Zentrum um ein Artefakt der Aufreinigung handeln könnte. Die Kristallstruktur eines Komplexes der E182A-Mutante von PqsE mit bis-pNPP wurde bestimmt und ermöglicht die Ableitung eines hypothetischen Hydrolysemechanismus. Ferner wurden Transkriptomanalysen eines PqsE-deletierten und eines PqsE-komplementierten *P. aeruginosa*-Stammes durchgeführt. Diese Daten legen es nahe, dass das natürliche Substrat von PqsE eine Verwandtschaft zu Anthranilsäure oder Catechol besitzt.

**Pyocyanin-Bindungsaktivität des hypothetischen Proteins PA0803**

Das ca. 6 Megabasenpaare große Genom von *Pseudomonas aeruginosa* enthält etwa 5500 Gene, von denen ein Großteil nicht untersucht ist und als “hypothetische Proteine” annotiert wurde. Die Unkenntnis eines Zusammenhangs mit bekannten biochemischen Auf- oder Abbauwegen bedeutet jedoch nicht, dass diese hypothetischen Proteine eine weniger wichtige Rolle für die Bakterien spielen.

Im zweiten hier vorgestellten Projekt wurde das Gen PA0803 aus I
*Pseudomonas aeruginosa* untersucht. PA0803 besitzt niedrige Sequenzhomologie zum Phenazin-Resistenzprotein EhpR aus *Pantoea agglomerans*, es ist im Genom allerdings nicht in der Nähe eines der beiden Phenazinbiosynthesecluster lokalisiert. Um herauszufinden, ob PA0803 Phenazine binden kann, wurde das Gen kloniert, exprimiert, gereinigt und charakterisiert, ebenso wurde die Kristallstruktur bei einer Auflösung von 1.6 Å bestimmt. Experimente mit isothermer Titrationskalorimetrie und die Kristallstruktur eines PA0803:Pyocyanin-Komplexes bestätigen, dass PA0803 Pyocyanin mit mikromolarer Affinität binden kann. Dies legt nahe, dass PA0803, zusammen mit anderen Genprodukten, als ein Transportprotein für kleine aromatische Moleküle dient.

# CURRICULUM VITAE

## EDUCATION

| | |
|---|---|
| 08/03 - present | **PhD Candidate** (expected Nov 2009) in Chemical Biology<br>Max-Planck Institute of Molecular Physiology, Dortmund |
| 08/99 - 07/03 | **Bachelor of Science** in Biological Sciences & Biotechnology<br>Tsinghua University, Beijing |

## RESEARCH EXPERIENCES

| | |
|---|---|
| 02/05 - present | Structural and functional study of PqsE, the *Pseudomonas* Quinolone Signal response protein (article to *Biochemistry* submited) **(Dissertation)** |
| 01/06 - present | Structural and functional study of a hypothetical protein PA0803 reveals its function as a pyocyanin binding protein (publication in preparation) |
| 08/03 - 02/05 | 1.0 Å structure of EhpR, a phenazine resistance protein from *pantoea agglomerans* Eh1087, suggests that phenazine resistance follows principles of GLYOXYLASE (I)-resistance mechanisms |

## PUBLICATION

**Yu S**, Jensen V, Seeliger J, Feldmann I, Weber S, Schleicher E, Häussler S, Blankenfeldt W*. Structure Elucidation and Preliminary Assessment of Hydrolase Activity of PqsE, the Pseudomonas Quinolone Signal (PQS) Response Protein. *Biochemistry* 2009 Nov 3; 48(43):10298-307.

Guo Z, Wu YW, Das D, Delon C, Cramer J, **Yu S**, Thuns S, Lupilova N, Waldmann H, Goody RS, Brunsveld L, Alexandrov K* and Blankenfeldt W*. Structures of Rab geranylgeranyl transferase: substrate/product complexes provide insights into evolution of protein prenylation. *EMBO J*. 2008 Sep 17; 27(18):2444-56.